Universidade do Minho
I3Bs - Instituto de Investigação em Biomateriais, Biodegradáveis e Biomiméticos

Sara Alexandra Correia Amorim

Extracellular matrix models to study the impact of Hyaluronan molecular weights on the behavior of gastric cancer cells

Fevereiro de 2020

Extracellular matrix models to study the impact of Hyaluronan molecular weights on the behavior of gastric cancer cells
Sara Alexandra Correia Amorim
UMinho | 2020

FCT Fundação para a Ciência e a Tecnologia
REPÚBLICA PORTUGUESA
UNIÃO EUROPEIA
Fundo Social Europeu
POCH

Universidade do Minho
I3Bs - Instituto de Investigação em Biomateriais, Biodegradáveis e Biomiméticos

Sara Alexandra Correia Amorim

Extracellular matrix models to study the impact of Hyaluronan molecular weights on the behavior of gastric cancer cells

Tese de Doutoramento
Doutoramento em Engenharia de Tecidos, Medicina Regenerativa e Células Estaminais

Trabalho efetuado sob a orientação de
Doutor Ricardo Alexandre Rodrigues Pires
Professor Doutor Rui Luís Gonçalves dos Reis

Fevereiro de 2020

ACKNOWLEDGMENTS

This thesis would not be possible without the contribution of several people, in a direct or indirect way.

Firstly, I would like to acknowledge Professor Rui Reis, not only to be my co-supervisor and support my work during this five year of PhD, but mostly for giving me the opportunity to join this prestigious Research Group. A special thanks to Prof. Rui Reis undoubtedly a visionary and great leader.

I would like to express my deeply gratitude to my supervisor Dr. Ricardo Pires for all the support, for believing in me even when I doubted. For all scientific and, sometimes, not so scientific discussions, but mostly for the patience to deal with a few "existential crises". More than a supervisor, Ricardo become also a friend.

To Professor Celso Reis, for the co-supervision during these five years of PhD and for being always available for scientific discussions.

I would like to acknowledge Diana Costa, to introduce me, a Chemist, to the Biology "world", for all the patience and the great contribution to this Thesis. To Iva Pashkuleva for the huge scientific support, to share her knowledge and support me from my early days in 3B's Research Group.

I would like to acknowledge all my co-workers, colleagues and friends in 3B's. A special appreciation to those who shared, closely, all the good and not so good moments, Ana Gi, Viviana and Ana Rita. A deep thanks to Ana Rita for being "there" when I needed, for listening, crying and laughing. To show me the "glass half full" when I saw it fully empty.

I would like to express my sincerely gratitude to my family, Mom, Dad and Sister for supporting me since the beginning and for all the unconditional love. I know that this Thesis and accomplishment make them very proud. Thank you for believe in me!

I am truly grateful to my husband, my friend, my partner for life and my shelter Nuno Mota. Without him nothing would make sense. His support, patience and love were crucial for giving strength to continue. Thank you for your love and unconditional support!

To my son Miguel! Thank you for your existence, for giving me strength and show me the true meaning of life and love. He born during this PhD and, undoubtedly, he made me a better professional, showing me that the time, that we always complain that we don't have, can be much more valuable. I am sorry for the moments that I missed. For that I dedicate this achievement to Miguel.

Finally, I would like to acknowledge the Foundation for Science and Technology (FCT) for my PhD scholarship SFRH/BD/112075/2015). This work was also supported by the European Commission: H2020-TWINN-2015-692333–CHEM2NATURE, H2020-WIDESPREAD-2014-2-668983–FORECAST and 739572-THE DISCOVERIES CTR

STATEMENT OF INTEGRITY

I hereby declare having conducted this academic work with integrity. I confirm that I have not used plagiarism or any form of undue use of information or falsification of results along the process leading to its elaboration.

I further declare that I have fully acknowledged the Code of Ethical Conduct of the University of Minho.

Extracellular matrix models to study the impact of Hyaluronan molecular weights on the behavior of gastric cancer cells

ABSTRACT

Gastric cancer (GC) is one of the most common types of cancers. At early stages, the tumor is confined to the primary site, however, at latter stages, its ability to metastasize to secondary sites reduces the efficiency of the current treatment strategies. There is a clear link between the invasive character of cancer cells and the composition and properties of the tumor microenvironment (TME). The TME is composed by cancer and healthy cells, as well as the extracellular matrix (ECM). The ECM is one of the main modulators of the proliferation, migration and invasion of cancer cells. In cancer, the unbalanced synthesis and degradation of glycosaminoglycans, proteoglycans and proteins, alters the ECM's physical properties and its biochemical composition, as for example the accumulation of hyaluronic acid (HA) with different molecular weights (Mws). It is known that HA of low Mw is implicated in the promotion of the migration and invasiveness of cancer cells, as well as in tumor growth and chemoresistance.

In this thesis, we developed 2D and 3D models, that mimic the physiological presentation of HA, and studied the influence of its Mw on the adhesion, migration and invasiveness of GC cells, *i.e.* MKN45 and AGS. 2D surfaces generated by Layer-by-Layer assembly, are able to present HA in an ECM-relevant manner, being recognized by its specific cell surface receptor, CD44 (Chapters 4 and 5). We tuned the surfaces' mechanical properties and showed that softer surfaces were generated as the Mw of HA increased (Chapters 4, 5 and 6), influencing the cancer cells' behavior. HA of low Mw (6.4kDa) promoted the migration of: *i)* AGS cells, in a process mediated by RHAMM and through the activation of the AKT signalling cascade (Chapter 6) and; *ii)* MKN45 cells, through a paxillin-mediated activation of focal adhesion sites (Chapter 7). We also used an Alginate-HA 3D model for the encapsulation of MKN45 and MSCs cells. A core of MKN45 cancer cells (mimicking the cancer site) and a shell of MSCs was a faithful mimic of the different cell types present in the TME. While the presence of HA of high Mw (*i.e.* 1500kDa) promoted the migration of MSCs into the MKN45 cancer cell niche; HA of low Mw induced the migration of the MKN45 cells into the shell of the 3D model (Chapter 8). In summary, we show that it is possible to mimic the biological role of HA using the developed models and that GC cells respond differently to the mechanical properties of these systems, as well as to the Mw of HA.

Keywords: Cancer models; ECM; Gastric cancer; Hyaluronic acid; Molecular weight

Modelos que mimetizam a matriz extracellular para estudar o impacto do peso molecular do Ácido hialuronico no comportamento das células do cancro gástrico

RESUMO

O cancro gástrico é um dos tipos mais comuns de cancro. Inicialmente, o tumor apresenta-se localizado, mas, com o avanço da doença, dissemina para outras zonas formando metástases. Neste contexto, existe uma estreita relação entre o carácter invasivo das células cancerígenas e a composição e propriedades do microambiente tumoral (TME, composto por células cancerígenas e saudáveis, e matriz extracellular, *i.e.* ECM). A ECM é capaz de modelar a capacidade invasiva das células cancerígenas. No cancro, a síntese e degradação descontrolada de glicosaminoglicanos, proteoglicanos e proteínas, alteram as propriedades físicas e bioquímicas da ECM levando à acumulação de ácido hialurónico (HA) com diferentes pesos moleculares (Mws). O HA de baixo Mw induz a migração e invasão das células cancerígenas, assim como o crescimento do tumor e resistência à quimioterapia.

Nesta tese, foram desenvolvidos modelos 2D e 3D que mimetizam a presença fisiológica do HA, de modo a estudar a influência do seu Mw na adesão, migração e invasão das células de cancro gástrico, *i.e.* MKN45 e AGS. As superfícies 2D geradas através da deposição sequencial de camadas (LbL), permitiu manter a bioatividade do HA sendo reconhecível pelo seu principal recetor celular, o CD44 (Capítulos 4 e 5). A rigidez das superfícies foram ajustadas, sendo que uma diminuição da rigidez foi observada à medida que aumentámos o Mw do HA, influenciando assim o comportamento celular (Capítulos 4, 5 e 6). O HA de baixo Mw (*i.e.* 6.4kDa) promoveu a migração das células: *i)* AGS, ativando a cascata de sinalização AKT mediada pela sobre-expressão de RHAMM (Capítulo 6); e *ii)* MKN45, através da ativação de proteínas de adesão, tais como paxilina (Capítulo 7). Foi também desenvolvido um modelo 3D composto por Alginato (Alg) e HA, onde células cancerígenas MKN45 foram encapsulados numa esfera central de Alg-HA (mimetizando o tumor) e células estaminais mesenquimais (MSCs) numa camada exterior de Alg (mimetizando as células saudáveis circundantes ao tumor). A presença de HA com alto Mw (*i.e.* 1500kDa) promoveu a migração de MSCs para a esfera central do modelo; enquanto que o HA de baixo Mw (*i.e.* 6.4kDa) induziu a migração das células MKN45 para a sua periferia (Capítulo 8). Resumindo, nesta tese demonstramos que, os modelos propostos mimetizam o papel biológico do HA, mostrando que as células cancerígenas respondem de forma diferente às propriedades mecânicas dos sistemas, assim como aos diferentes Mws do HA.

Palavras-chave: Ácido Hialurónico; Cancro Gástrico; ECM; Modelos de cancro; Peso Molecular

TABLE OF CONTENTS

LIST OF ABBREVIATIONS

A

αMEM – alfa Minimum Essential Medium

AFM – Atomic Force Microscopy

AHA-g-PNIPAAm – Aminated Hyaluronic Acid-g- poly(N-isopropylacrylamide)

ALDH - aldehyde dehydrogenase

Alg - Alginate

ALP – Alkaline Phosphatase

Au - gold

B

bCAFs – Breast cancer associated fibroblasts

BCMN - Block copolymer micelle nanolithography

BCSC - Breast cancer stem cells

bFGF – Basic fibroblast growth factor

bmMSCs – Bone marrow Mesenchymal stem cells

BSA – Bovine serum albumine

C

Ca^{2+} - Calcium ion

$CaCO_3$ – Calcium carbonate

CAFs – Cancer associated fibroblasts

calcein-AM - Calcein-Acetoxymethyl

CD24 - Cluster of differentiation 24

CD44 – Cluster of differentiation 44

CHI - Chitosan

cm - centimeter

CO_2- Carbon dioxide

Coll - Collagen

CS – Chondroitin sulphate

CSCs – Cancer stem cells

D

°C - Degree Celsius

DAPI - 4',6'-diamino-2-fenil-indol

DNA – Deoxyribonucleic Acid

DS – Dermatan surphate

E

EC – Endothelial cells

ECM - Extracellular matrix

EDC - N-(3-dimethylaminopropyl)-N′-ethylcarbodiimide hydrochloride

e.g. – "for example", form latin *exempli gratia*

EMT – Epithelial to mesenchymal transition

ERK1/2 – Extracellular signal-regulated kinase

F

FACS - Fluorescence-activated cell sorting

FAK – Focal adhesion kinase

FBS - Fetal bovine serum

FITC - Fluorescein isothiocyanate

FN - Fibronectin

G

G' - Storage modulus

G''- Loss modulus

GAGs - Glycosaminoglycans

GBM - Glioblastoma

GFs – Growth factors

GlcA – Glucuronic acid

GlcNac – N-acetyl-glucosamine

H

HA - Hyaluronic acido or Hyaluronan

HAADH – HA modified with adipic acid dihydrazide

HAALD - HA modified with aldehydes

HABP1 - Hyaluronan-binding protein 1

HARE - Hyaluronan receptor for endocytosis

HAS – Hyaluronan synthase

Hep - Heparin

HIF-1α- Hypoxia-inducible factor 1-alpha

HMF - human mammary fibroblast

HMw – High molecular weight

HS – Heparan sulphate

HS-HA – Thiolated-hyaluronan

Hyal – Hyaluronidases

H_2O - Water

Hz - Hertz

I

i.e. - "in other words", form latin *id est*

ICC - Immunocytochemistry

IL – Interleukin

K

KCl – Potassium chloride

kDa - Kilodalton

kg - Kilogram

kPa - Kilopascal

L

L - Liter

LbL – Layer-by-layer

LMw – Low molecular weight

LYVE-1 - Lymphatic vessel endothelial hyaluronan receptor 1

M

M - Molar

MA-HA – Methacrylated hyaluronic acid

mbar – Milibar

mg - Milligram

MHz – Mega Hertz

min - minute

mL – Mililiter

mm – Millimeter

mM - Millimolar

MMP - Metalloproteinase

MMw – Medium molecular weight

MPa - Megapascal

mPas – MiliPascal

Mws – Molecular weight

µg - Microgram

µm - Micrometer

N

NaCl - Sodium chloride

NaOH - Sodium hydroxide

NHS – N-hydroxysuccinimide

nm - Nanometers

O

OCN - Osteocalcin

P

Pa - Pascal

PBS - Phosphate-buffered saline

PCa – Pancreatic cancer

PCL - Polycaprolactone

PEG – Poly-ethylene glycol

PGA – Poly-glycolic acid

pH - Potential hydrogenionic

PI - Propidium iodide

PLA - Poly(lactic acid)

PLGA - Poly [(lactic acid) -co- (glycolic acid)]

PLL – Poly-L-lysine

p - Statistical level of significance

Q

QCM-D – Quartz crystal microbalance with dissipation

R

Ref. - Reference

RGD - Arginine-glycine-aspartic acid

RHAMM - Receptor for hyaluronan mediated motility

RPM - Rotations per minute

RPMI - Roswell Park Memorial Institute

RT - Room temperature

η – Refractive index

S

s - Seconds

SEM - Scanning Electron Microscopy

SiO_2 – Silicon oxide

SMCs – Smooth muscle cells

SPR – Surface plasmon resonance

T

TBS - Tris-buffered saline

TBS-T - Tris-buffered saline with tween 20

TCPS – Tissue culture polystyrene

TGF-β - Transforming growth factor-β3

TiO_2 – Titanium oxide

TME – Tumor microenvironment

TRL - Toll-like receptor

3D - Three-dimensional

2D – Two-dimensional

U

UV - Ultraviolet

V

VEGF - Vascular endothelial growth factor

W

λ – Wavelength

WB – Western blot or Western blotting

Y

YAP - Yes-associated protein

LIST OF EQUATIONS

LIST OF FIGURES

LIST OF SUPPLEMENTARY FIGURES

LIST OF TABLES

LIST OF SUPPLEMENTARY TABLES

SHORT *CURRICULUM VITAE*

Sara Amorim was born in 1984 in Oliveira de Azeméis. Her academic journey started on 2002 at the University of Minho, with a graduation in Applied Chemistry, which was concluded in 2007 with a final grade of 13/20. During her graduation she participated in the Erasmus Program, where she had the opportunity to visit the University of Pardubice in the Czech Republic. During 5 months she was developed her final research Project on "New Metal Complex Dyes with Thiol Group in Molecule" with a final degree of 18/20. In 2007 she enrolled in a Master degree course in Medicinal Chemistry (at the University of Minho), which she finished by 2009 with a final grade of 16/20. Her Master thesis was performed under the scope of the project "BIOPACK – In-situ biopolymers nanocomposites: high performance packaging materials for a clean environment".

Nowadays, Sara is a PhD student at the 3B's Research Group on the Tissue Engineering, Regenerative Medicine and Stem Cells Doctoral Program. She arrived at the 3B's Research Group in 2010, to work in the "BioActiveCork" project. Since then, she has been dedicated to the functionalization of 2D surfaces using different strategies, namely, using self-assembled monolayers (SAMs) for biosensing applications, under the scope of the project "Find & Bind" financed under the 7th Framework Program of the European Commission, as well as the synthesis of inorganic silica nanoparticles to induce osteogenic differentiation in the scope of the project "Polaris" also funded by the European Commission.

In September 2015, she was awarded an individual PhD scholarship by the Fundação para a Ciência e Tecnologia (FCT). Under the supervision of Dr. Ricardo Pires, Prof. Dr. Rui L. Reis and Prof. Dr. Celso Reis, she started her PhD on the development of 2D and 3D platforms to mimic the ECM of gastric cancer cells and to study their invasive behavior mediated by hyaluronic acid.

Sara Amorim was also involved in the Twinning project "Chem2Nature" and, more recently, on the H2020 funded ERA Chairs project "Forecast".

As result of her research work, she is author and co-author of 9 full length papers published in international scientific journals, 1 book chapter, 1 published conference abstract, 12 oral communications, 28 poster presentations and 2 oral poster presentations.

LIST OF PUBLICATIONS

The work performed during the PhD period resulted in the publications listed below.

Papers in international scientific journals with referees (as first author)

1. **Amorim, S.,** Reis, C. A., Reis, R. L. & Pires, R. A, (2020), Extracellular matrix mimics using hyaluronic acid-based materials (submitted)

2. **Amorim, S.,** Reis, C. A., Reis, R. L., Pashkuleva, I., & Pires, R. A. (2020), Tunable layer-by-layer films containing hyaluronic acid and their interactions with CD44. (submitted)

3. **Amorim, S.,** da Costa, D. S., Mereiter S., Reis, C. A., Reis, R. L., Pashkuleva, I., & Pires, R. A. (2020), Multilayer Platform to Model the Bioactivity of Hyaluronic Acid in Gastric Cancer. (submitted)

4. **Amorim, S.,** da Costa, D. S., Reis, C. A., Reis, R. L., Pashkuleva, I., & Pires, R. A. (2020), Hyaluronic Acid of low molecular weight triggers the invasive "hummingbird" phenotype on gastric cancer cells. (submitted)

5. **Amorim, S.,** da Costa, D. S., Reis, C. A., Reis, R. L., Pashkuleva, I., & Pires, R. A. (2020), 3D mimics of tumor microenvironment: interplay between hyaluronan, stem and cancer cells. (submitted)

6. **Amorim, S.,** da Costa, D. S., Freitas, D., Reis, C. A., Reis, R. L., Pashkuleva, I., & Pires, R. A. (2018). Molecular weight of surface immobilized hyaluronic acid influences CD44-mediated binding of gastric cancer cells. *Sci Rep, 8*(1), 16058. doi:10.1038/s41598-018-34445-0

Papers in international scientific journals with referees (as co-author)

1. Homem, N. C., de Camargo Lima Beluci, N., **Amorim, S.,** Reis, R. L., Vieira, A. M. S., Vieira, M. F., Bergamasco, R., Amorim, M. T. P. (**2019**). Surface modification of a polyethersulfone microfiltration membrane with graphene oxide for reactive dyes removal. *Applied Surface Science, 486*, 499-507. doi:10.1016/j.apsusc.2019.04.276

2. Vieira, S., Franco, A. R., Fernandes, E. M., **Amorim, S.,** Ferreira, H., Pires, R. A., Reis, R. L., Neves, N. M. (**2018**). Fish sarcoplasmic proteins as a high value marine material for wound dressing applications. *Colloids Surf B Biointerfaces, 167*, 310-317. doi:10.1016/j.colsurfb.2018.04.002

3. Ferreira, H., Martins, A., Alves da Silva, M. L., **Amorim, S.,** Faria, S., Pires, R. A., Reis, R. L., Neves, N. M. (**2018**). The functionalization of natural polymer-coated gold nanoparticles to carry bFGF to promote tissue regeneration. *Journal of Materials Chemistry B, 6*(14), 2104-2115. doi:10.1039/c7tb03273k

4. Araújo, A. R., Soares da Costa, D., **Amorim, S.,** Reis, R. L., Pires, R. A., & Pashkuleva, I. (**2016**). Surfaces Mimicking Glycosaminoglycans Trigger Different Response of Stem Cells via Distinct Fibronectin Adsorption and Reorganization. *ACS Appl Mater Interfaces, 8*(42), 28428-28436. doi:10.1021/acsami.6b04472

5. Francesko, A., Fernandes, M. M., Ivanova, K., **Amorim, S.,** Reis, R. L., Pashkuleva, I., Mendoza, E., Pfeifer, A., Heinze, T., Tzanov, T. (**2016**). Bacteria-responsive multilayer coatings comprising polycationic nanospheres for bacteria biofilm prevention on urinary catheters. *Acta Biomater, 33*, 203-212. doi:10.1016/j.actbio.2016.01.020

Book Chapter

1. **Amorim S.**, Reis R. L., Pires R. A. " Biomatrices that mimic the cancer extracellular environment" (*In Press*)

Conference oral presentations (as first author and as speaker)

1. **Amorim S.**, Soares da Costa D., Mereiter S., Pashkuleva I,Reis C., Reis R. L., Pires RA "Hyaluronan molecular weight regulates the dynamics of focal adhesions and cancer cell migration and invasiveness" 13º Reunião do Grupo de Glucidos, Porto, 2019.

2. **Amorim S.**, Soares da Costa D., Pashkuleva I,Reis C., Reis R. L., Pires RA, "Progression and invasiveness of gastric cancer in 3D matrices and in the presence of stem cells", Forecast Conference, Porto, 2019

3. **Amorim S.**, Soares da Costa D., Pashkuleva I., Reis C., Reis R. L., Pires RA, "Hyaluronan-based 3D extracellular matrix model to study cancer progression", Termis EU, Greece, 2019

4. **Amorim S.**, Soares da Costa D., Freitas D., Reis C. A., Reis R. L., Pashkuleva I., and Pires R. A., "Model surfaces to study Hyaluronan-CD44 interactions in gastric cancers", International Symposium on Bioinspired Macromolecular Systems, Aveiro, 2017.

5. **Amorim S.**, Soares da Costa D., Freitas D., Reis C. A., Reis R. L., Pashkuleva I., and Pires R. A., "The effect of immobilized Hyaluronic Acid on CD44-overexpressing MKN45 gastric cancer cell line ", 12º Reunião do Grupo de Glucidos, Aveiro, 2017.

6. **Amorim S.**, Soares da Costa D., Freitas D., Magalhães A., Reis C., Reis R.L., Pashkuleva I. and Pires R. A. "Molecular weight of surface immobilized hyaluronic acid influences CD44-mediated adhesion of gastric cancer cells", 27th European Conference on Biomaterials (ESB), Krakow, Poland,30th August to 3rd September, 2015

7. **Amorim S.**, Soares da Costa D., Freitas D., Magalhães A., Reis C., Reis R. L., Pashkuleva I., and Pires R. A., "Role of exogenous hyaluronic acid molecular weight on CD44-mediated adhesion", 2nd POLARIS Workshop, Guimarães, Portugal, 29 June to 1 July 2015.

Conference oral presentations (as co-author)

1. Ferreira H., Martins A., Silva M. L. A., **Amorim S.**, Faria S., Pires R. A., Reis R. L., Neves N. M., Layer-by-Layer assembly of natural polymers onto gold nanoparticles for imaging and regenerative strategies, Baltic Conference, Stockholm (Sweden) 8-11 October 2017.

2. Ferreira H., Martins A, Silva MLA, **Amorim S.,** Faria S., Pires R.A., Reis R. L., Neves N. M., "Coating of gold nanoparticles with natural polymers for imaging and regenerative strategies"- Term Stem, Guimarães, 2016

3. Araújo AR, Soares da Costa D., **Amorim S.,** Reis R.L., Pires R.A. and Pashkuleva I., "Glycosaminoglycan mimicking surfaces trigger distinct response of stem cells via fibronectin adsorption" 27th European Conference on Biomaterials (ESB), Krakow, Poland, 30th August to 3rd September 2015

Conference posters (as first author)

1. **Amorim S.**, Soares da Costa D., Reis C. A., Reis R. L., Pashkuleva I., and Pires R. A., "Adhesion and migration of AGS gastric cancer cell line via AKT pathway activation, influenced by the immobilized oligossacharide HA", TermStem Conference, November, 2019

2. **Amorim S.**, Soares da Costa D., Reis C. A., Reis R. L., Pashkuleva I., and Pires R. A. "Immobilized oligosaccharides of Hyaluronic Acid induce the migration and proliferation of AGS gastric cancer cells through the activation of the AKT pathway", 1st Discoveries Forum on Regenerative and Precision Medicine, September, 2019

3. **Amorim S.**, Reis R. L., Pashkuleva I., and Pires R. A. "Design and build up of Layer-by-Layer assemblies with targeted properties: the influence of crosslinking and polyelectrolytes molecular weights", Chem2Nature Final Conference, October, 2018

4. **Amorim S.**, Soares da Costa D., Reis C. A., Reis R. L., Pashkuleva I., and Pires R. A. "Molecular weight of Hyaluronic acid modulates the morphology of gastric cancer cell" European Society for Biomaterials (ESB) Conference, September, 2018

5. **Amorim S.**, Soares da Costa D., Reis C. A., Reis R. L., Pashkuleva I., and Pires R. A. "Epithelial mesenchymal transition of gastric cancer cell depends on the molecular weight of hyaluronic acid" Chem2Nature Third School, June, 2018

6. **Amorim S.**, Soares da Costa D., Freitas D., Reis C. A., Reis R. L., Pashkuleva I., and Pires R. A., "Extracellular matrix inspired models for gastric cancer development: focus on hyaluronan-CD44 interactions", Forecast Workshop, 2017.

7. **Amorim S.**, Soares da Costa D., Reis C. A., Reis R. L., Pashkuleva I., and Pires R. A., "Influence of the molecular weight of immobilized hyaluronic acid on the behavior of CD44-overexpressing cells", European Society for Biomaterials (ESB), September, 2017.

8. **Amorim S.**, Soares da Costa D., Reis C. A., Reis R. L., Pashkuleva I., and Pires R. A., "Response of cancer cells overexpressing CD44 to multilayer systems incorporating HA with different molecular weights", Chem2Nature, 2017.

9. **Amorim S.**, Soares da Costa D., Reis C., Reis R. L., Pashkuleva I., and Pires R. A., "Regulation of gastric cancer invasiveness by hyaluronic acid with specific molecular weight", Chem2Nature, 2016.

Conference posters (as co-author)

1. Dudik O., **Amorim S.**, Soares da Costa D., Silva T. H., Pires R. A., and Reis R. L., “Modified mesoporous silica nanoparticles improves BMP-2 loading and its release timeframe”, TermStem Conference, November, 2019

2. Dudik O., **Amorim S.**, Soares da Costa D., Silva T. H., Pires R. A., and Reis R. L., "Development of mesoporous silica-based nanoparticles as BMP-2 controlled release systems", 1st Discoveries Forum on Regenerative and Precision Medicine, September, 2019

3. Dudik O., **Amorim S.**, Soares da Costa D., Silva T. H., Pires R. A., and Reis R. L., "Silica-based nanoparticles as BMP-2 localized delivery systems for bone tissue engineering applications", First Achilles Conference, July, 2019

4. Dudik O., **Amorim S.**, Silva T. H., Pires R. A., and Reis R. L., "Mesoporous silica nanoparticles for the immobilization of BMP-2 targeting bone regeneration", Chem2Nature Final Conference, October, 2018

5. Dudik O., **Amorim S.**, Silva T. H., Pires R. A., and Reis R. L., "Silica-based particles for effective immobilization of BMP-2", Chem2Nature, June, 2018

6. Ferreira H., Martins A., Silva M. L. A., **Amorim S.**, Faria S., Pires R. A., Reis R. L., Neves N. M., AuNPs coated with natural polymers for monitoring tissues regeneration stimulated by bFGF immobilized at their surface, Chem2Nature, 21-25 November, 2016.

Awarded grants

1. Foundation for Science and Technology (FCT) PhD scholarship (SFRH/BD/112075/2015).

INTRODUCTION TO THE THESIS FORMAT

This thesis comprises four main **Section (I to IV)** including nine **Chapters (1 to 9)**. The **Section I** provides a general introduction to the theme of the thesis, based on Hyaluronic acid (HA) and their role on the extracellular matrix **(Chapter 1)** and an overview on 3D cancer models that mimics the tumor microenvironment **(Chapter 2)**. The **Section II** details the materials and methods **(Chapter 3)** used on the development of the experimental work. In **Section III**, the experimental work and results are described and discussed, divided in five **Chapters (4 to 8)**. Finally, the **Section IV** relies on the final conclusions of the thesis **(Chapter 9)**. The thesis format is based on published or submitted papers, comprising the following structure: abstract, introduction, experimental section, results and discussion and conclusion. The content of each chapter is summarized below.

Section I – General introduction

Chapter 1 – Extracellular matrix mimics using hyaluronic acid-based biomaterials: presents a comprehensive overview on the important role of hyaluronic acid on the extracellular matrix of healthy and pathological cells. This Chapter includes the state-of-art of hyaluronan-based materials, including HA-based particles for drugs delivery, 2D surfaces for cells attachment and 3D models for cells encapsulation. It comprised an outline on the current HA products available in the market and their applications.

Chapter 2 – Biomatrices that mimic the cancer extracellular environment: provides a deeper overview on the developed 3D biomatrices, based on the components of the extracellular matrix, that resembles the cancer microenvironment.

Section II – Detailed description of experimental materials and methodologies

Chapter 3 – Materials and Methods: presents the materials, experimental methodologies and characterization techniques used within the experimental work developed on Chapters 4 to 8.

Section III – Experimental studies

Chapter 4 – Tunable layer-by-layer films containing hyaluronic acid and their interactions with CD44: presents the physical properties, e.g. thickness and hydration, of the layer-by-layer film composed by Poly-l-lysine and Hyaluronic acid, $(PLL\text{-}HA)_5$, of different molecular weights in the presence

and absence of crosslinking. The biorecognition of $(PLL\text{-}HA)_5$ is studied by the interaction with CD44, the main receptor for hyaluronic acid.

Chapter 5 – Molecular weight of surface immobilized hyaluronic acid influences CD44-mediated binding of gastric cancer cells: shows the interaction of gastric cancer cell lines, MKN45 and AGS, with the HA-end film $(PLL\text{-}HA)_1$ in response to the expression of CD44 at the cell membrane, and their invasive character.

Chapter 6 – Hyaluronic acid of low molecular weight triggers the invasive "hummingbird" phenotype on gastric cancer cells: shows the activation of a specific invasive phenotype, associated to the "hummingbird" morphology, when AGS cells are in contact with the LbL film $(PLL\text{-}HA)_5$.

Chapter 7 – Multilayer platform to model the bioactivity of Hyaluronic acid in gastric cancer: demonstrates the interaction between cancer cells and the $(PLL\text{-}HA)_5$ film, by monitoring in real-time with QCM-D, the adhesion and remodeling of the LbL film when in contact with MKN45. Further analysis on focal adhesion activation and migration pathways is revealed.

Chapter 8 – 3D mimics of the tumor microenvironment: interplay between hyaluronic acid, stem and cancer cells: presents a core-shell hydrogel comprising hyaluronic acid, with different molecular weights, blended with alginate in the core and alginate in the shell. The core resembles the tumor where MKN45 cells are encapsulated and the shell mimic the mesenchymal stem cells present in the tumor microenvironment. This core-shell hydrogel allows to study the influence of mesenchymal stem cells and hyaluronic acid of different molecular weights on the cancer invasiveness.

Section IV – Final conclusions and perspectives

Chapter 9 – General Conclusions and Final remarks: contains a concluding summary of each Chapter presented on the thesis. General conclusions comprising the limitations and innovative features of the developed work is described. Finally, future perspectives and applications of the knowledge acquired on the thesis is also provided.

Section I

General introduction

Chapter 1

Extracellular matrix mimics using hyaluronic acid-based biomaterials

Chapter 1

Extracellular matrix mimics using hyaluronic acid-based biomaterials*

ABSTRACT

Hyaluronic acid (HA) is a critical element of the extracellular matrix (ECM). The regulated synthesis and degradation of HA modulates the ECM chemical and physical properties, that, in turn, influence the cellular behaviour. HA triggers different signalling pathways, associated to the adhesion, proliferation, migration and differentiation of cells, mediated by its interaction with specific cellular receptors or by tuning the mechanical properties of the ECM. This review, summarizes the recent advances on the current strategies used to mimic the HA present in the ECM to study healthy or pathological cellular behaviour. This includes the development of HA-based 2D and 3D models for the seeding and encapsulation of cells, respectively, and HA particles as carriers for the targeted delivery of therapeutic agents to cells.

Keywords: Hyaluronic acid, extracellular matrix, hydrogels, particles, 2D surfaces, 3D models

* This Chapter is based on the publication: "Amorim, S., Reis, C. A., Reis, R. L. & Pires, R. A, (2020), *Extracellular matrix mimics using hyaluronic acid-based* materials (submitted)"

1-1. INTRODUCTION

The extracellular matrix (ECM) is a rich and complex tridimensional environment mainly composed by different bioactive polymers, such as, proteins and glycosaminoglicans (GAGs), as well as their combinations, *e.g.* glycoproteins and proteoglycans. This ECM acts as a structural and functional support for the cells in the different tissues of our body. The dynamic interplay between cells and the biofunctional ECM components regulate the normal activities of tissues, through the activation of signaling cascades that modulate cellular behavior. [1] Of note, the ECM also present a highly dynamic character that includes the continuing production, degradation and remodeling of its components. The balanced composition of the ECM is of extreme importance to maintain the homeostasis of the extracellular environment. In general, the most abundant type of structural protein present in the ECM is collagen, mostly in its fibrillary form, that confer tridimensional structure and mechanical strength to the matrix [2]. Other important components of the ECM are the glycoproteins, usually referred to as *"multitasking"* proteins, such as fibronectin, laminins, elastins, vitronectin, thrombospondins, tenascins, nephronectin and fibrinogen. They comprise several molecular domains that bind to different molecules (including collagens), adding cohesiveness to the ECM and ability to recognize and interact with specific cell membrane receptors, initiating different biochemical signaling pathways. [3] Proteoglycans, are another type of ECM component, that combine a protein core that is functionalized with different GAGs. These GAGs (*i.e.* heparin, chondroitin sulphate, heparan sulphate and hyaluronic acid) are key components of the ECM, as they are responsible for most of their physical properties and, more recently, it has been found that they are key biofunctional elements responsible for the modulation of cellular behavior. [4] Among all the GAGs that constitute the ECM of human tissues, hyaluronic acid (HA) stands out for being the only non-sulphated and most abundant.

HA, also known as hyaluronan, is a linear, negatively charged polysaccharide, presenting a disaccharide repetitive unit, constituted by the combination of glucuronic acid (GlcA) and N-acetyl glucosamine (GlcNAc), which are linked together by alternate β1-3 and β1-4 linkages. [5] Despite its linear and simple primary structure, HA is involved in different biological events, *e.g.* cells proliferation [6] and differentiation [7], contributing to the physiological balance of the ECM, by conferring hydration, lubrification and matrix homeostasis. [8] HA is synthesized by cells, extruded to the extracellular space through the transmembrane hyaluronan synthases (HAS) and catabolized by the enzymes, hyaluronidases (Hyal). [9] The chain length of HA varies accordingly to the hyaluronan synthases

activity. In mammals three different HAS (HAS1-3) are responsible for the production of HA, and they mainly differ in their ability to produce and extrude HA of different molecular weights (Mws). [10, 11] On the other hand, the Hyals play an important role in maintaining a balanced distribution of HA chain lengths in the ECM, cleaving HA at the β1,4 linkages. [12]

HA presents a simple and linear chemical structure; however, this is not a synonym of lack of bioactivity. In fact, the role of HA in the extracellular and pericellular space is not only as a space filling molecule. In contrast to the sulphated GAGs, HA does not have the capacity to establish covalent links to proteins generating proteoglycans, however, it plays a unique role in the ECM, as its interaction with different proteins occurs to generate a biofunctional outcome, *e.g.* the hyaladherin CD44 or the receptor for HA-mediated motility, RHAMM, the specific HA cell surface receptors. [13-15] The interaction between HA and its receptors is known to initiate several signaling events, activating pathways related to cell adhesion (*e.g.* focal adhesion kinase, FAK), proliferation and migration (extracellular-regulated kinase, ERK1/2). [13, 16, 17] HA has been also associated to different pathological states, as for example cancer, being an active modulator of invasiveness and metastasis. [17, 18] The biological relevance of HA leads to an increasing interest in the evaluation of its bioactivities in the ECM and its ability to modulate cellular function. These activities are leading researchers to pursue the development of different HA-based platforms to study *in vitro* the interplay between HA and cells. These systems are being designed not only to evaluate the HA's bioactivities (*e.g.* interaction with different proteins, such as growth factors, GFs), but also how HA is able to modulate the ECM mechanical features through the deposition of HA of different Mws.

1-2. ROLE OF HYALURONIC ACID IN THE EXTRACELLULAR MATRIX

1-2.1. Hyaluronic acid as a structural element in the extracellular matrix

HA is one of the major constituents of the ECM being responsible for the maintenance of tissue homeostasis, assuming a function of space filling element in connective tissues. Depending on its Mw, this GAG assumes different important physiological functions as a structural element of the ECM, namely: maintenance of the hydration of tissues; modulator of diffusion and exchange of ions and biomolecules; and mechanical support for cells. [19] Moreover, its ability to interact with other

biomolecules present in the cellular milieu also alters the physical properties of the ECM, through the formation of crosslinking configurations. [20]

1-2.2. The molecular weight of hyaluronic acid

The linear structure of HA is generated and extruded through the plasma membrane to the pericellular and extracellular space, in a process mediated by the transmembrane synthases HASs. At their cytoplasmic domain, the HASs catalyzes the reaction between UDP-glucuronic acid (UDP-GlcA) and UDP-N-acetylglucosamine (UDP-GlcNAc) with the reducing end of the HA chain promoting its elongation. Depending on the type of HAS responsible for the synthesis, it is generated HA of different Mw, namely: while HAS3 produces the shortest chains, between $1x10^5$-$2x10^5$ Da; the HAS1 and HAS2 generate the longest ones, from $2x10^5$ up to $2x10^6$ Da, reaching polymer lengths of, approximately, 25μm. [21, 22]

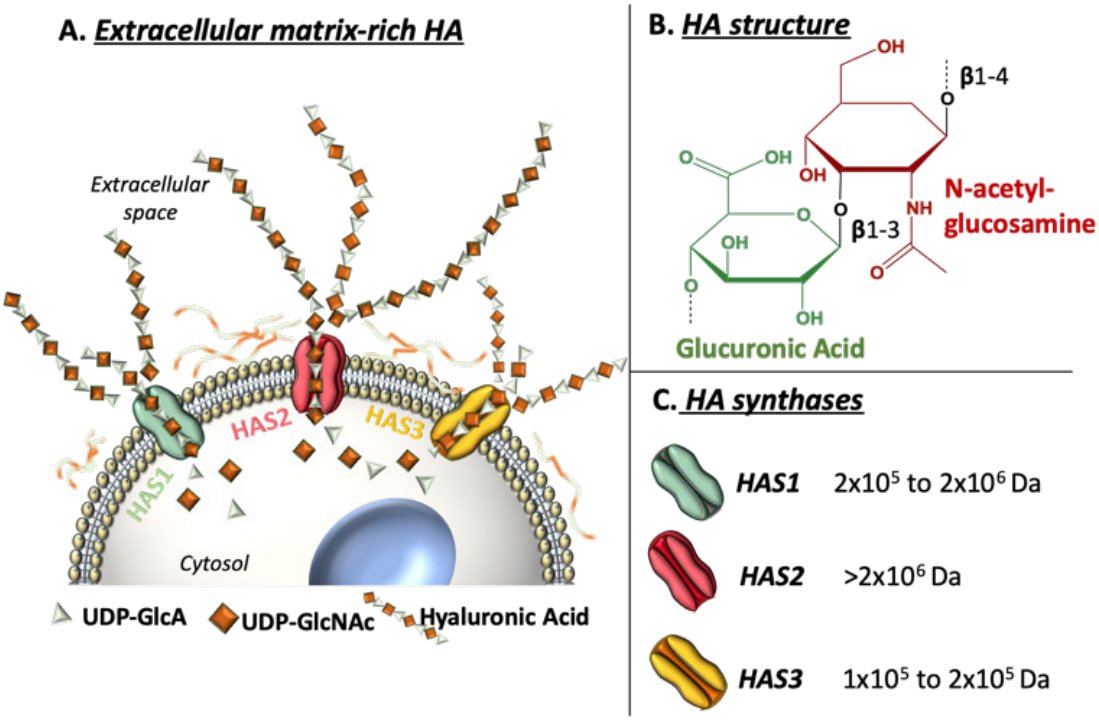

Figure 1-1. Chemical structure of HA composed by N-acetylglucosamine and glucuronic acid repeating units, linked by β1-3 and β1-4 glycosidic bonds. HA with different Mws is extruded from the cytoplasm to the ECM through the HA synthases (HAS1-3) pores, that links the intracellular with the extracellular space.

A balanced deposition and degradation of HA at the ECM is vital to keep the homeostasis of the cellular environment. In this context, while the above mentioned HASs regulate the deposition of HA, the Hyals and free radicals, such as reactive oxygen species (ROS), are key elements to control the degradation of HA contributing to their turnover at the ECM. [23] While Hyal1 is an intracellular enzyme, Hyal2, a glycosylphosphatidylinositol (GPI)-linked enzyme, is anchored to the cell membrane at the pericellular space. [24] Despite its independent mode of action, Hyal1 and Hyal2 are important contributors to biochemical pathways that lead to the degradation of HA. The Hyal2 cleaves HA at the cell surface, supported by the HA' major receptor, CD44, which holds the HA molecule in place for the enzyme to cleave it into small fragments; subsequently, HA is endocytically transported to the lysosomes to be degraded by the Hyal1. [24, 25]

The Mw of the HA present in the ECM, is known to be a key modulator of cellular behavior, while contributing to tissue homeostasis. HA has been described to be an inducer of numerous cellular responses mainly due to its interaction with different receptors. The most well-known, and widely described in the literature, are CD44 and RHAMM. However, others, such as toll-like receptors 2 and 4 (TLR-2,4), hyaluronan receptor for endocytosis (HARE), hyaluronan-binding protein 1 (HABP1) and lymphatic vessel endothelial receptor for hyaluronan 1 (LYVE1) are all HA binding proteins. [26] The Mw of HA is associated to different pathological states, such as osteoarthritis [27], fibrosis [28] and neuroinflammation [29]. The short chains of HA are usually associated with pro-inflammatory responses, pro-angiogenic activity and migration and proliferation of cells, whereas the longest chains are usually linked to cellular differentiation and anti-inflammatory responses (Table 1).

Table 1-1. HA molecular weights and their biological functions

HA Mws (kDa)	*HA target receptor*	*Function*	*Biological response*	*Ref.*
Low Mws (LMws)				
< 6	–	Pro-inflammatory	–	[30, 31]
	TRL-2; TLR-4;	NF-kB activation		
	CD44	Production of pro-inflammatory cytokines	Neuroinflammation	[29]
	–	Macrophage activation	Endothelialization	[32]
15 - 50	RHAMM	Activation of YAP1/TAZ protein	Mesotheliomas malignancy	[33]
	RHAMM	Activation of PI3K and MEK signaling pathways	Human choriocarcinoma cell migration	[34]
	TLR-4	Up-regulation of TGFβ-1, TNF-α, IL-6 Pro-inflammatory	Tissue repair	[31]
30 - 60	CD44	Migration of BRO cells	Melanoma cells invasion	[35]

Medium Mws (MMws)				
50 - 500	RHAMM	Up-regulation of TGFβ-1	Cellular migration and proliferation	[31]
60 - 800	–	Up-regulation of pro-resolving genes (*arg1*, *il10*, and *mrc1)*	–	[30]
High Mws (HMws)				
> 800	–	Pro-resolving mediators	–	[30]
1000 - 1800	CD44	Up-regulation of TGFβ-1	Cellular migration and proliferation	[31]
	–	Downregulation of TGFb1, CTGF, collagen I and collagen III	Endometrial fibrosis attenuation	[28]
	–	Anti-inflammatory; Anti-oxidant; Block the ERK1/2 signaling pathway	Protective role in nasal inflammation	[36]
	CD44	Migration of MKN45 cells; Cortactin phosphorylation	Invasion of gastric cancer cells	[37]
> 2000	CD44	Activation of ERK1/2 and	Embryonic stem cell differentiation,	[38]

	–	suppression of EGFR signaling pathways Up-regulation of ALP, Runx-2 and OCN	toward smooth muscle cells Osteogenic differentiation	[39]

In the last decades, HA has been increasingly linked to cancer invasiveness and progression, due to its overproduction, dysregulated degradation into short HA chains (< 100kDa) and accumulation at the ECM of tumors. [40, 41] The overexpression of HA synthases and hyaluronidases [42, 43] in cancer has been associated to the increased deposition of HA of different Mws on the ECM, inducing alterations on cellular behavior through the activation of different signaling pathways. In response to the HA present on the ECM, CD44 and RHAMM play the major roles on triggering biochemical cascades associated to cancer cells motility [37, 44], proliferation [45], or even apoptosis and latency [46]. Whereas CD44 presents a HA binding domain (HABD) with three different binding modes that are considered the CD44-HA fingerprints, RHAMM needs a host molecule such CD44, TRLs' and growth factors, to maintain the RHAMM-HA interaction and exert its bioactivities. [47, 48] However, the capacity of CD44 to bind to HA of different Mws, is associated to its free mobility at the membrane lipid rafts, as well as its ability to group into clusters, generating a range of possible interactions that have been studied in different pathologies.

1-2.3. Hyaluronic acid as space filling molecule and mechano-modulator/-transductor

The chemical structure of HA, in particular the presence of -OH groups, is related to its high capacity retain water and ability to swell, which makes it an ideal space filling element. Under physiological ionic strengths (*i.e.* 0.15M of NaCl), HA presents a stretched chain, rich in water molecules, that contributes to its large volume, which increases with the increment of the HA's Mw. [49] HA is found in most of the tissues, including the synovial fluid, the vitreous, the umbilical cord and amniotic fluid. In the latter ones, the Mw of the HA varies depending on the gestation stage. [50] The HA of HMw acts as a functional regulator of synovial joint fluid, giving the required viscosity and lubrication to act as a shock

absorber for compressive forces. [51, 52] In fact, osteoarthritis has been associated to the loss of HA of HMw through its cleavage into HAs of LMws. This change leads to a decrease in the viscoelastic properties of cartilage and, in consequence, the mechanical resistance of the joints. [53] The critical role of HA on the viscoelastic and biomechanical balance of tissues, is the basis of its ability to act as a structural support for cells to proliferate and migrate. [54] The non-covalent assembly of HA with proteoglycans (*e.g.* versican and aggrecan), GAGs (*e.g.* chondroitin sulfate, heparin) and glycoproteins (*e.g.* elastin, laminin, fibronectin and tenascin) is crucial for the generation of an ECM that confers the adequate biophysical and biochemical properties for cells to interact and play their normal function, keeping the structural equilibrium of the parenchyma of tissues. [19, 55] In addition, the unbalanced entanglement between HA and other ECM components induce alterations on the organization and stiffness of the tissues, being associated to several diseases, such as atherosclerosis and diabetic angiopathy [56], fibrosis [57] and cancer. [58]

The accumulation of HA *per se* in the ECM and/or changes in the HA's chemical properties, mainly through the alterations of its Mw, strongly affects the physical properties of the matrix and, consequently, affects downstream signaling cascades. As an example, the HA content of human articular cartilage varies from 0.5 μg/mg to 2.5 μg/mg (both under wet conditions), in an age-dependent manner. [59] However, the major alterations on the HA content are in cancer-related pathologies. [58] The HA levels in the urine from bladder cancer patients were found to be 4–9-fold higher when compared to healthy patients [60]. Of note, high levels of HA were associated to aggressiveness and poor prognosis of ovarian [61], breast [62], colorectal [63], pancreatic [64] and gastric [65] cancers. The secretion and degradation of HA of different Mws and their distribution throughout the ECM, largely affects the biomechanics of the matrix and, consequently, the biochemical sensing of cells. The mechanotransductor capacity of the HMw HA is reported to inhibit the proliferation of breast cancer cells thought the activation of the Hippo pathway, mediated by the formation of CD44 clusters. [66] On the other hand, the ECM-rich HMw HA on glioblastoma cancer tissues showed controversial results: while some reports show that the increased tissue density and stiffness, is linked to cancer cells' proliferation and motility [67], others studies report the less invasive character of cancer cells when in contact with hydrogels containing HA of 500kDa [68]. In addition, *Pogoda et al.* showed that glioblastoma cells seeded on softer HA surfaces presented nearly identical responses, *i.e.* cells spreading, proliferation, motility and IL-8 secretion, to those seeded on stiffer polyacrylamide substrates, showing that the main changes in the biomechanics might not be the main feature that drives HA bioactivities in cancer pathological states. [69]

The overproduction of Hyals in certain tumors (*e.g.* Hyal1 and Hyal2 on colorectal [70], Hyal1 on bladder [71] and breast [42] cancers, and Hyl1 and Hyal3 on lung cancer [72]) drives the average Mw of HA to lower values, which impacts in the density and viscosity of the ECM. [17, 49, 73] In fact, the presence of LMw HA are extensively linked to the biochemical stimulation of cellular motility rather than the physical and/or mechanical stimulus. However, the regulation of Yes-associated protein (YAP) expression, a mechanotransducer protein [74], has been linked to the expression and activation of CD44, the major receptor for HA. In this context, HA of LMw (*i.e.* 4kDa) is reported to reduce the expression of YAP, inhibiting its translocation to the nucleus (which is related with the proliferation and migration of cells [75]), through the upstream sensing of CD44 in hepatocellular carcinoma. [76] Additionally, the HA-responsive protein RHAMM, regulates the expression of YAP via HA/RHAMM activation. [33] Matrix remodeling and stiffening also leads to the activation of YAP, that in turn enables the expression of actomyosin cytoskeleton rearrangement in cancer-associated fibroblast (CAF's) [77], the activation of TGF-beta-induced fibrosis on fibroblasts [78] and laminin on breast cancer stem cells. [79] While the mechanical properties of the matrix can induce specific cellular responses (as previously detailed), YAP can also regulate matrix stiffness under a positive feedback loop, by activating the RhoA pathway increasing the actomyosin-based tension of the cytoskeleton. [74]

1-3. ENGINEERED HYALURONIC ACID-BASED BIOMATERIALS TO MIMIC THE EXTRACELULLAR MATRIX

The biological relevance of HA, in particular its recognized ability to modulate cellular behavior, lead to the development of biomaterials based on this GAG, in an attempt to mimic the bioactive cellular environments and/or generate responsive systems to deliver therapeutic agents. In the following subsections we will be review some of these HA-based biomaterials and their biological applications.

1-3.1. Particles

Particles, ranging from the nano to the macro scale, have been developed to selectively target the extracellular space, to reach the surface of cells, or even to be internalized by specific cells. The HA affinity with the transmembrane receptor CD44, which is overexpressed in several cell types, both healthy [80] and cancers [81] ones, has been exploited on the development of nanoparticles to target

the intracellular space, in a strategy usually referred as "trojan horse". [82] Different approaches are described to prepare the HA particles. The most reported methodology is its combinatory assembly with: organic nanoparticles, based on lipids [83, 84], chitosan [85, 86] or PEG [87, 88]; or inorganic ones, such as SiO_2 [89], Au [90], TiO_2 [91] and $CaCO_3$ [92]. The manipulation of these organic/inorganic cores allows the control of the particles' size, an important feature when internalization is targeted. The coating of these particles with HA induces an increment of surface porosity, which is important for the encapsulation of therapeutic agents. As an example, HA-coating of mesoporous SiO_2 nanoparticles (pore size of ≈ 2.5nm), encapsulated with a photosensitizer or doxorubicin has been used to target CD44-overexpressing cancer cells. [93, 94] The chemical composition of HA with available reactive groups (*e.g.* carboxylic acids), allows the exploitation of electrostatic or covalent interactions with other materials. For instance, the negative charge of HA ($-COO^-$) allows it to participate in electrostatic binding with the positively charge chitosan. This strategy has been used for the targeted deliver of siRNA or Everolimus drug to lung cancer cells. [85, 86] To promote the interaction between HA and the negative charged SiO_2 or Au particles, these cores are usually amine-functionalized ($-NH_2$), or the layer-by-layer (LbL) assembly is applied to revert the surface charge of the core particles. [95, 96] In the LbL strategy, poly-L-lysine (PLL) is the most common polycation used as a support layer, for the subsequent deposition of HA leading to its immobilization in the particles' surface. The LbL assembly of PLL-HA is pH sensitive, being disrupted in the acidic tumor microenvironment, leading to the release of the loaded therapeutic agent. [97] Drugs presenting low water solubility are usually difficult to deliver in the cellular milieu; however, this can be achieved using nanostructured lipid carriers decorated, electrostatically, with HA as a targeting ligand for lung cancer cells. [98] A different end-on presentation of HA can be achieved by using gold nanoparticles conjugated with end-thiolated HA (HS-HA) to promote its binding to the gold surface, generating a brush-like surface structure. [99] The recognition of the particles and their reversible/irreversible attachment to the cells' surface is mediated by the HA receptors. In this context, it is possible to tune the targeting capacity of these particles by the changing the Mws of the HA present in the shell of the particles. [100]

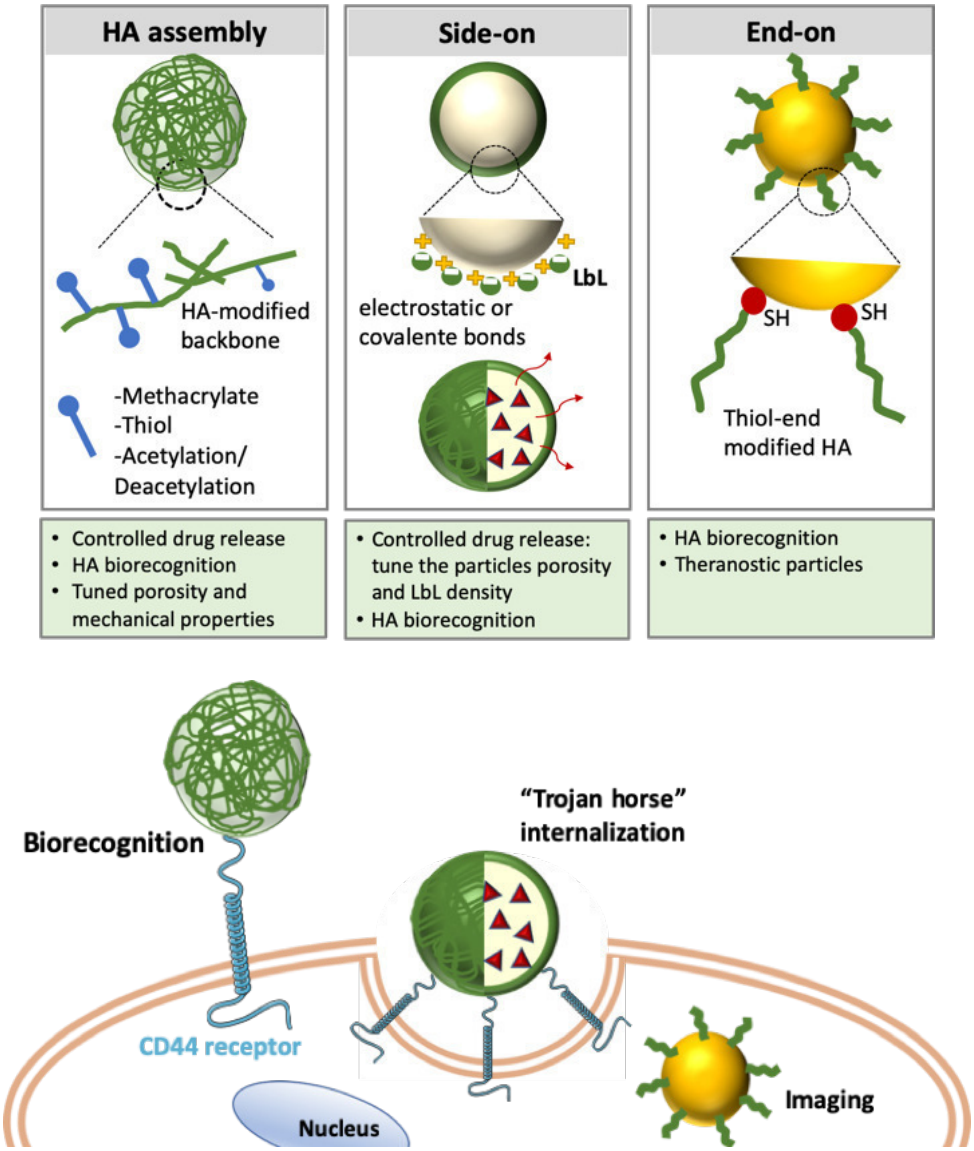

Figure 1-2. Active targeting of HA-based particles used as drug/proteins carriers: HA assembly from modified HA backbone; inorganic (e.g. SiO2, TiO2, Au, CaCO2) or organic (e.g. liposomes, lipids) particles cores coated with HA; and, thiol-end HA coated gold nanoparticles. Schematic representation of the multiple effects of HA particles as ECM mimic for cells biorecognition and for therapeutic drug release or imaging.

The development of polyelectrolyte complexes using native or modified HA has been reported. However, the biological instability of non-modified HA (native) structures requires the use of toxic reagents for the crosslinking (*e.g.* glutaraldehyde [101], carbodiimides [102] and hydrazides [103]) to maintain its structure and maintain its biostability with limited biodegradation. [104] In contrast, these harsh cross-linking conditions are not suitable for cell studies or the encapsulation of drugs/proteins due to their cytotoxicity. [105] In this sense, the modification of the HA backbone has been explored in order to obtain a biomaterial suitable for biomedical applications. One of the most reported chemical

modification performed on HA is the modification of its hydroxyl moieties into methacrylate groups, forming methacrylated-HA (MA-HA) that can be further cross-linked by UV light. This MA-HA present increased stability in physiological conditions and allows the loading and controlled release of proteins or drugs. [106, 107] Other approaches are reported to alter the HA chemical structure, such as thiol-modified HA [108], aminated HA-g-poly(N-isopropylacrylamide) (AHA-g-PNIPAAm) [109] or poly(ethylene glycol)-conjugated HA nanoparticles (PEG-HANPs) [110], so that it is possible to use HA to prepare hydrogel-like carriers. HA-decorated nanoparticles present multifunctional character, where the combination of its ability to act as a drug delivery system with their capacity to be recognized by different cellular targets is the most exploited HA capabilities.

1-3.2. 2D surfaces

The ability of HA to modulate cellular morphology, proliferation and motility has been studied *in vitro* using 2D substrates that mimic, in a very simplistic way, the characteristics of the ECM. The controlled side-on immobilization of HA (of different Mws) using different polycations, can be used to modulate the stiffness of the surface, the charge density, as well as the available HA epitopes that can be recognized by cells. [111, 112] Similar to the functionalization of particles, the Layer-by-Layer (LbL) assembly is used to immobilize HA and different polyelectrolytes for the construction of multilayered films. The alternate dipping of a glass slide on poly-L-lysine (PLL) and HA solutions, generates a $(PLL\text{-}HA)_x$ surface with controlled stiffness, through the manipulation of the crosslinker concentration. This approach has been used to evaluate the impact of stiffness on the behaviour of C2C12 myoblasts. It was observed a higher adhesion and cell's spreading on stiffer films, processes that were mediated by integrins. [113] Gold surfaces were also used to immobilized (PLL-HA) films to evaluate the influence of HA's Mws on gastric cancer cells invasiveness, mediated by the CD44 receptor. [37] It was also used the alternative end-thiolated-HA with different chain lengths to investigate the interactions between the immobilized HA with aggrecan (a proteoglycan from the ECM) and the protein LYVE-1 (an HA sensitive cellular receptor). [114] The surface topography has been also used to study the HA ability to modulate cellular behavior. [115, 116] Cells are sensitive to the ECM's mechanical and morphological features, and thus, micro and nanopatterned surfaces can provide insights on cell-matrix interactions, and its influence on the activation of downstream biochemical pathways. In fact, the spatial organization of focal adhesions (FAs), integrins, transmembrane receptors and cytoskeleton proteins, are responsible for cellular

adhesion and matrix remodeling. In this context, their influence on cellular responses can be assessed using micro and nanostructured substrates. [116] Different approaches can be used for micro and nanofabrication [117], such as photolithography [118], soft lithography and microcontact printing [119], electron beam lithography (EBL) [120] and block copolymer micelle nanolithography (BCMN) [121]. The selection of the best technique is dependent on the desired microstructure, *e.g.* pillars [122], stripes [123], micropatterned networks [124] or controlled inorganic nanoparticles' spacing. [125, 126] Parallel ridge stripes, that mimic the shape of vascular endothelial cells (EC) when exposed to the shear stress from the blood flow, generated under physiological conditions, were used to study the adhesion of EC and smooth muscle cells (SMCs) on HMw HA-modified stripes [127, 128] and the secretion of growth factors (TGF and VEGF) by SMCs. [129] More recently, gold-(PEI-(HA-PLL)$_{11}$-HA) nanostructured hexagonally arranged dots of crosslinked PEM with defined spacing (*i.e.* 733, 518 and 302nm) and tuned mechanical properties where used to differentiate human adipose derived stem cells, showing that highly crosslinked surfaces presenting HA-coated particles of smaller size (*i.e.* 302nm) induced osteogenesis. [130]

2D surfaces are simple substrates that can be used to give insights on the cellular biochemical and biophysical responses. However, these substrates lack the complexity of the ECM, that can only be fully achieved using a tridimensional environment where cells can be encapsulated.

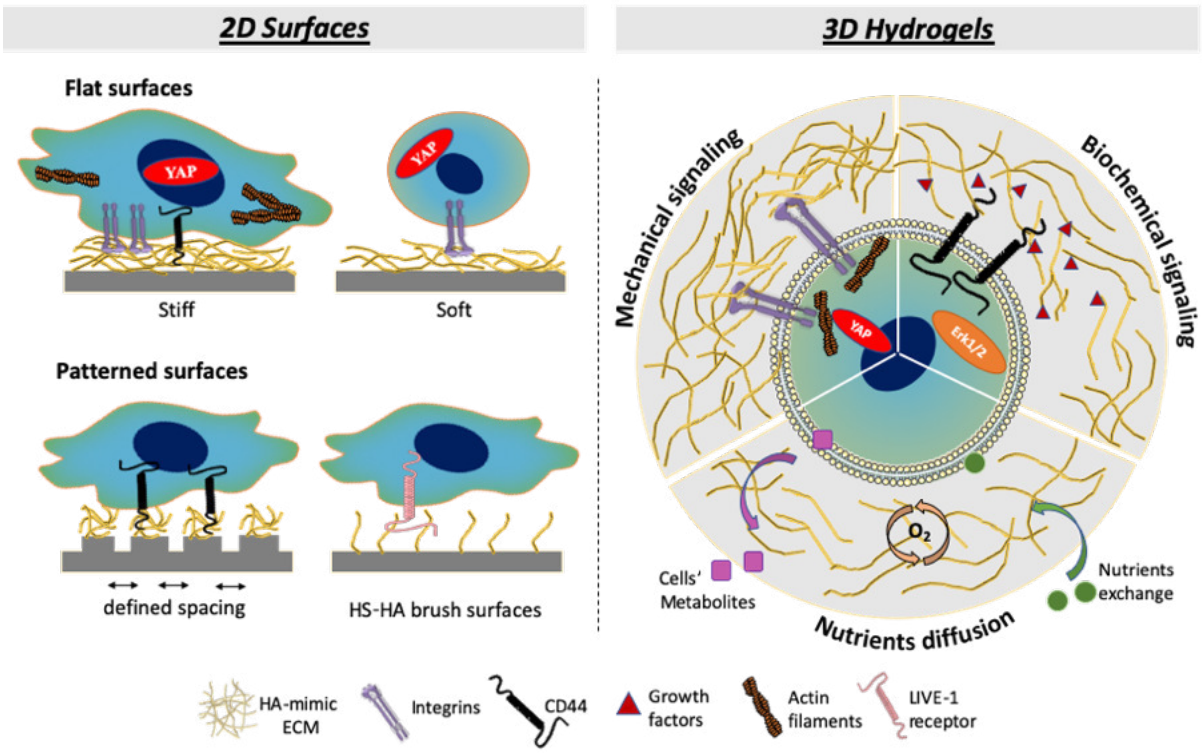

Figure 1-3. Schematic representation of 2D surfaces and 3D models used for cellular immobilization and encapsulation, respectively. Cellular adhesion, spreading and migration on 2D surfaces is restricted to the xy plane, being the external stimulus (mechanical and topographical) unidirectional. 2D patterned surfaces with controlled spacing used for integrins and/or HA receptor clustering studies. 3D models recreate the physical (e.g. porosity, topography), mechanical (e.g. hydrogel density, hydration, stiffness) and chemical (e.g. growth factors, proteins) cues of the ECM. Tridimensional systems are closer ECM mimics of the cell-cell and cell-matrix interactions.

1-3.3. 3D models

3D models able to mimic the complexity of the extracellular microenvironment have been proposed to overcome the limitations of the 2D platforms, leading to the development of hydrogels, comprising the chemical and physical composition of the pericellular and extracellular environment. [131] In this context, 3D hydrogels, allows to recapitulate fundamental parameters of the ECM, such as porosity, stiffness and hydration, which are able to tune the cellular adhesion and to act as mechanotransductors. In fact, altering the porosity and viscoelastic properties of the gels, it is possible to control the two-way diffusion of nutrients, oxygen and biochemical factors throughout the cell culture period. [132]

The above-mentioned importance of HA in the ECM and its ability to regulate the cellular behavior, lead to the development of *in vitro* 3D models to study the role of HA in cell-matrix and cell-cell interactions. Different approaches are used to prepare the 3D HA-based hydrogels. Usually, it involves the chemical modification of HA at the -COOH position from the glucuronic acid residue, one of the -OH positions of the N-acetylglucosamine, or the -$NHCOCH_3$ groups, using different chemical strategies, as for example deacetylation, amidation, esterification, among others. [133, 134] The 3D HA-based hydrogels require chemical or physical crosslinking to be able to maintain their structure and resemble the native HA network. One of the most common strategies is the use of methacrylated HA (MA-HA) which is crosslinked by UV after the encapsulation of cells. The precise control of the UV-crosslinking, by regulating the time and/or intensity to the UV exposure, allows the preparation of hydrogels with different mechanical properties. [135, 136] Studies using these systems functionalized by RGD on glioblastoma tumor invasion have been performed to mimic biochemical and biophysical cues of the brain HA-rich milieus. Glioblastoma cellular morphology and migration were probed on these hydrogels. An increased cell migration was observed on stiffer hydrogels. [137] In addition, the physiologically-relevant stiffness of HA-based hydrogels, resembling the ECM of healthy liver (*i.e.* 600-4600Pa) were mimicked using thiol-modified HA. The combination of the HA-based hydrogels with the ECM from the liver induced an increment on cellular adhesion and proliferation when stiffer hydrogels were used. [138] Modified HA with aldehydes (HAALD) and adipic acid dihydrazide (HAADH) were also used to produce 3D hydrogels. These systems were used to encapsulate prostate cancer cells (PCa) and crosslinked at 37°C. It was possible to show with these systems that the invasive features of PCa were mediated by the HA's receptor, RHAMM. [139] Modified furan-HA can be crosslinked with the bismaleimide PEG, cleavable by matrix - metalloproteinase (MMP). Upon encapsulation of MDA-MB-231 it was found that their invasive behavior was incremented in response to the density of the hydrogel and the concentration of the GRGDS ligand. [140] The most common way to generate HA-based hydrogels is to chemically modify the HA, however, this strategy derivates from its native chemical presentation in the ECM. In order to avoid these deviations, it has been attempted the used of native HA in the development of 3D hydrogels. This has been achieved by its incorporation into matrices of a supporting hydrogel. Alginate (Alg) is one of the most common material to immobilize native HA into a 3D hydrogel network, due to the easy handling and the possibility to crosslink the Alg chains using mild conditions, *e.g.* Ca^{2+}. [141] The role of the different Mws of HA on the migration of breast cancer cells (SKBR3) and phenotypic alterations was evaluated by immobilizing HA of lower (35kDa) and higher (117kDa) Mw in Alg matrices. It was possible to see that metastatic activity and

epithelial-mesenchymal transition (EMT) in the presence of HA of 35kDa. [142] The resemblance of the natural ECM using the native HA immobilized in an Alg network was also used to probe the chondrogenic differentiation of mesenchymal stem cells. [143] Other materials have been used to promote the ECM-like presentation of HA: it has been proposed the use of chitosan-HA hydrogels to mimic the ECM of glioblastoma, [144] or the EMT process of pancreatic cancer cells. [145] The combination of collagen (Coll) and HA, incorporating the ECM fibrillar elements from collagen, has been described. Altering the HA-Coll crosslinking it is possible to tune the mechanical properties of these hydrogels, which altered the ability of mesenchymal stem cells to adhere, change their morphology and to generate focal adhesions. [146] These strategies have been also used to mimic the heterogeneous network of the ECM of natural heart valve [147], or even, blending three different components such, chitosan-silk fibroin-HA for osteogenic differentiation. [148]

1-4. HA-RELATED PRODUCTS IN THE MARKET

The biological importance of HA has been extensively studied and its fundamental role on tissues homeostasis has been increasingly recognized by the scientific community. Based on this knowledge, the pharmaceutical, medical, cosmetic and food industries have been exploiting the development of HA-related products. Some of these products are already available in the market. These includes systems for ophthalmologic applications, dermatological fillers (*e.g.* anti-age products), for the treatment of osteoarthritis and vesicoureteral reflux. [149]

In the case of the ophthalmologic applications, the high hydrophilicity and viscoelastic properties of HA is able to reduce the dryness and irritation of the eyes [150], as well as to reduce the inflammation of different ophthalmological diseases. [151] The use of HMw HA in the knee to treat osteoarthritis is a current clinical treatment strategy. It takes advantage of the lubricant capacity of HA, that resembles the properties of the synovial fluid. The injection of HMw in the intra-articular area elicits an anti-inflammatory activity, while stimulating *de novo* synthesis of HA. [152, 153]

The most common application of HA is for dermatological applications, namely as wound healing dressings, as well as anti-aging dermal fillers. Some of these fillers contain the linear native HA, however, these have a limited half-life after injection. In order to overcome this drawback, it is becoming increasingly common the use of crosslinked HA. [154, 155]

Other commercially available HA-based materials for biomedical applications include: oral HA-containing gels as a barrier-forming ingredient for the treatment of mucositis [156]; HA solutions developed for intravesical instillation against interstitial cystitis [157], or optimized as a nasal douche to reduce the inflammation present in upper airways diseases while also improving the nasal clearance [149, 158]; or, more recently, as anti-aging microstructured patches comprising crosslinked HA as anti-wrinkle and moisturizer product. [159] The benefits of HA to improve skin function are beyond its topical administration. In fact, it has been developed HA-based food supplements that are able to reduce skin dryness over time. [160]

Despite the extensive studies (and reported literature) on the use of HA (and its derivatives) as drug delivery systems, these types of systems are still not widely available. The *in vitro* studies that report the ability of HA-based carriers to deliver bioactive drugs and proteins, with prolonged stability and therapeutic efficacy, still need to follow the translational pipeline that leads to their application in the clinical practice. [161]

1-5. CONCLUSIONS AND FUTURE REMARKS

In this review, we summarized the relevance of the HA-rich ECM on the cellular behavior and tissues homeostasis and the different type of platforms that have been proposed to study HA-mediated cell-cell or cell-ECM interactions. It is well established the importance of the HA's Mws on the biochemical and biophysical balance of the ECM. While HA of HMw is usually associated to the maintenance of tissue homeostasis, the LMw presents pro-inflammatory cues, as well as ability to activate cellular malignant phenotypes. Its important biological functions in combination with its chemical versatility, makes the HA backbone prone to different chemical modifications to improve its stability under physiological environments. Different approaches have been proposed to present HA on an ECM-relevant manner, mimicking its structural, mechanical and biochemical properties from the *in vivo* environment. Taking advantage of the ability of exogenous HA to be recognized by a series of biological elements (*e.g.* different HA-specific cell surface receptors), it has been proposed various HA-based materials as drug/proteins carriers for extra- or intra-cellular delivery. Despite the increasing knowledge on HA and its bioactivities, the structural and biological complexity of HA in the ECM is still not completely understood. As an example, the deposition of different Mws of HA in the ECM and its influence on the progression of cancers is still unclear and controversial. In these cases, the development of platforms that are able to mimic the HA present in the ECM are important tools to gain knowledge on its biological

functions. In this context, the development of 3D HA-based models that resembles the ECM, is a research topic gaining increasing relevance. However, the present state of the art is still far from the accurate mimic of the way HA is structurally organized in the ECM. The present models are still not able to completely mimic HA's bioactivity and its influence in cellular behavior. It is thus expected significant improvements in the models that are currently under development and that will be available in the following years.

1-6. REFERENCES

1. Jarvelainen, H., et al., *Extracellular matrix molecules: potential targets in pharmacotherapy.* Pharmacol Rev, 2009. **61**(2): p. 198-223.

2. Bella, J. and D.J. Hulmes, *Fibrillar Collagens.* Subcell Biochem, 2017. **82**: p. 457-490.

3. Brosicke, N., et al., *Extracellular Matrix Glycoprotein-Derived Synthetic Peptides Differentially Modulate Glioma and Sarcoma Cell Migration.* Cell Mol Neurobiol, 2015. **35**(5): p. 741-53.

4. Soares da Costa, D., R.L. Reis, and I. Pashkuleva, *Sulfation of Glycosaminoglycans and Its Implications in Human Health and Disorders.* Annu Rev Biomed Eng, 2017. **19**: p. 1-26.

5. Dicker, K.T., et al., *Hyaluronan: a simple polysaccharide with diverse biological functions.* Acta Biomater, 2014. **10**(4): p. 1558-70.

6. Murakami, T., et al., *Hyaluronic acid promotes proliferation and migration of human meniscus cells via a CD44-dependent mechanism.* Connect Tissue Res, 2019. **60**(2): p. 117-127.

7. Canibano-Hernandez, A., et al., *Hyaluronic Acid Promotes Differentiation of Mesenchymal Stem Cells from Different Sources toward Pancreatic Progenitors within Three-Dimensional Alginate Matrixes.* Molecular Pharmaceutics, 2019. **16**(2): p. 834-845.

8. Iturriaga, V., et al., *Role of Hyaluronic Acid in the Homeostasis and Therapeutics of Temporomandibular Joint Osteoarthritis.* International Journal of Morphology, 2017. **35**(3): p. 870-876.

9. Day, A.J. and J.K. Sheehan, *Hyaluronan: polysaccharide chaos to protein organisation.* Curr Opin Struct Biol, 2001. **11**(5): p. 617-22.

10. Theocharis, A.D., et al., *Extracellular matrix structure.* Adv Drug Deliv Rev, 2016. **97**: p. 4-27.

11. Vigetti, D., et al., *Metabolic control of hyaluronan synthases.* Matrix Biol, 2014. **35**: p. 8-13.

12. Stern, R. and M.J. Jedrzejas, *Hyaluronidases: Their genomics, structures, and mechanisms of action.* Chemical Reviews, 2006. **106**(3): p. 818-839.

13. Misra, S., et al., *Interactions between Hyaluronan and Its Receptors (CD44, RHAMM) Regulate the Activities of Inflammation and Cancer.* Frontiers in Immunology, 2015. **6**.

14. Senbanjo, L.T. and M.A. Chellaiah, *CD44: A Multifunctional Cell Surface Adhesion Receptor Is a Regulator of Progression and Metastasis of Cancer Cells.* Frontiers in Cell and Developmental Biology, 2017. **5**(18).

15. Day, A.J. and G.D. Prestwich, *Hyaluronan-binding proteins: tying up the giant.* J Biol Chem, 2002. **277**(7): p. 4585-8.

16. Kouvidi, K., et al., *Role of receptor for hyaluronic acid-mediated motility (RHAMM) in low molecular weight hyaluronan (LMWHA)-mediated fibrosarcoma cell adhesion.* J Biol Chem, 2011. **286**(44): p. 38509-20.

17. Chanmee, T., P. Ontong, and N. Itano, *Hyaluronan: A modulator of the tumor microenvironment.* Cancer Lett, 2016. **375**(1): p. 20-30.

18. Wu, R.-L., et al., *Hyaluronic acid in digestive cancers.* Journal of Cancer Research and Clinical Oncology, 2017. **143**(1): p. 1-16.

19. Richter, R.P., et al., *Glycosaminoglycans in extracellular matrix organisation: are concepts from soft matter physics key to understanding the formation of perineuronal nets?* Curr Opin Struct Biol, 2018. **50**: p. 65-74.

20. Herrera, J., C.A. Henke, and P.B. Bitterman, *Extracellular matrix as a driver of progressive fibrosis.* Journal of Clinical Investigation, 2018. **128**(1): p. 45-53.

21. Toole, B.P., *Hyaluronan: From extracellular glue to pericellular cue.* Nature Reviews Cancer, 2004. **4**(7): p. 528-539.

22. Zhu, Z., et al., *Hyaluronic acid: a versatile biomaterial in tissue engineering.* Plastic and Aesthetic Research, 2017. **4**(12).

23. Soltes, L., et al., *Degradative action of reactive oxygen species on hyaluronan.* Biomacromolecules, 2006. **7**(3): p. 659-68.

24. Bourguignon, V. and B. Flamion, *Respective roles of hyaluronidases 1 and 2 in endogenous hyaluronan turnover.* Faseb Journal, 2016. **30**(6): p. 2108-2114.

25. Higuchi, Y., et al., *Conditional knockdown of hyaluronidase 2 in articular cartilage stimulates osteoarthritic progression in a mice model.* Sci Rep, 2017. **7**(1): p. 7028.

26. Price, Z.K., N.A. Lokman, and C. Ricciardelli, *Differing Roles of Hyaluronan Molecular Weight on Cancer Cell Behavior and Chemotherapy Resistance.* Cancers, 2018. **10**(12).

27. Band, P.A., et al., *Hyaluronan molecular weight distribution is associated with the risk of knee osteoarthritis progression.* Osteoarthritis Cartilage, 2015. **23**(1): p. 70-6.

28. Zhu, Y., et al., *High Molecular Weight Hyaluronic Acid Inhibits Fibrosis of Endometrium.* Med Sci Monit, 2016. **22**: p. 3438-3445.

29. Scuruchi, M., et al., *6-Mer Hyaluronan Oligosaccharides Modulate Neuroinflammation and alpha-Synuclein Expression in Neuron-Like SH-SY5Y Cells.* J Cell Biochem, 2016. **117**(12): p. 2835-2843.

30. Rayahin, J.E., et al., *High and low molecular weight hyaluronic acid differentially influence macrophage activation.* ACS Biomater Sci Eng, 2015. **1**(7): p. 481-493.

31. D'Agostino, A., et al., *Is molecular size a discriminating factor in hyaluronan interaction with human cells?* Carbohydr Polym, 2017. **157**: p. 21-30.

32. Kang, L., et al., *Hyaluronic acid oligosaccharide-modified collagen nanofibers as vascular tissue-engineered scaffold for promoting endothelial cell proliferation.* Carbohydr Polym, 2019. **223**: p. 115106.

33. Shigeeda, W., et al., *Hyaluronic acid enhances cell migration and invasion via the YAP1/TAZ-RHAMM axis in malignant pleural mesothelioma.* Oncotarget, 2017. **8**(55): p. 93729-93740.

34. Mascaro, M., et al., *Low molecular weight hyaluronan induces migration of human choriocarcinoma JEG-3 cells mediated by RHAMM as well as by PI3K and MAPK pathways.* Histochem Cell Biol, 2017. **148**(2): p. 173-187.

35. Sapudom, J., et al., *Molecular weight specific impact of soluble and immobilized hyaluronan on CD44 expressing melanoma cells in 3D collagen matrices.* Acta Biomater, 2017. **50**: p. 259-270.

36. Albano, G.D., et al., *Effect of High, Medium, and Low Molecular Weight Hyaluronan on Inflammation and Oxidative Stress in an In Vitro Model of Human Nasal Epithelial Cells.* Mediators Inflamm, 2016. **2016**: p. 8727289.

37. Amorim, S., et al., *Molecular weight of surface immobilized hyaluronic acid influences CD44-mediated binding of gastric cancer cells.* Sci Rep, 2018. **8**(1): p. 16058.

38. Simpson, R.M., et al., *Hyaluronan Is Crucial for Stem Cell Differentiation into Smooth Muscle Lineage.* Stem Cells, 2016. **34**(5): p. 1225-38.

39. Zhao, N., et al., *Effect of molecular weight and concentration of hyaluronan on cell proliferation and osteogenic differentiation in vitro.* Biochem Biophys Res Commun, 2015. **465**(3): p. 569-74.

40. Carvalho, M.P., et al., *Tumor spheroid assembly on hyaluronic acid-based structures: A review.* Carbohydr Polym, 2016. **150**: p. 139-48.

41. Liu, M., C. Tolg, and E. Turley, *Dissecting the Dual Nature of Hyaluronan in the Tumor Microenvironment.* Front Immunol, 2019. **10**: p. 947.

42. Tan, J.X., et al., *HYAL1 overexpression is correlated with the malignant behavior of human breast cancer.* International Journal of Cancer, 2011. **128**(6): p. 1303-1315.

43. Udabage, L., et al., *The over-expression of HAS2, Hyal-2 and CD44 is implicated in the invasiveness of breast cancer.* Experimental Cell Research, 2005. **310**(1): p. 205-217.

44. Jiang, B., et al., *Probable Molecular Mechanism of Pancreatic Cancer Cells Migration Promoted by High Molecular Weight Hyaluronic Acid.* Acta Medica Mediterranea, 2019. **35**(4): p. 2099-2103.

45. Mele, V., et al., *The hyaluronan-mediated motility receptor RHAMM promotes growth, invasiveness and dissemination of colorectal cancer.* Oncotarget, 2017. **8**(41): p. 70617-70629.

46. Kassim, Y.L., et al., *Three Dimensional Tumor Engineering by Co-Culture of Breast Tumor and Endothelial Cells Using a Hyaluronic Acid Hydrogel Model.* Journal of Clinical & Experimental Oncology, 2017. **06**(05).

47. Tolg, C., et al., *Hyaluronan and RHAMM in wound repair and the "cancerization" of stromal tissues.* Biomed Res Int, 2014. **2014**: p. 103923.

48. Vuorio, J., I. Vattulainen, and H. Martinez-Seara, *Atomistic fingerprint of hyaluronan-CD44 binding.* PLoS Comput Biol, 2017. **13**(7): p. e1005663.

49. Cowman, M.K., et al., *Viscoelastic Properties of Hyaluronan in Physiological Conditions.* F1000Res, 2015. **4**: p. 622.

50. Cowman, M.K., et al., *The Content and Size of Hyaluronan in Biological Fluids and Tissues.* Front Immunol, 2015. **6**: p. 261.

51. Zhang, Z. and G.F. Christopher, *The nonlinear viscoelasticity of hyaluronic acid and its role in joint lubrication.* Soft Matter, 2015. **11**(13): p. 2596-2603.

52. Tamer, T.M., *Hyaluronan and synovial joint: function, distribution and healing.* Interdiscip Toxicol, 2013. **6**(3): p. 111-25.

53. Bowman, S., et al., *Recent advances in hyaluronic acid based therapy for osteoarthritis.* Clin Transl Med, 2018. **7**(1): p. 6.

54. Caires, R., et al., *Hyaluronan modulates TRPV1 channel opening, reducing peripheral nociceptor activity and pain.* Nat Commun, 2015. **6**: p. 8095.

55. Mouw, J.K., G.Q. Ou, and V.M. Weaver, *Extracellular matrix assembly: a multiscale deconstruction.* Nature Reviews Molecular Cell Biology, 2014. **15**(12): p. 771-785.

56. Lorentzen, K.A., et al., *Mechanisms involved in extracellular matrix remodeling and arterial stiffness induced by hyaluronan accumulation.* Atherosclerosis, 2016. **244**: p. 195-203.

57. Skandalis, S.S., et al., *Impact of Extracellular Matrix on Cellular Behavior: A Source of Molecular Targets in Disease.* Biomed Res Int, 2015. **2015**: p. 482879.

58. Voutouri, C. and T. Stylianopoulos, *Accumulation of mechanical forces in tumors is related to hyaluronan content and tissue stiffness.* Plos One, 2018. **13**(3).

59. Holmes, M.W., M.T. Bayliss, and H. Muir, *Hyaluronic acid in human articular cartilage. Age-related changes in content and size.* Biochem J, 1988. **250**(2): p. 435-41.

60. Lokeshwar, V.B., et al., *Tumor-associated hyaluronic acid: a new sensitive and specific urine marker for bladder cancer.* Cancer Res, 1997. **57**(4): p. 773-7.

61. Anttila, M.A., et al., *High levels of stromal hyaluronan predict poor disease outcome in epithelial ovarian cancer.* Cancer Res, 2000. **60**(1): p. 150-5.

62. Auvinen, P., et al., *Hyaluronan in peritumoral stroma and malignant cells associates with breast cancer spreading and predicts survival.* Am J Pathol, 2000. **156**(2): p. 529-36.

63. Ropponen, K., et al., *Tumor cell-associated hyaluronan as an unfavorable prognostic factor in colorectal cancer.* Cancer Research, 1998. **58**(2): p. 342-347.

64. Kultti, A., et al., *Accumulation of extracellular hyaluronan by hyaluronan synthase 3 promotes tumor growth and modulates the pancreatic cancer microenvironment.* Biomed Res Int, 2014. **2014**: p. 817613.

65. Setala, L.P., et al., *Hyaluronan expression in gastric cancer cells is associated with local and nodal spread and reduced survival rate.* British Journal of Cancer, 1999. **79**(7-8): p. 1133-1138.

66. Ooki, T., et al., *High-Molecular-Weight Hyaluronan Is a Hippo Pathway Ligand Directing Cell Density-Dependent Growth Inhibition via PAR1b.* Developmental Cell, 2019. **49**(4): p. 590-+.

67. Kim, Y. and S. Kumar, *CD44-Mediated Adhesion to Hyaluronic Acid Contributes to Mechanosensing and Invasive Motility.* Molecular Cancer Research, 2014. **12**(10): p. 1416-1429.

68. Chen, J.W.E., et al., *Influence of Hyaluronic Acid Transitions in Tumor Microenvironment on Glioblastoma Malignancy and Invasive Behavior.* Frontiers in Materials, 2018. **5**.

69. Pogoda, K., et al., *Soft Substrates Containing Hyaluronan Mimic the Effects of Increased Stiffness on Morphology, Motility, and Proliferation of Glioma Cells.* Biomacromolecules, 2017. **18**(10): p. 3040-3051.

70. Bouga, H., et al., *Involvement of hyaluronidases in colorectal cancer.* BMC Cancer, 2010. **10**: p. 499.

71. Kramer, M.W., et al., *HYAL-1 hyaluronidase: a potential prognostic indicator for progression to muscle invasion and recurrence in bladder cancer.* Eur Urol, 2010. **57**(1): p. 86-93.

72. de Sa, V.K., et al., *Hyaluronidase splice variants are associated with histology and outcome in adenocarcinoma and squamous cell carcinoma of the lung.* Hum Pathol, 2012. **43**(5): p. 675-83.

73. McAtee, C.O., J.J. Barycki, and M.A. Simpson, *Emerging roles for hyaluronidase in cancer metastasis and therapy.* Adv Cancer Res, 2014. **123**: p. 1-34.

74. Dobrokhotov, O., et al., *Mechanoregulation and pathology of YAP/TAZ via Hippo and non-Hippo mechanisms.* Clin Transl Med, 2018. **7**(1): p. 23.

75. *Control of cellular responses to mechanical cues through YAP/TAZ regulation.*

76. Fan, Z.H., et al., *Standard CD44 modulates YAP1 through a positive feedback loop in hepatocellular carcinoma.* Biomedicine & Pharmacotherapy, 2018. **103**: p. 147-156.

77. Calvo, F., et al., *Mechanotransduction and YAP-dependent matrix remodelling is required for the generation and maintenance of cancer-associated fibroblasts.* Nature Cell Biology, 2013. **15**(6): p. 637-+.

78. Liu, F., et al., *Mechanosignaling through YAP and TAZ drives fibroblast activation and fibrosis.* American Journal of Physiology-Lung Cellular and Molecular Physiology, 2015. **308**(4): p. L344-L357.

79. Mercurio, A., et al., *A Laminin 511 Matrix is Regulated by TAZ and Functions as the Ligand for the a6Bb1 Integrin to Sustain Breast Cancer Stem Cells.* The FASEB Journal, 2015. **29**(1_supplement): p. 890.4.

80. Ponta, H., L. Sherman, and P.A. Herrlich, *CD44: from adhesion molecules to signalling regulators.* Nat Rev Mol Cell Biol, 2003. **4**(1): p. 33-45.

81. Orian-Rousseau, V., *CD44, a therapeutic target for metastasising tumours.* Eur J Cancer, 2010. **46**(7): p. 1271-7.

82. Montanari, E., et al., *Pursuing Intracellular Pathogens with Hyaluronan. From a 'Pro-Infection' Polymer to a Biomaterial for 'Trojan Horse' Systems.* Molecules, 2018. **23**(4).

83. Lee, S.-E., et al., *Hyaluronic acid-coated solid lipid nanoparticles to overcome drug-resistance in tumor cells.* Journal of Drug Delivery Science and Technology, 2019. **50**: p. 365-371.

84. Arpicco, S., G. De Rosa, and E. Fattal, *Lipid-Based Nanovectors for Targeting of CD44-Overexpressing Tumor Cells.* J Drug Deliv, 2013. **2013**: p. 860780.

85. Chiesa, E., et al., *Hyaluronic Acid-Decorated Chitosan Nanoparticles for CD44-Targeted Delivery of Everolimus.* Int J Mol Sci, 2018. **19**(8).

86. Zhang, W., et al., *Antitumor effect of hyaluronic-acid-modified chitosan nanoparticles loaded with siRNA for targeted therapy for non-small cell lung cancer.* Int J Nanomedicine, 2019. **14**: p. 5287-5301.

87. Yan, X.J., et al., *Hyaluronic acid/PEGylated amphiphilic nanoparticles for pursuit of selective intracellular doxorubicin release.* Journal of Materials Chemistry B, 2019. **7**(1): p. 95-102.

88. Sargazi, A., et al., *Hyaluronic acid/polyethylene glycol nanoparticles for controlled delivery of mitoxantrone.* Artif Cells Nanomed Biotechnol, 2018. **46**(3): p. 500-509.

89. Lu, J., et al., *Host-guest fabrication of dual-responsive hyaluronic acid/mesoporous silica nanoparticle based drug delivery system for targeted cancer therapy.* Int J Biol Macromol, 2020. **146**: p. 363-373.

90. Gotov, O., et al., *Hyaluronic acid-coated cisplatin conjugated gold nanoparticles for combined cancer treatment.* Journal of Industrial and Engineering Chemistry, 2018. **65**: p. 236-243.

91. Gupta, B., et al., *Hyaluronic acid-capped compact silica-supported mesoporous titania nanoparticles for ligand-directed delivery of doxorubicin.* Acta Biomaterialia, 2018. **80**: p. 364-377.

92. Szarpak, A., et al., *Designing Hyaluronic Acid-Based Layer-by-Layer Capsules as a Carrier for Intracellular Drug Delivery.* Biomacromolecules, 2010. **11**(3): p. 713-720.

93. Yu, M., et al., *Hyaluronic acid modified mesoporous silica nanoparticles for targeted drug delivery to CD44-overexpressing cancer cells.* Nanoscale, 2013. **5**(1): p. 178-83.

94. Gary-Bobo, M., et al., *Hyaluronic acid-functionalized mesoporous silica nanoparticles for efficient photodynamic therapy of cancer cells.* Photodiagnosis Photodyn Ther, 2012. **9**(3): p. 256-60.

95. Amorim, S., et al., *Hyaluronic acid/poly-L-lysine bilayered silica nanoparticles enhance the osteogenic differentiation of human mesenchymal stem cells.* Journal of Materials Chemistry B, 2014. **2**: p. 6939-6946.

96. Ferreira, H., et al., *The functionalization of natural polymer-coated gold nanoparticles to carry bFGF to promote tissue regeneration.* Journal of Materials Chemistry B, 2018. **6**(14): p. 2104-2115.

97. Dreaden, E.C., et al., *Bimodal tumor-targeting from microenvironment responsive hyaluronan layer-by-layer (LbL) nanoparticles.* ACS Nano, 2014. **8**(8): p. 8374-82.

98. Mahmoudi, S., et al., *Targeted hyaluronic acid-based lipid nanoparticle for apigenin delivery to induce Nrf2-dependent apoptosis in lung cancer cells.* Journal of Drug Delivery Science and Technology, 2019. **49**: p. 268-276.

99. Karakocak, B.B., et al., *Hyaluronate coating enhances the delivery and biocompatibility of gold nanoparticles.* Carbohydr Polym, 2018. **186**: p. 243-251.

100. Mizrahy, S., et al., *Hyaluronan-coated nanoparticles: the influence of the molecular weight on CD44-hyaluronan interactions and on the immune response.* Journal of controlled release : official journal of the Controlled Release Society, 2011. **156**(2): p. 231-8.

101. Tomihata, K. and Y. Ikada, *Crosslinking of hyaluronic acid with glutaraldehyde.* Journal of Polymer Science Part a-Polymer Chemistry, 1997. **35**(16): p. 3553-3559.

102. Bodnar, M., et al., *Preparation and characterization of cross-linked hyaluronan nanoparticles.* Colloid and Polymer Science, 2009. **287**(8): p. 991-1000.

103. Garcia, F.P., et al., *A versatile method for the selective core-crosslinking of hyaluronic acid nanogels via ketone-hydrazide chemistry: from chemical characterization to in vivo biodistribution.* Biomater Sci, 2018. **6**(7): p. 1754-1763.

104. Khunmanee, S., Y. Jeong, and H. Park, *Crosslinking method of hyaluronic-based hydrogel for biomedical applications.* Journal of Tissue Engineering, 2017. **8**.

105. Xu, X., et al., *Hyaluronic Acid-Based Hydrogels: from a Natural Polysaccharide to Complex Networks.* Soft Matter, 2012. **8**(12): p. 3280-3294.

106. Messager, L., et al., *Photochemical crosslinking of hyaluronic acid confined in nanoemulsions: towards nanogels with a controlled structure.* Journal of Materials Chemistry B, 2013. **1**(27): p. 3369-3379.

107. Kim, K., et al., *Hyaluronic Acid-Coated Nanomedicine for Targeted Cancer Therapy.* Pharmaceutics, 2019. **11**(7).

108. Gurav, D.D., et al., *pH-responsive targeted and controlled doxorubicin delivery using hyaluronic acid nanocarriers.* Colloids and Surfaces B-Biointerfaces, 2016. **143**: p. 352-358.

109. Tan, H.P., et al., *Thermosensitive injectable hyaluronic acid hydrogel for adipose tissue engineering.* Biomaterials, 2009. **30**(36): p. 6844-6853.

110. Han, H.S., et al., *Robust PEGylated hyaluronic acid nanoparticles as the carrier of doxorubicin: Mineralization and its effect on tumor targetability in vivo.* Journal of Controlled Release, 2013. **168**(2): p. 105-114.

111. Boudou, T., et al., *Multiple functionalities of polyelectrolyte multilayer films: new biomedical applications.* Adv Mater, 2010. **22**(4): p. 441-67.

112. Costa, R.R. and J.F. Mano, *Polyelectrolyte multilayered assemblies in biomedical technologies.* Chem Soc Rev, 2014. **43**(10): p. 3453-79.

113. Ren, K., et al., *Manipulation of the adhesive behaviour of skeletal muscle cells on soft and stiff polyelectrolyte multilayers.* Acta Biomater, 2010. **6**(11): p. 4238-48.

114. Minsky, B.B., C.H. Antoni, and H. Boehm, *Controlled Immobilization Strategies to Probe Short Hyaluronan-Protein Interactions.* Sci Rep, 2016. **6**: p. 21608.

115. Smulovitz, C., L.E. Dickinson, and S. Gerecht, *Micropatterned Surfaces for the Study of Cancer and Endothelial Cell Interactions with Hyaluronic Acid.* Israel Journal of Chemistry, 2013: p. n/a-n/a.

116. Arnold, M., et al., *Cell interactions with hierarchically structured nano-patterned adhesive surfaces.* Soft Matter, 2009. **5**(1): p. 72-77.

117. Ermis, M., E. Antmen, and V. Hasirci, *Micro and Nanofabrication methods to control cell-substrate interactions and cell behavior: A review from the tissue engineering perspective.* Bioactive Materials, 2018. **3**(3): p. 355-369.

118. Hong, H.J., W.S. Koom, and W.G. Koh, *Cell Microarray Technologies for High-Throughput Cell-Based Biosensors.* Sensors (Basel), 2017. **17**(6).

119. Jeong, H.H., et al., *Selectable Nanopattern Arrays for Nanolithographic Imprint and Etch - Mask Applications.* Advanced Science, 2017. **2**(7).

120. Vinje, J., K.S. Beckwith, and P. Sikorski, *Electron beam lithography fabrication of SU-8 polymer structures for cell studies.* bioRxiv, 2019: p. 849745.

121. Lohmuller, T., et al., *Nanopatterning by block copolymer micelle nanolithography and bioinspired applications.* Biointerphases, 2011. **6**(1): p. MR1-12.

122. Ghezzi, B., et al., *Sub-Micropillar Spacing Modulates the Spatial Arrangement of Mouse MC3T3-E1 Osteoblastic Cells.* Nanomaterials (Basel), 2019. **9**(12).

123. Joo, S., et al., *Effects of ECM protein micropatterns on the migration and differentiation of adult neural stem cells.* Sci Rep, 2015. **5**: p. 13043.

124. Albert, P.J. and U.S. Schwarz, *Modeling cell shape and dynamics on micropatterns.* Cell Adhesion & Migration, 2016. **10**(5): p. 516-528.

125. Liu, Y., et al., *Nanoparticle Tension Probes Patterned at the Nanoscale: Impact of Integrin Clustering on Force Transmission.* 2014.

126. Schaufler, V., et al., *Selective binding and lateral clustering of α5β1 and αvβ3 integrins: Unraveling the spatial requirements for cell spreading and focal adhesion assembly.* Cell Adh Migr, 2016.

127. Li, J.G., et al., *Co-culture of vascular endothelial cells and smooth muscle cells by hyaluronic acid micro-pattern on titanium surface.* Applied Surface Science, 2013. **273**: p. 24-31.

128. Li, J.G., et al., *Tailoring of the titanium surface by preparing cardiovascular endothelial extracellular matrix layer on the hyaluronic acid micro-pattern for improving biocompatibility.* Colloids and Surfaces B-Biointerfaces, 2015. **128**: p. 201-210.

129. Li, J.G., et al., *Research of smooth muscle cells response to fluid flow shear stress by hyaluronic acid micro-pattern on a titanium surface.* Experimental Cell Research, 2013. **319**(17): p. 2663-2672.

130. Niepel, M.S., et al., *Polyelectrolyte multilayers of poly (l-lysine) and hyaluronic acid on nanostructured surfaces affect stem cell response.* Nanoscale, 2019. **11**(6): p. 2878-2891.

131. Hinderer, S., S.L. Layland, and K. Schenke-Layland, *ECM and ECM-like materials — Biomaterials for applications in regenerative medicine and cancer therapy.* Advanced Drug Delivery Reviews, 2016. **97**: p. 260-269.

132. Tibbitt, M.W. and K.S. Anseth, *Hydrogels as Extracellular Matrix Mimics for 3D Cell Culture.* Biotechnology and Bioengineering, 2009. **103**(4): p. 655-663.

133. Highley, C.B., G.D. Prestwich, and J.A. Burdick, *Recent advances in hyaluronic acid hydrogels for biomedical applications.* Curr Opin Biotechnol, 2016. **40**: p. 35-40.

134. Schante, C.E., et al., *Chemical modifications of hyaluronic acid for the synthesis of derivatives for a broad range of biomedical applications.* Carbohydrate Polymers, 2011. **85**(3): p. 469-489.

135. Ondeck, M.G. and A.J. Engler, *Mechanical Characterization of a Dynamic and Tunable Methacrylated Hyaluronic Acid Hydrogel.* J Biomech Eng, 2016. **138**(2): p. 021003.

136. Poldervaart, M.T., et al., *3D bioprinting of methacrylated hyaluronic acid (MeHA) hydrogel with intrinsic osteogenicity.* PLoS One, 2017. **12**(6): p. e0177628.

137. Ananthanarayanan, B., Y. Kim, and S. Kumar, *Elucidating the mechanobiology of malignant brain tumors using a brain matrix-mimetic hyaluronic acid hydrogel platform.* Biomaterials, 2011. **32**(31): p. 7913-7923.

138. Deegan, D.B., et al., *Stiffness of hyaluronic acid gels containing liver extracellular matrix supports human hepatocyte function and alters cell morphology.* J Mech Behav Biomed Mater, 2015. **55**: p. 87-103.

139. Gurski, L.A., et al., *Hyaluronan (HA) interacting proteins RHAMM and hyaluronidase impact prostate cancer cell behavior and invadopodia formation in 3D HA-based hydrogels.* PLoS One, 2012. **7**(11): p. e50075.

140. Fisher, S.A., et al., *Tuning the Microenvironment: Click-Crosslinked Hyaluronic Acid-Based Hydrogels Provide a Platform for Studying Breast Cancer Cell Invasion.* Advanced Functional Materials, 2015. **25**(46): p. 7163-7172.

141. Andersen, T., P. Auk-Emblem, and M. Dornish, *3D Cell Culture in Alginate Hydrogels.* Microarrays (Basel), 2015. **4**(2): p. 133-61.

142. Zhao, Y.F., et al., *Modulating Three-Dimensional Microenvironment with Hyaluronan of Different Molecular Weights Alters Breast Cancer Cell Invasion Behavior.* ACS Appl Mater Interfaces, 2017. **9**(11): p. 9327-9338.

143. Canibano-Hernandez, A., et al., *Alginate Microcapsules Incorporating Hyaluronic Acid Recreate Closer in Vivo Environment for Mesenchymal Stem Cells.* Mol Pharm, 2017. **14**(7): p. 2390-2399.

144. Florczyk, S.J., et al., *Porous chitosan-hyaluronic acid scaffolds as a mimic of glioblastoma microenvironment ECM.* Biomaterials, 2013. **34**(38): p. 10143-50.

145. Wong, C.W., et al., *Biomaterial substrate-derived compact cellular spheroids mimicking the behavior of pancreatic cancer and microenvironment.* Biomaterials, 2019. **213**: p. 119202.

146. Lou, J., et al., *Stress relaxing hyaluronic acid-collagen hydrogels promote cell spreading, fiber remodeling, and focal adhesion formation in 3D cell culture.* Biomaterials, 2018. **154**: p. 213-222.

147. Nazir, R., et al., *Collagen type I and hyaluronic acid based hybrid scaffolds for heart valve tissue engineering.* Biopolymers, 2019. **110**(8): p. e23278.

148. Gokila, S., et al., *Development of 3D scaffolds using nanochitosan/silk-fibroin/hyaluronic acid biomaterials for tissue engineering applications.* International Journal of Biological Macromolecules, 2018. **120**: p. 876-885.

149. Vasvani, S., P. Kulkarni, and D. Rawtani, *Hyaluronic acid: A review on its biology, aspects of drug delivery, route of administrations and a special emphasis on its approved marketed products and recent clinical studies.* Int J Biol Macromol, 2019.

150. Rinaudo, M., *Main properties and current applications of some polysaccharides as biomaterials.* Polymer International, 2008. **57**(3): p. 397-430.

151. Jarvis, B. and D.P. Figgitt, *Topical 3% diclofenac in 2.5% hyaluronic acid gel: a review of its use in patients with actinic keratoses.* Am J Clin Dermatol, 2003. **4**(3): p. 203-13.

152. Li, X., et al., *Arthroscopic debridement of the osteoarthritic knee combined with hyaluronic acid (Orthovisc®) treatment: A case series and review of the literature.* Journal of Orthopaedic Surgery and Research, 2008. **3**(1): p. 43.

153. Curran, M.P., *Hyaluronic Acid (Supartz®).* Drugs & Aging, 2010. **27**(11): p. 925-941.

154. Keizers, P.H.J., et al., *A high crosslinking grade of hyaluronic acid found in a dermal filler causing adverse effects.* Journal of Pharmaceutical and Biomedical Analysis, 2018. **159**: p. 173-178.

155. Gutowski, K.A., *Hyaluronic Acid Fillers Science and Clinical Uses.* Clinics in Plastic Surgery, 2016. **43**(3): p. 489-+.

156. Smith, T., *Gelclair: managing the symptoms of oral mucositis.* Hospital Medicine, 2001. **62**(10): p. 623-626.

157. Kallestrup, E.B., et al., *Treatment of interstitial cystitis with Cystistat (R): A hyaluronic acid product.* Scandinavian Journal of Urology and Nephrology, 2005. **39**(2): p. 143-147.

158. Furnari, M.L., et al., *Nebulized hypertonic saline containing hyaluronic acid improves tolerability in patients with cystic fibrosis and lung disease compared with nebulized hypertonic saline alone: a prospective, randomized, double-blind, controlled study.* Ther Adv Respir Dis, 2012. **6**(6): p. 315-22.

159. Lee, Y.J., et al., *Anti-aging and hydration efficacy of a cross-linked hyaluronic acid microstructure patch.* Dermatol Ther, 2019. **32**(3): p. e12888.

160. Kawada, C., et al., *Ingested hyaluronan moisturizes dry skin.* Nutr J, 2014. **13**: p. 70.

161. Fallacara, A., et al., *Hyaluronic Acid in the Third Millennium.* Polymers (Basel), 2018. **10**(7).

Chapter 2

Biomatrices that mimic the cancer extracellular environment

Chapter 2

Biomatrices that mimic the cancer extracellular environment

ABSTRACT

The tumor microenvironment (TME), in particular its extracellular matrix (ECM) has been increasingly linked to the tumor pathological behaviour, e.g. its aggressiveness and invasion. The dynamic interplay between cells and the healthy ECM regulates the normal function of tissues, modulating the cell behaviour and activating signalling events, mainly triggered through the well-structured and organized components of the ECM. In cancer, changes on the ECM composition, derived from the deregulation of production and degradation of its constituents, alters the biochemical (e.g. upregulation of metalloproteinases, deposition of proteins, etc.) and mechanical (e.g. crosslinking extension of the matrix) features of the extracellular space, changing the normal functioning of tissues. In this context, the engineering of 3D models that mimic the TME is a difficult task, however, it has the potential to allow the in vitro study of cancer cells has they would behave in their native environment. Recently, it has been proposed a series of 3D cancer models to screen the role of the ECM components, such, proteins and glycans on cancer pathology, and on the progression of the disease. These developments have proven to be efficient in recapitulating some of the biological and biochemical features of the TME. In this chapter we will review the biomaterials used for the development of 3D cancer models and the advantages and disadvantages of each one. In general, we will focus on natural materials, such collagen, hyaluronic acid, fibronectin or laminin - components of the ECM. However, we also give a brief overview on the use of components from other natural sources, such as, alginate and chitosan. In addition, the use of PEG, PLA and PLGA that has been widely used to generate 3D cancer models due to their biocompatibility and ability to be easily tune the model's physical properties, will be also revised.

2-1. INTRODUCTION

The tumor microenvironment (TME) is a complex matrix of blood vessels, malignant and non-malignant cells, proteins, glycosaminoglycans, signalling molecules, among other components of the extracellular matrix (ECM) [1, 2]. The ECM is the major component of the TME and has been increasingly linked to cancer progression and metastasis [3-5]. The dynamic character of the ECM involves a series of mechanisms related with its production, degradation and remodelling. In turn, these mechanisms regulate the normal function of the cells and the composition of their extracellular environment. In pathological frameworks, such as the TME, these key regulatory features are disturbed altering the composition of the ECM through the uncontrolled synthesis and degradation of proteins and glycans that accumulate on the basement membrane and the extracellular/pericellular space. In addition, the reorganization of ECM components, alters the crosslinking extension of the interstitial matrix, affecting the homeostasis and normal functioning of tissues [6-8] (Figure 1). In this view, the complexity of the ECM in healthy tissues is significantly amplified in the TMEs.

During the last few years, the development of 3D TME mimics emerged as model platforms for the *in vitro* study of cancer, as well as the behaviour of its cells as a function of the composition of the TME. These models have been used for the screening of the role of each TME component on tumor progression and invasiveness. These 3D models provide architectural support for cell-cell interactions, offering the biochemical and mechanical cues of the 3D TME. Moreover, the third dimension of the models, confers the ability to tune key parameters, such as porosity and water content, which, in turn, regulate the transport of oxygen and nutrients, as well as the two-way exchange of soluble biochemical factors [9]. The controlled diffusion and distribution of these elements throughout the 3D network are fundamental to recapitulate the cancer cell behaviour and to control the homeostasis of the TME. These properties can be tuned through the chemical and/or physical manipulation of the 3D models.

In addition to its spatial organization, the TME is composed by different types of collagens (types I-V), elastin, fibronectin, laminin, as well as different glycoproteins, glycosaminoglycans, proteoglycans and ECM regulators [10]. The recent developments to recreate the TME network includes the natural and synthetic-based materials. Using specific ECM constituents, such collagen [11], the glycosaminoglycan hyaluronic acid (HA) [12], or natural non-mammalian materials, such as alginate (Alg) [13], it is possible to recreate *in vitro* the cell-cell and cell-ECM interactions that recapitulate the TME. Advances on the development of 3D TME models, led to the use of synthetic polymers with

bioactive, biocompatible and biodegradable properties. The recreation of the cellular surroundings using synthetic materials allowed to: i) manipulate and functionalize the materials, with specific bioactive motifs able to induce cellular adhesion, spreading and/or migration [14]; ii) easily tune the mechanical properties of the 3D networks through the manipulation of the concentration of the polymer or the type and extension of crosslinking [15].

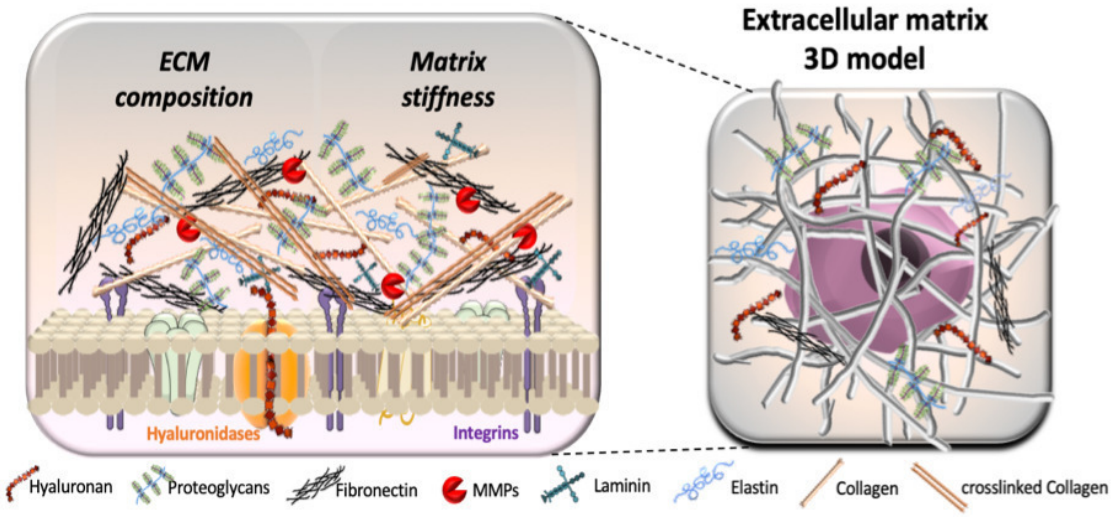

Figure 2-1. Schematic representation of the dysregulated ECM in the TME. In summary, there is: an accumulation of ECM, through the overexpression of HA, and an increment of the ECM stiffness through the crosslinking of collagen, leading to an upregulation of matrix metalloproteinases (MMPs), accelerating ECM degradation and promoting the extravasation of tumor cells [16].

In the following sections we will review the recently reported methodologies and materials used to develop 3D TME mimics, based on the above-mentioned strategies. We will also make an overview of the advantages and disadvantages of each one, in an attempt to elucidate the reader about which ones are more suitable to recapitulate the TME of different tumors.

2-2. 3D *IN VITRO* MODELS

2-2.1. Natural-based models

Natural-based materials have been exploited in the development of 3D models that mimic the TME. They are regarded as mimics of the ECM due to their close resemblance to the chemical and morphological presentation of its components. In fact, the chemical similarity between the proposed natural materials, e.g. proteins, polysaccharides, etc., with the ones that are present in the ECM that constitutes the TME allows the presentation of different bioactive motifs (e.g. aminoacid sequences, monosaccharides and their sequences, etc.) that are recognized by the cells and able to modulate their behaviour [17]. In the following sections, we will give an overview on the different biomaterials that have been used to mimic the 3D TME and in particular its ECM. These includes the use of proteins, glycoproteins and polysaccharides extracted from natural sources. It will be detailed the advantages and disadvantages of each one and it will be given an overview of the most relevant biochemical features from the *in vivo* TME that they are able to recapitulate in these *in vitro* 3D models.

2-2.2. Protein-based systems

Collagens are the most abundant type of protein present in the ECM and are the most tested for the development of 3D tissue models. They are present in nature (and in the human body) under different conformations and aminoacid sequences. The most common one is type I but there are more than 20 different types already identified [18]. One of the main advantages of using collagen type I to produce 3D matrices is associated with the mild crosslinking conditions (i.e. pH and temperature) [19], which is compatible with cell encapsulation. The self-assembly capacity of collagens is another advantage, as they readily organize into fibres [20, 21], generating meshes of different pore sizes and densities [21, 22]. The generation of 3D collagen-based models have been used to screen its role in the TME. In fact, it is known that the increased expression and deposition of collagens on the ECM, is correlated with cancer progression and poor patient prognosis on different cancers, e.g. breast cancer [23]. MDA-MB-231 and MCF-7 cells (human breast cancer cell lines) cultured on 3D collagen matrices, showed to be more elongated with higher invasive behaviour, which was correlated with fibril thickness, intrafibrillar crosslinking, as well as the fibril's stiffness (Figure 2) [24]. On the other hand, Plou *et al* demonstrated

that the non-small cell lung cancer (NSCLC) H1299 cells, adhere and proliferate in highly concentrated collagen matrices. However, they present reduced migration, and tend to spontaneously form cell clusters while inhibiting single cell invasion [25]. The variation of the thickness of collagen I-based hydrogel (between 1.5 and 3.0mm) was also tested to study the impact on cell-cell and cell-matrix interactions using MDA-MB-231 cells [26]. The expression of hypoxia-inducible factor (HIF)-1α, associated to the formation of tumor spheroids, and the angiogenic potential through the expression of vascular endothelial growth factor (VEGF) was evaluated. The results showed that in the higher thickness of collagen hydrogel, 3.0mm, HIF-1α and VEGF-A gene expression was upregulated, as a result of lack of oxygen and nutrient-induced cell death after day 5.

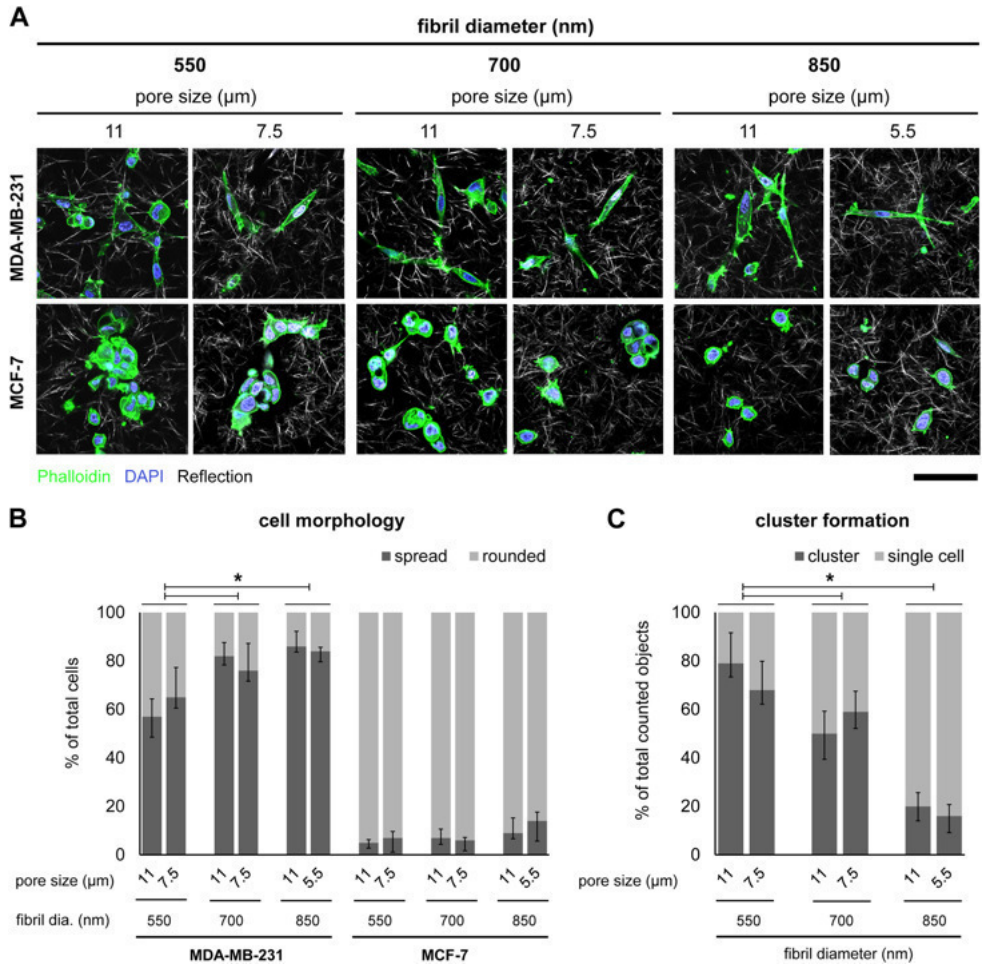

Figure 2-2. Influence of collagen fibril diameter and hydrogel pore size on cluster formation and cell morphology of breast cancer cells, MDA-MB-231 and MCF-7. (A) Confocal laser scanning microscopy images of breast cancer cells seeded on the 3D collagen I matrices; (B) percentage of spread and rounded cells; and (C) quantification of single cells and clusters formation cultivated in the different collagen matrices. Reprinted from Sapudom *et al.* [24] Copyright (2019), with permission from Elsevier.

Similar to collagen, the glycoprotein fibronectin (FN) forms fibrillar structures in the ECM [5]. FN occurs in a soluble form in the plasma, however it can also self-assemble into linear and branched supramolecular fibres, that surrounds the cells, allowing the interplay between ECM components [27]. In contrast to collagen, FN is secreted as a soluble dimer and its cell-surface interaction is necessary for its assembly into longer fibrils [28]. To our knowledge, FN on its own has not been used for the formulation of 3D matrices, however, due to its overexpression in the interstitial ECM and its association with cancer cell migration and tumor growth [29], it has been used in the formulation of different 3D cancer models, as a cellular adhesive component. The combination of collagen and FN are reported as a close mimic of the ECM. The presence of increasing concentrations of FN within a collagen matrix has

been studied and it has been reported that it alters the collagen fibrillization kinetics, where a faster fibril formation results in an altered microstructure network [30, 31]. The adsorptive immobilization of FN on the collagen network, as well as the evaluation of its ability to modulate the cellular behaviour was investigated by Sapudom *et al.* The authors showed that the presence of FN at high concentrations induces the migration of fibroblasts, accompanied by a reduction of their proliferation rate [30]. The induced differentiation of fibroblasts into myofibroblasts is associated to cancer invasion through the production of pro-invasive proteinases [32], however, Sapudom *et al* [30] did not observe any cellular differentiation in the developed collagen-FN 3D matrices. An important feature to be considered, and that is relevant to be recapitulated in the 3D cancer models, is the fact that the remodelling and activation of fibroblasts induces a stiffening of the ECM matrix and tissue desmoplasia [33]. These observations show that the mechanical properties of the ECM present in the TME is an important parameter to be considered when developing cancer models, a topic that will be discussed further in a later section.

Laminin, is another glycoprotein present at the cellular basement membrane that has been used to model the 3D laminin-rich ECM. It is secreted by healthy myofibroblasts and plays a crucial role in maintaining epithelial polarity. In breast tumors, this polarity is altered due to the reduced expression of laminin [34]. A 3D laminin-rich ECM model is commercially available (3D IrECM). It has been used to study the cancer cells behaviours, mimicking physiologic *in vivo* growth conditions [35]. A panel of cancer cells were already evaluated under this 3D culture conditions, by screening their morphologies, proliferation and expression of signalling proteins. Cells seeded on this 3D model exhibited different morphologies (round, mass, grape-like and stellate), which was dependent on the cell type, and was associated with gene and protein expression profiles, as well as correlated with invasiveness characteristics of the tested tumor cells [36]. The 3D IrECM has been also applied to evaluate the response of human breast cancer cells to doxorubicin (a common anti-cancer drug). Under the laminin rich microenvironment, MCF-7 cells presented morphological alterations, a decreased proliferation rate and an elevated sensitivity to doxorubicin [37], showing the suitability of the model for drug screening purposes.

2-2.3. Polysaccharide-based systems

The polysaccharides that are present in the ECM (i.e. the glycosaminoglycans - GAGs), play an important role in the biological milieu. They are usually regulating the cell-cell communication and cell-ECM interactions [38]. They can also initiate intracellular pathways, through the interaction with cell membrane receptors, that modulate gene expression and protein secretion, as well as cell proliferation and differentiation [39]. The GAGs are composed by repeating disaccharides units, one is an amino sugar (d-glucosamine or d-galactosamine), and the other is a uronic acid residue (d-glucuronic acid or iduronic acid) [40]. One or both of this units can be additionally sulphated, generating a range of five different GAGs, namely: HA, heparan sulphate (HS), Heparin (Hep), chondroitin sulphate (CS) and dermatan sulphate (DS). These different types of GAGs are distinguished by the degree of sulphation and the distribution of their sulphation motifs throughout the repeating unit and the polymeric chain [41]. These structural features present in the GAGs, namely the changes on their sulphation degree, have been linked to cancer cell migration and tumor aggressiveness [42-45].

The most studied and the only non-sulphated GAG, associated to cancer pathology, is HA. The deposition of HA in the TME has been related to the proliferation and migration of cancer cells. In particular, the molecular weight (Mw) of HA have been reported to generate different biological outcomes. While, in some studies, low Mw HA (i.e. oligomers) are associated with tumor invasiveness, others suggest that HAs of high Mw are the cause of invasive cellular character [46-48]. Moreover, the CD44 transmembrane protein (a major HA receptor) is known to be overexpressed in some cancers (e.g. colorectal, pancreatic and gastric), in particular the isoforms between CD44v6-CD44v15 have been related to cancer migration and invasiveness [49].

Different approaches have been used to fabricate 3D HA-based culture systems to study its influence on cancer progression [12]. Usually HA-based systems require crosslinking to generate stable 3D structures that resemble the *in vivo* HA network. The most common procedure to generate 3D HA hydrogels is to chemically modify HA into its methacrylated form (Me-HA), that can be crosslinked by UV light [50-52]. 3D glioblastoma (GMB) models were developed using these Me-HA-based hydrogels [53], where cellular morphology and motility were dependent on the hydrogel stiffness. Pedron *et al* also used Me-HA but in combination with methacrylated-gelatin or PEG; they found that the addition of Me-HA (0.3-0.5 wt%) modulated the glioma proliferation and morphology, as well as the expression of invasive-associated genes (VEGF, HIF-1, MMP-9, FN) [54]. Modification of HA with aldehyde (HAALD) and hydrazide (HAADH) groups have been also described. In this case, the hydrogel can be crosslinked

via the hydrazine bonds, allowing the encapsulation of prostate cancer cells. This system was proposed as a platform to screen anticancer drugs, namely, camptothecin, docetaxel, and rapamycin [55, 56]. The mixture of HA with Alg is another approach to immobilize and mimic the presentation of HA under a 3D environment. In this case, the physical dispersion of HA into an Alg solution [57] or the crosslinking of HA-Alg through the oxidation of Alg has been described. In both cases, the generated systems were used to study the role of the HA's Mws on breast cancer cells, namely on their proliferation and invasiveness [12]. The presence of HA of low Mw (35 kDa) significantly enhances the migration ability of SKBR3 (breast cancer) cells, as well as 4T-1 (pancreatic cancer cells); behaviour that was suppressed by the HA of higher Mw (117 kDa). Moreover, it was observed that the HA of 35 kDa potentiates the epithelial-mesenchymal transition (EMT) phenotype, associated to cancer metastasis.

Among the sulphated GAGs, CS, a linear polysaccharide, in particular its sulphation degree has been reported to be involved in cancer cell proliferation, migration and adhesion, being one relevant factor that induces cancer progression [58, 59]. CS is present on the cell surface and found in extracellular/pericellular space covalently attached to different core proteins [60]. In the TME, CS is detected at high concentration within the collagen network, altering its structure and viscoelastic properties [61]. The 3D models generated by the combination of collagen and CS (Coll-CS) have been reported. The pore sizes of the Coll-CS structures have been shown to influence cell adhesion, where larger pores reduce cell viability, and smaller pores (with the correspondent increase in surface area) leads to higher viability of MC3T3 cells [62]. Coll-CS hydrogels have been also used as a neuroblastoma model using two different cell lines: KellyLuc and KellyCis83Luc. It was observed cellular penetration and proliferation into the Coll-CS matrix, with increased resistance to cisplatin (platin-containing drugs are used in neuroblastoma treatment) when compared to 2D cell cultures [63], a result that resembles better the *in vivo* environment. Other researchers have reported the modification of Alg hydrogels with CS, for the encapsulation of Hepatocellular carcinoma cells (HCCLM3), as well as head and neck squamous carcinoma cells (HNSCC). They found an upregulation on the gene expression of matrix metalloproteinase (MMPs), namely MMP2, MMP9 and MMP14, on cells cultured in Alg-CS with higher invasion ability [64].

2-2.4. Other natural occurring materials

In the previous sections we outlined a series of materials present in the human biological tissues, in both healthy and pathological states, and that have been used to develop 3D models that mimic the ECM present in the TME. However, there are a vast range of other natural materials (that are not present in the human body) but, due to its chemical similarity, has been tested as 3D TME mimics.

Another widely studied material for the development of 3D cancer model is Alg, a polysaccharide obtained from brown seaweeds that has been widely used in the biomedical field, in particular as a biomaterial for 3D cell culture [65]. Its main advantages are related with the easy handling, the possibility to cross-link and gel under mild conditions (e.g. in the presence of divalent cations, Ca^{2+}), the ability to tune the physical properties of the Alg hydrogels through the manipulation of the concentration of Alg and its crosslinking agent (e.g. Ca^{2+}) [66]. However, and despite these important advantages, the main drawback of using Alg-based systems for cell culture studies is the limited cell adhesion. To overcome this weakness, Alg has been modified with cell adhesive peptide sequences, such as Arg-Gly-Asp (RGD) [67], or has been formulated through its combination with other biomolecules present in the ECM, such collagen or hyaluronic acid, as detailed below [65, 68]. The blending of Alg with collagen, an ECM-occurring protein, has been tested in the development of 3D models suitable for the encapsulation of human breast cancer cells [69, 70], as well as a combination of MDA-MB-231 cells and human mammary fibroblast (HMF) spheroids. Under this co-culture conditions it was observed the secretion of CXCL12-CXCR4 signalling molecules as inductors of directional cell migration into the 3D hydrogel [70]. The incorporation of HA on Alg matrices has been also reported to mimic the cancer stem cells (CSCs) microenvironment and used to isolate and enrich CSCs from 4T1 breast cancer cells. The incorporation of HA and growth factors, EGF and bFGF, on the Alg matrices, allowed the efficient isolation of CSCs that highly expresses CD44 and SCa-1, with low expression of CD24, usually referred as cancer stem cells markers. [71] The encapsulation of mono and co-culture of human dermal fibroblasts (HDF) and human breast cancer cells (MCF-7) have been also attempted [72]: in this case, the 3D culture system provided a favourable microenvironment to study the crosstalk between tumor cells and fibroblasts. It was detected the synthesis and deposition of ECM and the accumulation of soluble factors that promote tumor progression.

CHI is another widely used material in the biomedical field. It is a polysaccharide derived from the partially deacetylation of chitin, that occurs in nature in the shells of crab and shrimp (among other sources). Its partial deacetylation under alkaline conditions yields CHI [73], a cationic polymer,

presenting cell adhesive properties due to its positive charge. CHI is also biocompatible, biodegradable and non-toxic [74, 75]. CHI scaffolds with different degrees of deacetylation has been used as a support for the culture of human breast cancer cells (MCF-7). Increased proliferation rate and formation of cells' clusters has been correlated with a higher degree of deacetylation and higher swelling ability. This CHI-based system revealed to be a 3D model to consider for drug-screening purposes, namely the evaluation of anticancer drugs [76]. 3D culture systems based on CHI have been also described to mimic the glioma tumor microenvironment: the combination of CHI and Alg it has been proposed to support the viability of hepatocellular carcinoma cells (HCC) [77], prostate cancer cells [78], U-87 MG [79, 80] and U-118 MG [80] human glioma cells. In these latter cases, glioma cells showed round morphology with interconnectivity characteristic of solid tumor cells. Moreover, the upregulation of growth factors upon culture on these 3D systems, rather than on 2D surfaces, indicates that cells are able to modify its surroundings into a more invasive environment [80]. CHI has been also formulated with HA for the generation of 3D systems that are able to support the encapsulation of glioblastoma cells (GBM). This blending of CHI and HA was used as a close mimic of the native TME, through the incorporation of HA, a TME-occurring GAG. The incorporation of HA induced the expression of CD44, a stem cell surface marker, on GBM cells. The stemness of GBM cells cultured in the CHI/HA 3D system was confirmed by the genetic up-regulation of stem cells markers, namely, Nestin, Musashi-1 and GFAP. Moreover, under this culture conditions, genes associated with tumor invasiveness, metastasis and EMT, such as SNAIL1, SNAIL2 and TWIST were altered in the GBM cells [81, 82]. The EMT process was also observed on pancreatic cancer cells encapsulated on the HA-rich CHI model, through the upregulation of different markers, such as E-cadherin, N-cadherin, Vimentin, TWIST1 and SNAIL [83].

2-2.5. Synthetic and other bio-based models

Synthetic materials, such as polyethylene glycol (PEG), polyglycolide (PGA) polylactide-co-glycolide (PLGA), or bio-based ones, such as poly(lactic acid) (PLA) have been also described for the formulation of 3D systems with tuneable biochemical and mechanical properties [84]. The main drawback of these materials is the limited cell adhesion, which hinders the cell's cytoskeleton organization, necessary for cell proliferation and migration. To overcome this hurdle, these 3D matrices can be functionalized with: 1) the RGD peptide sequence, a known cell-adhesion motif present in FN but also identified in many

other ECM proteins such laminin and collagen [85-87]; 2) peptide cross-linkers that are degradable by MMPs, allowing the cells to degrade the matrix, creating space for cell proliferation and migration [88, 89]. PEG is widely used as a scaffold material to mimic the ECM part of the TME [15, 90]. PEG conjugated with fibrinogen (PEG-Fb) enables integrin-mediated signalling mechanisms required for cell attachment, spreading, and proliferation. This system has been proposed as 3D photo-crosslinkable hydrogels able to encapsulate breast cancer cells [91, 92]. It has been shown that PEG-Fb of varying composition influences the morphology of MCF7 and SK-BR-3 cells with epithelial phenotype, while inducing the formation of colonies. In addition, MDA-MB-231 cells presenting mesenchymal character, exhibited invasive behaviour under the same experimental conditions. The physical properties of these hydrogels (namely their crosslinking density and higher pore size) promoted the formation of a high number of cellular protrusions and an invasive character [91]. Microspheres of PLA-based hydrogels have been used to mimic the tumor shape and as a support that facilitates the formation of tumor spheroids [92]. The advantage of using PLA to generate 3D tumor models is based on its processing flexibility using different methodologies. As an example, it is possible to produce PLA-based electrospun scaffolds, using different PLA concentration (12% and 15%) [93], that supported the viability of the breast cancer cells MDA-MB-231. In this case, it was observed an increase in the STAT3 phosphorylation levels, a transcription factor that regulates the expression of different genes crucial for tumor progression. In addition, the physical characteristics of PLA has been tuned in the development of 3D TME models, including variations on the pore sizes, filament density, infill pattern or layer height [94]. In this case, the MDA-MB-231 cells were tested and, upon 3 days of cell culture, it was detected an upregulation of ALDH, that is associated to the stemness character of cancer cells. Variations om the intensity of this upregulation was dependent on the pore sizes of the model. PLGA has been also used as a 3D TME mimic. In this case, the U251 glioma cells were evaluated, in particular their resistance to hypoxia conditions [95]. PLGA presents low stability under physiological conditions due to its fast degradation rates [96]. In order to improve the stability of the TME mimic, PCL has been tested as an alternative to PLGA. Its suitability to mimic the TME has been evaluated using bone cancer cells [97]. In particular, the Ewing sarcoma cells cultured on electrospun PCL 3D system presented enhanced resistance to doxorubicin, showing favourable results on the application of these materials for the screening of the activity of anticancer therapeutic agents. Moreover, PCL-based models are also suitable to mimic the TME of breast cancers being closer to the physiological environment of the subpopulation of breast cancer stem cells (BCSCs) mimicking its native behaviour [98].

2-3. MIMICKING THE TME MECHANICAL FEATURES

The TME, is a complex environment with different cell types and ECM molecules. Importantly, it provides mechanical support for cell adhesion and motility and, consequently, to tumor growth [8, 99]. The TME stiffness influences the ability of cancer cells to spread and invade the neighbouring tissues. In fact, invasive cells tend to alter the TME mechanical properties, through the deposition of different ECM proteins that changes its biomechanical characteristics [100]. In general, the cancer stroma is usually stiffer than the healthy one, increasing from 150 to 400 Pa, and in pre-malignant breast tissues an increased ECM remodelling and stiffness is observed (~350 Pa) contributing to the development of malignancy [101, 102]. One of the major contributors for the increased stiffness of the TME is the deposition of fibrillar collagen. The crosslinking and reorganization of collagen into thick and organized fibres, induces the generation of intracellular tension, inducing an increment of cellular traction forces, while enhancing ECM stiffness [103]. In this context, collagen has been explored to generate 3D cancer models to study the intracellular tension in response to collagen concentration.

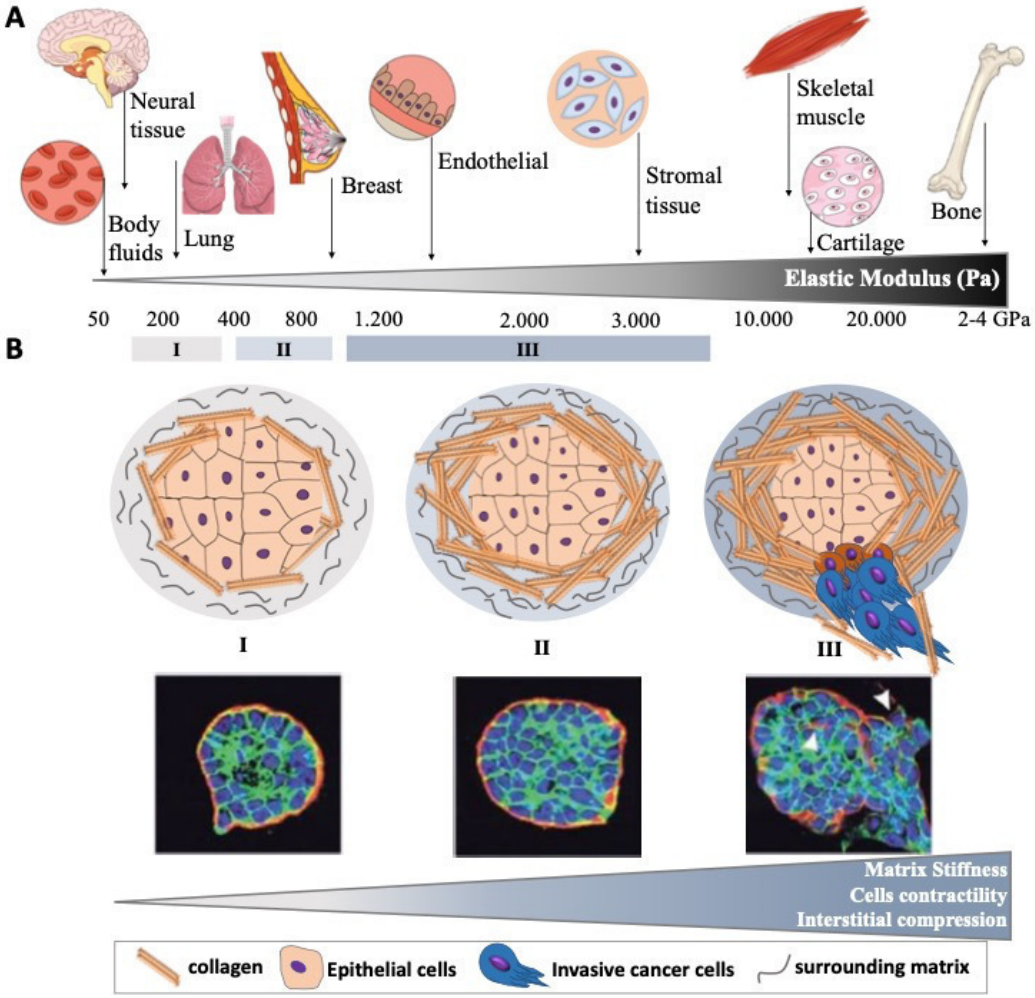

Figure 2-3. (A) Biomechanical properties of human tissues and their elastic modulus values and (B) Increased accumulation and alignment of collagen fibres with high stiffness on the extracellular and pericellular matrix. Disruption of the basement membrane promoting invasion and tumor migration. Adapted from Paszek et al [104] and Cox et al [101]. Copyright (2005), with permission from Elsevier.

Collagen concentrations between 1 and 4 mg/mL, increased the Young's modulus of the hydrogels from ~370 to 1200 Pa, a range that is comparable to the physiological stiffness of healthy soft tissues, e.g. lung, breast or endothelial tissues [104]. The breast adenocarcinoma cells MDA-MB-231, were cultured on these collagen hydrogels of varying stiffness values and a direct correlation was observed between the cellular and hydrogel stiffness [105]. In more detail, the modulus of the TME of breast cancer tissues can reach a value of 1500 Pa, close to the one for the stiffer collagen hydrogels. Wullkopf *et al* used the same concentration of collagen to screen the invasive potential of cells from different sources. Breast (4T1, 67NR, MDA-MB-231 and MCF7), colorectal (SW620 and SW480) and pancreatic ($KP^{R172H}C$ and KPflC) cancer cells were evaluated in the presence of 1 and 4 mg/mL of

collagen hydrogels. In general, more invasive cells (MDA-MD-231, 4T1, $KP^{R172H}C$ and SW620) increased their viscoelastic properties with the increment of the hydrogel stiffness. However, this type of change is dependent of the type of cells, for example, the MDA-MB-231 and $KP^{R172H}C$ changed from a viscous cytoplasm to a more elastic phenotype when exposed to the denser collagen networks, while the 4T1 and SW620 cells, that were more elastic on soft matrices, had an opposite response, increasing their viscosity on dense collagen matrices [104]. Moreover, paediatric osteosarcoma cell line U2OS and the breast adenocarcinoma cells MDA-MB-231, behave differently when culture on 3D collagen hydrogels with modulus from 10 to 200 kPa. [106] Larger osteosarcoma spheroids (335-395) were formed on the stiffest hydrogels, whereas bigger adenocarcinoma spheroids (550-800 μm) are present in softer gel. Actually, the formation of cancer cells spheroids is also sensitive to the surrounding matrix stiffness. MCF-7 breast cancer cells were encapsulated into 3D PEG-heparin hydrogels and the formation of tumor spheroids were evaluated in response to the mechanical properties of the surrounding 3D environment [107]. The PEG-heparin matrix presenting a Young's modulus between 2 000 and 20 000 Pa showed a relevant impact on the size of cellular spheroids. The mechanical stress induced by the stiffer hydrogels lead to an increased cellular packing density in the spheroids, without a relevant impact on cell proliferation or apoptosis. MCF7 cells isolated from stiffer hydrogels showed increase CK8/18 expression that are reported to play a critical role in protecting tissues and cells from mechanical stress [108]. In fact, the mechanical properties of PEG-based hydrogels modulate the proliferation of prostate cancer cells (LNCaP). Higher inhibition of cellular proliferation was observed in hydrogels prepared with 2.5% of PEG, when compared with the hydrogels prepared with 1.5% or 2% of PEG. This was described as a consequence of the depletion of nutrients in the cellular environment due to their limited diffusion through the TME [90]. The chemical modification of PEG with thiol groups, allows the crosslinking of the hydrogels through the formation of PEG-dithiol linkages [109, 110]. This strategy is also a feasible approach to tune the mechanical properties of the hydrogels, by changing the concentrations of linker and initiator, without changing the PEG concentration. The creation of patterned regions with alternated stiffness and concentrations of RGD sequences has been also tested. Results with HT-1080 human fibrosarcoma cells, showed that, well cultured on softer (100 Pa) regions, cells invert their direction or form aggregates at the interface with stiffer domains (i.e. 360 Pa). The same type of cells seeded on stiffer regions were less motile, while they tend to migrate to the softer domains [88, 111]. 3D Alg-Collagen blends have been also reported has a platform to study the impact of mechanical properties of the extracellular space in the morphology and phenotype of breast cancer-associated fibroblasts (bCAFs). It was found a linear relationship between the hydrogel's stiffness, cell

morphology and expression of mechanosensitive proteins. In particular, bCAFs assume a spindle-like shape on soft matrices (≈100 Pa), in contrast, cells encapsulated on stiffer networks (≈ 900 Pa) presented a round shape. The expression and nuclear translocation of YAP/TAZ mechanosignalling protein was also observed in softer 3D matrices [69]. Alg beads of varying stiffness, from 21 to 105 kPa were used as 3D models to encapsulate human head and neck squamous cell carcinoma (HNSCC) tumor initiating cells (TICs) [112]. In this case, CD44 and ABCG2 were used as TICs markers and an upregulation was detected on cells seeded on a matrix of moderate stiffness (i.e. 70 kPa). The same matrix induced high cellular proliferation, however, this Alg-based system does not provide any enriched adhesive sites for cellular attachment. Despite this drawback, it was detected cell-cell contacts leading to the formation of spheroids and to the secretion of ECM, maintaining cellular viability. Fibrin-based gels with stiffness of 90 Pa [113] were also used to evaluate its capacity to support the proliferation of murine B16-F1 melanoma cells. This system was able to induce the formation of larger tumor spheroids, when compared to the gels of higher stiffness (i.e. 420 and 1 050 Pa). Moreover, when different cell types were compared, namely, murine H22 hepatocarcinoma cells, murine EL4 lymphoma cells (suspension growth cell types), murine P815 lymphoblast-like mastocytoma cells, human A2780 ovarian cancer cells and human HepG2 liver carcinoma cells (all adherent-dependent cells), the softer 90 Pa fibrin hydrogels were preferable for the formation of spheroids. In general, the impact of the mechanical properties in cancer cell behaviour is dependent on the specific cell type and their original TME mechanical features.

2-4. Conclusions and Future Remarks

The development of matrices that mimic the characteristics of the TME is of great interest and a reliable approach for the *in vitro* study of cancer behaviour under different experimental conditions. The inability of the 2D systems to completely recapitulate the TME and the *in vivo* cellular behaviour, led to the recent developments that tries to mimic the TME under a 3D configuration. The present state of the proposed 3D models mimics some important biochemical and biomechanical features, closer to the ones that are present in the *in vivo* environment. The use of natural materials to generate this 3D environment has the major advantage of being a close mimic of components present in the native ECM, however, its main disadvantage is the presence of a high batch to batch variability. The use of materials that present a high level of control over their chemical composition is desirable to fully mimic the TME.

Analysing the presently proposed systems, it is clear that they can recapitulate some of the TME biochemical or biomechanical features (e.g. porosity, stiffness, topography, and investigate single components involved in the tumor progression by the incorporation of single ECM cues, such as, growth factors, cytokines, enzymes, etc.). However, a complete mimic of the TME is still to be developed. Anyway, the present systems are able to study the TME dynamics, as well as to evaluate the efficacy of anti-cancer compounds under a drug screening approach. The further increase in complexity of these 3D systems (being closer mimics of the TME) is expected to lead to the generation of models that better recapitulate the *in vivo* scenario. These 3D matrices expected to be proposed in the near future can be a valid alternative to the use of animal models, where relevant conclusions can be drawn on the mechanisms of tumor progression and the suitability of these systems to evaluate the efficacy of different anti-cancer drugs to treat cancer or to control its progression.

2-5. REFERENCES

1. Hui, L.L. and Y. Chen, *Tumor microenvironment: Sanctuary of the devil.* Cancer Letters, 2015. **368**(1): p. 7-13.

2. Quail, D.F. and J.A. Joyce, *Microenvironmental regulation of tumor progression and metastasis.* Nat Med, 2013. **19**(11): p. 1423-37.

3. Filipe, E.C., J.L. Chitty, and T.R. Cox, *Charting the unexplored extracellular matrix in cancer.* Int J Exp Pathol, 2018. **99**(2): p. 58-76.

4. Xiong, G.-F. and R. Xu, *Function of cancer cell-derived extracellular matrix in tumor progression.* Journal of Cancer Metastasis and Treatment, 2016. **2**(9).

5. Walker, C., E. Mojares, and A. Del Rio Hernandez, *Role of Extracellular Matrix in Development and Cancer Progression.* Int J Mol Sci, 2018. **19**(10).

6. Bonnans, C., J. Chou, and Z. Werb, *Remodelling the extracellular matrix in development and disease.* Nature Reviews Molecular Cell Biology, 2014. **15**(12): p. 786-801.

7. Lu, P.F., V.M. Weaver, and Z. Werb, *The extracellular matrix: A dynamic niche in cancer progression.* Journal of Cell Biology, 2012. **196**(4): p. 395-406.

8. Malandrino, A., et al., *Complex mechanics of the heterogeneous extracellular matrix in cancer.* Extreme Mech Lett, 2018. **21**: p. 25-34.

9. Tibbitt, M.W. and K.S. Anseth, *Hydrogels as Extracellular Matrix Mimics for 3D Cell Culture.* Biotechnology and Bioengineering, 2009. **103**(4): p. 655-663.

10. Hynes, R.O. and A. Naba, *Overview of the Matrisome-An Inventory of Extracellular Matrix Constituents and Functions.* Cold Spring Harbor Perspectives in Biology, 2012. **4**(1).

11. Sapudom, J., et al., *Molecular weight specific impact of soluble and immobilized hyaluronan on CD44 expressing melanoma cells in 3D collagen matrices.* Acta Biomater, 2017. **50**: p. 259-270.

12. Zhao, Y.F., et al., *Modulating Three-Dimensional Microenvironment with Hyaluronan of Different Molecular Weights Alters Breast Cancer Cell Invasion Behavior.* ACS Appl Mater Interfaces, 2017. **9**(11): p. 9327-9338.

13. Canibano-Hernandez, A., et al., *Alginate Microcapsules Incorporating Hyaluronic Acid Recreate Closer in Vivo Environment for Mesenchymal Stem Cells.* Mol Pharm, 2017. **14**(7): p. 2390-2399.

14. Weiss, M.S., et al., *The impact of adhesion peptides within hydrogels on the phenotype and signaling of normal and cancerous mammary epithelial cells.* Biomaterials, 2012. **33**(13): p. 3548-59.

15. Pranav, S., et al., *Cancer cell migration within 3D layer-by-layer microfabricated photocrosslinked PEG scaffolds with tunable stiffness.* Biomaterials, 2012. **33**(29): p. 7064-7070.

16. Kaushik, N., et al., *Proinvasive extracellular matrix remodeling for tumor progression.* Arch Pharm Res, 2019. **42**(1): p. 40-47.

17. Turner, N.J. and S.F. Badylak, *Biologic scaffolds for musculotendinous tissue repair.* Eur Cell Mater, 2013. **25**: p. 130-43.

18. Kular, J.K., S. Basu, and R.I. Sharma, *The extracellular matrix: Structure, composition, age-related differences, tools for analysis and applications for tissue engineering.* Journal of Tissue Engineering, 2014. **5**: p. 2041731414557112.

19. Chuang, C.H., et al., *Comparison of covalently and physically cross-linked collagen hydrogels on mediating vascular network formation for engineering adipose tissue.* Artif Cells Nanomed Biotechnol, 2018. **46**(sup3): p. S434-S447.

20. Chevallay, B. and D. Herbage, *Collagen-based biomaterials as 3D scaffold for cell cultures: applications for tissue engineering and gene therapy.* Med Biol Eng Comput, 2000. **38**(2): p. 211-8.

21. Sapudom, J., et al., *The phenotype of cancer cell invasion controlled by fibril diameter and pore size of 3D collagen networks.* Biomaterials, 2015. **52**: p. 367-75.

22. Wolf, K., et al., *Physical limits of cell migration: control by ECM space and nuclear deformation and tuning by proteolysis and traction force.* J Cell Biol, 2013. **201**(7): p. 1069-84.

23. Zhang, H., et al., *Membrane associated collagen XIII promotes cancer metastasis and enhances anoikis resistance.* Breast Cancer Res, 2018. **20**(1): p. 116.

24. Sapudom, J., et al., *Fibril bending stiffness of 3D collagen matrices instructs spreading and clustering of invasive and non-invasive breast cancer cells.* Biomaterials, 2019. **193**: p. 47-57.

25. Plou, J., et al., *From individual to collective 3D cancer dissemination: roles of collagen concentration and TGF-beta.* Sci Rep, 2018. **8**(1): p. 12723.

26. Szot, C.S., et al., *3D in vitro bioengineered tumors based on collagen I hydrogels.* Biomaterials, 2011. **32**(31): p. 7905-12.

27. Theocharis, A.D., D. Manou, and N.K. Karamanos, *The extracellular matrix as a multitasking player in disease.* FEBS J, 2019.

28. Mao, Y. and J.E. Schwarzbauer, *Fibronectin fibrillogenesis, a cell-mediated matrix assembly process.* Matrix Biol, 2005. **24**(6): p. 389-99.

29. Wang, J.P. and A. Hielscher, *Fibronectin: How Its Aberrant Expression in Tumors May Improve Therapeutic Targeting.* Journal of Cancer, 2017. **8**(4): p. 674-682.

30. Sapudom, J., et al., *The interplay of fibronectin functionalization and TGF-beta1 presence on fibroblast proliferation, differentiation and migration in 3D matrices.* Biomater Sci, 2015. **3**(9): p. 1291-301.

31. Sapudom, J. and T. Pompe, *Biomimetic tumor microenvironments based on collagen matrices.* Biomater Sci, 2018. **6**(8): p. 2009-2024.

32. De Wever, O., et al., *Stromal myofibroblasts are drivers of invasive cancer growth.* Int J Cancer, 2008. **123**(10): p. 2229-38.

33. Frantz, C., K.M. Stewart, and V.M. Weaver, *The extracellular matrix at a glance.* Journal of Cell Science, 2010. **123**(24): p. 4195-4200.

34. Insua-Rodriguez, J. and T. Oskarsson, *The extracellular matrix in breast cancer.* Adv Drug Deliv Rev, 2016. **97**: p. 41-55.

35. Eke, I., et al., *3D matrix-based cell cultures: Automated analysis of tumor cell survival and proliferation.* Int J Oncol, 2016. **48**(1): p. 313-21.

36. Kenny, P.A., et al., *The morphologies of breast cancer cell lines in three-dimensional assays correlate with their profiles of gene expression.* Molecular Oncology, 2007. **1**(1): p. 84-96.

37. Gomes, L.R., A.T. Vessoni, and C.F. Menck, *Three-dimensional microenvironment confers enhanced sensitivity to doxorubicin by reducing p53-dependent induction of autophagy.* Oncogene, 2015. **34**(42): p. 5329-40.

38. Stavolone, L. and V. Lionetti, *Extracellular Matrix in Plants and Animals: Hooks and Locks for Viruses.* Front Microbiol, 2017. **8**: p. 1760.

39. Kowitsch, A., A. Chhalotre, and T. Groth, *Effect of thiolated glycosaminoglycans on the behavior of breast cancer cells: toward the development of in vitro models of cancer.* Int J Artif Organs, 2017. **40**(1): p. 31-39.

40. Wang, M., et al., *Glycosaminoglycans (GAGs) and GAG mimetics regulate the behavior of stem cell differentiation.* Colloids Surf B Biointerfaces, 2017. **150**: p. 175-182.

41. Richter, R.P., et al., *Glycosaminoglycans in extracellular matrix organisation: are concepts from soft matter physics key to understanding the formation of perineuronal nets?* Curr Opin Struct Biol, 2018. **50**: p. 65-74.

42. Soares da Costa, D., R.L. Reis, and I. Pashkuleva, *Sulfation of Glycosaminoglycans and Its Implications in Human Health and Disorders.* Annu Rev Biomed Eng, 2017. **19**: p. 1-26.

43. Fernandez-Vega, I., et al., *Specific genes involved in synthesis and editing of heparan sulfate proteoglycans show altered expression patterns in breast cancer.* Bmc Cancer, 2013. **13**.

44. Kalathas, D., et al., *Alterations of glycosaminoglycan disaccharide content and composition in colorectal cancer: Structural and expressional studies.* Oncology Reports, 2009. **22**(2): p. 369-375.

45. Vallen, M.J.E., et al., *Highly sulfated chondroitin sulfates, a novel class of prognostic biomarkers in ovarian cancer tissue.* Gynecologic Oncology, 2012. **127**(1): p. 202-209.

46. Kultti, A., et al., *Accumulation of extracellular hyaluronan by hyaluronan synthase 3 promotes tumor growth and modulates the pancreatic cancer microenvironment.* Biomed Res Int, 2014. **2014**: p. 817613.

47. Toole, B.P., *Hyaluronan: From extracellular glue to pericellular cue.* Nature Reviews Cancer, 2004. **4**(7): p. 528-539.

48. Price, Z.K., N.A. Lokman, and C. Ricciardelli, *Differing Roles of Hyaluronan Molecular Weight on Cancer Cell Behavior and Chemotherapy Resistance.* Cancers (Basel), 2018. **10**(12).

49. Senbanjo, L.T. and M.A. Chellaiah, *CD44: A Multifunctional Cell Surface Adhesion Receptor Is a Regulator of Progression and Metastasis of Cancer Cells.* Frontiers in Cell and Developmental Biology, 2017. **5**(18).

50. Freudenberg, U., et al., *Glycosaminoglycan-Based Biohybrid Hydrogels: A Sweet and Smart Choice for Multifunctional Biomaterials.* Adv Mater, 2016. **28**(40): p. 8861-8891.

51. Gil, M.S., et al., *Injectable hydrogel-incorporated cancer cell-specific cisplatin releasing nanogels for targeted drug delivery.* Journal of Materials Chemistry B, 2017. **5**(34): p. 7140-7152.

52. Wang, Y., et al., *3D hydrogel breast cancer models for studying the effects of hypoxia on epithelial to mesenchymal transition.* Oncotarget, 2018. **9**(63): p. 32191-32203.

53. Ananthanarayanan, B., Y. Kim, and S. Kumar, *Elucidating the mechanobiology of malignant brain tumors using a brain matrix-mimetic hyaluronic acid hydrogel platform.* Biomaterials, 2011. **32**(31): p. 7913-7923.

54. Pedron, S., E. Becka, and B.A.C. Harley, *Regulation of glioma cell phenotype in 3D matrices by hyaluronic acid.* Biomaterials, 2013. **34**(30): p. 7408-7417.

55. Gurski, L.A., et al., *Hyaluronic acid-based hydrogels as 3D matrices for in vitro evaluation of chemotherapeutic drugs using poorly adherent prostate cancer cells.* Biomaterials, 2009. **30**(30): p. 6076-6085.

56. Gurski, L.A., et al., *Hyaluronan (HA) Interacting Proteins RHAMM and Hyaluronidase Impact Prostate Cancer Cell Behavior and Invadopodia Formation in 3D HA-Based Hydrogels.* PLOS ONE, 2012. **7**(11): p. e50075.

57. Tang, Y., et al., *Three-dimensional prostate tumor model based on a hyaluronic acid-alginate hydrogel for evaluation of anti-cancer drug efficacy.* J Biomater Sci Polym Ed, 2017. **28**(14): p. 1603-1616.

58. Mikami, T. and H. Kitagawa, *Biosynthesis and function of chondroitin sulfate.* Biochimica et Biophysica Acta (BBA) - General Subjects, 2013. **1830**(10): p. 4719-4733.

59. Theocharis, A.D., et al., *Chondroitin Sulfate as a Key Molecule in the Development of Atherosclerosis and Cancer Progression.* Chondroitin Sulfate: Structure, Role and Pharmacological Activity, 2006. **53**: p. 281-295.

60. Sugahara, K. and H. Kitagawa, *Recent advances in the study of the biosynthesis and functions of sulfated glycosaminoglycans.* Current Opinion in Structural Biology, 2000. **10**(5): p. 518-527.

61. Brauchle, E., et al., *Biomechanical and biomolecular characterization of extracellular matrix structures in human colon carcinomas.* Matrix Biol, 2018. **68-69**: p. 180-193.

62. O'Brien, F.J., et al., *The effect of pore size on cell adhesion in collagen-GAG scaffolds.* Biomaterials, 2005. **26**(4): p. 433-41.

63. Curtin, C., et al., *A physiologically relevant 3D collagen-based scaffold-neuroblastoma cell system exhibits chemosensitivity similar to orthotopic xenograft models.* Acta Biomater, 2018. **70**: p. 84-97.

64. Liu, Y., et al., *Development of a Biomimetic Chondroitin Sulfate-modified Hydrogel to Enhance the Metastasis of Tumor Cells.* Sci Rep, 2016. **6**: p. 29858.

65. Andersen, T., P. Auk-Emblem, and M. Dornish, *3D Cell Culture in Alginate Hydrogels.* Microarrays (Basel), 2015. **4**(2): p. 133-61.

66. Wisdom, K. and O. Chaudhuri, *3D Cell Culture in Interpenetrating Networks of Alginate and rBM Matrix.* Methods Mol Biol, 2017. **1612**: p. 29-37.

67. Kang, S.W., et al., *The Effect of Conjugating RGD into 3D Alginate Hydrogels on Adipogenic Differentiation of Human Adipose-Derived Stromal Cells.* Macromolecular Bioscience, 2011. **11**(5): p. 673-679.

68. Little, C.J., W.M. Kulyk, and X. Chen, *The Effect of Chondroitin Sulphate and Hyaluronic Acid on Chondrocytes Cultured within a Fibrin-Alginate Hydrogel.* J Funct Biomater, 2014. **5**(3): p. 197-210.

69. Cao, H., et al., *Mechanoregulation of Cancer-Associated Fibroblast Phenotype in Three-Dimensional Interpenetrating Hydrogel Networks.* Langmuir, 2019. **35**(23): p. 7487-7495.

70. Liu, C., et al., *Hybrid collagen alginate hydrogel as a platform for 3D tumor spheroid invasion.* Acta Biomater, 2018. **75**: p. 213-225.

71. Qiao, S.P., et al., *An alginate-based platform for cancer stem cell research.* Acta Biomater, 2016. **37**: p. 83-92.

72. Estrada, M.F., et al., *Modelling the tumour microenvironment in long-term microencapsulated 3D co-cultures recapitulates phenotypic features of disease progression.* Biomaterials, 2016. **78**: p. 50-61.

73. Rinaudo, M., *Main properties and current applications of some polysaccharides as biomaterials.* Polymer International, 2008. **57**(3): p. 397-430.

74. Jayakumar, R., et al., *Biomedical applications of chitin and chitosan based nanomaterials-A short review.* Carbohydrate Polymers, 2010. **82**(2): p. 227-232.

75. Ahmadi, F., et al., *Chitosan based hydrogels: characteristics and pharmaceutical applications.* Research in Pharmaceutical Sciences, 2015. **10**(1): p. 1-16.

76. Dhiman, H.K., A.R. Ray, and A.K. Panda, *Characterization and evaluation of chitosan matrix for in vitro growth of MCF-7 breast cancer cell lines.* Biomaterials, 2004. **25**(21): p. 5147-54.

77. Leung, M., et al., *Chitosan-alginate scaffold culture system for hepatocellular carcinoma increases malignancy and drug resistance.* Pharm Res, 2010. **27**(9): p. 1939-48.

78. Florczyk, S.J., et al., *3D porous chitosan-alginate scaffolds: a new matrix for studying prostate cancer cell-lymphocyte interactions in vitro.* Adv Healthc Mater, 2012. **1**(5): p. 590-9.

79. Kievit, F.M., et al., *Modeling the tumor microenvironment using chitosan-alginate scaffolds to control the stem-like state of glioblastoma cells.* Biomater Sci, 2016. **4**(4): p. 610-3.

80. Kievit, F.M., et al., *Chitosan-alginate 3D scaffolds as a mimic of the glioma tumor microenvironment.* Biomaterials, 2010. **31**(22): p. 5903-10.

81. Wang, K., et al., *Culture on 3D Chitosan-Hyaluronic Acid Scaffolds Enhances Stem Cell Marker Expression and Drug Resistance in Human Glioblastoma Cancer Stem Cells.* Adv Healthc Mater, 2016. **5**(24): p. 3173-3181.

82. Florczyk, S.J., et al., *Porous chitosan-hyaluronic acid scaffolds as a mimic of glioblastoma microenvironment ECM.* Biomaterials, 2013. **34**(38): p. 10143-50.

83. Wong, C.W., et al., *Biomaterial substrate-derived compact cellular spheroids mimicking the behavior of pancreatic cancer and microenvironment.* Biomaterials, 2019. **213**: p. 119202.

84. Gu, L. and D.J. Mooney, *Biomaterials and Emerging Anticancer Therapeutics: Engineering the Microenvironment.* Nat Rev Cancer, 2016. **16**(1): p. 56-66.

85. Cruz-Acuna, R. and A.J. Garcia, *Synthetic hydrogels mimicking basement membrane matrices to promote cell-matrix interactions.* Matrix Biol, 2017. **57-58**: p. 324-333.

86. Enemchukwu, N.O., et al., *Synthetic matrices reveal contributions of ECM biophysical and biochemical properties to epithelial morphogenesis.* J Cell Biol, 2016. **212**(1): p. 113-24.

87. Bellis, S.L., *Advantages of RGD peptides for directing cell association with biomaterials.* Biomaterials, 2011. **32**(18): p. 4205-10.

88. Singh, S.P., et al., *A peptide functionalized poly(ethylene glycol) (PEG) hydrogel for investigating the influence of biochemical and biophysical matrix properties on tumor cell migration.* Biomater Sci, 2014. **2**(7): p. 1024-1034.

89. Sridhar, B.V., et al., *Development of a cellularly degradable PEG hydrogel to promote articular cartilage extracellular matrix deposition.* Adv Healthc Mater, 2015. **4**(5): p. 702-13.

90. Sieh, S., et al., *Phenotypic Characterization of Prostate Cancer LNCaP Cells Cultured within a Bioengineered Microenvironment.* Plos One, 2012. **7**(9).

91. Pradhan, S., et al., *PEG-fibrinogen hydrogels for three-dimensional breast cancer cell culture.* J Biomed Mater Res A, 2017. **105**(1): p. 236-252.

92. Pradhan, S., et al., *A three-dimensional spheroidal cancer model based on PEG-fibrinogen hydrogel microspheres.* Biomaterials, 2017. **115**: p. 141-154.

93. Polonio-Alcala, E., et al., *PLA Electrospun Scaffolds for Three-Dimensional Triple-Negative Breast Cancer Cell Culture.* Polymers (Basel), 2019. **11**(5).

94. Polonio-Alcala, E., et al., *Screening of Additive Manufactured Scaffolds Designs for Triple Negative Breast Cancer 3D Cell Culture and Stem-Like Expansion.* Int J Mol Sci, 2018. **19**(10): p. 3148.

95. Kim, J.W., W.J. Ho, and B.M. Wu, *The role of the 3D environment in hypoxia-induced drug and apoptosis resistance.* Anticancer Res, 2011. **31**(10): p. 3237-45.

96. Rezvantalab, S., et al., *PLGA-Based Nanoparticles in Cancer Treatment.* Front Pharmacol, 2018. **9**: p. 1260.

97. Fong, E.L., et al., *Modeling Ewing sarcoma tumors in vitro with 3D scaffolds.* Proc Natl Acad Sci U S A, 2013. **110**(16): p. 6500-5.

98. Rabionet, M., et al., *Electrospinning PCL Scaffolds Manufacture for Three-Dimensional Breast Cancer Cell Culture.* Polymers (Basel), 2017. **9**(8).

99. Yingzi, L., et al., *Effects of mechanical properties on tumor invasion: insights from a cellular model.* Conf Proc IEEE Eng Med Biol Soc, 2014. **2014**: p. 6818-21.

100. Yu, H., J.K. Mouw, and V.M. Weaver, *Forcing form and function: biomechanical regulation of tumor evolution.* Trends Cell Biol, 2011. **21**(1): p. 47-56.

101. Cox, T.R. and J.T. Erler, *Remodeling and homeostasis of the extracellular matrix: implications for fibrotic diseases and cancer.* Dis Model Mech, 2011. **4**(2): p. 165-78.

102. Butcher, D.T., T. Alliston, and V.M. Weaver, *A tense situation: forcing tumour progression.* Nat Rev Cancer, 2009. **9**(2): p. 108-22.

103. Northcott, J.M., et al., *Feeling Stress: The Mechanics of Cancer Progression and Aggression.* Front Cell Dev Biol, 2018. **6**: p. 17.

104. Wullkopf, L., et al., *Cancer cells' ability to mechanically adjust to extracellular matrix stiffness correlates with their invasive potential.* Mol Biol Cell, 2018. **29**(20): p. 2378-2385.

105. Kim, J.E., et al., *Characterization of the mechanical properties of cancer cells in 3D matrices in response to collagen concentration and cytoskeletal inhibitors.* Integr Biol (Camb), 2018. **10**(4): p. 232-241.

106. Charoen, K.M., et al., *Embedded multicellular spheroids as a biomimetic 3D cancer model for evaluating drug and drug-device combinations.* Biomaterials, 2014. **35**(7): p. 2264-71.

107. Taubenberger, A.V., et al., *3D microenvironment stiffness regulates tumor spheroid growth and mechanics via p21 and ROCK.* bioRxiv, 2019: p. 586784.

108. Pastuszak, M., et al., *Cytokeratins in gastroenterology. Systematic review.* Prz Gastroenterol, 2015. **10**(2): p. 61-70.

109. Lin, C.C., A. Raza, and H. Shih, *PEG hydrogels formed by thiol-ene photo-click chemistry and their effect on the formation and recovery of insulin-secreting cell spheroids.* Biomaterials, 2011. **32**(36): p. 9685-95.

110. Xin, S., O.M. Wyman, and D.L. Alge, *Assembly of PEG Microgels into Porous Cell-Instructive 3D Scaffolds via Thiol-Ene Click Chemistry.* Adv Healthc Mater, 2018. **7**(11): p. e1800160.

111. Hoffmann, J.C. and J.L. West, *Three-dimensional photolithographic micropatterning: a novel tool to probe the complexities of cell migration.* Integr Biol (Camb), 2013. **5**(5): p. 817-27.

112. Liu, C., et al., *Potential effect of matrix stiffness on the enrichment of tumor initiating cells under three-dimensional culture conditions.* Exp Cell Res, 2015. **330**(1): p. 123-34.

113. Liu, J., et al., *Soft fibrin gels promote selection and growth of tumorigenic cells.* Nat Mater, 2012. **11**(8): p. 734-744.

Section II

Experimental materials and methodologies

Chapter 3

Materials and Methods

Chapter 3

Materials and Methods

This Chapter contains detailed information on the experimental procedures, that were used throughout this thesis, and that are briefly described in the subsequent chapters. In general, herein is described the materials and methods used for the preparation of the 2D and 3D systems used in chapters 4-8, as well as the experimental conditions and techniques used to characterize the developed biomaterials.

3-1. MATERIALS

The following section describes the main biomaterials used for the preparation of the 2D and 3D systems developed under this thesis.

3-1.1. Hyaluronic Acid

Hyaluronic Acid or Hyaluronan (HA) is a linear polysaccharide derived from the repeating unit of glucuronic acid and N-acetylglucosamine, linked by glycosidic bonds. [1] The most common HA used on biomedical applications is of recombinant origin, obtained from pathogenic bacteria such *Streptococcus zooepidemicus,* through fermentation processes [2], as a mild acid but when under physiological conditions becomes a salt, typically as a sodium salt. [3] For the build-up of the multilayered films, HA was used as a polyanion, taking advantage of the charged carboxylic acid group - COO^-, allowing for the formation of ionic or covalent bonds, when in contact with a polycation or reactive amine groups, respectively. Under physiological salt conditions, as the ones used in the experimental chapters (*i.e.* 0.15M sodium chloride), HA acquires an extended random coil conformation [4], which allows it to better interact with positively charged surfaces (as in the layer-by-layer assembly, as

discussed later). The HA used throughout this thesis was obtained from Lifecore Biomedical as Sodium Hyaluronate, with three different molecular weights (Mws): HA of low Mw, *i.e.* 6.4kDa, HA of medium Mw, *i.e.* 752 kDa and HA of high Mw, *i.e.* 1500kDa. The HA was used as received without any additional purification step.

3-1.2. Poly-L-lysine

Poly-l-lysine (PLL) is a polypeptide derived from the natural occurring amino acid lysine, with a positive charge when protonated. [5] PLL is usually used as a polymer used to functionalize surfaces to promote the adhesion of cells and different biomolecules. [6] It is also widely reported as an element of the layer-by-layer (LbL) technique, due to its easy handling and ability to spontaneously adsorb onto negatively-charged surfaces [7], spheres [8] or 3D hydrogels [9]. In this thesis, the PLL was used as a polycation for the immobilization of the negatively charged HA. The PLL hydrobromide of 30-70 kDa (33 200Da characterized by viscosity) was purchased from Sigma and used as received without any additional purification.

3-1.3. Alginate

Alginate (Alg) is a polysaccharide harvested from brown seaweeds and widely used for biomedical applications. [10] It is widely used for the development of 3D hydrogels, due to its mild crosslinking conditions, *i.e.* in the presence of divalent calcium cations, Ca^{2+}, forming the so-called “egg-box” structure. [11, 12] The main drawback of Alg is the lack on cell adhesive sites, which is typically overcome with its combination with peptides or other biomolecules that can be recognized by cells. [13] On chapter 8, it was used sodium Alg, Pronova UP VLVG, with very low viscosity <20 mPas, obtained from NovaMatrix (Norway). Alg was used as received to prepare the 3D Alg and Alg-HA hydrogels.

3-2. PROCESSING OF BIOMATERIALS

The processing methodologies used to develop the biomedical devices evaluated during this thesis is described in the following section.

3-2.1. Layer-by-layer assembly

The layer-by-layer (LbL) is a well-known assembly technique to build-up multi-layered films, taking advantage of the electrostatic interactions between oppositely charged polyelectrolytes. [14] LbL is a highly versatile method that allows the construction of films presenting nano- to microscale thicknesses, with tunable chemical and physical composition (*e.g.* thickness, stiffness, hydration, etc.). [15] In this thesis, the LbL assembly was used to develop multi-layered films composed by PLL and HA. The assembly between the polycation PLL and the polyanion HA is driven by electrostatic interactions through their oppositely charged groups, *i.e.* $-NH_4^+$ and $-COO^-$, respectively. In Chapter 4 we also tested the impact of covalent crosslinking to improve the bioactivity and stability of the LbL systems. A typical process for the assembly of the LbL films was the immobilization of the polyelectrolytes on a gold-coated glasses 1x1 cm^2 (Chapters 4 and 5) or on tissue culture polystyrene, TCPS discs of 13mm diameter (Chapters 6 and 7), through the alternating dipping of positively charged polyelectrolyte, PLL, and negatively charged polyelectrolyte, HA. In all the cases, the LbL build-up was performed using a first layer of PLL, generated by dipping the surface in a PLL solution (0.5 $mg.mL^{-1}$ in 0.15M NaCl) for 15min; followed by washing (0.15M NaCl, pH ≈ 6.0 – 6.5) and immersion into the HA solution (1$mg.mL^{-1}$ in 0.15M NaCl). The alternate dipping of the surfaces into the PLL and HA solutions were repeated until the desired number of layers were assembled. On Chapters 4, 6 and 7 we generated 10-layers' systems $(PLL\text{-}HA)_5$, while on Chapter 5, 2-layers' system were assembled, *i.e.* (PLL-HA). In all the cases, upon assembly, the LbL coated substrates were rinsed with water (to remove the excess of NaCl), dried at room temperature and characterized or used in further studies.

3-2.2. Covalent crosslinking of the LbL systems

During the film construction, covalent bonds between PLL and HA was formed using a carbodiimide-based crosslinking. This reaction was promoted by using a combination of N-(3-dimethylaminopropyl)-N′-ethylcarbodiimide hydrochloride (EDC) and N-hydroxysuccinimide (NHS), a commonly-employed crosslinking system, that induces the reaction between primary amines and carboxylic acids. This EDC/NHS system and have been described in the literature to generate PLL-HA assemblies with improved stability [16]. Briefly, EDC reacts with the carboxylic acid groups from the HA to form an active O-acylisourea intermediate, which can further react directly with the amine groups of PLL. The presence of NHS improves the coupling efficiency between HA and the primary amines of PLL: O-acylisourea intermediates (from HA) react with NHS, forming NHS-ester intermediates, increasing the kinetics of the reaction with the PLL amines to form the final amide bonds (Figure 1).

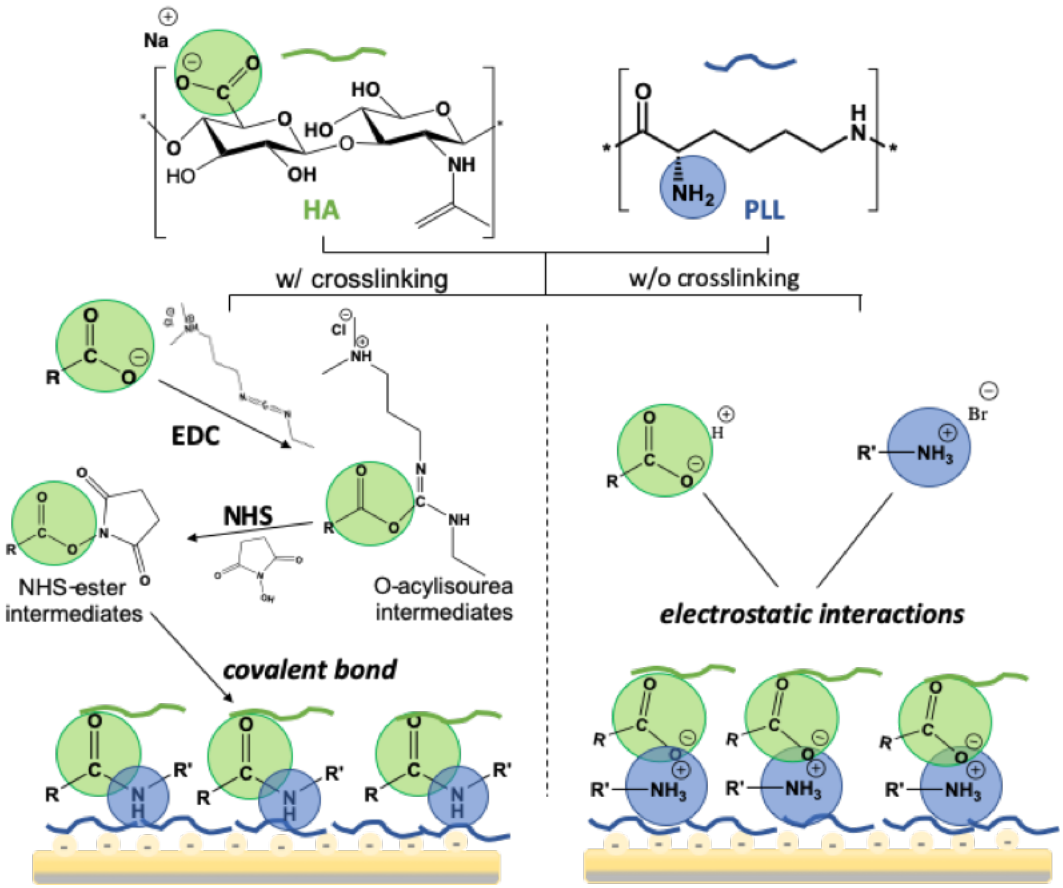

Figure 3-1. Schematic representation of PLL-HA interactions generated during the LbL assembly, in the absence/presence of covalent crosslinking (EDC/NHS).

In the absence of EDC/NHS the stability of the LbL system is based on the electrostatic interactions between the polycation and polyanion, PLL and HA in our case. Due to the complexity of the system and the process of LbL assembly and to improve the efficiency of the the covalent crosslinking, each layer was individually activated and covalently bond to the adsorbed LbL system. This was executed through the supplementation of the HA solution with EDC (at a concentration of 0.4M) and NHS (at 0.100M). All the remaining process was similar to the one typically used to generate LbL systems in the absence of crosslinker, *i.e.* based only in electrostatic interactions.

3-2.3. Alginate-based 3D hydrogels

On Chapter 8 the 3D Alg-based hydrogels were used as an extracellular matrix (ECM) model for the immobilization and presentation of HA of different Mws in a biologically relevant manner. As mentioned before, the lack of adhesive sites on the Alg molecule, confers to this polysaccharide a non-bioactive character, which results in the generation of a simple physical support for the immobilization of HA, as well as for the encapsulation of cells, being biologically inert, *i.e.* without cellular recognition motifs. The 3D system consisted on a core-shell hydrogel, that mimics the tumor parenchyma, in the core, and the surrounding healthy cells, in the shell.

To generate this system, the Alg and HA were dissolved in Milli-Q water (with 0.15M NaCl), and mixed to a final concentration of 20mg.mL^{-1} of Alg and 1mg.mL^{-1} of HA. For the preparation of the core hydrogels, a sphere was generated by the extrusion of the mixture through a 27G syringe into a 100mM $CaCl_2$ bath under constant magnetic stirring. After gelation, the spheres were washed with TBS supplemented with 15mM of $CaCl_2$. The Alg or Alg-HA_{Mw} spheres were embedded on a pre-gelated Alg disc and the core-shell hydrogels were allowed to crosslink on a QGel® mould, filled with 50mM of $CaCl_2$ for 15min. Finally, the hydrogel was washed with TBS-$CaCl_2$.

For the encapsulation of cancer cells, MKN45, in the core they were suspended (at a concentration of 5x10^6 cells/mL) in the solution of Alg or Alg-HA prior to the extrusion of the sphere. To encapsulate the healthy cells, bone marrow mesenchymal stem cells (bmMSCs), they were suspended (at a concentration of 2x10^6 cell/mL) on the Alg solution before the formation of the shell (see Figure 2). To generate the core-shell system, Alg or Alg-HA_{Mw} core spheres (47μL sphere volume) containing MKN45, were further embedded in an Alg disc (70μL shell volume) encapsulated with bmMSCs. This core-shell

system was incubated for 10 days under alpha Medium (αMEM) or with conditioned medium (CM) from bmMSCs expansion (3 days of cell growth). In the case of the CM, it was diluted with fresh medium (1:1 ratio) and used for the incubation of the hydrogels.

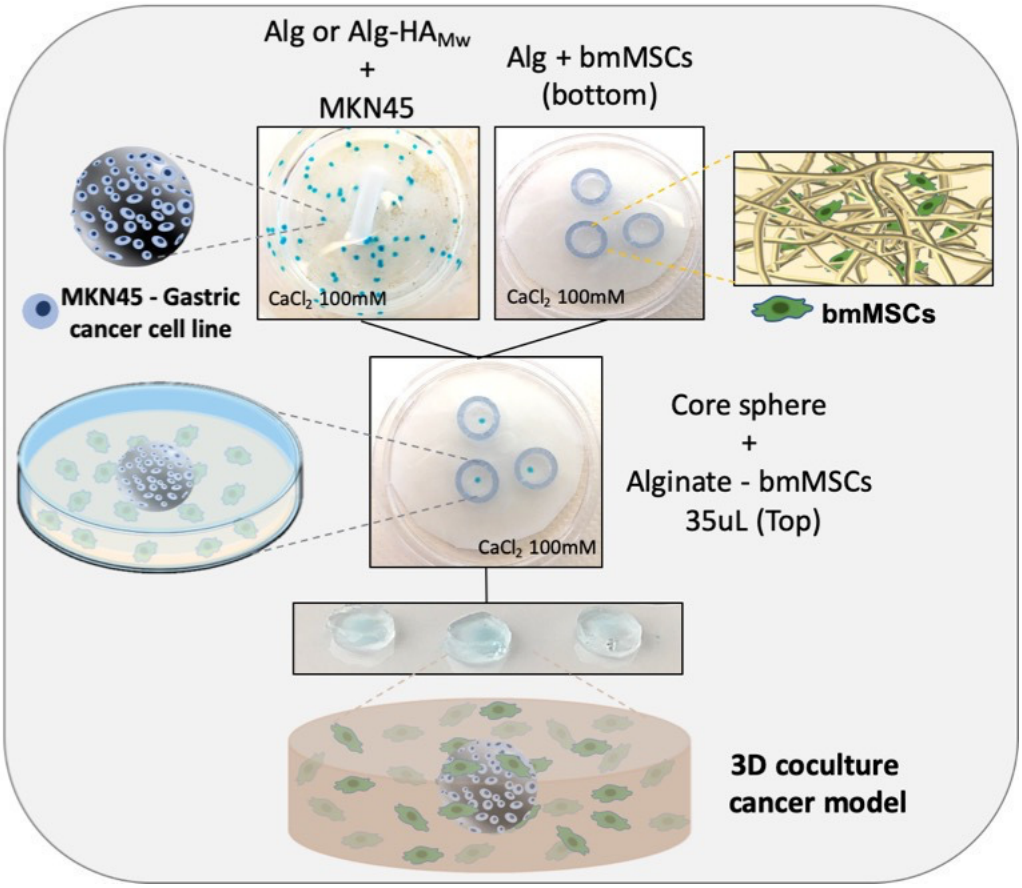

Figure 3-2. Schematic representation of the procedure used to generate the 3D core-shell systems presenting MKN45 cells in the core and bmMSCs in the shell.

The cancer cell line MKN45 (derived from a Human gastric adenocarcinoma) was used on 6th to 7th passage and cultured in RPMI-1640 medium (Sigma-Aldrich, Portugal) supplemented with 10% of foetal bovine serum (FBS; Gibco) and 1% antibiotic/antimycotic solution (final concentration of penicillin 100units/mL, streptomycin 100mg.mL^{-1} and 25μg.mL^{-1} amphotericin B; Gibco, UK).

Mesenchymal stem cells were obtained from Human bone marrow aspirates, collected from healthy patients under the scope of an agreement with Hospital da Prelada (Porto, Portugal). Bone marrow mesenchymal stem cells (bmMSCs) were isolated according to the procedure described elsewhere. [17] Upon isolation, bmMSCs were tested for mesenchymal stem cell markers (CD73,

CD90, CD105) by flow cytometry at different passages to confirm the maintenance of their stemness phenotype. bmMSCs were then expanded in Minimum Essential Medium Eagle with alpha modifications (αMEM) (Sigma-Aldrich, Germany) supplemented with 1% Antibiotic/Antimycotic (Gibco, UK), 10% foetal bovine serum (FBS, Gibco, UK) (final concentration of penicillin 100 units.mL^{-1} and streptomycin 100 mg.mL^{-1}; Gibco, UK), and used at 3rd passage. Both cell types, MKN45 and bmMSCs, were cultured in a 5% CO_2 incubator at 37°C. For the cells' encapsulation studies, MKN45 and bmMSCs were washed with PBS and harvested with TrypLE™ Express before suspension in the respective Alg or Alg-HA_{Mw} solutions.

3-3. MATERIALS CHARACTERIZATION AND BIOLOGICAL ANALYSIS

3-3.1. Quartz Crystal Microbalance with Dissipation (QCM-D)

The Quartz Crystal Microbalance with Dissipation (QCM-D) is a useful technique to study the interaction of different polymers, polymers-proteins, or even the interaction of cells with different surfaces. [18] In this thesis, we used the QCM-D to assess the assembly of PLL and HA of different Mws (Chapter 4 and 5). In addition, the MKN45 cell adhesion was also studied by QCM-D, as well as the cells' capacity to remodel the assembled LbL films (Chapter 7). The adsorption of the CD44 protein (one of the main HA cell surface receptor) onto the $(PLL\text{-}HA)_n$ LbL films was also followed in real-time by QCM-D by monitoring changes in Frequency (Δf, mass) and Dissipation (ΔD, viscoelastic properties).

The QCM-D analysis is based on an acoustic piezoelectric principle. The propagation of an acoustic wave through a solid substrate deposited onto a sensor (*i.e.* gold-coated AT-cut quartz crystals), generated by an alternating voltage. The frequency of the propagation of this acoustic wave through the surface is dependent on the mass of the adsorbed material. [19] Thus, as the adsorbed mass deposited on the quartz crystal increases, the frequency of the sensor decreases. In fact, the frequency shift (*i.e.* Δf) is directly correlated with the adsorbed mass (Δm) as shown in the following equation:

Equation 3-1

$$\Delta m = -\frac{C}{n}\Delta f_n$$

where C is the mass sensitivity constant of the instrument (*i.e.* 17.7 ng/Hz·cm^2) and Δf_n is the change in the resonance frequency at the nth harmonic (n = 1, 3, etc.). [20]

In presence of viscoelastic materials, the shift on the resonance frequency is also sensitive to the adsorbed water, that allows the additional collection of data related with the energy Dissipation (*i.e.* ΔD). The combined analysis of the ΔD and Δf data (which are intimately related) in the presence of the adsorbed layer, we can collect information related with the total adsorbed mass (water included), the hydration, viscoelastic properties, as well as the stability of the adsorbed materials.

We used the QCM-D to study the construction of the LbL films using PLL and HA_{Mw} (Chapter 4 and 5). In this case, the gold-coated AT-cut quartz crystals (QSX301) were placed in the QCM-D flow chamber (Q-Sense E4, Sweden). The temperature was set to 25°C and a stable baseline was acquired using an aqueous solution of NaCl 150mM. Afterwards, a PLL solution (0.5mg/mL in 150mM NaCl) was added to the chamber for 15min. The sensor was rinsed with an aqueous solution of NaCl 150mM to remove loosely bound material. The following HA layer was deposited onto the sensor using a solution of HA_{Mw} (1mg/mL in an aqueous solution of 150mM NaCl) injected into the flow chamber during 15min, followed by a washing step. When in presence of crosslinked films, the HA_{Mw} solutions were supplemented with the crosslinking agents (EDC, 400mM and NHS, 100mM).

On Chapter 4 the adsorption of PLL and HA_{Mw} was repeated until a 10-layers film was obtained, *i.e.* $(PLL\text{-}HA)_5$, while on Chapter 5 only 2-layers were adsorbed, *i.e.* (PLL-HA). In all the cases, the adsorption and washing steps were performed using a flow rate of 50μL.min^{-1}. In both Chapters, the adsorption of CD44 hist-tag protein (orb84335, 10 μg.mL^{-1} in PBS solution with 1% BSA) was injected into the QCM-D chamber using the same flow rate until reaching a stable Δf and ΔD signal.

On Chapter 7 the QCM-D was also used to monitor in real-time the adhesion of MKN45 cells and to evaluate their interaction with the $(PLL\text{-}HA)_5$ LbL films. The $(PLL\text{-}HA_n)_5$ were coated on commercially available gold coated QCM-D crystals (Biolin Scientific, Sweden) using a spin-coater. Briefly, 100μL of each polyelectrolyte solution was allowed to adsorb onto the sensor during 15 min. In this case, upon the adsorption steps, the sensors were spun during 10s at 3000rpm (using a spin

coater) to remove excess solution and unbound material, with an additional spinning at the washing steps (using an aqueous solution of 0.15M NaCl). The coated sensors were placed in the QCM-D flow chamber and a stable baseline was acquired by flowing the RPMI medium at a flow rate of 50μL.min^{-1}. Afterwards, MKN45 cells (0.400×10^{6} cells/mL) were then flowed over the substrates at a flux of 50μL.min^{-1} for at least 1h. The flow was stopped for 1h to allow cell attachment monitored by the QCM-D system (*i.e.* Δf and ΔD). Finally, the sensors were rinsed with RPMI to remove unbound cells, at flow rate of 100μL.min^{-1}.

All measurements were performed at several harmonics (n = 1, 3, 5, 7, 9 and 11, corresponding to 5, 15, 25, 35, 45, 55, and 65MHz, respectively). The $\Delta f_n/n$ and ΔD data were fitted using the Voigt model for the 5th, 7th and 9th overtone using the Q-Sense DFind software or the QTools Software provided by the manufacturer.

3-3.2. Surface Plasmon Resonance (SPR)

The Surface Plasmon Resonance (SPR) provides information about the build-up of a LbL systems or the interaction between polymer-proteins in a similar fashion as the QCM-D technique. SPR is an optical-based method, that monitors changes on the refractive index (n) of a gold surface, in response to the adsorption of a material or the presence of a different media, that alters the detected reflected angle of an incident laser at a certain wavelength (Figure 3). [21]

SPR was used on Chapter 4 to complement the information obtained from the QCM-D. As mentioned in section 3.1, the QCM-D measures the adsorbed mass on a quartz sensor including the polymer and water, which allows the determination of the film properties (thickness, mass and hydration) taking into consideration the coupled water and, thus, the viscoelastic properties of the LbL structure. From the SPR analysis, the water adsorbed during the film buildup is not taken into consideration and only the adsorbed polymer/protein properties are analysed., making the use of both techniques highly complementary.

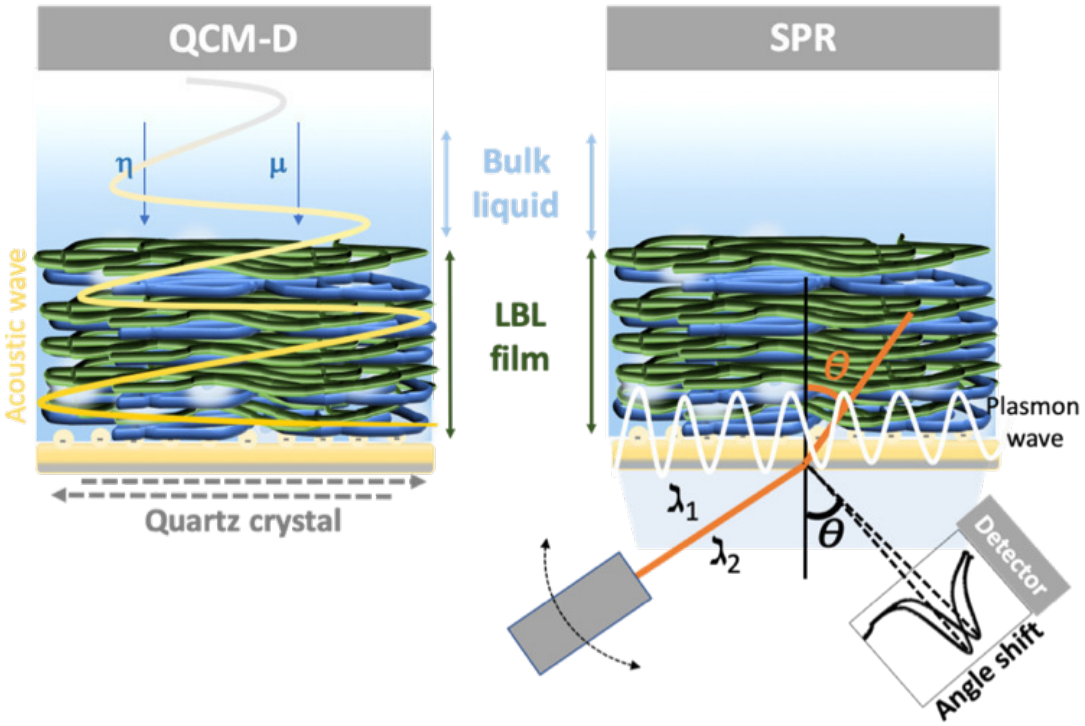

Figure 3-3. Graphical representation of QCM-D and SPR techniques. In the QCM-D experiment, an acoustic sensor under a liquid environment will lose the mechanical energy stored in the oscillation during a specific timeframe, due to the flexibility of the molecules, that move with the oscillating surface [178]. On the SPR measurements, at a certain wavelength and incident angle of light, the changes on the refractive index (n) is detected through an evanescent wave on the sensor. The changes on n at the sensor's surface, through fluctuations on the media or by the adsorption of a material, leads to a loss of the reflected light intensity originating a shift on the SPR angle [177, 179].

We used the multi-parametric SPR (MP-SPR, BioNavis Navi 200, Finland) which performs the full angle scans at two wavelengths, 670 and 785nm. In our case, the $(PLL\text{-}HA)_5$ film was generated in a similar fashion as for the QCM-D experiments. Each layer of PLL or HA, was allowed to adsorb for 5min, followed by a washing step, using an aqueous NaCl 150mM solution, between the injection of each polyelectrolyte. The CD44 his-tag protein was adsorbed under the same conditions, always after the $(PLL\text{-}HA)_5$ build-up. SPR data for the LbL construction were analysed using the Layer Solver software (version 1.3.8, Max Planck Institute for Polymer Research, Mainz, Germany), applying the Fresnels' equation, using the dual-wavelengths method (670 and 785nm). Briefly, the dual-wavelength method correlates linearly the dispersion coefficient and the wavelength changes, which is used to determine the refractive index (*n*). In this method, the LayerSolver software automatically computes the obtained data and returns the values for thickness and *n*. [22]

3-3.3. Atomic Force Microscopy (AFM)

The characterization of the LbL films with the HAs of different Mws was complemented by Atomic Force Microscopy (AFM). The AFM provides information about the mechanical properties (Young's Modulus) of the generated LbL surfaces, as well as, the topographical characteristics (roughness) of the films used on Chapter 4, 5 and 6. The Young's modulus of the 3D culture model, studied on Chapter 8 was also evaluated by AFM.

Both LbL surfaces and 3D hydrogels were analysed using a JPK NanoWizard 3 (JPK, Germany). The Young's Modulus of the $(PLL\text{-}HA)_5$ films were measured under QI Advanced Mode using qp-BioAC-CB3 probes (calibrated using the non-contact method in the JPK software; a resonance frequency of ~23-37kHz and a calibrated spring constant of ~0.065N/m, NanoSensors, Germany) and the Young's Moduli values were obtained by fitting the approach curves with the Hertz/Sneddon model, using a cone tip shape (applying a very short indentation range, 0.5-1nm – to avoid the influence of the substrate). All the experiments were performed under air, while the surfaces were humidified using a drop of PBS. The stiffness of the core Alg and Alg-HA_{Mw} hydrogels with and without MKN45 cells, were measured under QI Advanced Mode using qp-BioAC-CB1 probes (resonance frequency of ~65kHz; spring constant of ~0.30N/m; NanoSensors, Germany). To obtain the Young's Modulus values the approach curves were fitted with the Hertz/Sneddon model, using a cone tip shape. All the experiments were performed under humidified environment using TBS-$CaCl_2$ buffer.

3-3.4. SURPASS – Electrokinetic Analyzer

The zeta potential is an important chemical characteristic that describes the surface charge of a surface when in contact with an electrolyte solution. From the Electrokinetic Analyzer it is possible to obtain information about the surface charge in a wide range of pHs (between 3-11), as well as the isoelectric point. It is also possible to, indirectly, speculate about the functional groups that are exposed on the surface under analysis. [23]

On Chapters 4 and 5, the assembled $(PLL\text{-}HA)_5$ and (PLL-HA) films, respectively, were analysed using an electrokinetic analyzer (SurPASS, Anton Paar, Graz, Austria), assessing the charge of the end-layer of the LbL film. The $(PLL\text{-}HA)_5$ films (gold coated glasses covered with the LbL systems) were mounted in an adjustable gap cell (1x2cm^2). On Chapter 4, the (PLL-HA) immobilized on TCPS were

mounted on an adjustable disk gap cell (14mm diameter). The gap between the samples was adjusted to apx. 110µm and an electrolyte (1mM KCl, at a pressure of 400mbar) was flowed through the cell. The streaming current (I_{str}) was determined at different pH values within the range of 5.5 to 10, automatically adjusted by the addition of NaOH (0.05M) to the solution. The respective ζ-potential was calculated and averaged over three measurements using Attract 2.0 software, which uses Smoluchowski equation to calculate the ζ-potential from I_{str}.

3-4. IN VITRO STUDIES AND BIOLOGICAL ANALYSIS

3-4.1. Cells adhesion, morphology and protein expression by immunocytochemistry

The behaviour of the gastric cancer cell lines MKN45 and AGS, was evaluated after culture onto 2D LbL surfaces or in the 3D hydrogel. The cells on 2D surfaces were analysed after 3 days of culture (Chapter 5, 6 and 7) or in shorter time frames, 3 and 6 hours (Chapter 7), in terms of cell adhesion and morphology. The immunocytochemistry (ICC) was performed in order to analyse the cellular morphology and to count the number of cells adhered in each surface (Chapter 5 and 6). After the incubation period, cells were washed twice with PBS, fixed in 10% neutral buffered formalin for 30min at 4°C, permeabilized with 1% Triton X-100 in PBS for 30min at 4°C, and blocked with 3% BSA in PBS for 30min at room temperature. A phalloidin–TRITC conjugate was used (1:200 in PBS for 30min) to assess cytoskeleton organization. Nuclei were counter-stained with DAPI (1mg.mL^{-1} in 1% BSA in PBS for 30min). The expression of specific proteins, such CD44 (mouse monoclonal antibody, clone 8E2F3, 1:400 in 1% w/v BSA/PBS), Paxillin (Anti-Paxillin monoclonal antibody [Y113], AB32084, 1:250 in 1% w/v BSA/PBS), Cortactin (rabbit polyclonal antibody, H-191, 1:400), E-Cadherin (rabbit monoclonal antibody, EP700Y, 1:500), RHAMM (mouse monoclonal antibody, H-8, 1:400) and YAP human anti-mouse antibody (SC-101199; 1:500 in 1% BSA in PBS) were stained followed by the secondary anti-mouse or anti-rabbit Alexafluor-488 (1:500 in 1% w/v BSA/PBS). The cells were observed under confocal laser scanning microscope (TCS SP8, Leica, Germany). The ICC of cells cultured in the 3D hydrogels (Chapter 8) was performed with an adapted procedure due to the difficulty to stain cells encapsulated into the gels. In this case, the washing steps were performed using TBS-$CaCl_2$ instead of PBS, to increase the stability of the hydrogels and the cells were fixed in 16% formaldehyde (Pierce™,

P1304MP) for at least 1h at room temperature under shaking. Cells were permeabilized with 0.1% Triton X-100 in TBS-$CaCl_2$ for 30min under shaking, and blocked with 3% BSA in TBS-$CaCl_2$ for 1h at room temperature. The immunostaining with Phalloidin, DAPI and the specific cellular receptors, e.g. CD44 and CD90 (CD90-FITC, 1:250 in 1% w/v BSA/TBS-$CaCl_2$) was performed in TBS-$CaCl_2$ overnight at 4°C.

The cellular migration analysis reported under Chapter 5, 6 and 7 was executed under an inverted microscope (Zeiss Axio Observer, Germany) equipped with a temperature (37°C) and CO_2 control (5% CO_2) unit. Cancer cells were allowed to adhere for 24h before the time-lapse procedure. Continuous images of the cells (obtained under a 20x objective) were captured every 5min for 16h using the Zen software. The image stacks and cells displacement were analysed with Fiji software package (http://fiji.sc/wiki/index.php/Fiji) using the Manual Tracking Plugin.

3-4.2. Cells morphology by Scanning Electron Microscopy (SEM)

Cell spreading and morphology was also evaluated by high resolution Scanning Electron Microscopy (SEM), allowed to quantify the cells' filopodia number and length. The MKN45 cells cultured on $(PLL\text{-}HA_n)_5$ surfaces, presented on Chapter 7, were washed with PBS, fixed with 10% formalin and dehydrated using ethanol of increasing concentrations (50%, 70%, 90% and 100%). The samples were coated with 0.6nm Pt and examined at an accelerating voltage of 3.00kV in an Auriga Compact SEM (Zeiss, Germany). The morphometric analysis of the cells was performed using the Fiji software package (Version 2.0.0-rc-68/1.52c).

3-4.3. Protein expression by Western-blotting

On Chapters 6 and 8, Western Blots (WBs) were used to identify specific proteins in the pool extracted from the AGS and MKN45 cells culture obtained from the 2D and 3D experiments, respectively. This technique is very useful not only to identify different proteins, but also to quantify them through the intensity of the respective band. WBs were obtained upon transferring the protein into a membrane, which was subsequently exposed to the corresponding primary and secondary antibodies. [24]

Proteins were extracted from the lysis of MKN45 and AGS cancer cells. The AGS cells cultured on 2D surfaces (Chapter 6) were washed with cold PBS and 200μL of lysis buffer (RIPA buffer, *i.e.* 150mM NaCl; 1% Triton-X100; 0.5% Sodium Deoxycholate; 0.1% Sodium Dodecyl Sulphate; 50mM Tris-Base; pH=8) supplemented with 1x Protease (cOmplete™, ROCHE) and 1x Phosphatase (PhosSTOP™, ROCHE) inhibitor cocktails) and scratched gently. In the case of the 3D hydrogel's core (Chapter 8) the spheres containing MKN45 cells were washed with cold TBS-$CaCl_2$ and placed on an Eppendorf containing 200μL of lysis buffer. To obtain the necessary amount of protein, at least 3 core spheres were recovered. In all the above-mentioned Chapters, the protein lysates were incubated for 30min on ice and vortexed with 5min intervals. The extracts were centrifuged (18,000g, 16min, 4°C), and the supernatant was transferred to a fresh tube and stored on ice for further quantification. The total protein concentration was quantified using the Pierce™ BCA Protein Assay Kit and measured using a spectrophotometer. Before using the protein lysate for WB, 6x Laemmli buffer was added (to reach a 1x dilution), they were denatured at 37°C for 1h30min and 95° for 5min prior to use. The lysates containing 20-40μg of protein were resolved using 4-12% Bis-Tris Protein Gels (Novex™) and transferred to nitrocellulose membranes (Thermo Fischer Scientific). The membranes were incubated in 4% (m/v) bovine serum albumin (BSA) in Tris-buffered saline-Tween (TBS-T, Cell Signalling Technology). On Chapter 6 the membranes were stained for α-smooth muscle actin (1:5000), CD44 (1:1000), RHAMM (1:1000), p-AKT and AKT (1:1000) and Annexin (1:1000), while on Chapter 8 membranes were stained for α-smooth muscle actin (1:5000), Vimentin (1:1000) and E-cadherin (1:5000) antibodies. After 3 cycles of 5min washing steps with TBS-T, the membranes were incubated with IRDye®800CW anti-Rabbit or anti-Mouse (1:10000) for 1h and imaged on the Odyssey Infrared Imaging System (LI-COR Biosciences).

3-4.4. Cells viability

On Chapter 8 the cellular viability was assessed by Live/Dead assay using calcein-AM (1μg/mL - green staining, live cells) and propidium iodide (PI) (1μL/mL - red staining, dead cells). This procedure allows the fast visualization of the distribution of living and dead cells: the reaction of Calcein AM with the intracellular esterase (lacking in dead cells) stains living cells and PI (not membrane permeable) that binds to DNA of disrupted cells staining dead cells with red. [25] Briefly, the core-shell hydrogels were incubated for 30min at 37°C in a solution containing TBS-$CaCl_2$ with Calcein-AM and PI. The

fluorescence of the cells was observed with a Confocal laser scanning microscope (TCS SP8, Leica, Germany).

3-4.5. Flow Cytometry analysis

On Chapter 5, AGS and MKN45 cells were analysed by flow cytometry to identify and quantify the CD44 expressing cells. In this case, cancer cells seeded on (PLL-HA_{Mw}) were detached with TrypLE Express. TrypLE is a mixture of recombinant cell-dissociation enzymes. Its action is milder than the commonly used porcine trypsin: TrypLE preserves better cell-surface epitopes when compared to trypsin. Detached cells were re-suspended in PBS and incubated for 20min at room temperature with mouse anti-human CD44-PE antibody (clone 515) (BD Bioscience, USA) and mouse anti-human CD44v6 monoclonal antibody (MA54) (Invitrogen, USA), following manufacturer-recommended concentrations. Cells were subsequently washed with PBS, centrifuged, fixed in 1% paraformaldehyde (Alfa Aesar, USA), and analysed on a FACs Calibur Flow Cytometer (BD Biosciences, USA) using the Flowing Software v2.5.1.

3-4.6. Proteome Profiler™ Human Phospho-MAPK Array

On Chapter 7 a proteomics phosphoantibody array kit was used to determine the phosphorylation of multiple kinases by using a single membrane-based immunoassay. The identification of the phosphorylation of the major families of mitogen-activated protein kinase (MAPK) and the extracellular signal-regulated kinases (ERK1/2) allows to understand the signalling molecules and activated pathways involved in the cellular function. The phosphorylation status of the intracellular proteins was performed using the Proteome Profiler™ Human Phospho-MAPK Array (R&D Systems, USA). The phosphorylation of 26 kinases, Akt (1, 2, 3), Akt pan, CREB, Erk(1, 2), GSK-3α/β and GSK-3β, HSP27, JNK (1, 2, 3), JNK pan, MKK (3, 6), MSK2, p38 (α, β, δ, γ), p53, p70 S6 kinase, RSK (1 , 2) and TOR were identified using a 20μg protein lysate extracted, as described in section 3.5.3, from the cells seeded on the LbL surfaces (presenting HA of 6.4 and 1500kDa) and cultured under dynamic conditions, *i.e.* QCM-D, following the manufacture's protocol. Briefly, the cells lysates were diluted in a cocktail of biotinylated detection antibodies, and incubated overnight with the Phospho-MAPK array membrane. After the washing step, to remove the unbound materials, streptavidin-HRP and

chemiluminescent detection reagents (Chemi Reagent Mix) were applied. Signals produced at each capture spot corresponds to the amount of bound phosphorylated protein.

3-5. REFERENCES

1. Toole, B.P., *Hyaluronan: From extracellular glue to pericellular cue.* Nature Reviews Cancer, 2004. **4**(7): p. 528-539.

2. Sze, J.H., J.C. Brownlie, and C.A. Love, *Biotechnological production of hyaluronic acid: a mini review.* 3 Biotech, 2016. **6**(1): p. 67.

3. Dicker, K.T., et al., *Hyaluronan: a simple polysaccharide with diverse biological functions.* Acta Biomater, 2014. **10**(4): p. 1558-70.

4. Kim, B., et al., *Ionic strength effect on molecular structure of hyaluronic acid investigated by flow field-flow fractionation and multiangle light scattering.* Anal Bioanal Chem, 2015. **407**(5): p. 1327-34.

5. Morga, M., et al., *Monolayers of poly-L-lysine on mica - Electrokinetic characteristics.* Journal of Colloid and Interface Science, 2015. **456**: p. 116-124.

6. Choi, J.H., et al., *Influence of pH and Surface Chemistry on Poly(L-lysine) Adsorption onto Solid Supports Investigated by Quartz Crystal Microbalance with Dissipation Monitoring.* J Phys Chem B, 2015. **119**(33): p. 10554-65.

7. Crouzier, T. and C. Picart, *Ion pairing and hydration in polyelectrolyte multilayer films containing polysaccharides.* Biomacromolecules, 2009. **10**(2): p. 433-42.

8. Amorim, S., et al., *Hyaluronic acid/poly-L-lysine bilayered silica nanoparticles enhance the osteogenic differentiation of human mesenchymal stem cells.* Journal of Materials Chemistry B, 2014. **2**: p. 6939-6946.

9. Cai, L., et al., *Optimal poly(L-lysine) grafting density in hydrogels for promoting neural progenitor cell functions.* Biomacromolecules, 2012. **13**(5): p. 1663-74.

10. Andersen, T., P. Auk-Emblem, and M. Dornish, *3D Cell Culture in Alginate Hydrogels.* Microarrays (Basel), 2015. **4**(2): p. 133-61.

11. Braccini, I. and S. Perez, *Molecular basis of Ca2+-induced gelation in alginates and pectins: The egg-box model revisited.* Biomacromolecules, 2001. **2**(4): p. 1089-1096.

12. Lee, K.Y. and D.J. Mooney, *Alginate: properties and biomedical applications.* Prog Polym Sci, 2012. **37**(1): p. 106-126.

13. Qiao, S.P., et al., *An alginate-based platform for cancer stem cell research.* Acta Biomater, 2016. **37**: p. 83-92.

14. Zeng, J.F. and M. Matsusaki, *Layer-by-layer assembly of nanofilms to control cell functions.* Polymer Chemistry, 2019. **10**(23): p. 2960-2974.

15. Costa, R.R. and J.F. Mano, *Polyelectrolyte multilayered assemblies in biomedical technologies.* Chem Soc Rev, 2014. **43**(10): p. 3453-79.

16. Richert, L., et al., *Improvement of stability and cell adhesion properties of polyelectrolyte multilayer films by chemical cross-linking.* Biomacromolecules, 2004. **5**(2): p. 284-294.

17. da Costa, D.S., et al., *Sulfonic groups induce formation of filopodia in mesenchymal stem cells.* Journal of Materials Chemistry, 2012. **22**(15): p. 7172-7178.

18. Höök, F., *The QCM-D Technique for Probing Biomacromolecular Recognition Reactions*, in *Piezoelectric Sensors*. 2007, Springer. p. 425-447.

19. Saitakis, M. and E. Gizeli, *Acoustic sensors as a biophysical tool for probing cell attachment and cell/surface interactions.* Cell Mol Life Sci, 2012. **69**(3): p. 357-71.

20. Chen, J.Y., L.S. Penn, and J. Xi, *Quartz crystal microbalance: Sensing cell-substrate adhesion and beyond.* Biosens Bioelectron, 2018. **99**: p. 593-602.

21. Tang, Y.J., X.Q. Zeng, and J. Liang, *Surface Plasmon Resonance: An Introduction to a Surface Spectroscopy Technique.* Journal of Chemical Education, 2010. **87**(7): p. 742-746.

22. Parkkila, P., et al., *Biophysical Characterization of Supported Lipid Bilayers Using Parallel Dual-Wavelength Surface Plasmon Resonance and Quartz Crystal Microbalance Measurements.* Langmuir, 2018. **34**(27): p. 8081-8091.

23. Ferraris, S., et al., *Zeta Potential Measurements on Solid Surfaces for in Vitro Biomaterials Testing: Surface Charge, Reactivity Upon Contact With Fluids and Protein Absorption.* Frontiers in Bioengineering and Biotechnology, 2018. **6**.

24. Mahmood, T. and P.C. Yang, *Western blot: technique, theory, and trouble shooting.* N Am J Med Sci, 2012. **4**(9): p. 429-34.

25. Hassan, W., Y. Dong, and W. Wang, *Encapsulation and 3D culture of human adipose-derived stem cells in an in-situ crosslinked hybrid hydrogel composed of PEG-based hyperbranched copolymer and hyaluronic acid.* Stem Cell Res Ther, 2013. **4**(2): p. 32.

Section III

Experimental Studies

Chapter 4

Tunable layer-by-layer films containing hyaluronic acid and their interactions with CD44

Chapter 4

Tunable layer-by-layer films containing hyaluronic acid and their interactions with CD44[†]

ABSTRACT

We report on the development of layer-by-layer (LbL) constructs whose viscoelastic properties and bioactivity can be finely tuned by using polyanions of different size and/or crosslinking. As a polyanion we used hyaluronic acid (HA) - a multi-signaling biomolecule whose bioactivity depends on its molecular weight. We investigated the interplay between the mechanical properties of the LbL systems built using HA of different sizes, with the specific HA-mediated biochemical interactions. We characterized the assembled materials and their interactions with CD44, the main HA receptor, by Quartz Crystal Microbalance with Dissipation (QCM-D), Surface Plasmon Resonance (SPR) and Atomic Force Microscopy (AFM). We observed that the presence of CD44 resulted in the disruption of the non-crosslinked multilayers, while crosslinked films remain stable and bind CD44 in a HA's molecular weight and charge specific fashion.

[†] This Chapter is based on the publication "Amorim, S., Reis, C. A., Reis, R. L., Pashkuleva, I., & Pires, R. A. (2020), *Tunable layer-by-layer films containing hyaluronic acid and their interactions with CD44*. (submitted)"

4-1. INTRODUCTION

Layer by layer (LbL) assembly is the hierarchical and controlled association of oppositely charged polyelectrolytes (PEs). It is usually applied to generate coatings or self-standing membranes relevant for different technological fields [1, 2]. In the biomedical area, biodegradable and biocompatible PEs have been used to generate LbL-based drug delivery systems [3]; substrates that induce stem cells differentiation[4], surfaces promoting cell adhesion and proliferation [2, 5]; mimics of the extracellular matrix (ECM)[6] and the cancer microenvironment [5, 7].

One of the most studied LbL system is built by the sequential deposition of hyaluronic acid (HA) and poly-L-lysine (PLL) (Fig. 1a) [8-10]. PLL is a common polycation used in LbL assembly because of its biocompatibility and the fact that is usually used as a coating that promote cell attachment [11, 12]. On the other hand, HA is a negatively-charged, non-sulphated glycosaminoglycan, that is one of the main components of mammalian connective tissue [13, 14]. HA is also an important multi-signalling molecule, that interacts with specific cell surface receptors/proteins (*e.g.* CD44) and regulates different cellular functions [15, 16]. As an example, HA is a key player in cancer cell biology and the acquisition of malignant phenotypes [17]. In fact, the tumor microenvironment is characterized by an excessive deposition of HA[18]. Its molecular weight (Mw) is also altered mostly due to the overexpression of hyaluronidases. These changes affect the mechanical properties (usually leading to a higher stiffness) and the biofunctionality of the matrix of the cancerous tissues [19].

Based on the importance of the HA size on its biological signalling [20, 21], HA is usually used for the assembly of LbL systems in the biomedical field [22]. However, whereas HA of high Mw (*e.g.* >100kDa) are the most studied [23, 24], the data about short HAs (*e.g.* HA's oligosaccharides <10kDa) are scarce. Moreover, the developed LbL systems are well characterized in terms of physico-chemical properties but the correlation between these properties and the bioactivity of the generated LbL constructs is not thoroughly studied. In this work, we use HA of different sizes, not only to modulate the viscoelastic properties of the LbL constructs, but also to impart different bioactivities of these constructs. We provide systematic data about the thickness, stiffness and hydration of the LbL assemblies, as well as on their ability to recognize and interact with CD44 (one of the main HA cell surface receptors), whose overexpression is one of the main cancer markers [25].

4-2. MATERIALS AND METHODS

4-2.1. Materials.

We studied two PEs with different Mws: poly-L-lysine hydrobromide (PLL; Mws 4-15, 15-30 and 30-70 kDa) from Sigma-Aldrich, and hyaluronic acid (HA; Mws of 6.4, 752 and 1500kDa) obtained from Lifecore. For the crosslinking of the multilayers we used N-(3-dimethylaminopropyl)-N′-ethylcarbodiimide hydrochloride (EDC, ≥98.0%) and N-hydroxysuccinimide (NHS) purchased from Sigma-Aldrich. Both PEs and chemicals were used as received without any further purification.

4-2.2. Methods

4-2.2.1. Quartz Crystal Microbalance with Dissipation (QCM-D)

Gold-coated AT-cut quartz crystals (QSX301) were placed in the QCM-D flow chamber (E4 instrument, Q-Sense, Sweden). The temperature was set to 25°C and a stable baseline was acquired using NaCl 150mM aqueous solution. A PLL solution (0.5mg/mL in 150mM NaCl) was added to the chamber for 15min. The sensor was rinsed with the NaCl 150mM aqueous solution to remove loosely bound material. A HA solution (1mg/mL in 150mM NaCl aqueous solution) was injected in the flow chamber for 15min. For the crosslinked assemblies, the HA solutions were supplemented with the crosslinking agents (EDC, 400mM and NHS, 100mM). A new washing step was performed, followed by the injection of PLL solution on the QCM-D chambers. The adsorption of PLL and HA was repeated until the ten layers were obtained, *i.e.* $(PLL\text{-}HA)_5$. The adsorption and washing steps were performed with a flow rate of $50\mu L.min^{-1}$. The adsorption of CD44 his-tag protein (orb84335), $10\mu g.mL^{-1}$ in PBS solution with 1% BSA, was injected using the same flow rate until stabilization of the frequency and dissipation signal. All measurements were performed at several harmonics (n = 1, 3, 5, 7, 9 and 11, corresponding to 5, 15, 25, 35, 45, 55, and 65 MHz, respectively). $\Delta f_n/n$ and ΔD were fitted using the Voigt model for the 5^{th}, 7^{th} and 9^{th} overtone using the Q-Sense DFind software.

4-2.2.2. Surface plasmon resonance (SPR)

SPR full angle scans were performed simultaneously at 670 and 785nm with a multi-parametric instrument (MP-SPR), SPR Navi 200 (BioNavis, Finland). As in the case of the QCM-D experiments, the assemblies of the 5 bilayers was performed and monitored *in situ*. Each layer was allowed to adsorb for 5min, with a washing step, using an aqueous NaCl 150mM solution, between the injection of each PE. The CD44 his-tag protein was adsorbed in the same conditions. SPR data for the LbL construction were analyzed using the Layer Solver software (version 1.3.8, Max Planck Institute for Polymer Research, Mainz, Germany), applying the Fresnels' equation, using the dual-wavelengths method (670 and 785nm). Briefly, the dual-wavelength method correlates linearly the dispersion coefficient and the wavelength changes, which is used to determine the refractive index (η), accordingly to the equation:

Equation 4-1

$$dn/_{d\lambda} = (n_{785} - n_{670})/_{785 - 670}$$

In this method, the LayerSolver software automatically fits the obtained data and returns the values for thickness (*Th* or *d*) and η. To be able to retrieve the *Th*, the parameters (d,η) are introduced as dependent variables between the 670/785nm, being the coefficient $d\eta/d\lambda$ a fixed value and used as linearly dependent[26]. Based on De Feijter equation (Eq. 2), the adsorbed mass (Γ) is calculated, considering the SPR measured optical thickness, *Thf* and refractive index, ηf, of the films:

Equation 4-2

$$\Gamma = Th_f \times (n_f - n_b)/_{(dn/dc)}$$

where ηb is the refractive index of the buffer (RI of the water 1.332) and ($d\eta/dc$) is the incremental change in the η of the solution of the polymers, that was assumed to be 0.15cm3/g [27-29].

4-2.2.3. Atomic Force Microscopy

The generated LbL surfaces were analyzed using a JPK NanoWizard 3 (JPK, Germany). The Young's modulus of the films were measured under QI Advanced Imaging Mode using qp-BioAC-CB3 probes (calibrated using the non-contact method in the JPK software; a resonance frequency of ~23-37kHz and a calibrated spring constant of ~0.065N/m, NanoSensors, Germany) and the values were obtained by fitting the approach curves with the Hertz/Sneddon model, using a cone tip shape (applying a very short indentation range, 0.5-1nm, to avoid the influence of the substrate). All the experiments were performed in air, while the surfaces were humidified using a drop of PBS.

4-2.2.4. ζ-potential measurements

The ζ-potential of the assembled films was analysed using an electrokinetic analyzer (SurPASS, Anton Paar, Graz, Austria). The $(PLL\text{-}HA)_5$ samples were mounted in an adjustable gap cell (1x2cm^2). The gap between the samples was adjusted to apx. 110μm and an electrolyte (1mM KCl, pressure of 400mbar) was flowed through the cell. The streaming current (I_{str}) was determined at different pH values within the range of 5.5 to 10, automatically adjusted by the addition of NaOH (0.05M) to the solution. The respective ζ-potential was calculated and averaged over three measurements using Attract 2.0 software, which uses the Smoluchowski equation for calculation of ζ-potential from I_{str}.

4-2.3. Theoretical models and equations

4-2.3.1. Hyaluronic acid conformation: depending on the Mw of HA, the radius of gyration (Rg) and hydrodynamic radius (Rh) varies [30]. Accordingly, the Rg and Rh were calculated using Eqs. 3 and 4, respectively:

Equation 4-3

$$Rg = 2.35\,(\text{HA Mw in kDa})^{0.57}$$

Equation 4-4

$$Rh = 0.87\,(\text{HA Mw in kDa})^{0.63}$$

4-2.3.2. Storage and elastic modulus: the viscoelastic properties of the films were obtained using the Voigt model, from which it was determined the shear modulus (G') and the viscous modulus (loss modulus - G'') of each LbL film, as detailed in Eqs 5 and 6:

Equation 4-5

$$\mu = G'$$

Equation 4-6

$$\eta' = {G''}/{\varpi}$$

where μ is the shear modulus (in Pa), representing the elastic component of viscoelastic material, η' is the dynamic viscosity (in Pa.s) and ϖ the angular frequency (ϖ=2πf7).[31]

4-2.3.3. Hydration of the films: the hydration (Hyd) of the assembled LbL films was calculated using the following equation:

Equation 4-7

$$\%\ of\ hydration\ = {(m_{QCM-D} - m_{SPR})}/{m_{QCM-D}} \times 100$$

where *m*QCM-D and *m*SPR are the acoustic and optical thickness of the films, respectively. [32]

4-3. RESULTS AND DISCUSSION

4-3.1. Real time characterization of LbL generated by the combination of PLL and HA of different Mw

QCM-D and SPR were used to follow in real-time the construction of the 10-layered films, *i.e.* (PLL-HA)$_5$. QCM-D gives information about mass adsorption, viscoelastic properties and hydration of the materials. [33, 34] Upon mass adsorption, the frequency of the quartz sensor decreases (Δf). Together with changes in frequency, QCM-D instrument allows simultaneous collection of data related with the energy Dissipation (ΔD), which are intimately related with the presence of water in the adsorbed layer. [35]

We used two sets of experiments: (i) electrostatically deposited (PLL-HA)$_5$ and (ii) covalently crosslinked (PLL-HA)$_5$ (Fig. 1b). In both sets of LbL films we used HA of different Mw. The QCM-D results showed that Δf and ΔD values depend on the size of HA and on the type of crosslinking (Fig. 1c-e).

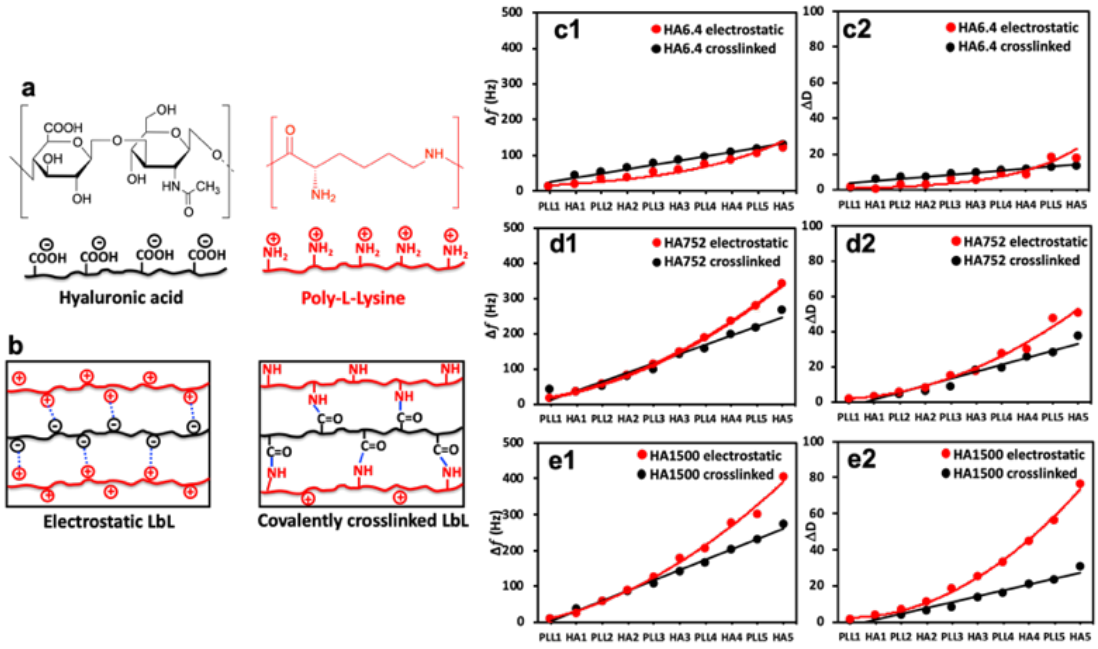

Figure 4-1. (a) Chemical structure of the used polyelectrolytes and (b) schematic presentation of their interactions in the two experimental setups. (c-e) QCM-D data (7th overtone) showing changes in (c1-e1) frequency (Δf) and (c2-e2) dissipation (ΔD) for the electrostatic (red) and covalently (black) crosslinking (PLL-HA)$_5$ systems. LbL assembly was executed with PLL (Mw = 30-70kDa) and HA of (c) 6.4, (d) 752 and (e) 1500kDa. Raw data are presented in Supplementary Fig. 1.

The $(PLL\text{-}HA)_5$ film growth (increased Δf and ΔD values) is directly proportional to the increment of the HA's Mw (Fig 1c1-e1): $\Delta f(PLL\text{-}HA6.4)5 << \Delta f(PLL\text{-}HA752)5 \approx \Delta f(PLL\text{-}HA_{1500})_5$. Previous reports describe an exponential growth for LbL of the PLL/HA combination.[36-38] This behavior is typical for weak PEs, such as HA, and is related with the diffusion of the PLL chains into the interior of the film.[39] In accordance with these studies, we also observed exponential growth of the electrostatic LbLs (Fig. 1c-e, red) regardless of the size of the used HA. The crosslinked LbLs behaved differently - they followed a linear growth (Fig. 1c-e, black). On one hand, this difference can be explained by the reduced PLL mobility as a result of the crosslinking.[9] On the other hand, the deposited mass for the crosslinked LbLs is systematically lower and the films are thinner and less dissipative when compared to the constructs built by electrostatic interactions (Figs. 1c2-e2, 2a red *vs* black, Table 1). These differences are more pronounced for the HA of higher Mws (*i.e.* HA_{752} and HA_{1500}) and can be explained either with less deposited material or/and closer packing of the PEs, *i.e.* formation of less hydrated and denser LbL films as a result of the formation of covalent bonds between PLL and HA.[38]

The storage modulus (G', elastic component) and loss modulus (G'', viscous component) were calculated from the QCM-D data (Supplementary Fig. 2). The ratio G''/G' gives an indication about the changes in the viscous and elastic component of the assembled films (Figs. 2b and Supplementary Fig. 3). The electrostatically assembled films present a higher G''/G' ratio than the crosslinked ones, showing a higher contribution of the viscous component (water content) to the properties of the films (Fig. 2b). In the case of the crosslinked films, a sharp decrease in G''/G' is observed for the shortest HA (6.4kDa). This behavior is consistent with the conversion from a gel-like assembly to a compact film formation.[40] The assemblies generated with the HA of higher Mws presented the same trend but the difference is not significant.

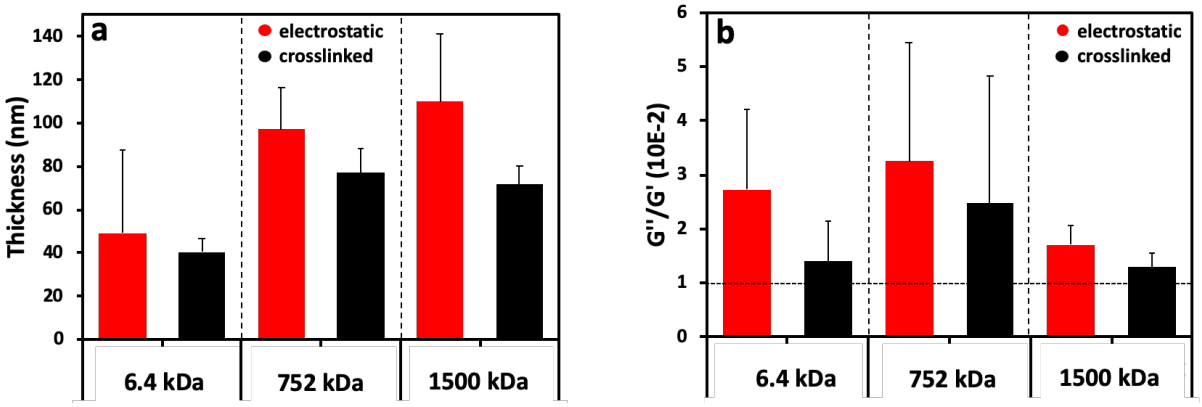

Figure 4-2. (a) Hydrodynamic film thickness, obtained by fitting the QCM-D data (5th, 7th and 9th overtones) according to Voigt model and (b) viscoelastic properties shown by the ratio G"/G' of the $(PLL\text{-}HA)_5$ assemblies prepared with HA of different Mws.

We then used SPR to complement the QCM-D data, and provide information about the whole LbL construct, including water. The optical-based SPR differs from the acoustic QCM-D as it provides information only about the "dry mass".

SPR data showed that the angle shift (Θ) increases with the HA size, following the same trend as the one observed by QCM-D (Fig. 2a), *i.e.* formation of thicker LbLs by the HA of highest Mw (1500kDa) and thinner constructs when assembled using the shortest HA (6.4kDa) for the electrostatic films (Fig. 3c, red symbols). All crosslinked LbLs are thinner when compared to the respective constructs formed by electrostatic interactions (Fig. 3c, red *vs* black symbols). Of note, this thickness difference is less pronounced for HA of 6. kDa and increases with the HA size. Another important result is the ηf that shows similar material density for all constructs except for the crosslinked LbL film generated using HA of 6.4kDa. The combination of high η and low thickness demonstrates densification of these films.[41, 42] Comparing the mass determined by QCM-D (mQCM) with the one measured by SPR (mSPR) allows to determine the hydration of the studied layers (Table 1). As expected, all films are highly hydrated[43], and the crosslinking reduces significantly (10%) the hydration of the LbL films generated using short HA. However, it does not affect significantly the hydration of the LbL films generated using HA752 and HA1500. In fact, as the Mw of HA increases the higher is the Rg (see Supplementary Table 1) potentiating the intramolecular interactions, leading to an increased entrapment of water (higher hydrodynamic radius)[44].

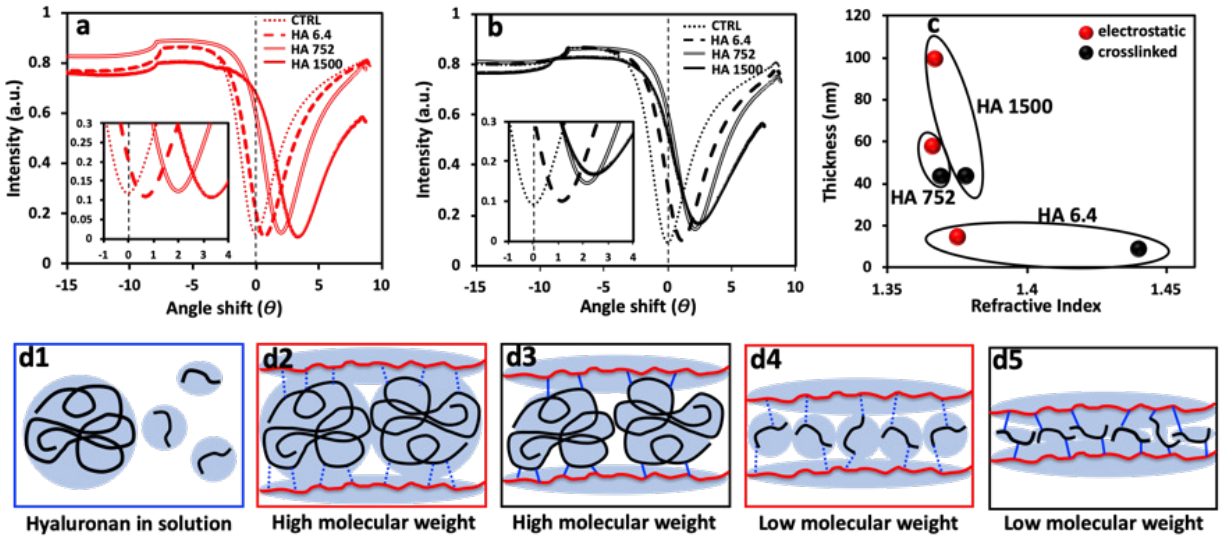

Figure 4-3. SPR data for the studied LbLs: reflectivity curves for (a) electrostatically assembled and (b) crosslinked (PLL-HA)5; (c) plot presenting the calculated thickness vs refractive index for these films. (d) Schematic presentation of the observed differences between long HA chains and short ones: (d1) hydration of HA in aqueous media; electrostatic assembly of (d2) high Mw HA and (d4) HA of low Mw; crosslinked LbLs assembled from (d3) longer HA chains that keep the intramolecularly entrapped water and (d5) short HA.

Altogether these results suggest the existence of size-dependent mechanisms of the interactions between PLL and HA. Previous studies showed that this dependence is due to the mobility of the polycation (PLL).[24] Herein, we demonstrate that different hydration/dehydration of longer and shorter HA chains plays also a role of this process (Fig. 3d).

In general, it is expected that the reduction of the film thickness, observed upon crosslinking, will lead to the densification and dehydration of the crosslinked LbL systems, as compared to their electrostatic analogues. Indeed, this is the result observed for the constructs assembled from the shortest HA (*i.e.* 6.4kDa). In the case of LbL systems generated using HA of longer chains, the use of crosslinking does not affect significantly the hydration level.

4-3.2. Mechanical properties of the (PLL-HA)5 systems generated with HA of different Mw

To better understand the impact of hydration and crosslinking on the properties of the $(PLL\text{-}HA)_5$ LbL systems, we evaluated their mechanical properties by AFM. Of note, the information obtained by AFM is limited to the surface of the construct and differs from the data generated via QCM-D that present

average values for the whole construct. Another difference is that the AFM measurements are performed through nanoindentation in a direction perpendicular to the deposition plane and to the direction of the HA/PLL fibers, while QCM-D measures the *G'* in a direction parallel to the deposited fibers.

In the case of the electrostatically-assembled films we observed a decrease of the Young's modulus with the increment of the HA Mw (Fig. 4). These results are in contradiction with the hydration of these constructs (Table 1), *i.e.* lower hydration with the increase of the HA Mw. However, the surface of the construct (last deposited bi-layer) differs from its bulk and the obtained results are due to the formation of a surface hydration shell that contains water molecules[39], loosely bound to the HA end-layer and that increases with the HA's Mw.

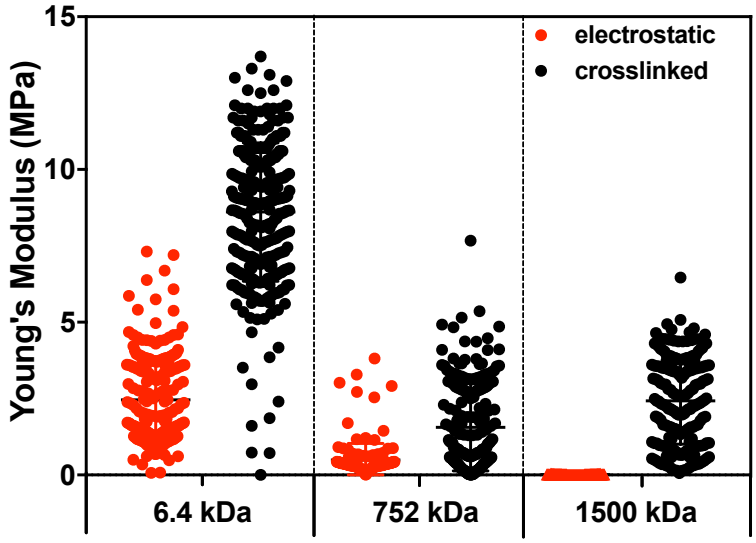

Figure 4-4. Young's Modulus of the (PLL-HA)5 LbL films generated using PLL of 30-70kDa and HA of 6.4, 752 and 1500kDa.

Crosslinked LbL systems are stiffer than the respective electrostatic constructs (increased Young's modulus), however, it is observed the same tendency in stiffness as a function of the HA size, as the one observed for the electrostatically deposited assemblies, *i.e.* decrease in the Young's modulus with the increment of the Mw of HA.

4-3.3. Bioactivity of the LbL systems generated with HA of different molecular weights

Besides generation of constructs with different mechanical properties, HA of different size can also code different bioinformation [45, 46]. Moreover, HA incorporation in the constructs via crosslinking (covalent interactions), introduces chemical modifications in its main backbone that can also alter the bioinformation coded by this glycosaminoglycan. We then assessed the interactions between the generated LbLs and CD44, one of the main cell surface receptors for HA, using QCM-D and SPR (Fig. 5). $\Delta D/\Delta f$ plots showed a reduction of Δf (mass loss) upon the addition of CD44 His-tag protein to the electrostatically assembled systems, independently of the HA size. The SPR data corroborated these results for the LbLs assembled with HA of 752 and 1500kDa (Fig. 5e, f, red curve) and showed that the specific interactions between CD44 and HA are stronger than the electrostatic interactions driving the LbL assembly and thus, results in the partial disassembly of the films. In the case of the system generated using short HA (Fig. 5d, red), we observe an increase in the adsorbed "dry" mass, showing that the reduction of Δf and ΔD (observed by QCM-D) for this system is mainly driven by dehydration/compactation.

Table 4-1. QCM-D and SPR parameters obtained for the LbL systems prepared using HA of different Mws (in the presence and absence of crosslinking) and PLL (Mw of 30-70kDa). The acoustic film thickness, Th_{QCM}, and mass, m_{QCM}, was determined using the Voigt model; the optical film thickness, Th_{SPR} and mass, m_{SPR}, was determined using the multiparameter SPR, based on the equations described in the experimental section (Eq. 1 and 2, respectively); film hydration (*Hyd*) was determined from the m_{QCM} and m_{SPR} data using Eq. 7. Mass of CD44 obtained from the difference between m_{SPR} and $m_{SPR}^{LbL+CD44}$.

	Electrostatic LbL			**Crosslinked LbL**							
HA	$(PLL\text{-}HA)_5$			$(PLL\text{-}HA)_5$			$(PLL\text{-}HA)_5$-CD44				
Mw kDa	m_{QCM} ng.cm^{-2}	m_{SPR} ng.cm^{-2}	*Hyd* %	m_{QCM} ng.cm^{-2}	m_{SPR} ng.cm^{-2}	*Hyd* %	Th_{SPR} nm	m_{QCM} ng.cm^{-2}	m_{SPR} ng.cm^{-2}	m_{SPR} CD44	*Hyd* %
6.4	5571.8 (1861.5)	421.4	92.4	4340.9 (502.0)	669.6	84.6	10.0 (1.450)	5050.6 (1039.9)	786.7	117.8	84.4
752	10665.2 (3440.3)	1312.4	87.7	8593.3 (1404.4)	1337.9	84.4	43.9 (1.381)	8233.2 (1220.0)	1427.5	89.6	82.7
1500	12494.8 (4057.2)	2321.2	81.4	7882.0 (951.2)	1343.2	82.9	48.8 (1.376)	8237.3 (484.9)	1431.5	106.1	82.6

The disassembly observed for the electrostatically generated systems is abolished in the crosslinked films: QCM-D and SPR sensograms (Supplementary Fig. 4) showed the retention of CD44 by these systems, independently of the HA's Mw (Figs. 5, Supplementary Fig. 1 and 4). Of note, the adsorption of CD44 does not significantly affect the viscoelastic properties of these LbL films. SPR data allows the quantification of the adsorbed protein and demonstrated a dependence on the Mw of the HA (Table 1). Highest retention of CD44 was measured for crosslinked construct with shortest HA. The higher ηf of these LbLs is consistent with a densification of the film upon protein adsorption. When longer HAs (752 and 1500kDa) are used for the construction of the crosslinked films, less CD44 is adsorbed. A possible reason for this observation is the different mechanisms of interaction of CD44 with the $(PLL\text{-}HA)_5$ systems: while in the films generated using $HA_{6.4}$, besides the specific affinity between CD44 and HA, the higher amount of PLL available on the surface (as shown by a higher ζ, *i.e.* -8.6±20.9 mV, Supplementary Fig. 5) allows the existence of non-specific electrostatic interactions between CD44 and PLL. In the presence of HA_{752} and HA_{1500}, the CD44 binds almost exclusively to HA, leading to an increment of the adsorbed mass with the augmentation of the HA's Mw, as a higher

number of HA motifs are available at the surface of the LbL systems. In fact, the enhanced and irreversible interaction between CD44 and HA of higher Mws has been previously observed [47].

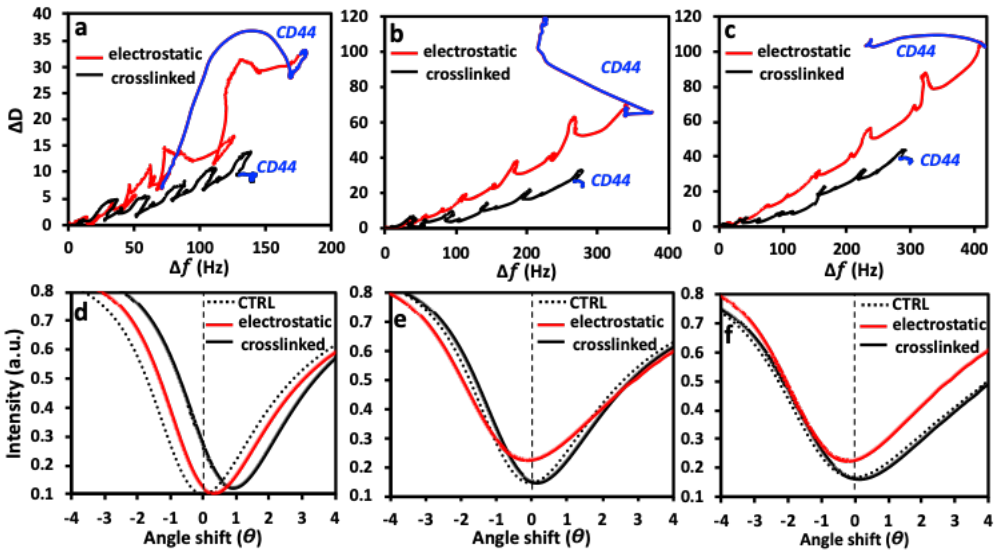

Figure 4-5. a-c) QCM-D ΔD/Δf plots (7th overtone) and (d-e) SPR reflectivity curves (D-F) showing the interaction of CD44-his tag protein with electrostatically deposited and crosslinked $(PLL\text{-}HA)_5$ films assembled from HA of different size, i.e. (a, d) 6.4, (b, e) 752 and (c, f) 1500 kDa. On the SPR curves, the black dashed line represents the normalized angle shift of $(PLL\text{-}HA)_5$, *i.e.* the SPR signal of the construct alone.

Altogether, our results demonstrate that electrostatically assembled LbL systems generated from PLL and HA are not feasible solutions when specific HA-mediated biomolecular interactions are in quest, due to their low stability. Crosslinking of the layers increases the construct biostability and allows quantification of HA-CD44 interactions without disruption of the assembled multilayers. Finally, the bioactivity of these crosslinked systems is also sensitive to the Mw of HA, reflected in their different ability to bind to CD44.

4-3.4. Conclusions

The stability of LbL films from PLL and HA depends on the HA size: more stable multilayers are generated by electrostatic interactions between longer HA with PLL. However, these systems are not stable enough when specific biomolecular interactions are at play, *e.g.* HA-CD44. In this context, crosslinking is an efficient strategy to increase the stability of the LbL systems. These processes affect not only the stability, but also the mechanical properties of the constructs: higher elastic and Young's

modulus were determined for all crosslinked coatings when compared to the respective electrostatically deposited films. These changes were most pronounced for the crosslinked LbLs generated from HA of 6.4kDa, for which significant reduction of the hydration and formation of denser films was observed. Finally, we demonstrate that PLL-HA chemical crosslinking do not compromise HA bioactivity, *i.e.* HA capacity to interact with CD44 in a Mw (HA)-dependent manner.

4-4. REFERENCES

1. Liu, X.; Chen, Z.; Xu, R.; Zhang, R.; Hu, Z.; Huang, F.; Cao, Y., Finely Tuned Composition in Conjugated Polyelectrolytes for Interfacial Engineering of Efficient Polymer Solar Cells. *Small Methods* **2018,** *2* (4).

2. Ren, K.; Fourel, L.; Rouviere, C. G.; Albiges-Rizo, C.; Picart, C., Manipulation of the adhesive behaviour of skeletal muscle cells on soft and stiff polyelectrolyte multilayers. *Acta biomaterialia* **2010,** *6* (11), 4238-48.

3. Liu, X. Q.; Picart, C., Layer-by-Layer Assemblies for Cancer Treatment and Diagnosis. *Adv Mater* **2016,** *28* (6), 1295-301.

4. Amorim, S.; Martins, A.; Neves, N. M.; Reis, R. L.; Pires, R. A., Hyaluronic acid/poly-L-lysine bilayered silica nanoparticles enhance the osteogenic differentiation of human mesenchymal stem cells. *Journal of Materials Chemistry B* **2014,** *2*, 6939-6946.

5. Aggarwal, N.; Altgarde, N.; Svedhem, S.; Zhang, K.; Fischer, S.; Groth, T., Effect of molecular composition of heparin and cellulose sulfate on multilayer formation and cell response. *Langmuir* **2013,** *29* (45), 13853-64.

6. Matsusaki, M.; Kadowaki, K.; Nakahara, Y.; Akashi, M., Fabrication of cellular multilayers with nanometer-sized extracellular matrix films. *Angewandte Chemie* **2007,** *46* (25), 4689-92.

7. Amorim, S.; da Costa, D. S.; Freitas, D.; Reis, C. A.; Reis, R. L.; Pashkuleva, I.; Pires, R. A., Molecular weight of surface immobilized hyaluronic acid influences CD44-mediated binding of gastric cancer cells. *Sci Rep* **2018,** *8* (1), 16058.

8. Niepel, M. S.; Almouhanna, F.; Ekambaram, B. K.; Menzel, M.; Heilmann, A.; Groth, T., Cross-linking multilayers of poly-l-lysine and hyaluronic acid: Effect on mesenchymal stem cell behavior. *Int J Artif Organs* **2018,** *41* (4), 223-235.

9. Boudou, T.; Crouzier, T.; Auzely-Velty, R.; Glinel, K.; Picart, C., Internal composition versus the mechanical properties of polyelectrolyte multilayer films: the influence of chemical cross-linking. *Langmuir* **2009,** *25* (24), 13809-19.

10. Bütergerds, D.; Cramer, C.; Schönhoff, M., pH-Dependent Growth Laws and Viscoelastic Parameters of Poly-l-Lysine/Hyaluronic Acid Multilayers. *Advanced Materials Interfaces* **2017,** *4* (1).

11. Morga, M.; Adamczyk, Z.; Godrich, S.; Ocwieja, M.; Papastavrou, G., Monolayers of poly-L-lysine on mica - Electrokinetic characteristics. *J Colloid Interf Sci* **2015,** *456*, 116-124.

12. Shan, C.; Yang, H.; Han, D.; Zhang, Q.; Ivaska, A.; Niu, L., Water-soluble graphene covalently functionalized by biocompatible poly-L-lysine. *Langmuir* **2009,** *25* (20), 12030-3.

13. Richter, R. P.; Baranova, N. S.; Day, A. J.; Kwok, J. C., Glycosaminoglycans in extracellular matrix organisation: are concepts from soft matter physics key to understanding the formation of perineuronal nets? *Curr Opin Struct Biol* **2018,** *50*, 65-74.

14. Haxaire, K.; Braccini, I.; Milas, M.; Rinaudo, M.; Perez, S., Conformational behavior of hyaluronan in relation to its physical properties as probed by molecular modeling. *Glycobiology* **2000,** *10* (6), 587-594.

15. Dicker, K. T.; Gurski, L. A.; Pradhan-Bhatt, S.; Witt, R. L.; Farach-Carson, M. C.; Jia, X., Hyaluronan: a simple polysaccharide with diverse biological functions. *Acta biomaterialia* **2014,** *10* (4), 1558-70.

16. Toole, B. P., Hyaluronan: From extracellular glue to pericellular cue. *Nat Rev Cancer* **2004,** *4* (7), 528-539.

17. Carvalho, M. P.; Costa, E. C.; Miguel, S. P.; Correia, I. J., Tumor spheroid assembly on hyaluronic acid-based structures: A review. *Carbohydr Polym* **2016,** *150*, 139-48.

18. Chanmee, T.; Ontong, P.; Itano, N., Hyaluronan: A modulator of the tumor microenvironment. *Cancer Lett* **2016,** *375* (1), 20-30.

19. Theocharis, A. D.; Skandalis, S. S.; Gialeli, C.; Karamanos, N. K., Extracellular matrix structure. *Adv Drug Deliv Rev* **2016,** *97*, 4-27.

20. Wu, R. L.; Huang, L.; Zhao, H. C.; Geng, X. P., Hyaluronic acid in digestive cancers. *Journal of cancer research and clinical oncology* **2017,** *143* (1), 1-16.

21. Price, Z. K.; Lokman, N. A.; Ricciardelli, C., Differing Roles of Hyaluronan Molecular Weight on Cancer Cell Behavior and Chemotherapy Resistance. *Cancers (Basel)* **2018,** *10* (12).

22. Szarpak, A.; Cui, D.; Dubreuil, F.; De Geest, B. G.; De Cock, L. J.; Picart, C.; Auzely-Velty, R., Designing Hyaluronic Acid-Based Layer-by-Layer Capsules as a Carrier for Intracellular Drug Delivery. *Biomacromolecules* **2010,** *11* (3), 713-720.

23. Richert, L.; Boulmedais, F.; Lavalle, P.; Mutterer, J.; Ferreux, E.; Decher, G.; Schaaf, P.; Voegel, J. C.; Picart, C., Improvement of stability and cell adhesion properties of polyelectrolyte multilayer films by chemical cross-linking. *Biomacromolecules* **2004,** *5* (2), 284-294.

24. Shen, L.; Chaudouet, P.; Ji, J.; Picart, C., pH-Amplified multilayer films based on hyaluronan: influence of HA molecular weight and concentration on film growth and stability. *Biomacromolecules* **2011,** *12* (4), 1322-31.

25. Senbanjo, L. T.; Chellaiah, M. A., CD44: A Multifunctional Cell Surface Adhesion Receptor Is a Regulator of Progression and Metastasis of Cancer Cells. *Frontiers in Cell and Developmental Biology* **2017,** *5* (18).

26. Parkkila, P.; Elderdfi, M.; Bunker, A.; Viitala, T., Biophysical Characterization of Supported Lipid Bilayers Using Parallel Dual-Wavelength Surface Plasmon Resonance and Quartz Crystal Microbalance Measurements. *Langmuir* **2018,** *34* (27), 8081-8091.

27. Westwood, M.; Noel, T. R.; Parker, R., The effect of poly-L-lysine structure on the pH response of polygalacturonic acid-based multilayers. *Carbohyd Polym* **2013,** *94* (1), 137-146.

28. Mendichi, R.; Schieroni, A. G.; Grassi, C.; Re, A., Characterization of ultra-high molar mass hyaluronan: 1. Off-line static methods. *Polymer* **1998,** *39* (25), 6611-6620.

29. Minsky, B. B.; Antoni, C. H.; Boehm, H., Controlled Immobilization Strategies to Probe Short Hyaluronan-Protein Interactions. *Sci Rep* **2016,** *6*, 21608.

30. Kuehl, C.; Zhang, T.; Kaminskas, L. M.; Porter, C. J.; Davies, N. M.; Forrest, L.; Berkland, C., Hyaluronic Acid Molecular Weight Determines Lung Clearance and Biodistribution after Instillation. *Molecular pharmaceutics* **2016,** *13* (6), 1904-14.

31. Patel, A. R.; Kerwin, B. A.; Kanapuram, S. R., Viscoelastic Characterization of High Concentration Antibody Formulations Using Quartz Crystal Microbalance with Dissipation Monitoring. *Journal of pharmaceutical sciences* **2009,** *98* (9), 3108-3116.

32. Liu, X.; Wu, D.; Turgman-Cohen, S.; Genzer, J.; Theyson, T. W.; Rojas, O. J., Adsorption of a nonionic symmetric triblock copolymer on surfaces with different hydrophobicity. *Langmuir* **2010,** *26* (12), 9565-74.

33. Zhang, S. L.; Bai, H. H.; Yang, P. H., Real-time monitoring of mechanical changes during dynamic adhesion of erythrocytes to endothelial cells by QCM-D. *Chem Commun* **2015,** *51* (57), 11449-11451.

34. Duner, G.; Thormann, E.; Dedinaite, A., Quartz Crystal Microbalance with Dissipation (QCM-D) studies of the viscoelastic response from a continuously growing grafted polyelectrolyte layer. *J Colloid Interface Sci* **2013,** *408*, 229-34.

35. Höök, F., The QCM-D Technique for Probing Biomacromolecular Recognition Reactions. In *Piezoelectric Sensors*, Springer: 2007; Vol. 5, pp 425-447.

36. Picart, C.; Mutterer, J.; Richert, L.; Luo, Y.; Prestwich, G. D.; Schaaf, P.; Voegel, J. C.; Lavalle, P., Molecular basis for the explanation of the exponential growth of polyelectrolyte multilayers. *Proceedings of the National Academy of Sciences of the United States of America* **2002,** *99* (20), 12531-5.

37. Lavalle, P.; Picart, C.; Mutterer, J.; Gergely, C.; Reiss, H.; Voegel, J. C.; Senger, B.; Schaaf, P., Modeling the buildup of polyelectrolyte multilayer films having exponential growth. *J Phys Chem B* **2004,** *108* (2), 635-648.

38. Teixeira, R.; Reis, R. L.; Pashkuleva, I., Influence of the sulfation degree of glycosaminoglycans on their multilayer assembly with poly-l-lysine. *Colloids Surf B Biointerfaces* **2016,** *145*, 567-575.

39. Picart, C.; Lavalle, P.; Hubert, P.; Cuisinier, F. J. G.; Decher, G.; Schaaf, P.; Voegel, J. C., Buildup Mechanism for Poly(l -lysine)/Hyaluronic Acid Films onto a Solid Surface. *Langmuir : the ACS journal of surfaces and colloids* **2001,** *17* (23), 7414-7424.

40. Hook, F.; Kasemo, B.; Nylander, T.; Fant, C.; Sott, K.; Elwing, H., Variations in coupled water, viscoelastic properties, and film thickness of a Mefp-1 protein film during adsorption and cross-linking: a quartz crystal microbalance with dissipation monitoring, ellipsometry, and surface plasmon resonance study. *Anal Chem* **2001,** *73* (24), 5796-804.

41. Granqvist, N.; Liang, H.; Laurila, T.; Sadowski, J.; Yliperttula, M.; Viitala, T., Characterizing ultrathin and thick organic layers by surface plasmon resonance three-wavelength and waveguide mode analysis. *Langmuir : the ACS journal of surfaces and colloids* **2013,** *29* (27), 8561-71.

42. Korhonen, K.; Granqvist, N.; Ketolainen, J.; Laitinen, R., Monitoring of drug release kinetics from thin polymer films by multi-parametric surface plasmon resonance. *Int J Pharm* **2015,** *494* (1), 531-6.

43. Altgarde, N.; Nileback, E.; de Battice, L.; Pashkuleva, I.; Reis, R. L.; Becher, J.; Moller, S.; Schnabelrauch, M.; Svedhem, S., Probing the biofunctionality of biotinylated hyaluronan and chondroitin sulfate by hyaluronidase degradation and aggrecan interaction. *Acta biomaterialia* **2013,** *9* (9), 8158-66.

44. Beldowski, P.; Andrysiak, T.; Mrela, A.; Pawlak, Z.; Auge, W. K., 2nd; Gadomski, A., The Anomalies of Hyaluronan Structures in Presence of Surface Active Phospholipids-Molecular Mass Dependence. *Polymers (Basel)* **2018,** *10* (3).

45. Maharjan, A. S.; Pilling, D.; Gomer, R. H., High and Low Molecular Weight Hyaluronic Acid Differentially Regulate Human Fibrocyte Differentiation. *PloS one* **2011,** *6* (10).

46. Yang, C.; Cao, M.; Liu, H.; He, Y.; Xu, J.; Du, Y.; Liu, Y.; Wang, W.; Cui, L.; Hu, J.; Gao, F., The high and low molecular weight forms of hyaluronan have distinct effects on CD44 clustering. *The Journal of biological chemistry* **2012,** *287* (51), 43094-107.

47. Wolny, P. M.; Banerji, S.; Gounou, C.; Brisson, A. R.; Day, A. J.; Jackson, D. G.; Richter, R. P., Analysis of CD44-hyaluronan interactions in an artificial membrane system: insights into the distinct binding properties of high and low molecular weight hyaluronan. *The Journal of biological chemistry* **2010,** *285* (39), 30170-80.

SUPPLEMENTARY INFORMATION

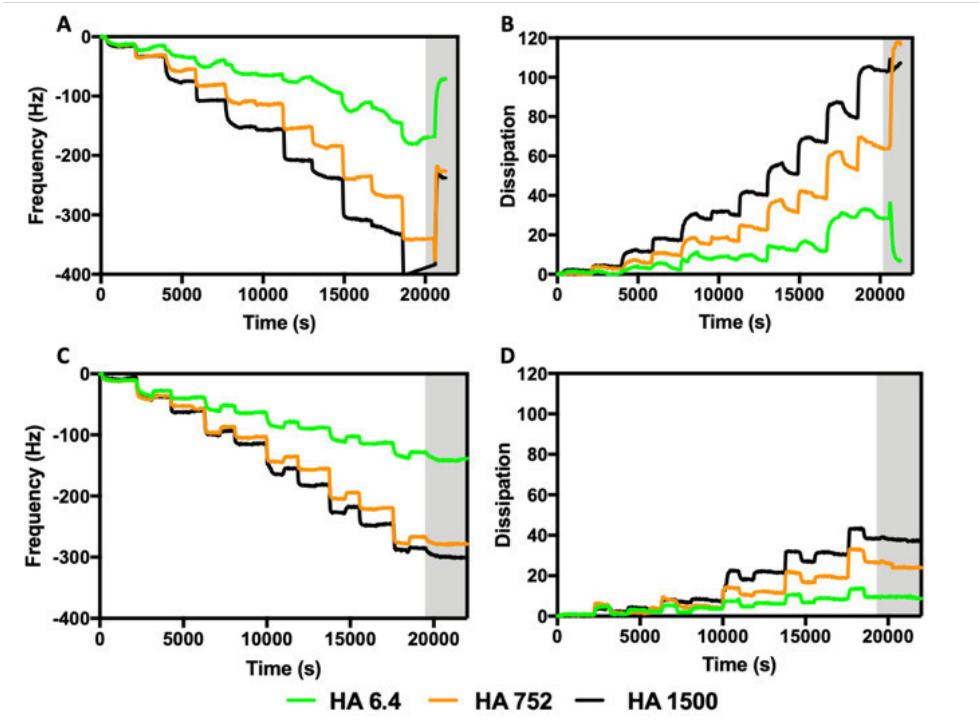

Supplementary Fig. 4-1. QCM-D real-time frequency and dissipation shifts for the 7th overtone, for the adsorption of PLL (30-70kDa) and HA (6.4, 752 and 1500kDa) without (A and B) and with (C and D) covalent crosslinking. His-tag CD44 adsorption (10μg/mL) after the buildup of the ten layers' film (grey zone).

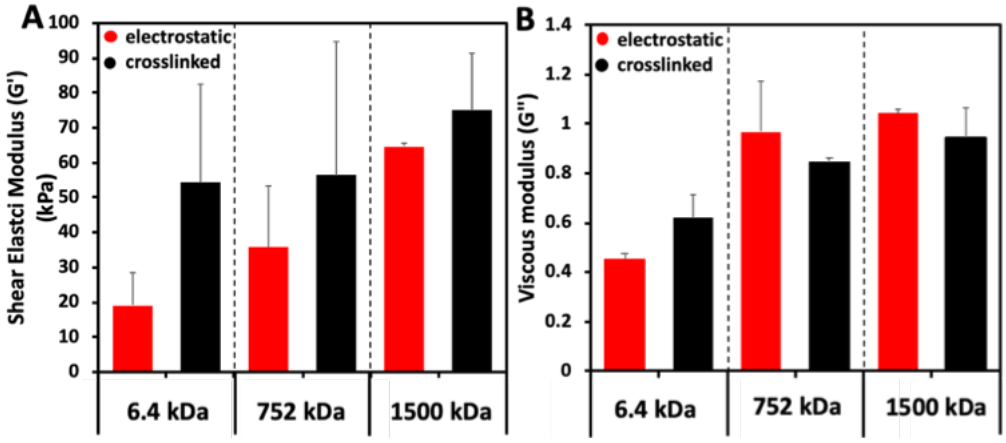

Supplementary Fig. 4-2. Shear elastic modulus (A) and viscous modulus (B) of LbL assembly generating using HA of different Mws, with and without covalent crosslinking. Mechanical properties obtained from Voigt modelling of the QCM-D data

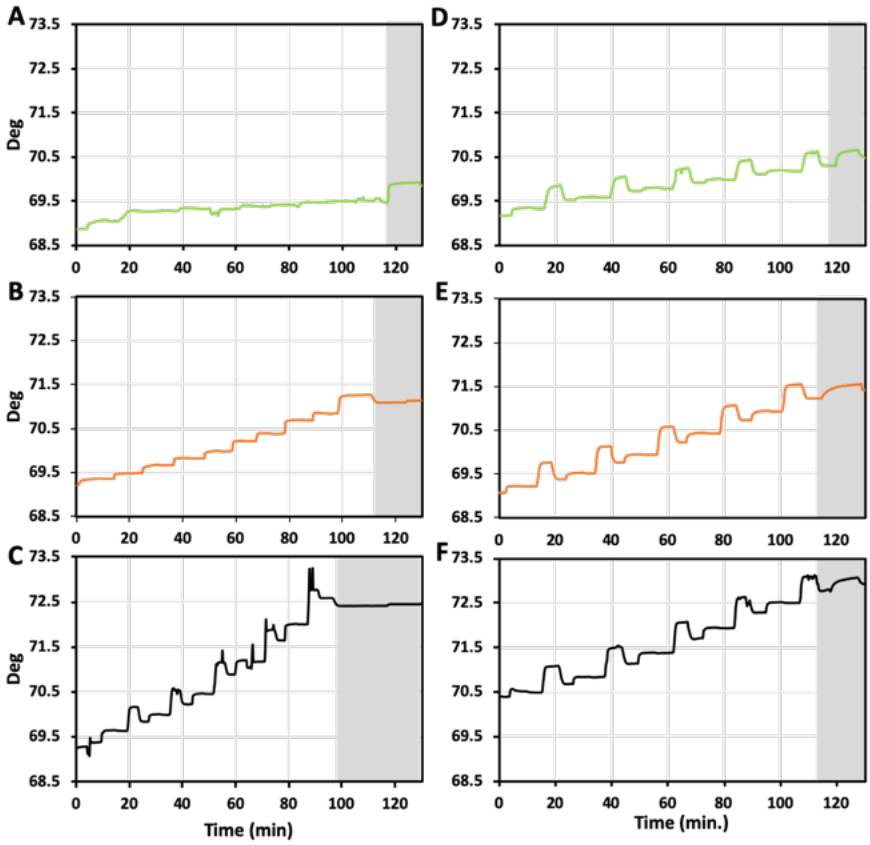

Supplementary Fig. 4-3. SPR real-time adsorption of PLL and HA (white zone), followed by CD44 protein injection (grey zone). Sensograms for PLL 30-70kDa without (A, B and C) and with (D, E and F) covalent crosslinking, using the HA of 6.4kDa (A and D), 752kDa (B and E) and 1500kDa (C and F).

Supplementary Table 4-1. Theoretical radius of gyration (R_g) and hydrodynamic radius (R_h) of HA, as a function of its molecular weight, calculated from Eq. 3 and 4, respectively.

	HA6.4	HA752	HA1500
R_g (nm)	6.8	102.4	151.9
R_h (nm)	2.8	56.4	87.2

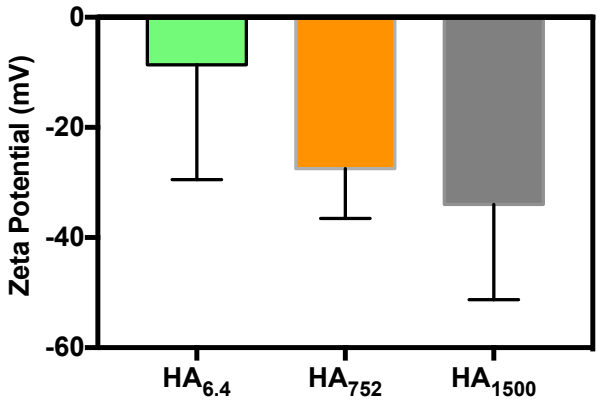

Supplementary Fig. 4-4. Zeta Potential of the LbL films using HA of Mws.

Chapter 5

Molecular weight of surface immobilized hyaluronic acid influences CD44-mediated binding of gastric cancer cells

Chapter 5

Molecular weight of surface immobilized hyaluronic acid influences CD44-mediated binding of gastric cancer cells[‡]

ABSTRACT

The physiological importance of the interactions between hyaluronic acid (HA) and its main membrane receptor, CD44, in pathological processes, e.g. cancer, is well recognized. However, these interactions are mainly studied in solution, whereas HA in the extracellular matrix (ECM) is partially immobilized via its interactions with other ECM components. We therefore, developed substrates in which HA is presented in an ECM-relevant manner. We immobilized HA with different molecular weights (Mw) in a Layer-by-Layer (LbL) fashion and studied the interactions of the substrates with CD44 and two human gastric cancer cell lines that overexpress this receptor, namely AGS and MKN45. We demonstrate that MKN45 cells are more sensitive to the LbL substrates as compared with AGS. This difference is due to different CD44 expression: while CD44 is detected mainly in the cytoplasm of AGS, MKN45 express CD44 predominantly at the cell membrane where it is involved in the recognition and binding of HA. The invasiveness of the studied cell lines was also evaluated as a function of HA Mw. Invasive profile characterized by low cell adhesion, high cell motility, high expression of cortactin, formation of invadopodia and cell clusters was observed for MKN45 cells when they are in contact with substrates presenting HA of high Mw.

[‡] This Chapter is based on the publication "Amorim, S., da Costa, D. S., Freitas, D., Reis, C. A., Reis, R. L., Pashkuleva, I., & Pires, R. A. (2018). *Molecular weight of surface immobilized hyaluronic acid influences CD44-mediated binding of gastric cancer cells*. Sci Rep, 8(1)"

5-1. INTRODUCTION

Hyaluronic acid (HA) is a non-sulfated glycosaminoglycan (GAG) that is present in the extracellular matrix (ECM) of all mammalian cells.[1] It is involved in key signaling pathways determining cell fate but also progression of some malignant tumors.[1-4] One of the main transmitters of the HA bioactivity is the transmembrane glycoprotein CD44 – the principal cell surface receptor of HA.[1-3, 5, 6] CD44 can be expressed as different isoforms: the most common standard isoform, CD44s, is expressed in most cells, while some CD44v (CD44 variants containing variable exons) are associated with specific tumors.[5-8] In fact, the CD44+ subpopulation of cancer stem cells (CSCs) in solid tumors have been identified as cancer-initiating cells.[9] This subpopulation is resistant to chemo- and radio-therapies commonly employed in cancer treatment.[10] Under specific culture conditions, cancer cell lines, such as AGS and MKN45, behave as CSCs, i.e. they express CSC markers (e.g. CD44) and have self-renewal capacity, present high proliferation rate, and exhibit high drug resistance, among other characteristics.[11]

Together with CD44, endogenous HA is also involved in different stages of malignant tumor progression. HA expression is usually up-regulated in the tumor microenvironment.[1, 3, 4] The interactions between HA and the membrane receptors of cancer cells activate several signaling pathways that promote tumor cell growth, survival, and migration, thereby increasing metastatic spread.[1, 3, 4] The concentration of HA and its Mw is of crucial importance for these interactions. In humans, cells secret HAs with different Mws in ECM: HAs of high Mw (up to 2 MDa) are generated by hyaluronan synthases HAS1 and HAS2, while the analogues with lower Mw (up to 200 kDa) are produced by HAS3.[12] When secreted by the cells, these HAs can be further modified by hyaluronidases (HYALs) – specific enzyme family that catalyze the degradation of HA – to generate species with even lower Mw HAs, including the oligo-HAs that present Mws of up to 6.4 kDa (16 disaccharide units).[13] The delicate balance between synthases and hyaluronidases determines the HAs composition in the ECM and depends on the specific cells/tissues and their pathological state. Generally, HAs with high Mw (Mw > 500 kDa) are space-filling molecules involved in normal biological processes. They have anti-angiogenic and immunosuppressive properties. Usually, they are associated with inhibition of cellular differentiation by suppressing cell–cell interactions or ligand access to cell surface receptors. In contrast, the shorter HA fragments (Mw = 20-200 kDa) have pro-inflammatory, immuno-stimulatory and angiogenic properties. HAs with low Mw are detected in cancers. Their effect is

contradictable: some studies relate low Mw HA with enhanced cancer cell invasion[14-16], while others report reduced invasiveness in the presence of these HAs.[17] These contradictions can be explained with the used models to study this effect and their relevance to the *in vivo* scenario.

Different approaches have been developed to elucidate the HA-CD44 interactions.[18, 19] Of note, most of these approaches focus on interactions occurring between molecules in solutions, however there is limited information regarding the interactions between immobilized HA and CD44 and/or cancer cells. The presentation of HA in such context of spatial confinement, with restricted flexibility, is of great interest in the design and development of ECM mimics and biomedical devices, e.g. biosensors, in which functionalization with HA is required.

In the present work, we report on the interactions of immobilized exogenous HA of different Mws (oligo, 6.4 kDa; medium, 752 kDa; and high, 1500 kDa) with two gastric cancer cell lines (AGS and MKN45). We applied the Layer-by-Layer (LbL) approach to deposit HA of different Mws on tissue culture polystyrene (TCPS). This approach allows surface immobilization of biomolecules with minimal or no changes of their chemistry, i.e. with preserved bioactivity. Moreover, the immobilized molecules are presented in an ECM fashion: they are spatially restricted but enough flexible to reorganize and bind CD44.

5-2. MATERIALS AND METHODS

5-2.1. Materials.

Unless otherwise stated, chemicals were used without further purification. Poly-L-lysine hydrobromide (PLL; Mw 30-70 kDa), N-(3-dimethylaminopropyl)-N′-ethylcarbodiimide hydrochloride (EDC) ≥98.0% and N-hydroxysuccinimide (NHS) were obtained from Sigma-Aldrich. Hyaluronic acid (HA; Mw 6.4 kDa, 752 kDa and 1500 kDa) was purchased from Lifecore. We used Anti-CD44 antibody [KM201] (ab25340) and Mouse IgG1 Kappa [MOPC-21]-Isotype 1 (ab18443) from Abcam for the CD44 blocking. Recombinant Human CD44 His tag protein was purchased from Biorbyt. Phalloidin–tetramethylrhodamine B isothiocyanate (phalloidin–TRITC), 4,6-diamidino-2-phenyindole, dilactate (DAPI) from Sigma-Aldrich and the monoclonal antibody to CD44 from Acris-Antibodies were used for immunostaining. The secondary antibody, Alexa Fluor 488 Rabbit Anti-Mouse IgG, was obtained from

Invitrogen. The primary antibody Cortactin (H-191), sc-11408, was obtained from Santa Cruz Biotechnology.

5-2.2. Methods

5-2.2.1. Formation and characterization of the PLL-HA bilayer system

The substrates used in this study were TCPS coverslips (13 mm diameter). The bilayer deposition was performed as previously described.[20] Briefly, the coverslips were immersed into a polycation solution (PLL, 0.5 mg/mL in 0.15 M NaCl) for 15 min, then removed and washed (0.15 M NaCl, pH ≈ 6.0 – 6.5) and then immersed into the polyanion solution (HA, 1 mg/mL in 0.15 M NaCl) supplemented with a crosslinking agent (EDC, 400mM and NHS, 100 mM) for 15 min. The coated TCPS (TCPS-PLL-HA_m, where m represents the Mw of the HA) were rinsed with water to remove the excess of salt, dried at room temperature and characterized or used in further studies.

5-2.2.2. ζ-potential measurements

SurPASS electrokinetic analyzer (Anton Paar, Graz, Austria), was used to determine the zeta potentials of the assembled films. The TCPS-PLL-HA_m were mounted in an adjustable disk gap cell (14 mm diameter). The gap between the discs was adjusted to approx. 110 μm and an electrolyte (1 mM NaCl, pressure of 400 mbar) was flowed through the cell. The streaming currents (I_{str}) were determined at different pH values within the range 5.5 to 10 automatically adjusted by the addition of NaOH (0.05 M) to the solution. The respective ζ-potentials were calculated and averaged over three measurements using Attract 2.0 software (this software uses Smoluchowski equation for calculation of ζ-potentials from I_{str}).

5-2.2.3. Atomic Force Measurement (AFM)

The experiments were performed on a JPK NanoWizard 3 (JPK, Germany). The roughness and mechanical properties of the films were measured under QI Advanced Mode using SNL-10 probes (resonance frequency of ~65kHz; spring constant of ~0.34N/m; Bruker, Germany) with the exception of the PLL coated surface where a TAP525 probe (resonance frequency of ~525kHz; spring constant of

~200N/m, Bruker, Germany) was used. The Young modulus of the films were calculated by fitting the approach curves with the Hertz model, using a paraboloid tip shape (applying a very short indentation range, 0.5-1nm – to eliminate contribution of the underlying substrate). All the probes were calibrated by contact with the underlying surfaces, from which sensitivity was determined, and by fitting the cantilever resonance frequency. All the experiments were performed in air, while the surfaces were humidified using a drop of water.

5-2.2.4. Quartz Crystal Microbalance (QCM-D) *in situ* measurements and modelling

The substrates used for this characterization were gold-coated AT-cut quartz crystals (QSX301, Q-Sense, Sweden). The crystals were washed several times with ethanol, dried under N_2, and immediately placed in the QCM-D flow chamber (E4 instrument, Q-Sense). A stable baseline was acquired in 0.15 M solution of NaCl at 25 °C. The PLL solution (0.5 mg/mL in 0.15 M NaCl) was added to the chamber under a flow rate of 50 μL/min for 15 minutes. The sensor was rinsed with 0.15 M NaCl aqueous solution to remove loosely bound material and HA solution (1 mg/mL in 0.15 M NaCl) supplemented with the crosslinking agents 4 EDC:1 NHS was injected (50 μL/min) in the flow chamber for 15 min. After rinsing (0.15 M NaCl), Human CD44 His-tag protein (2 μg/mL in 1% BSA in phosphate-buffered saline (PBS)) was flowed onto the deposited PLL-HA bilayer until signal stabilization. Finally, the sensor was rinsed (0.15 M NaCl) to remove loosely bound protein. All measurements were performed at several harmonics (n = 3, 5, 7, 9 and 11). $\Delta F/n$ and ΔD were fitted for the 5th, 7th and 9th overtone using the Q-Tools software (v 3.0.6.213). Voigt element-based model was applied to obtain the thickness of the PLL-HA bilayers. The mass of the wet films and of the adsorbed CD44, was calculated by fitting the data in an interactive fashion, and by assuming a fluid density of 1020 kg/m^3, a fluid viscosity of 0.001 kg/m.s, and a layer density of 1200 kg/m^3.

5-2.2.5.Culture, expansion and seeding of gastric cancer cell lines

Human gastric cancer cell lines AGS and MKN45 were cultured in RPMI-1640 medium (Sigma-Aldrich) supplemented with 10% heat-inactivated fetal bovine serum (FBS; Biochrom AG, Germany) and 1% antibiotic/antimycotic solution (final concentration of penicillin 100 units/mL and streptomycin 100 mg/mL; Gibco, UK). Cells were cultured in a 5% CO_2 incubator at 37°C. Before the *in vitro* studies, the substrates (TCPS-PLL-HA$_m$) were sterilized by exposing them to UV light for 30 min. Confluent AGS and

MKN45, were harvested and seeded on TCPS-PLL-HA_m at a density of 11000 cells/cm^2. The cells were cultured for 3 days. Uncoated TCPS substrates were processed as the other samples and used as control.

5-2.2.6. Protein expression

After each time point the samples were washed twice with PBS, fixed in 10% neutral buffered formalin for 30 min at 4°C, permeabilized with 0.2% Triton X-100 in PBS for 5 min, and blocked with 3% BSA in PBS for 30 min at room temperature. The CD44 expression was evaluated by CD44 monoclonal antibody (clone 8E2F3, 1:400 in 1% w/v BSA/PBS), followed by rabbit anti-mouse Alexafluor-488 (1:500 in 1% w/v BSA/PBS). Cortactin was visualized by using cortactin rabbit polyclonal antibody (H-191, 1:400), followed by the secondary rabbit anti-mouse Alexafluor-488 (1:500 in 1% w/v BSA/PBS). E-Cadherin was stained using rabbit monoclonal antibody (EP700Y, 1:500), followed by the secondary rabbit anti-mouse Alexafluor-488 (1:500 in 1% w/v BSA/PBS). The cells were observed under confocal laser scanning microscope (TCS SP8, Leica, Germany).

5-2.2.7. Morphology, distribution and motility of AGS and MKN45

A phalloidin–TRITC conjugate was used (1:200 in PBS for 30 min) to assess cytoskeleton organization and cell morphology of the studied cell lines. Nuclei were counter-stained with DAPI (1 mg/mL in 1% BSA in PBS for 30 min). Samples were washed with PBS, mounted with Vectashield (Vector) on glass slides and observed under an Imager Z1 microscope (Zeiss, Germany) and photographed using an Axio Cam MRm camera (Zeiss, Germany) to evaluate the number of adherent cells. Confocal laser scanning microscope (TCS SP8, Leica, Germany) was used to evaluate the morphology of adherent cells. Live monitoring of individual cell motility was performed at 37 °C in an inverted microscope (Zeiss Axio Observer) equipped with a temperature and CO_2 control device (5% CO_2). Time-lapse images (40X) were captured every 1 min using Zen software. Cells were continuously observed for 60 min. Image stacks were analyzed with the image processing software Fiji (http://fiji.sc/wiki/index.php/Fiji) and cell displacement quantified using Track Mate Plugin.

5-2.2.8. Flow Cytometry analysis

AGS (P8) and MKN45 (P7) were detached with TrypLe. TrypLe is a mix of recombinant cell-dissociation enzymes. Its action is milder than the commonly used porcine trypsin: TrypLe preserves better cell-surface epitope expression when compared to trypsin[21]. Detached cells were re-suspended in PBS and incubated for 20 min at room temperature with mouse anti-human CD44-PE antibody (clone 515) and mouse anti-human CD44v6 monoclonal antibody (MA54), following manufacturer-recommended concentrations. Cells were subsequently washed with PBS, centrifuged, fixed in 1% paraformaldehyde (Sigma), and analyzed on a FACs Calibur Flow Cytometer (BD Biosciences) using the Flowing Software v2.5.1.

5-2.2.9. Image analysis

The quantification of adherent cells and the time for adhesion were performed using ImageJ analysis software (Version 2.0.0-rc-34/1.50a).

5-2.2.10. Statistical Analysis

The normality of the data was evaluated using Shapiro–Wilk test (p<0.05). When the data did not follow a normal distribution an initial Kruskal–Wallis test was executed followed by Mann-Whitney test. T-test was performed for data with a normal distribution. In all the cases, a significant variation was only considered for a $p < 0.001$ (***).

5-3. RESULTS AND DISCUSSION

5-3.1. Immobilization of HA

Biomacromolecules can be immobilized on different substrates following two general approaches. In the first one, a covalent bond between the substrates and the biomolecule is formed. This approach generates stable and chemically defined platforms but usually requires functionalization of the support and the biomolecule – a process that can compromise the bioactivity of the immobilized component

either by modifying its active centers or by restricting its mobility, i.e. ability of binding sites alignment.[22-24] On the other hand, non-covalent immobilization does not require any pre-functionalization of the biomacromolecules. It relies on their simple deposition (usually by physical adsorption) on properly modified substrates. These approaches are associated with higher flexibility of the deposited molecules but also with a limited stability: while polymers with high Mw assemble in relatively stable coatings, their oligo-derivatives form unstable surfaces.[23] Herein, we applied the LbL approach to immobilize and present HA in an ECM resembling manner. The most common LbL assembly relies on alternate deposition of polyelectrolytes with opposite charges.[25, 26] We therefore used HA (a weak polyanion) in combination with poly-L-lysine (PLL, strong polycation). This system is well studied by us and others: it has been shown that the Mw of the polyions can alter dramatically both the structure of the multilayer system and its stability.[20, 27-31] Based on these previous findings and the requirement to test HA with different Mw, we have used a bilayer system that was crosslinked via common carbodiimide chemistry. We expected that such constructs would be stable and with limited "in and out" mobility, i.e. the layers would be defined, and that HA present on the surface of the construct would be enough flexible to reorganize and bind CD44 (Fig. 1A).

The deposition of the layers was followed *in situ* by quartz crystal microbalance with dissipation (QCM-D, Fig. 1B). This acoustic technique is based on a quartz crystal disk (QCM-D sensor) that oscillates at its resonance frequency when an alternating potential is applied. The resonance frequency (F) changes upon mass adsorption on the surface and the deposited mass can be calculated from the Sauerbrey's equation when rigid films are formed. Beyond the Sauerbrey limit, the viscoelastic properties of the films can be accessed using an appropriate model such as the Voigt one.[32] Besides the deposited mass, QCM-D also allows quantification of the viscoelastic properties of the deposited films. Such measurements are performed by continuous switch on and off of the driving potential that result in a decay of the freely oscillating crystal and allows measurement of the energy dissipation (D).

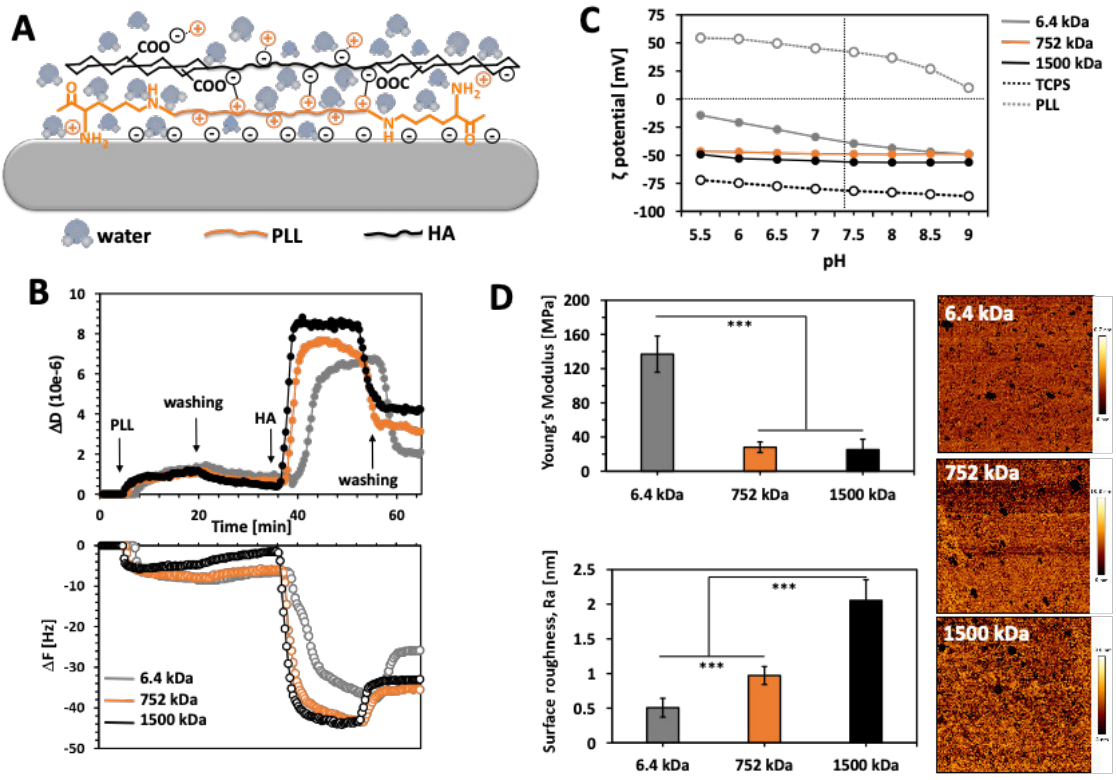

Figure 5-1. Schematic presentation of the used substrates (A) and their characterization by QCM-D (B), electrokinetic analysis (C) and AFM (D). All AFM data were obtained after scanning areas of 150x150 nm. The significant differences are marked by (***) for $p < 0.001$.

The adsorption of PLL and HA was confirmed by a decrease of F and an increase of D (Fig. 1B). The changes were more pronounced during the build-up of the HA layer (regardless the Mw) than during the PLL deposition. These results are in a very good agreement with previous reports that refer to the high hydration state of the HA as a main reason behind this difference.[27, 28, 31] In fact, the AFM characterization confirmed this explanation (Fig. 1D): the deposition of the first PLL layer resulted in a formation of relatively stiff surface (~600 MPa, data not shown). The following adsorption of the HA led to a sharp decrease of the Young's Modulus that is a result from the high capacity of HA to adsorb and retain water, i.e. to form very swelled films.[33] This difference was much bigger for the HA with medium and high Mw (~25 MPa for 752 and 1500 kDa) than for the oligo-HA (~140 MPa for HA of 6.4 kDa) and it is consistent with previous reports.[29, 33, 34] The results obtained for the roughness (Ra) of the substrates are also in agreement with the literature. We observed formation of "islets" upon adsorption of the HA (brighter areas in Fig. 1D).[31, 34] The size of these islets and the Ra of respective bilayer depends on the Mw of the HA - larger islets are formed from HA with higher Mw.

The preservation of the LbL structure, i.e. lack of layers' migration and the presence of the HA on the substrate's surface, was confirmed by electrokinetic analysis (Fig. 1C). This characterization method gives information about the ζ-potential of the surface. The deposition of PLL onto TCPS altered the ζ-potential, from negative to positive: at pH 7.4 (physiological pH) the surface charge of the substrate changed from -82 mV to +42 mV. The following deposition of HA led to a reversion of the ζ-potential to negative values. Of note, the ζ-potentials of the surfaces presenting HA of 752 and 1500 kDa do not change significantly with the pH, indicating the formation of stable and chemically defined constructs. The bilayers formed from oligo-HA, i.e. 6.4 kDa, present similar behavior at basic and neutral pHs. However, at acidic pH we observed an increasing ζ-potential for this system, indicating instability or possible layer migration at these pH values.[29]

5-3.2. Interactions of LbL with CD44

The Mw and presentation of HA (soluble or immobilized) affect tremendously the activation of its receptors, the binding to these receptors and the resulting downstream signaling.[15, 16, 35, 36] The most widely accepted theory suggests that the HA-receptor binding relies on multivalent interactions and the downstream signaling is related with the ability of HA to cluster the receptors on the cell surface (Supplementary Fig. 1). The minimal binding size of HA depends on the receptor: 6-mer of HA binds to CD44, while 4-mer does not interact with this receptor.[2, 15] Importantly, 6- to 18-mers of HA bind CD44 monovalently and thus, impede the following clustering and signaling. Size-dependent HA signaling can also differ according to cell type and HA presentation. So far, most of the generated results consider HA in solution, usually as a supplement to the cell culture media. However, *in vivo* HA is embedded in the ECM, where it interacts with other bioentities that restricts HA spatial freedom and defines spatially its binding sites.[16] The LbL substrates designed by us are reductionist model of this environment. We characterized their interactions with CD44 *in situ* using QCM-D (Fig. 2).

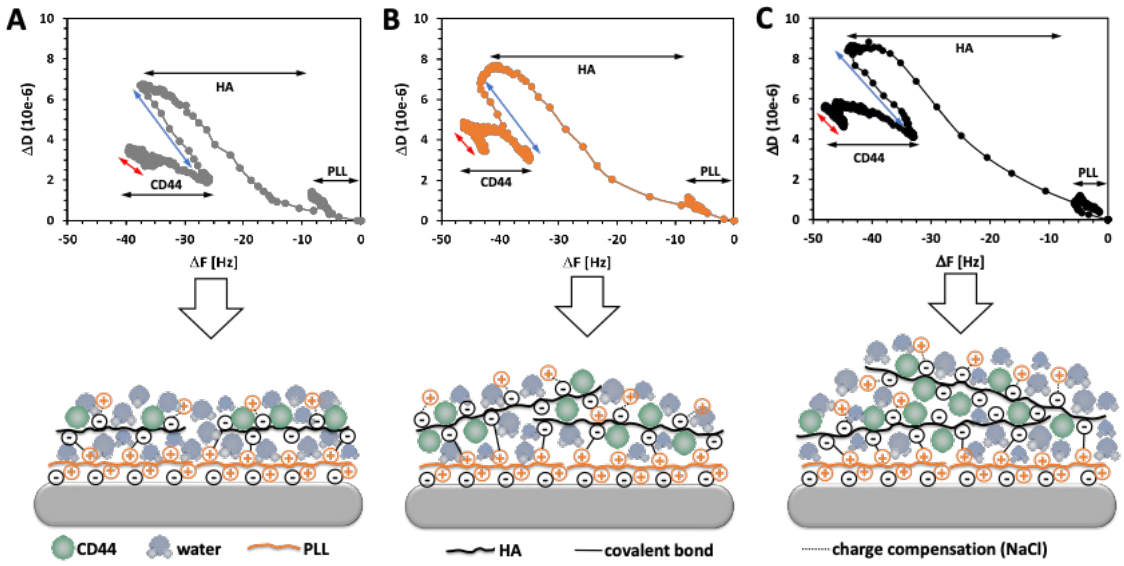

Figure 5-2. D/F plots and respective models for the interactions between CD44 and the surfaces prepared with HA of 6.4 kDa (A), 752 kDa (B) and 1500 kDa (C). The arrows indicate each layer build-up (black) and the respective washing steps after HA (blue) and CD44 (red) depositions.

Herein, we present the QCM-D data as D/F plots because this kind of presentation visualize readily the dissipation caused by a unit of frequency (mass).[37, 38] The results clearly demonstrate that CD44 interacts with all LbLs. While this technique does not allow quantification of the retained protein (because the signal change includes also the water retained in the LbL), it is interesting to see differences among the studied substrates. The CD44 deposition on the surface presenting HA of 6.4 kDa resulted in a decrease of F and an increase of D, i.e. in a linear change of D/F plots (Fig. 2A), indicating formation of a protein monolayer on the top of the constructs. Different signal shape is observed for the LbL formed from HA with medium and high Mws (752 and 1500 kDa). The initial CD44 deposition follows the same trend as for the surface presenting HA of 6.4 kDa but then, we observe deposition of mass (decrease of F) that is not accompanied with changes of D (Fig. 2B and C, the plateau of the CD44 part in D/F plots). This signal indicates that after initial deposition on the substrate surface, CD44 penetrate within the constructs where it replaces the water (the schemes in Fig. 2B and C). This process is only valid for longer HA chains that form LbL with more free volume in their vicinity (as shown by the QCM-D data in Fig. 2: grey line vs orange and black ones in ΔD plot). Moreover, the degree of freedom of these HA chains is higher and they are able to reorganize better and capture the CD44 from the solution.

5-3.3. Cell adhesion and morphology of AGS and MKN45 seeded on LbL

We studied the behavior of two different gastric cancer cells, namely AGS (intestinal type of gastric carcinoma) and MKN45 (diffuse type of gastric carcinoma). According to previous reports, these cell lines overexpress CD44s and some CD44v, e.g. CD44v6, which are associated with cancer.[39, 40] Patients with gastric carcinoma and high expression of CD44v6+ are usually diagnosed with advanced stage of the disease, related with high metastasis potential and mortality.[10, 41-44]

Our results confirm that indeed both cell lines express CD44 when cultured on TCPS, although there are differences among them: while all MKN45 are CD44s+ and very big population is CD44v6+, only about half of AGS cells are CD44s+ and CD44v6+ (Table 1 and Supplementary Fig. 3).[10] Besides larger CD44+ population, MKN45 cells express much higher amount of CD44s as demonstrated by the mean fluorescence intensity (MFI, Table 1).

In the absence of HA, i.e. on TCPS and on PLL substrates, we observed comparable number of adherent AGS and MKN45 cells (Fig. 3 white bars). Upon addition of HA to the cell culture medium, we did not observe any effect of the Mw of the supplemented HA either for AGS or for MKN45 cells (Supplementary Fig. 2). When cells were cultured on the LbL constructs with HA, the number of the adhered AGS cells did not change significant (about 100 cells/mm^2, Fig. 3A), while less attached MKN45 cells (maximum 58 cells/mm^2) were determined on these substrates and this difference was most significant for the surface presenting HA of 1500 kDa. Possible explanations of this result are the different expression and/or availability of the CD44 (CD44s and CD44v) on the surface of the studied cell lines in response to the substrate change or/and different adhesion mechanism of AGS and MKN45 cells. We, therefore, used flow cytometry to quantify the percentage of cells that expresses CD44s and the CD44v6 (positive cell population) and the quantity of the protein they express on their surface (Mean Fluorescence Intensity, MFI) in contact with the surfaces presenting HA of different Mws (Table 1 and Supplementary Fig. 3).

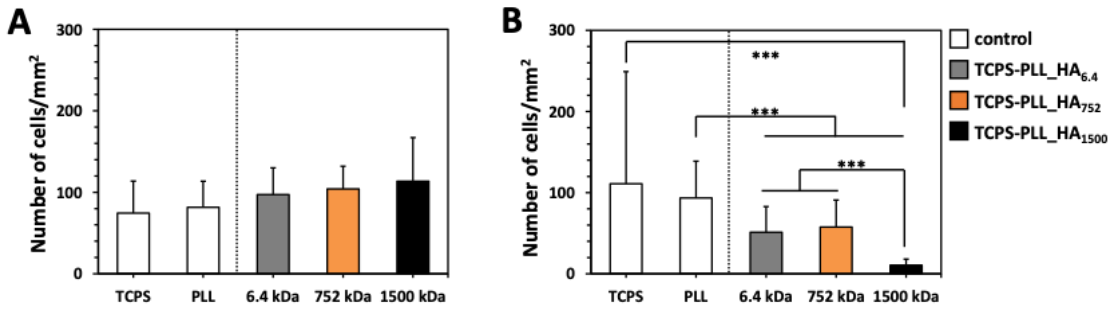

Figure 5-3. Number of adherent AGS (A) and MKN45 (B) cells after 72h of culture on different substrates. Significant differences are marked with * ($p < 0.001$).**

The presence of HA on the substrates induces different response of the studied cells. AGS cells recruit CD44s on their surface: bigger CD44+ populations and higher expression (MFI, Table 1) of CD44s were determined for these cells in contact with LbL as compared with cells cultured on TCPS. While the trend is the same for all LbL substrates, cells cultured on LbL of the oligomeric HA (6.4 kDa) show smaller increase in terms of both population size and MFI. The substrate change affects less the expression of CD44v6 in AGS but in this case the LbL of shortest HA analogue induces the bigger change. Opposite effect was observed for MKN45 cells. The CD44s(+) population is preserved but the cells express less protein on the surfaces (smaller MFI as compared with the TCPS one) in contact with LbL and this effect was less pronounced for the substrates with HA of 6.4 kDa (Table 1). The presence of HA affects also the expression of CD44v6 by MKN45: smaller CD44v6(+) populations were determined in this case.

Table 5-1. Expression of CD44s and CD44v6 in AGS and MKN45 cells as a function of the substrate surface composition. The quantification was performed by fluorescence-activated cell sorter (FACS) after 72 h of cell culture in contact with the respective substrates.

	AGS				MKN45			
	TCPS	HA6.4	HA752	HA1500	TCPS	HA6.4	HA752	HA1500
	$CD44^+$ cell populations [% from the total cell population]							
CD44s	47.08	85.07	94.10	94.96	99.08	94.81	95.14	95.13
CD44v6	50.30	77.37	57.14	56.25	83.11	63.30	73.94	76.69
	Mean Fluorescence Intensity (MFI)							
CD44s	13.41	20.61	30.71	31.23	193.51	164.25	137.37	140.91
CD44v6	14.12	16.50	14.96	14.41	20.57	18.76	19.36	22.51

The involvement of these receptors in the adhesion to the LbL was evaluated by blocking them and studied the behavior of AGS and MKN45 in contact with the same substrates (Fig. 4). The CD44 blocking did not affect AGS attachment (Fig. 4A) but significantly less MKN45 cells were observed on all HA functionalized substrates (Fig. 4B) indicating that MKN45 cells adhesion is CD44-mediated. AGS cells used other mechanisms of adhesion, which do not involve CD44-HA interactions, possibly through integrin mediation.[45, 46] These seemingly contradictory results for AGS cells (recruiting CD44 but not using them for HA binding) can be explained by structural differences of the CD44 expressed by these cells. Differences in the Mw (different variant isoforms generated by alternative splicing) and glycosylation profile can affect tremendously the HA binding.[40, 47] Usually, poor HA binding is related with steric hindrance of the binding sites caused by extensive CD44 glycosylation or/and significant elongation of the receptor.

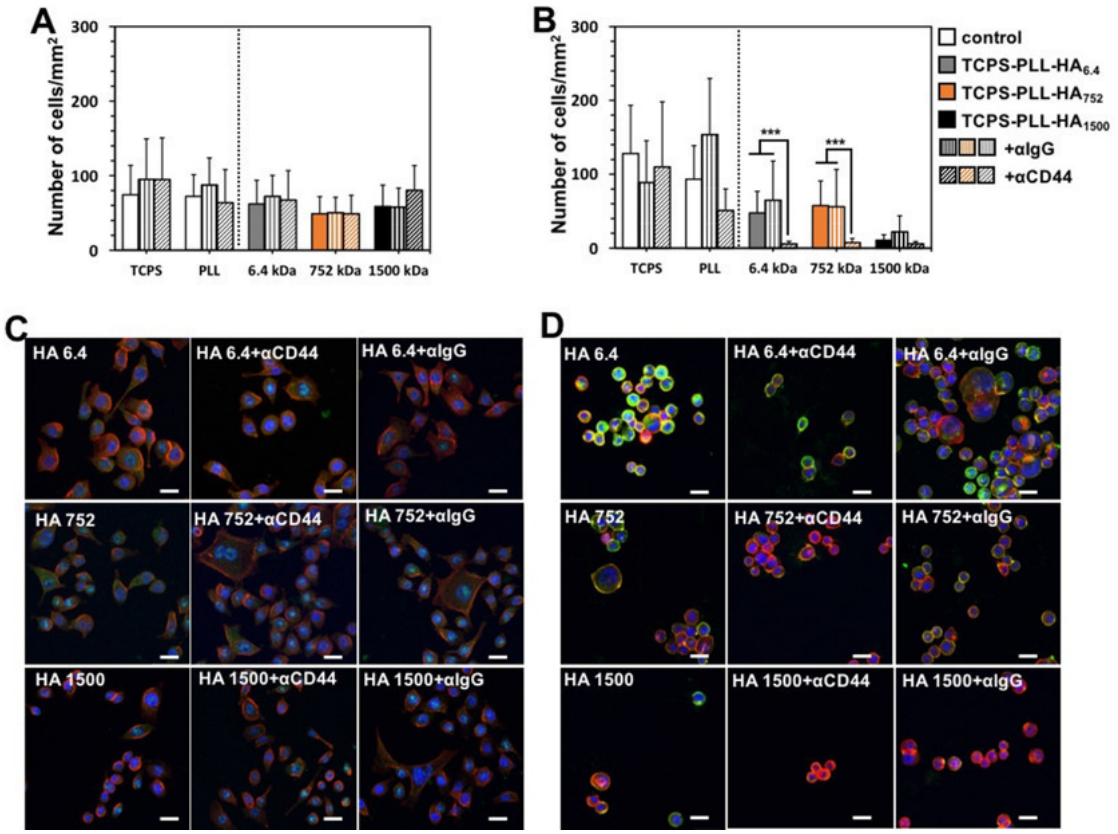

Figure 5-4. Effect of CD44 blocking on the adhesion of AGS (A, C) and MKN45 (B, D) presented as number of adherent cells (A, B) and visualized by immunohistochemistry (green for CD44, red for actin and blue for nuclei). The results were obtained for cell cultured during 78 h. Bars correspond to 50 µm. IgG was used as an isotype control. Significant differences (Kruskal–Wallis, Mann-Whitney test, $p < 0.001$) are marked with *. Images for the control substrates (TCPS and TCPS-PLL) are presented in Supplementary Fig. 4.**

The adhesion assay was complemented by immunofluorescence analysis that confirmed this hypothesis. This analysis visualizes the CD44s expression/distribution and cell morphology (Fig. 4C and D). In agreement with flow cytometry results (MFI, Table 1), we can see that the CD44 expression (all CD44 isoforms) is much higher for the MKN45 (Fig. 4D) than for the AGS cell line (Fig. 4B). Another important difference that is visible from the immunofluorescence analysis is the tendency of the MKN45 to adhere in clusters, i.e. their adhesion is dependent on cell-cell contacts. This behavior is important especially in the case of the surface presenting HA of 1500 kDa, where we observed very few adherent cells/clusters and thus, we were not able to conclude on the influence of the CD44 blocking on the MKN45 cell adhesion to these substrates. Last, but not least important remark is that CD44 in AGS is detected mainly in the cytoplasm, while MKN45 express it at the cell membrane (green staining in Fig. 4C vs 4D). This different expression may lead to a higher sensitivity of the MKN45 cells towards the surface immobilized HA.

5-3.4. Invadopodia formation by CD44 downstream activation

Cancer invasion and metastasis is linked to the existence of specific actin-rich membrane protrusions called invadopodia.[48, 49] Several proteins are involved in the formation and development of these protrusions: Tks5, cortactin and neural Wiskott-Aldrich syndrome protein (N-WASP) compose the core structure of invadopodia.[50, 51] Among these, cortactin is overexpressed in several cancer cells, where it regulates the secretion of matrix metalloproteinases (MMPs) to the stubs of degrading invadopodia, being crucial for the formation and function of these protrusions.[52, 53] CD44-HA crosstalk is also involved in this process: it induces stabilization and maturation of invadopodia through the activation of $\alpha 5\beta 1$ integrin and phosphorylation of cortactin.[54] We therefore evaluated the formation of invadopodia and expression of cortactin by AGS and MKN45 cells cultured on the surfaces presenting the HA of different Mws (Fig. 5). Generally, MKN45 cells express more cortactin than AGS regardless of the used substrate (Fig. 5A vs 5B). The expression was affected by the Mw: HA with higher Mw stimulate cortactin expression in both AGS (higher expression on HA of 752 kDa) and MKN45 cells (6.4 kDa<<752 kDa<1500 kDa). Cortactin co-localizes with actin at the cell membrane, which is associated with cortactin recruitment to cell–cell adhesive contacts in response to homophilic cadherin ligation.[55] This co-localization is well pronounced for MKN45 cells when HA of higher Mw is used on the substrates (Fig. 5B, yellow dots) and associated with the presence of cell clusters. In fact, these results are in good agreement with the E-cadherin expression observed for the MKN45 cells at the same type of cell-cell contacts (Fig. 5D). Cortactin also co-localizes with actin in punctate structures situated in the ventral surface of the cell, below its nucleus (Fig. 5A, B yellow staining shown by the white arrows). This co-localization together with the observed morphology and positioning of the structures is consistent with the formation of invadopodia.[56, 57]

Invadopodia formation can be related with mechanical properties of the substrate.[56, 58] In fact, the LbLs developed by us have different stiffness (Fig. 1D) that could trigger this process. LbL built-up from HA with lowest Mw (6.4 kDa) has highest surface stiffness. However, cells in contact with these substrates exhibit lower expression of cortactin/number of invadopodia, which is in contradiction with previous studies reporting higher surface stiffness as a promotor of invadopodia formation. We, therefore, conclude that the Mw of the HA is the key regulator of the invadopodia formation for the studied substrates. These results are in agreement with the observed expression of CD44 on the cell membrane in response of the HA's Mw: CD44 activates Src-kinase, which regulates the phosphorylation of cortactin and consequently, the formation of invadopodia.[59]

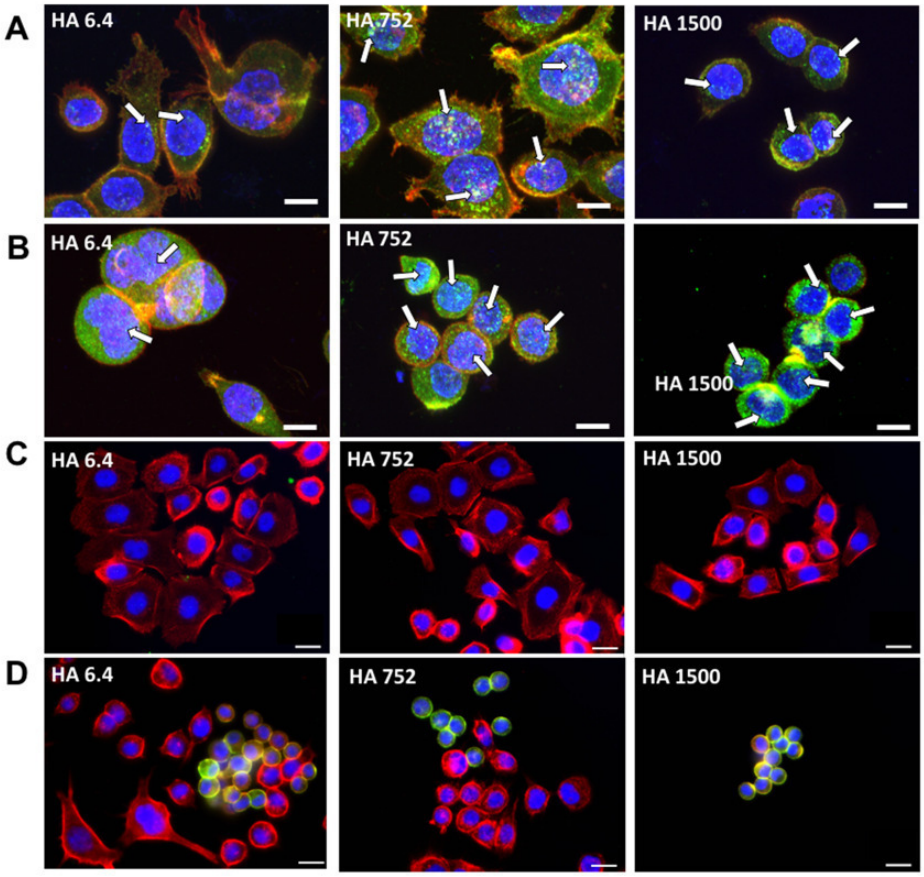

Figure 5-5. Expression of cortactin (A, B) and E-cadherin (C, D) by AGS (A, C) and MKN45 (B, D) cell lines. Cortactin, E-cadherin: green; actin: red; and nuclei: blue. Co-localization of actin/cortactin (A, B; white arrows) and actin/E-cadherin (C, D): yellow. Bars correspond to 10 µm for A and B and 20 µm for C and D.

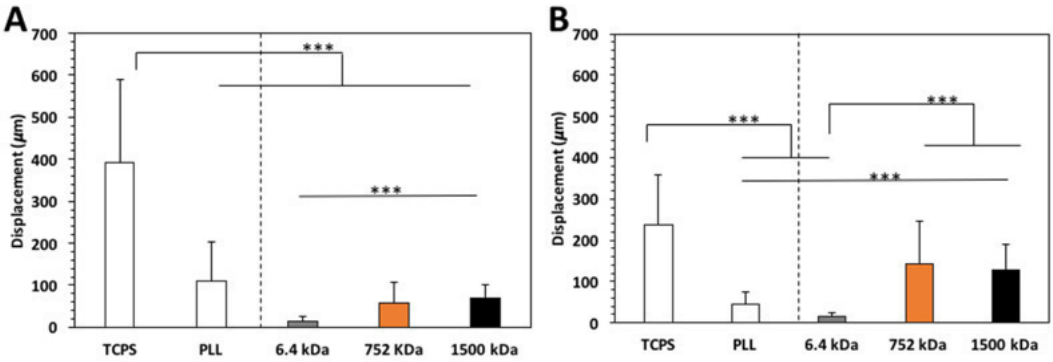

Figure 5-6. Single cell motility assay for AGS (A) and MKN45 (B) during 60 min of incubation. Significant differences (t-test) are marked with *** for a $p < 0.001$.

The Mw of the HA affected also the individual cell migration (Fig. 6A-B). Lowest cell motility and the shorter cell tracks (Supplementary Fig. 5) were observed for cells in contact with HA of 6.4 kDa. The migration ability of both AGS and MKN45 cells increased on substrates with HA of higher Mw. Moreover, MKN45 cells present lower displacements than AGS on the control substrates (TCPS and PLL, i.e. no HA) but this behavior was switched on surfaces presenting HA of higher Mws (752 and 1500 kDa), where MKN45 cells (high surface expression of CD44) exhibit a higher cell motility than AGS cells.

5-4. CONCLUSIONS

We demonstrate that immobilized HA have different effect on cancer cell behavior as compared with soluble HA supplemented with the culture media. The effect of HA depends not only on its presentation but also on the cancer cell type and the expression of CD44. We observed a relationship between the cell behavior and the Mw of the immobilized HA for cells that have high surface expression of CD44. Invasiveness properties such as low cell adhesion, high cell motility, high expression of cortactin, formation of invadopodia and cell clusters were enhanced for such cells when they are in contact with substrates presenting HA of high Mw. While our results demonstrate that HA Mw influences cancer cell behavior, it also indicates that the way HA is presented (soluble vs immobilized) is of relevance for its biological functions. The use of platforms of immobilized HA resembling its presentation in the ECM (similar to the ones that we describe) to study cancer cell biology are probably more adequate than the use of soluble HA.[60, 61] These platforms can be used to screen the activity of drugs on cancer cell invasion (whose evolution is dependent on the interaction between CD44-HA), leading to the achievement of consistent data that supports the further evaluation of selected drugs in the pipeline that leads to their use in the clinical practice.

5-5. REFERENCES

1. Toole, B.P., *Hyaluronan: From extracellular glue to pericellular cue.* Nature Reviews Cancer, 2004. **4**(7): p. 528-539.

2. Misra, S., et al., *Interactions between hyaluronan and its receptors (CD44, RHAMM) regulate the activities of inflammation and cancer.* Frontiers in Immunology, 2015. **6**.

3. Fuster, M.M. and J.D. Esko, *The sweet and sour of cancer: Glycans as novel therapeutic targets.* Nature Reviews Cancer, 2005. **5**(7): p. 526-542.

4. Pinho, S.S. and C.A. Reis, *Glycosylation in cancer: mechanisms and clinical implications.* Nat Rev Cancer, 2015. **15**(9): p. 540-55.

5. Borland, G., J.A. Ross, and K. Guy, *Forms and functions of CD44.* Immunology, 1998. **93**(2): p. 139-148.

6. Isacke, C.M. and H. Yarwood, *The hyaluronan receptor, CD44.* International Journal of Biochemistry & Cell Biology, 2002. **34**(7): p. 718-721.

7. Hsieh, H.F., et al., *Molecular studies into the role of CD44 variants in metastasis in gastric cancer.* Journal of Clinical Pathology-Molecular Pathology, 1999. **52**(1): p. 25-28.

8. da Cunha, C.B., et al., *De novo expression of CD44 variants in sporadic and hereditary gastric cancer.* Lab Invest, 2010. **90**(11): p. 1604-14.

9. Yu, D., et al., *Proteomic analysis of CD44(+) and CD44(-) gastric cancer cells.* Molecular and Cellular Biochemistry, 2014. **396**(1-2): p. 213-220.

10. Takaishi, S., et al., *Identification of Gastric Cancer Stem Cells Using the Cell Surface Marker CD44.* Stem Cells, 2009. **27**(5): p. 1006-1020.

11. Singh, S.R., *Gastric cancer stem cells: A novel therapeutic target.* Cancer Letters, 2013. **338**(1): p. 110-119.

12. Karousou, E., et al., *Roles and targeting of the HAS/hyaluronan/CD44 molecular system in cancer.* Matrix Biology, 2017. **59**: p. 3-22.

13. Chanmee, T., P. Ontong, and N. Itano, *Hyaluronan: A modulator of the tumor microenvironment.* Cancer Letters, 2016. **375**(1): p. 20-30.

14. Stern, R., A.A. Asari, and K.N. Sugahara, *Hyaluronan fragments: An information-rich system.* European Journal of Cell Biology, 2006. **85**(8): p. 699-715.

15. Cyphert, J.M., C.S. Trempus, and S. Garantziotis, *Size Matters: Molecular Weight Specificity of Hyaluronan Effects in Cell Biology.* International journal of cell biology, 2015. **2015**: p. 563818.

16. Sapudom, J., et al., *Molecular weight specific impact of soluble and immobilized hyaluronan on CD44 expressing melanoma cells in 3D collagen matrices.* Acta Biomaterialia, 2017. **50**: p. 259-270.

17. Wu, R.L., et al., *Hyaluronic acid in digestive cancers.* Journal of Cancer Research and Clinical Oncology, 2017. **143**(1): p. 1-16.

18. Yao, H.J., et al., *The effect of hyaluronic acid functionalized carbon nanotubes loaded with salinomycin on gastric cancer stem cells.* Biomaterials, 2014. **35**(33): p. 9208-23.

19. Zhu, H., et al., *The role of the hyaluronan receptor CD44 in mesenchymal stem cell migration in the extracellular matrix.* Stem Cells, 2006. **24**(4): p. 928-935.

20. Amorim, S., et al., *Hyaluronic acid/poly-L-lysine bilayered silica nanoparticles enhance the osteogenic differentiation of human mesenchymal stem cells.* Journal of Materials Chemistry B, 2014. **2**(40): p. 6939-6946.

21. Tsuji, K., et al., *Effects of Different Cell-Detaching Methods on the Viability and Cell Surface Antigen Expression of Synovial Mesenchymal Stem Cells.* Cell Transplantation, 2017. **26**: p. 1089-1102.

22. Altgarde, N., et al., *Probing the biofunctionality of biotinylated hyaluronan and chondroitin sulfate by hyaluronidase degradation and aggrecan interaction.* Acta Biomaterialia, 2013. **9**(9): p. 8158-8166.

23. Pashkuleva, I. and R.L. Reis, *Sugars: burden or biomaterials of the future?* Journal of Materials Chemistry, 2010. **20**(40): p. 8803-8818.

24. da Costa, D.S., et al., *Adhesion of Adipose-Derived Mesenchymal Stem Cells to Glycosaminoglycan Surfaces with Different Protein Patterns.* Acs Applied Materials & Interfaces, 2015. **7**(18): p. 10034-10043.

25. Boudou, T., et al., *Multiple Functionalities of Polyelectrolyte Multilayer Films: New Biomedical Applications.* Advanced Materials, 2010. **22**(4): p. 441-467.

26. Borges, J. and J.F. Mano, *Molecular Interactions Driving the Layer-by-Layer Assembly of Multilayers.* Chemical Reviews, 2014. **114**(18): p. 8883-8942.

27. Teixeira, R., R.L. Reis, and I. Pashkuleva, *Influence of the sulfation degree of glycosaminoglycans on their multilayer assembly with poly-L-lysine.* Colloids and Surfaces B-Biointerfaces, 2016. **145**: p. 567-575.

28. Crouzier, T. and C. Picart, *Ion Pairing and Hydration in Polyelectrolyte Multilayer Films Containing Polysaccharides.* Biomacromolecules, 2009. **10**(2): p. 433-442.

29. Porcel, C., et al., *Influence of the polyelectrolyte molecular weight on exponentially growing multilayer films in the linear regime.* Langmuir, 2007. **23**(4): p. 1898-1904.

30. Shen, L.Y., et al., *pH-Amplified Multilayer Films Based on Hyaluronan: Influence of HA Molecular Weight and Concentration on Film Growth and Stability.* Biomacromolecules, 2011. **12**(4): p. 1322-1331.

31. Picart, C., et al., *Buildup mechanism for poly(L-lysine)/hyaluronic acid films onto a solid surface.* Langmuir, 2001. **17**(23): p. 7414-7424.

32. Voinova, M.V., et al., *Viscoelastic acoustic response of layered polymer films at fluid-solid interfaces: Continuum mechanics approach.* Physica Scripta, 1999. **59**(5): p. 391-396.

33. Grohmann, S., et al., *Colloidal force spectroscopy and cell biological investigations on biomimetic polyelectrolyte multilayer coatings composed of chondroitin sulfate and heparin.* Biomacromolecules, 2011. **12**(6): p. 1987-97.

34. Kujawa, P., et al., *Effect of molecular weight on the exponential growth and morphology of hyaluronan/chitosan multilayers: A surface plasmon resonance spectroscopy and atomic force microscopy investigation.* Journal of the American Chemical Society, 2005. **127**(25): p. 9224-9234.

35. Yang, C.X., et al., *The High and Low Molecular Weight Forms of Hyaluronan Have Distinct Effects on CD44 Clustering.* Journal of Biological Chemistry, 2012. **287**(51): p. 43094-43107.

36. Wolny, P.M., et al., *Analysis of CD44-Hyaluronan Interactions in an Artificial Membrane System: Insights Into The Distinct Binding Properties Of High And Low Molecular Weight Hyaluronan.* Journal of Biological Chemistry, 2010. **285**(39): p. 30170-30180.

37. Hook, F., et al., *Structural changes in hemoglobin during adsorption to solid surfaces: Effects of pH, ionic strength, and ligand binding.* PNAS, 1998. **95**: p. 12271-12276.

38. Amorim, S., et al., *Interactions between Exogenous FGF-2 and Sulfonic Groups: in Situ Characterization and Impact on the Morphology of Human Adipose-Derived Stem Cells.* Langmuir, 2013. **29**(25): p. 7983-7992.

39. Fang, M., et al., *CD44 and CD44v6 are Correlated with Gastric Cancer Progression and Poor Patient Prognosis: Evidence from 42 Studies.* Cellular Physiology and Biochemistry, 2016. **40**(3-4): p. 567-578.

40. Rios de la Rosa Julio, M., A. Tirella, and N. Tirelli, *Receptor-Targeted Drug Delivery and the (Many) Problems We Know of: The Case of CD44 and Hyaluronic Acid.* Advanced Biosystems. **0**(0): p. 1800049.

41. Jang, B.I., et al., *The Role of CD44 in the Pathogenesis, Diagnosis, and Therapy of Gastric Cancer.* Gut and Liver, 2011. **5**(4): p. 397-405.

42. Xin, Y., et al., *CD44V6 in gastric carcinoma: A marker of tumor progression.* Applied Immunohistochemistry & Molecular Morphology, 2001. **9**(2): p. 138-142.

43. Yamaguchi, A., et al., *Expression of CD44v6 in advanced gastric cancer and its relationship to hematogenous metastasis and long-term prognosis.* Journal of Surgical Oncology, 2002. **79**(4): p. 230-235.

44. Campos, D., et al., *Probing the O-Glycoproteome of Gastric Cancer Cell Lines for Biomarker Discovery.* Molecular & Cellular Proteomics, 2015. **14**(6): p. 1616-1629.

45. Choi, H.R., et al., *Oligosaccharides of hyaluronic acid increased epidermal cell stemness by modulation of integrin expression.* Journal of Cosmetic Dermatology, 2012. **11**(4): p. 290-296.

46. Chopra, A., et al., *Augmentation of integrin-mediated mechanotransduction by hyaluronic acid.* Biomaterials, 2014. **35**(1): p. 71-82.

47. Bartolazzi, A., et al., *Glycosylation of CD44 is implicated in CD44-mediated cell adhesion to hyaluronan.* The Journal of Cell Biology, 1996. **132**(6): p. 1199-1208.

48. Weaver, A.M., *Invadopodia: specialized cell structures for cancer invasion.* Clinical & Experimental Metastasis, 2006. **23**(2): p. 97-105.

49. Bergman, A., J.S. Condeelis, and B. Gligorijevic, *Invadopodia in context.* Cell Adhesion & Migration, 2014. **8**(3): p. 273-279.

50. Gould, C.M. and S.A. Courtneidge, *Regulation of invadopodia by the tumor microenvironment.* Cell Adhesion & Migration, 2014. **8**(3): p. 226-235.

51. Yamaguchi, H. and J. Condeelis, *Regulation of the actin cytoskeleton in cancer cell migration and invasion.* Biochimica Et Biophysica Acta-Molecular Cell Research, 2007. **1773**(5): p. 642-652.

52. MacGrath, S.M. and A.J. Koleske, *Cortactin in cell migration and cancer at a glance.* Journal of Cell Science, 2012. **125**(7): p. 1621-1626.

53. Webb, B.A., et al., *Dissecting the functional domain requirements of cortactin in invadopodia formation.* European Journal of Cell Biology, 2007. **86**(4): p. 189-206.

54. Eddy, R.J., et al., *Tumor Cell Invadopodia: Invasive Protrusions that Orchestrate Metastasis.* Trends in Cell Biology, 2017. **27**(8): p. 595-607.

55. Helwani, F.M., et al., *Cortactin is necessary for E-cadherin–mediated contact formation and actin reorganization.* The Journal of Cell Biology, 2004. **164**(6): p. 899-910.

56. Murphy, D.A. and S.A. Courtneidge, *The 'ins' and 'outs' of podosomes and invadopodia: characteristics, formation and function.* Nature Reviews Molecular Cell Biology, 2011. **12**(7): p. 413-426.

57. Oser, M., et al., *Cortactin regulates cofilin and N-WASp activities to control the stages of invadopodium assembly and maturation.* Journal of Cell Biology, 2009. **186**(4): p. 571-587.

58. Alexander, N.R., et al., *Extracellular matrix rigidity promotes invadopodia activity.* Current Biology, 2008. **18**(17): p. 1295-1299.

59. Chellaiah, M.A., *CD44-Src signaling promotes invadopodia formation in prostate cancer (PC3) cells.* OA Cancer, 2013. **1**(2).

60. Chen, J.W.E., et al., *Influence of Hyaluronic Acid Transitions in Tumor Microenvironment on Glioblastoma Malignancy and Invasive Behavior.* Frontiers in Materials, 2018. **5**.

61. Minsky, B.B., C.H. Antoni, and H. Boehm, *Controlled Immobilization Strategies to Probe Short Hyaluronan-Protein Interactions.* Scientific Reports, 2016. **6**.

SUPPLEMENTARY INFORMATION

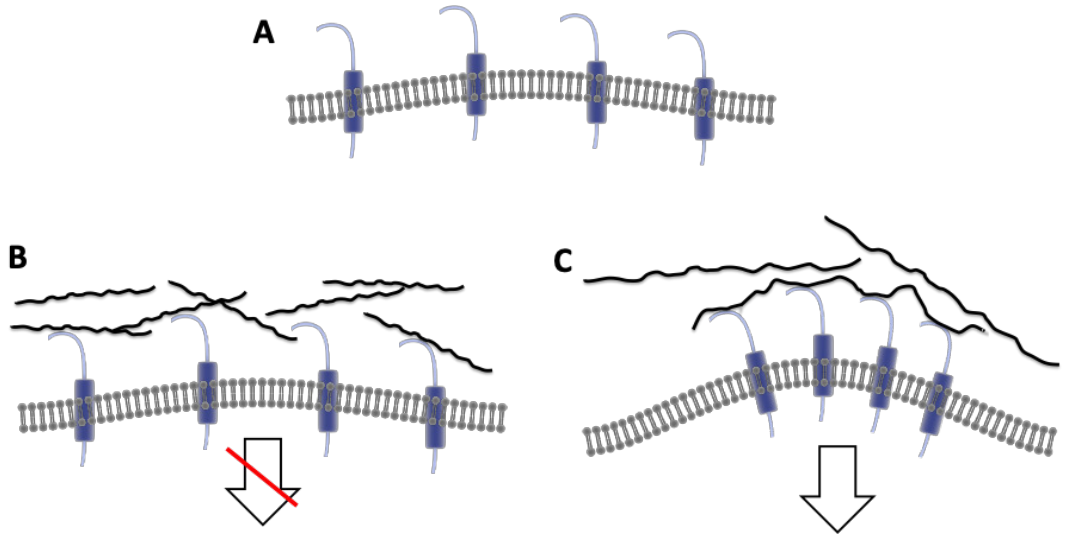

Supplementary Fig. 5-1. Schematic presentation of the interactions between the cell-surface glycoprotein CD44 (A) and hyaluronan in solution (B and C). Oligomers of hyaluronan bind monovalently to CD44 and do not activate the following intracellular signaling (B). In fact, they can replace the endogenous hyaluronan of high molecular weight and attenuate the signaling. On the contrary, hyaluronan of high molecular weight bind CD44 multivalently resulting in CD44 clustering and activation in different downstream signaling.

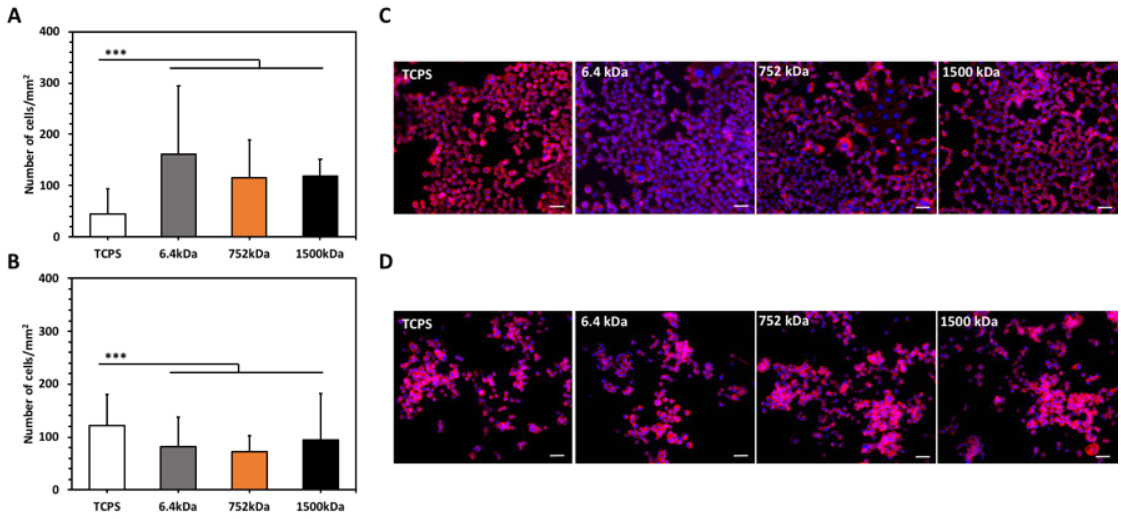

Supplementary Fig. 5-2. Number of adherent cells (AGS, A and MKN45, B) and morphology of AGS (C) and MKN45 (D) after 72h of culture on TCPS in the presence of hyaluronan with different Mws supplemented to the culture media at concentration of 1 mg/mL.

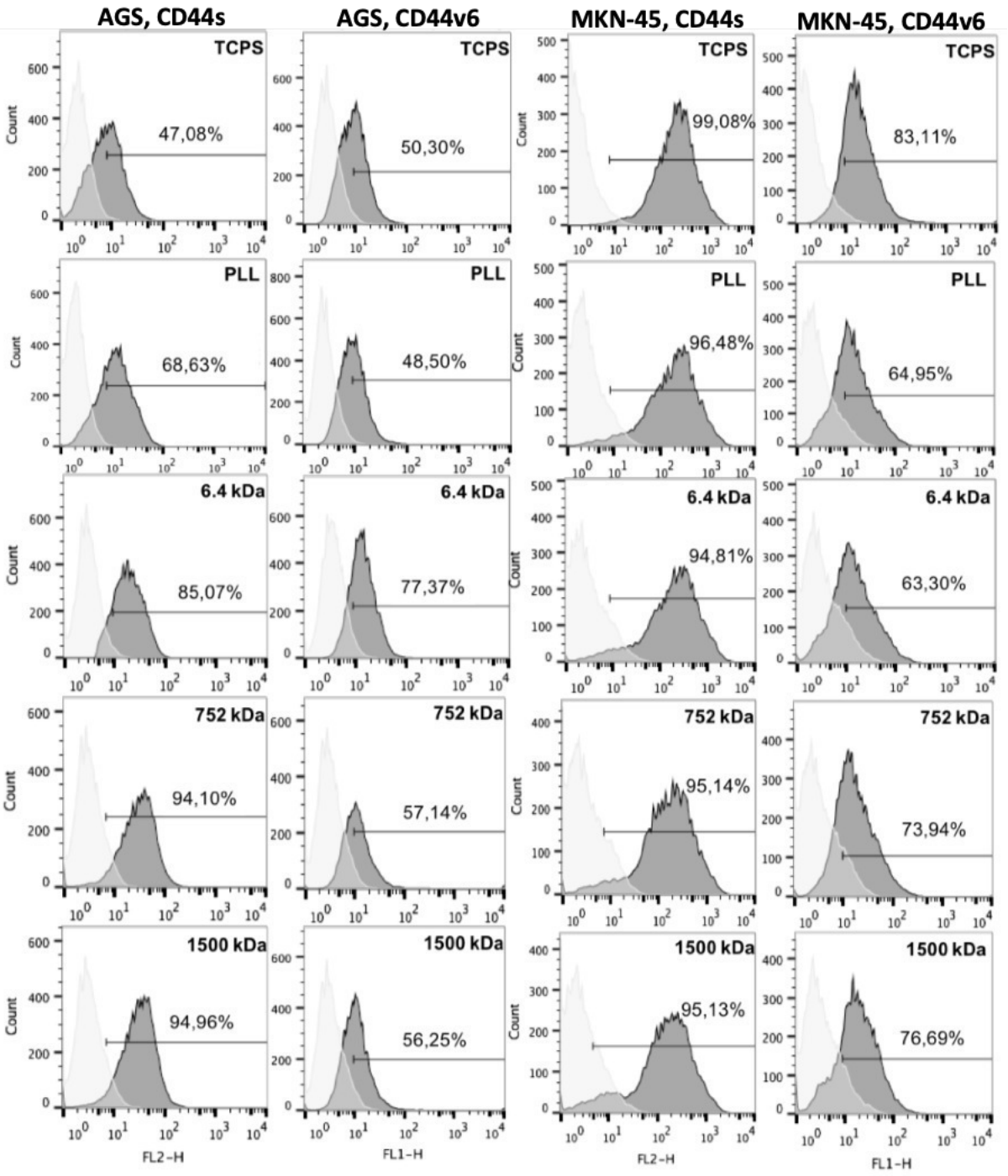

Supplementary Fig. 5-3. Fluorescence-activated cell sorter (FACS) analysis of surface marker CD44s and CD44v6 for the AGS and MKN-45, after 72h of cell culture in each surface.

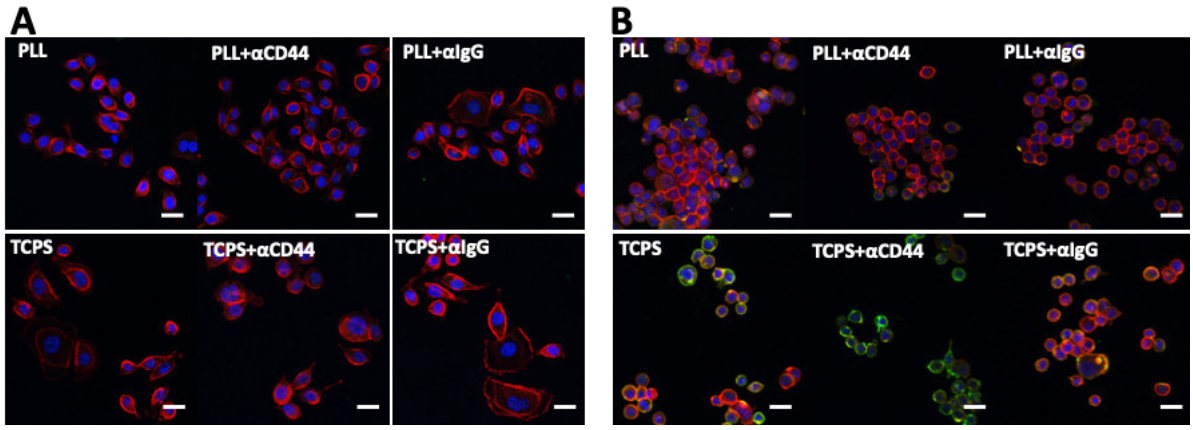

Supplementary Fig. 5-4. Immunohistochemistry of AGS (A) and MKN-45 (B) cultured on control surfaces (TCPS and PLL) during 78 h without or after CD44 blocking (green for CD44, red for actin and blue for nuclei). IgG was used as an isotype control. Bars correspond to 50 µm.

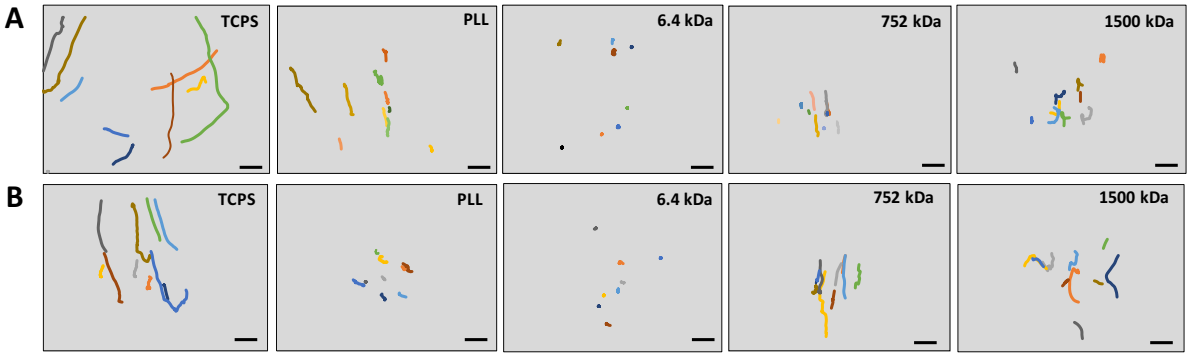

Supplementary Fig. 5-5. Representative example of single cell paths. Images show the cells tracking during 60 minutes of incubation, of AGS (A) and MKN-45 (B) cells on the different surfaces. The displacements of cells are represented as color lines. Each plot represents 1 individual cell track. Bars correspond to 100 µm.

Chapter 6

Hyaluronic acid of low molecular weight triggers the invasive “hummingbird” phenotype on gastric cancer cells

Chapter 6

Hyaluronic acid of low molecular weight triggers the invasive "hummingbird" phenotype on gastric cancer cells[§]

ABSTRACT

The overproduction and deposition of hyaluronic acid (HA) of different size in the tumor microenvironment is associated with cancer metastasis. Here, we report on the development of Layer-by-Layer (LbL) constructs containing HA of different molecular weights (*i.e.* 6.4, 752 and 1500kDa) that mimic the HA-rich cancer ECM. We studied the effect of the HA's size on the behaviour of gastric cancer cell (AGS). Our results demonstrate that LbL constructs with short HA, *i.e.* 6.4kDa, activate the cytoskeleton rearrangement leading to the "hummingbird" morphology, promote high cellular motility and increase the expression of p-ERK1/2 and p-AKT, which are involved in the migration of cancer cells. In addition, we show that this malignant transformation involves an active participation of the HA co-receptor RHAMM in AGS cells.

[§] This Chapter is based on the publication "Amorim, S., da Costa, D. S., Reis, C. A., Reis, R. L., Pashkuleva, I., & Pires, R. A. (2020), *Hyaluronic Acid of low molecular weight triggers the invasive "hummingbird" phenotype on gastric cancer cells*. (submitted)"

6-1. INTRODUCTION

Gastric cancer (GC) is one of the most incident cancer-related deaths. [1] Its onset and progression are commonly associated with the infection by the Gram-negative bacterium Helicobacter pylori (H. pylori). Approximately half of the World's population is colonized with this bacterium, however, the majority of the individuals are asymptomatic. [2] The long-term infection with H. pylori in combination with other factors, such as genetic background and dietary habits, among others, can potentiate gastric carcinogenesis. [3] The most severe GC outcomes are usually related with the translocation of the cytotoxin-associated gene A antigen (CagA) from the H. pylori to the host epithelial cells through the cag pathogenicity island (PAI). [4, 5] The presence of the oncoprotein CagA in the epithelial cell membrane and its phosphorylation induce an elongation of epithelial GC cells to an "hummingbird"-like shape that is usually associated with the epithelial mesenchymal transition (EMT). [6, 7] In EMT the epithelial cells gain a mesenchymal character, lose cell-cell contacts and increase their migration and invasive capacity. [8]

Hyaluronic acid (HA), is one of the most abundant glycosaminoglycans (GAGs) in the extracellular matrix (ECM). Structurally, this is the simplest GAG as it is composed by repeating disaccharides of N-acetylglucosamine and glucuronic acid. Besides this simple composition, HA is involved in different signalling pathways and thus, able to modulate pathological and physiological processes. An example is cancer cell behaviour, which depends on HA size: short HA (<100 kDa) is linked to cancer progression and poor GC prognosis [9, 10]; whilst long HA is associated with cancer latency. [11] The main cell surface receptor for HA, the transmembrane protein CD44, is a GC stem cell marker associated with H. pylori-induced cancer cell proliferation. [12] Considering these HA bioactivities, we develop a 2D platform to assess the impact of HA size on the formation of an invasive "hummingbird" phenotype on the AGS cell line (derived from an epithelial GC). We build Layer-by-Layer (LbL) constructs through the sequential deposition of five bilayers made of poly-L-lysine (PLL, a polycation) and HA (a polyanion) of different size. [13] In all generated constructs (PLL-HA_{Mw})5 the final, surface-exposed layer is made of HA. GC cells were seeded on these constructs and the influence of HA size on the transition to the "hummingbird" phenotype and its link to GC invasiveness was investigated.

6-2. MATERIALS AND METHODS

6-2.1. Materials

Hyaluronic acid (HA) sodium salts of 6.4 kDa, 752 kDa (HA700K-5) and 1500 kDa (HA15M-5) were purchased from Lifecore (USA) and poly-L-lysine (PLL) hydrobromide (P2636) was acquired from Sigma-Aldrich. N-(3-dimethylaminopropyl)-N′-ethylcarbodiimide hydrochloride (EDC, ≥ 98.0%) and N-hydroxysuccinimide (NHS) were purchased from Sigma-Aldrich. The reagents were used as received without further purification.

6-2.2. Layer-by-layer film construction

The layer-by-layer (LbL) constructs ere build-up on tissue culture polystyrene (TCPS) coverslips of 13mm diameter by alternate dipping into a solution of PLL (0.5 mg.mL-1 in NaCl 0.15M) and in a solution of HAMw (1 mg.mL-1 in NaCl 0.15M) containing the crosslinker EDC (400mM) and NHS (100mM). After each layer deposition, the substrate was washed with NaCl 0.15M at pH ≈ 6.0–6.5. The sequential layer deposition was repeated 10 times generating a $(PLL\text{-}HA)_5$ film. The final constructs were washed with water and sterilized under UV light for 30min prior cell seeding.

6-2.3. Cell seeding and immunocytochemistry analysis

Adenocarcinoma Human gastric cancer cells (i.e. AGS), at passage 6, were expanded in RPMI-1640 medium (Sigma-Aldrich, Portugal) supplemented with 10% of fetal bovine serum (FBS, Gibco) and 1% antibiotic/antimycotic solution (final concentration of penicillin 100units/mL, streptomycin 100mg.mL-1 and 25 g.mL-1 amphotericin B; Gibco, UK) and incubated at 37°C in the presence of 5% CO2 until reaching confluence. Cells were harvested with TrypLE and seeded (11000 cells/cm2) on the TCPS (control) and (PLL-HAMw)5-coated TCPS for 3 days. For immunostaining, cells were washed with PBS, fixed with 10% buffered formalin, followed by permeabilization with 0.2% Triton X-100 in PBS for 5min. Cells were blocked with 3%BSA in PBS for 30min at room temperature and the monoclonal antibody to CD44 (AM06286SU-N from ACRIS) was used at a 1:400 dilution in 1%BSA in PBS (w/v) for 1h at room temperature. The rabbit anti-mouse Alexafluor-488 (1:500 dilution, 1% BSA in PBS (w/v)) was used as a secondary antibody. For the staining of nuclei and actin, DAPI (1:500 dilution in 1% BSA

in PBS (w/v)) and Phalloidin-TRITC (1:250 dilution, 1% BSA in PBS (w/v)) were used, respectively. RHAMM was stained with RHAMM (H-8) mouse monoclonal antibody (1:400 dilution) and for YAP a human anti-mouse antibody was employed (SC-101199; 1:500 dilution, 1% BSA in PBS), followed by the secondary rabbit anti-mouse Alexafluor-488 (1:500 dilution, 1% BSA in PBS) for both primary antibodies. Stained cells were observed under confocal laser scanning microscope (TCS SP8, Leica, Germany).

6-2.4. Real-time qPCR

Total RNA was extracted from AGS cells seeded on $(PLL\text{-}HA_{Mw})_5$ coated T25 culture flasks. Briefly, after 3 days of culture the flasks were washed with PBS, the Tri® reagent (Sigma-Aldrich, USA) was added and the flask was gently scratched to remove the cells from the bottom. The cells were stored at -80°C. After the removal of proteins by chloroform extraction, the RNA pellet was washed with isopropyl alcohol and ethanol (70%). The RNA pellet was rebuilt in RNAse-free water (Gibco, Invitrogen, UK). Reverse transcriptase (RT)-PCR was performed according to the protocol from the iScript cDNA synthesis kit (Quanta BioSciencesTM, Gaithersburg, MD, USA). The transcripts' expression data were normalized with the housekeeping gene 18S and the relative quantification calculated according to the Livak (2_ ΔΔCT) method using the cells seeded on TCPS as the calibrator.

6-2.5. Cells migration through time-lapse analysis

After 24h of incubation, the cells seeded on the different surfaces were analysed using an inverted microscope (Zeiss Axio Observer, Germany) equipped with a temperature (37°C) and CO2 control device (5%CO2). Images of the cells (20x objective) were continuously captured every 5min for 16h using the Zen software (Zeiss, Germany). Image stacks and cellular displacement were analysed with the Fiji software (http://fiji.sc/wiki/index.php/Fiji) using the Manual Tracking Plugin.

6-2.6. Flow Cytometry analysis

AGS cancer cells (passage 7) were seeded on a T25 flask pre-coated with $(PLL\text{-}HA_{Mw})_5$ as described in section 4.2. After 3 days of incubation the cells were detached with TrypLe. The cell's suspension was centrifuged and re-suspended in PBS. After incubation for 20min with mouse anti-human CD44-PE

antibody (clone 515), the cells were washed with PBS and after centrifugation, they were fixed with 1% formalin in PBS (Sigma). The cells were analyzed on a FACs Calibur Flow Cytometer (BD Biosciences) using the Flowing Software v2.5.1.

6-2.7. Western-blot analysis

AGS protein lysates were extracted in RIPA buffer (150mM NaCl, 1% Triton-X100, 0.5% sodium deoxycholate, 0.1% sodium dodecyl sulphate, 50mM Tris-Base, pH=8) supplemented with 1x Protease (cOmpleteTM, ROCHE) and 1x Phosphatase (PhosSTOPTM, ROCHE) inhibitor cocktails for 30min with 5min intervals of vortexing. The extracts were centrifuged (18,000g, 16min, 4°C), and the supernatant was further analysed by Western-Blotting. The protein, with the Laemmli buffer, was denatured at 37°C for 1h30min and 95°C for 5min prior to use. The lysates containing 40μg of protein were resolved using 4-12% Bis-Tris Protein Gels (NovexTM) and transferred to nitrocellulose membranes (Thermo Fischer Scientific). The membranes were incubated in 4% (m/v) bovine serum albumin (BSA) in Tris-buffered saline-Tween (TBS-T, Cell Signalling Technology) and probed with -smooth muscle actin (rabbit monoclonal [E184], 1:5000 dilution), p-AKT (rabbit monoclonal antibody [EP2109Y], 1:1000 dilution), AKT (rabbit monoclonal antibody (B-1), 1:1000 dilution), RHAMM (mouse monoclonal antibody (H-8), 1:1000 dilution), p-ERK1/2 (rabbit monoclonal antibody, 1:1000 dilution), CD44 (rabbit monoclonal antibody, 1:1000 dilution) and Annexin-4 (rabbit monoclonal antibody, 1:1000 dilution). After 3 cycles of 5min washing with TBS-T, the membranes were incubated with IRDye®800CW anti-Rabbit or anti-Mouse (1:10000 dilution) for 1h and imaged on the Odyssey Infrared Imaging System (LI-COR Biosciences).

6-2.8. Statistical analysis

Shapiro-Wilk test was used to evaluate the normality of the distribution of the data ($p < 0.05$). Kruskal–Wallis test followed by Mann-Whitney test was applied when the data showed non-normal distribution. Significant variations are considered for *** for $p < 0.001$ and ** for $p < 0.01$.

6-3. RESULTS AND DISCUSSION

6-3.1. Hummingbird phenotype in the presence of HA of low Mw

To evaluate the influence of the HA's Mws on the cellular morphology we cultured AGS cells on the $(PLL\text{-}HA)_5$ LbL constructs generated using HA of 6.4, 752 and 1500 kDa (Fig. 1). We observe a clear morphological differences between AGS cells cultured on the LbL with the shortest $HA_{6.4}$ that exhibited a spindle-like shape typical of the "hummingbird" phenotype [1, 2] and the other constructs presenting HA of higher Mws (Fig. 1A) for which round cells were observed (Fig. 1B). Of note, multinucleated giant cells (MGC), typical for AGS cultures were observed on the control surface (*i.e.* tissue culture polystyrene, TCPS). [3]

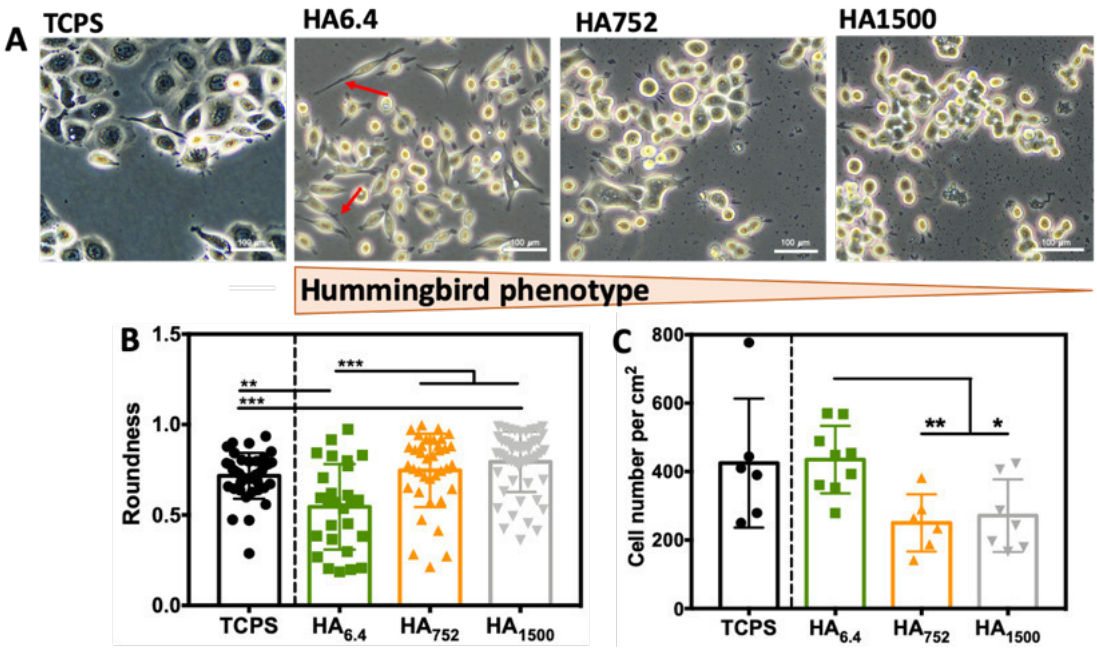

Figure 6-1. Microscope images showing the morphology (A), morphometric analysis (B) and number (C), of AGS cells seeded on the LbL surfaces presenting HA of different Mws, i.e. 6.4, 752 and 1500kDa. Scale bars correspond to 100µm. Statistical differences are marked with * for $p < 0.001$, ** for $p < 0.01$ and * for $p < 0.05$.**

The number of adherent cells was also different: significantly more cells adhered on the $(PLL\text{-}HA_{6.4})_5$ when compared to the constructs presenting longer HA chains (Fig. 1C). These results clearly demonstrate the distinct effect of the shortest $HA_{6.4}$ on AGS cells: it induces changes in cell morphology,

to a spindle shaped morphology and maintains the high cell proliferation level confirmed by Ki-67 staining (Supplementary Fig. 1)

6-3.2. Different mechanotransduction induced by the LbL constructs

The use of HA with different sizes affect the mechanical properties of the LbL constructs. Cells can sense these differences via a process called mechanotransduction. [4] We measured the surface stiffness of the constructs as a function of the HA's size (AFM nanomechanical mapping) and observed that the shorter HA form stiffer layers - a result that is consistent with the enhanced hydration capacity of longer HA. [5]

Yes-associated protein (YAP) is typically involved in the transduction of mechanical cues. [6] In cancer, the increased expression of YAP together with its nuclear translocation is associated with tumor growth and metastasis. [7, 8] We observed that cells cultured on softer surfaces, *i.e.* $(PLL\text{-}HA_{752})_5$ and $(PLL\text{-}HA_{1500})_5$, express YAP mainly in the cytoplasm (Fig. 2A). YAP translocation to the nucleus occurred in cells seeded on the stiffer surfaces, *i.e.* TCPS and $(PLL\text{-}HA_{6.4})_5$. This translocation is usually associated with the formation of stress fibres that flattens the nucleus to the substrate [9]

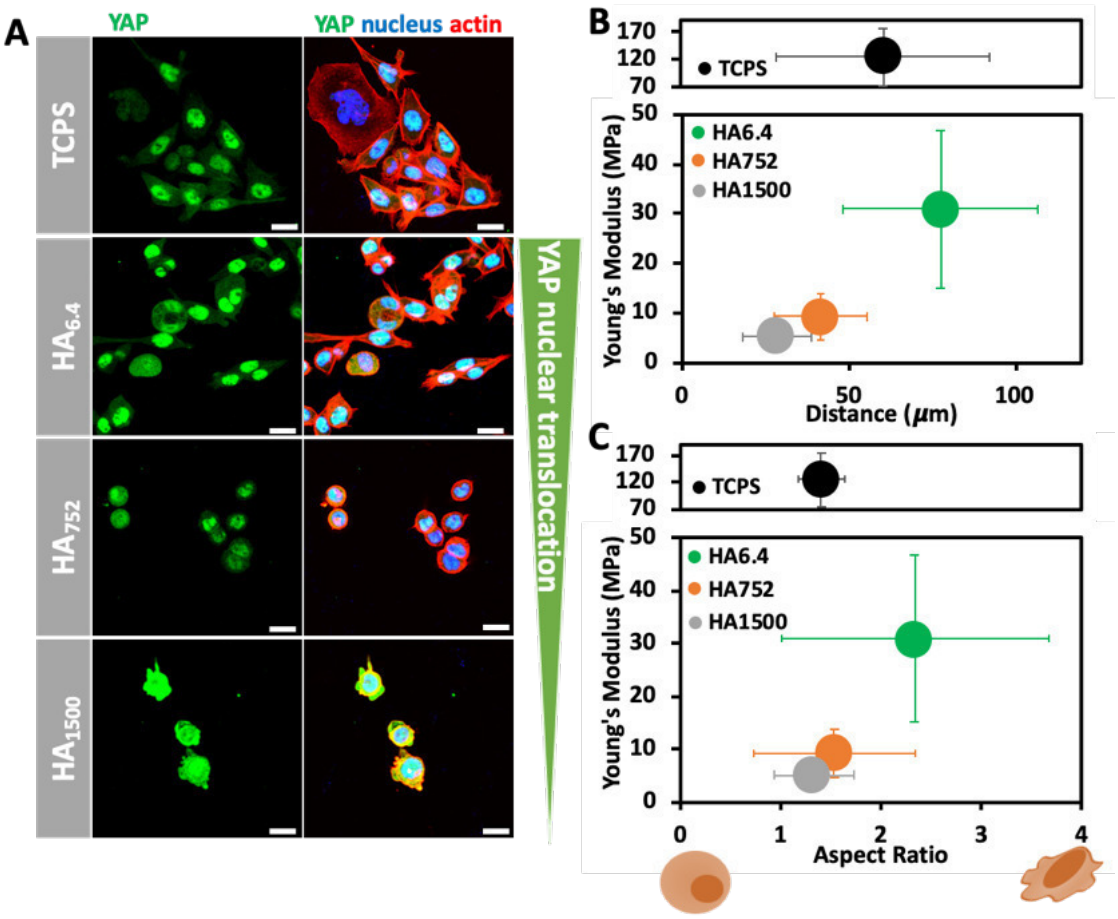

Figure 6-2. A. Confocal microscopy images showing the immunofluorescence of YAP protein. B. Young's Modulus vs Distance and C. Young's Modulus vs Aspect Ratio of AGS cells cultured on LbL constructs presenting HA of different size. Scale bars correspond to 20μm.

Surface stiffness can also modulate the cell's migration pattern. We used time-lapse live cell imaging to determine the cellular paths and distances. AGS cultured on stiffer substrates, i.e. TCPS and $(PLL\text{-}HA_{6.4})_5$ presented the longest distance (Fig. 2B). However, the morphology of the cells cultured on these substrates is significantly different as demonstrated by the determined aspect ratio (AR) (Figs. 2C, Supplementary Fig. 2 and 3): round cells were observed on TCPS surface, while cells with spindle-like morphology was induced by the $(PLL\text{-}HA_{6.4})_5$ substrates showing that the mechanotransduction is not the only factor that influence the morphological transition.

6-3.3. Hyaluronic acid Mw modulates the expression of CD44 and RHAMM receptors

CD44, the major cell surface receptor for HA, is a cancer stem cell marker that is overexpressed in GCs. [10, 11] AGS cells cultured on $(PLL\text{-}HA)_5$ expressed more CD44 when compared with cells on TCPS and this difference is most pronounced for the constructs containing HA of higher Mws (Fig. 3A-C). Such increment of the CD44 expression in function of the HA size is in good agreement with our previous results obtained with bilayered constructs. [12]

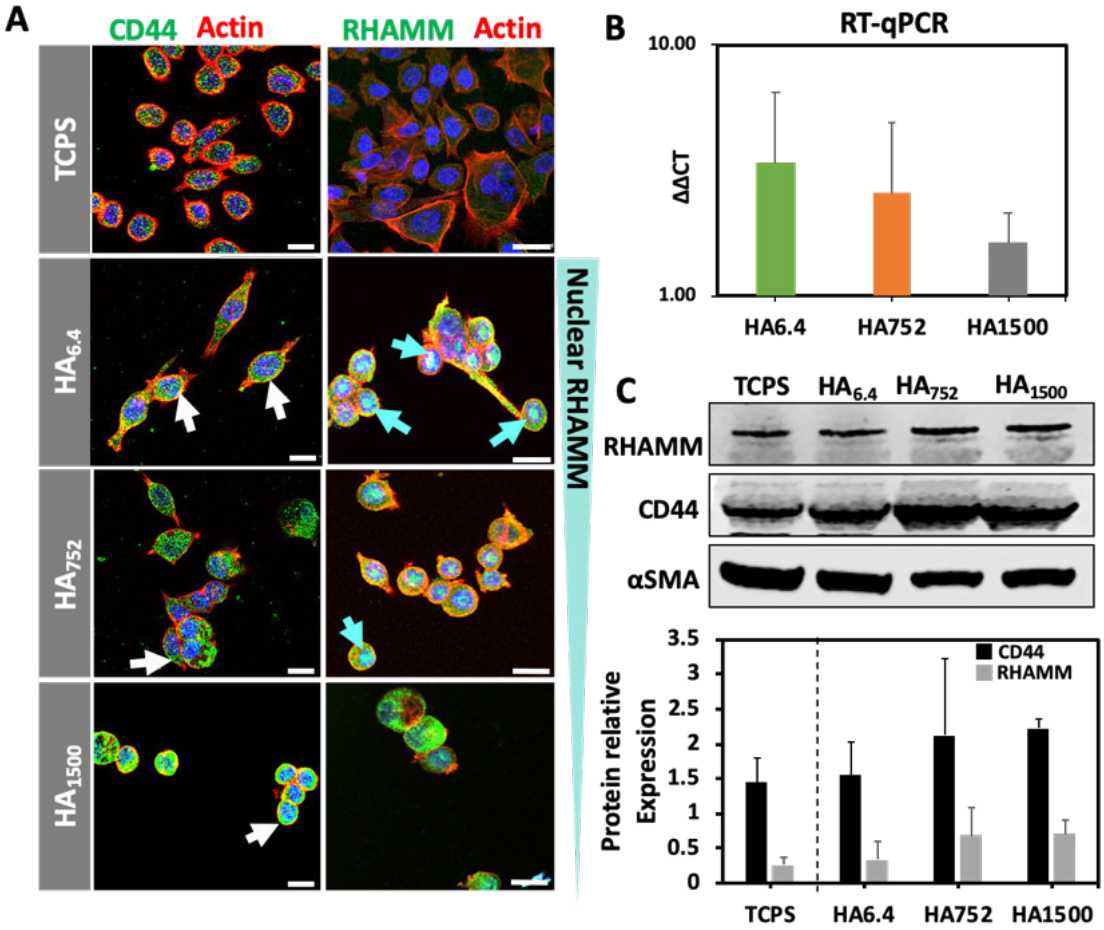

Figure 6-3. A. Fluorescence images showing AGS cells cultured on TCPS, $(PLL\text{-}HA_{6.4})_5$, $(PLL\text{-}HA_{752})_5$ $(PLL\text{-}HA_{1500})_5$ and immunostained for CD44 and RHAMM. B. CD44 gene expression on AGS cells seeded on the same LbL surfaces. C. Western-blot analysis of CD44 (120kDa) and RHAMM (90 kDa) after 3 days of cell culture. Scale bars correspond to 20μm.

CD44 expressed by AGS cells seeded on TCPS is mainly located in the cytoplasm. When cells are in contact with substrate containing HA, *i.e.* LbL constructs, CD44 is recruited to the cells' surface (Fig. 3A, white arrows) regardless the HA size.

RHAMM is another HA receptor that is expressed only during tissue remodelling and in pathological scenarios. As an example, overexpression of RHAMM in cancer promote the invasive phenotype [13, 14] and its co-localization with actin is associated with increased cellular motility. [15] RHAMM can be localized in different cellular compartments and its role depends on the localization: intracellular RHAMM promotes cell polarity and migration, and regulates the microtubule dynamics [16, 17] through the interaction with phosphorylated ERK1/2 protein (*i.e. p*-ERK1/2), while nuclear RHAMM co-localize with *p*-ERK1/2, controlling gene expression responsible for cellular motility. [18, 19] RHAMM was expressed by AGS cells cultured on different LbLs but its localization depends on the HA's Mws: AGS cultured on $(PLL\text{-}HA_{6.4})_5$ have RHAMM localized in the nucleus (Fig. 3A, blue arrows) and in the cytoplasm, whilst cells cultured on the $(PLL\text{-}HA_{1500})_5$ lack nuclear RHAMM. The immunostaining also revealed that AGS cells cultured on LbL with short $HA_{6.4}$ co-localized RHAMM and actin (Fig. 3A) and indeed, these are the substrates that promote higher cellular motility (Fig. 2B). On the other hand, the nuclear RHAMM co-localizes with p-ERK in AGS cells seeded on the same substrates (Figs. 3A and Supplementary Fig. 4). The proliferation, migration and invasion of cancer cells are often associated with the activation of the ERK1/2 signalling pathway, and their nuclear translocation is a hallmark for cancer aggressiveness, as observed for the surfaces presenting $HA_{6.4}$. [20, 21]

6-3.4. HA regulates the downstream signalling pathways associated with cancer migration

Tissues infected with *H. pylori* overexpress Annexin 4 (ANX4). [22] ANX4 is a protein predominantly expressed in epithelial cells. Its overexpression is a hallmark of the development of different epithelial tumors, such as the gastric adenocarcinoma. ANX4 is involved in the regulation of downstream signalling cascades, such as the activation of AKT pathway associated with the proliferation and migration of cancer cells as well as with the tumor aggressiveness. [23-25]

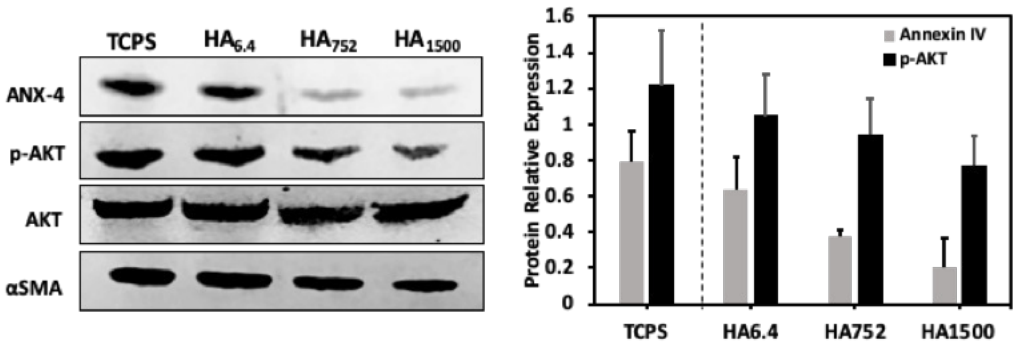

Figure 6-4. Western blot analysis and the respective densitometry showing the expression of ANX4 (35 kD) and p-AKT (62 kDa) by the AGS cells cultured on the studied LbLs.

AGS have high expression of ANX4 as shown by the results obtained for the cells cultured on TCPS (Fig. 4). Such high expression is consistent with the malignant phenotype of this cancer cells. A similar observation has been reported to the infected tissues by *H. pylori*. [26] An inhibition of ANX4 expression and its activated form *p*-AKT was observed in AGS cultures on LbL, especially when constructs presenting HA of higher Mws, *i.e.* 752 and 1500kDa were used as substrates (Fig. 4). Contrarily, the malignant phenotype associated to the high expression of ANX4 and p-AKT pathway is maintained on the surfaces presenting $HA_{6.4}$. The overexpression of ANX4 has been reported to be correlated with an upregulation of RHAMM. [27] However, our results show that the increment of HA Mw is accompanied by an increase in RHAMM expression (Fig. 3B). Of note, it is known that CD44 binds to all sizes of HA, while RHAMM preferentially binds to low Mw HA (*i.e.* < 7 kDa). [28] This preferential binding of RHAMM to low Mw HA could be one of the reasons for the maintenance of the malignant phenotype.

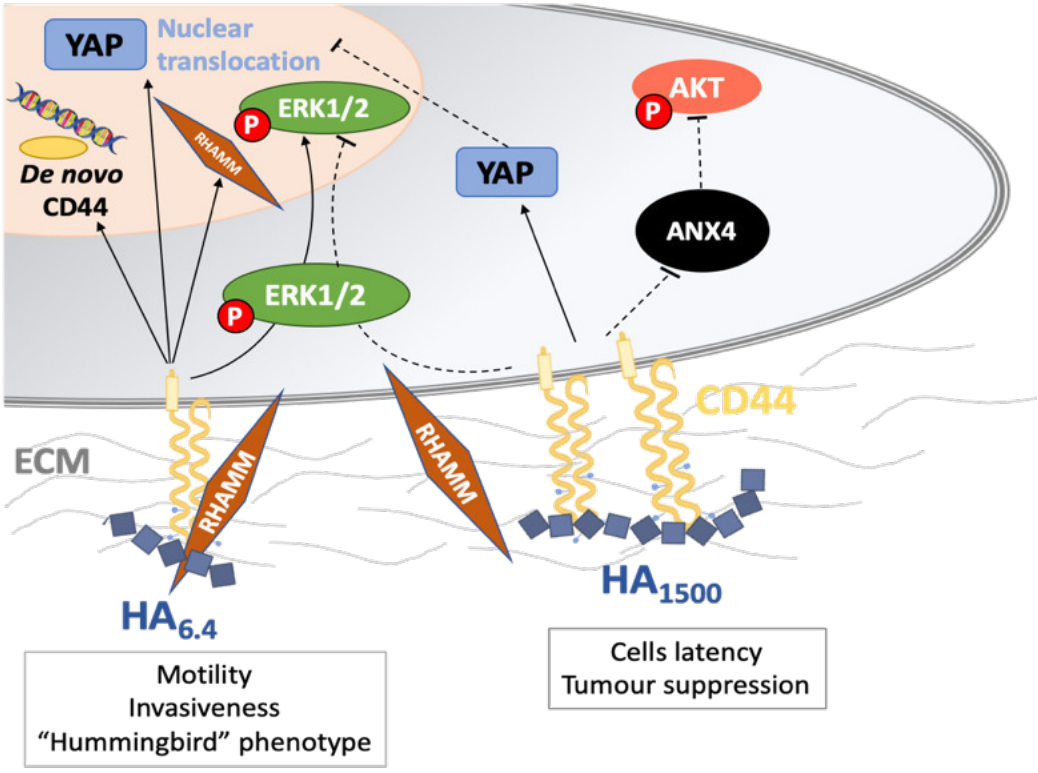

Figure 6-5. Schematic representation of the proposed mechanisms (and signalling pathways) promoted by the HA of different Mws.

Our results are consistent with a dual effect of HA on the invasiveness of GC, under size-mediated pathways. The $HA_{6.4}$ recruits CD44 to the cell surface and stimulates the synthesis of *de novo* CD44, which could be associated to the stemness behaviour of AGS cells. In addition, cells cultured on $(PLL\text{-}HA_{6.4})_5$ have an elongated shape which is characteristic for invasive cells [29] and agrees with the protein expression of p-ERK1/2, ANX4 and p-AKT confirming the invasive phenotype of these cells. In contrast, long HA_{1500} recruit CD44 to the cell surface but does not trigger *de novo* CD44 synthesis. In addition, it is also observed an inhibition of ANX4 accompanied by a reduced expression of p-AKT (Fig. 5). AGS attachment to $(PLL\text{-}HA_{1500})_5$ is decreased and the migration and invasive pathways are downregulated in the presence of HA_{1500}, being consistent with a promotion of cancer latency by long HA. [28]

6-4. CONCLUSIONS

We demonstrated that HA of different sizes can induce distinct cancer cell behaviour. AGS GC cells displayed increased polarity and morphometric changes associated with the invasive "hummingbird" phenotype in the presence of short HA, *i.e.* 6.4kDa. We further demonstrated that long HA, *i.e.* HA_{1500}, inhibits the migration of AGS cells, being consistent with the promotion of cancer latency. In conclusion, we prove that the developed LbL surfaces are relevant model systems that can be used to study cancer cell behaviour, in particular the different signalling cascades involved in HA-mediated cancer invasiveness.

6-5. REFERENCES

1. Bessede, E., et al., *Helicobacter pylori generates cells with cancer stem cell properties via epithelial-mesenchymal transition-like changes.* Oncogene, 2014. **33**(32): p. 4123-31.

2. Schneider, S., C. Weydig, and S. Wessler, *Targeting focal adhesions:Helicobacter pylori-host communication in cell migration.* Cell Communication and Signaling, 2008. **6**(1): p. 2.

3. Iwakura K, W.H., Nakano T, Daikoku E, Shimamoto C, Katsu K, Sano K, *Unique Enhancement of Multinuclear Giant Cell Formation in AGS Cell Line Infected with Helicobacter pylori.* Bull OMC, 2007. **53**(1): p. 1-9.

4. Cantini, M., et al., *The Plot Thickens: The Emerging Role of Matrix Viscosity in Cell Mechanotransduction.* Adv Healthc Mater, 2019: p. e1901259.

5. Cowman, M.K., et al., *Viscoelastic Properties of Hyaluronan in Physiological Conditions.* F1000Res, 2015. **4**: p. 622.

6. *Control of cellular responses to mechanical cues through YAP/TAZ regulation.*

7. Li, N., et al., *Helicobacter pylori CagA promotes epithelial mesenchymal transition in gastric carcinogenesis via triggering oncogenic YAP pathway.* J Exp Clin Cancer Res, 2018. **37**(1): p. 280.

8. Zhang, X., et al., *The Ambivalent Function of YAP in Apoptosis and Cancer.* Int J Mol Sci, 2018. **19**(12).

9. Elosegui-Artola, A., et al., *Force Triggers YAP Nuclear Entry by Regulating Transport across Nuclear Pores.* Cell, 2017. **171**(6): p. 1397-1410 e14.

10. Misra, S., et al., *HA/CD44 interactions as potential targets for cancer therapy.* FEBS J, 2011. **278**: p. 1429-43.

11. *Targeting cancer stem cells in gastric cancer.* Gastrointestinal Cancer: Targets and Therapy, 2014.

12. Amorim, S., et al., *Molecular weight of surface immobilized hyaluronic acid influences CD44-mediated binding of gastric cancer cells.* Sci Rep, 2018. **8**(1): p. 16058.

13. Entwistle, J., C.L. Hall, and E.A. Turley, *HA receptors: regulators of signalling to the cytoskeleton.* J Cell Biochem, 1996. **61**(4): p. 569-77.

14. Mele, V., et al., *The hyaluronan-mediated motility receptor RHAMM promotes growth, invasiveness and dissemination of colorectal cancer.* Oncotarget, 2017. **8**(41): p. 70617-70629.

15. Assmann, V., et al., *The intracellular hyaluronan receptor RHAMM/IHABP interacts with microtubules and actin filaments.* J Cell Sci, 1999. **112 (Pt 22)**: p. 3943-54.

16. Muroyama, A. and T. Lechler, *Microtubule organization, dynamics and functions in differentiated cells.* Development, 2017. **144**(17): p. 3012-3021.

17. Maxwell, C.A., J. McCarthy, and E. Turley, *Cell-surface and mitotic-spindle RHAMM: moonlighting or dual oncogenic functions?* J Cell Sci, 2008. **121**(Pt 7): p. 925-32.

18. Misra, S., et al., *Interactions between Hyaluronan and Its Receptors (CD44, RHAMM) Regulate the Activities of Inflammation and Cancer.* Frontiers in Immunology, 2015. **6**.

19. Tolg, C., et al., *Hyaluronan and RHAMM in wound repair and the "cancerization" of stromal tissues.* Biomed Res Int, 2014. **2014**: p. 103923.

20. Plotnikov, A., et al., *The nuclear translocation of ERK1/2 as an anticancer target.* Nature Communications, 2015. **6**: p. 6685.

21. Olea-Flores, M., et al., *Extracellular-Signal Regulated Kinase: A Central Molecule Driving Epithelial-Mesenchymal Transition in Cancer.* Int J Mol Sci, 2019. **20**(12).

22. Lin, L.L., et al., *Annexin A4: A novel molecular marker for gastric cancer with Helicobacter pylori infection using proteomics approach.* Proteomics Clin Appl, 2008. **2**(4): p. 619-34.

23. Chen, W., et al., *Overexpression of annexin A4 indicates poor prognosis and promotes tumor metastasis of hepatocellular carcinoma.* Tumour Biol, 2016. **37**(7): p. 9343-55.

24. Mogami, T., et al., *Annexin A4 Is Involved in Proliferation, Chemo-Resistance and Migration and Invasion in Ovarian Clear Cell Adenocarcinoma Cells.* Plos One, 2013. **8**(11).

25. Yao, H., et al., *The role of annexin A4 in cancer.* Front Biosci (Landmark Ed), 2016. **21**: p. 949-57.

26. Wei, B., et al., *Annexin A4 and cancer.* Clin Chim Acta, 2015. **447**: p. 72-8.

27. Lin, L.-L., et al., *Membrane repair against H. pylori promotes cancer cell proliferation.* Nature Precedings, 2010.

28. Liu, M., C. Tolg, and E. Turley, *Dissecting the Dual Nature of Hyaluronan in the Tumor Microenvironment.* Front Immunol, 2019. **10**: p. 947.

29. Bourzac, K.M., C.M. Botham, and K. Guillemin, *Helicobacter pylori CagA Induces AGS Cell Elongation through a Cell Retraction Defect That Is Independent of Cdc42, Rac1, and Arp2/3.* 2007.

SUPPLEMENTARY INFORMATION

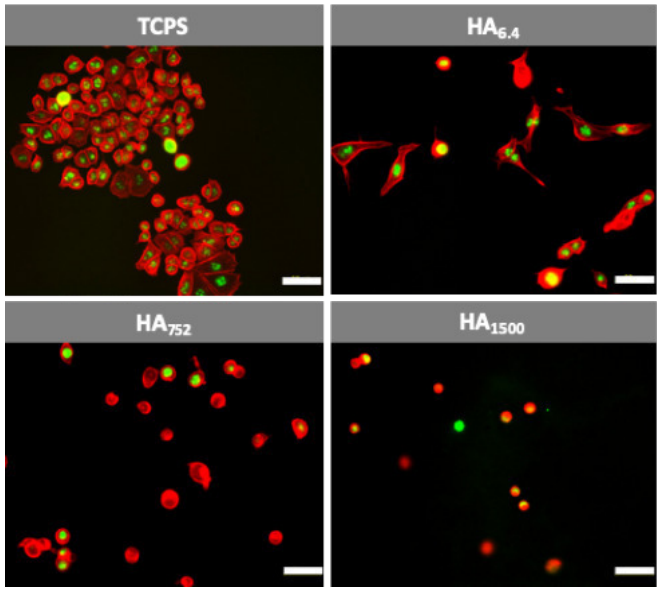

Supplementary Fig. 6-1. Nuclear Ki-67 immunostaining (green) on cells seeded on TCPS and surfaces presenting HA with the different Mws. Scale bars correspond to 50μm.

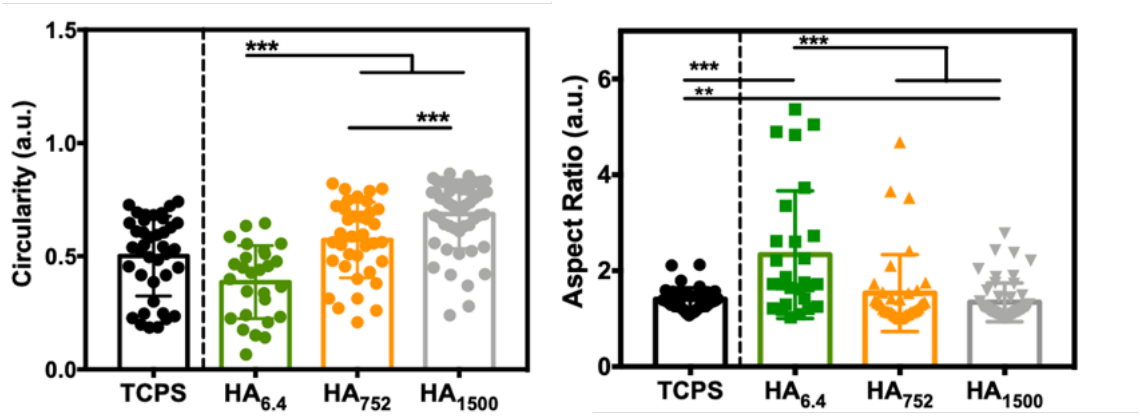

Supplementary Fig. 6-2. Morphometric analysis of AGS cells seeded on TCPS and LbL with HA_{Mw} after 3 days of culture. Significant differences are marked with *** for $p < 0.001$, ** for $p < 0.01$.

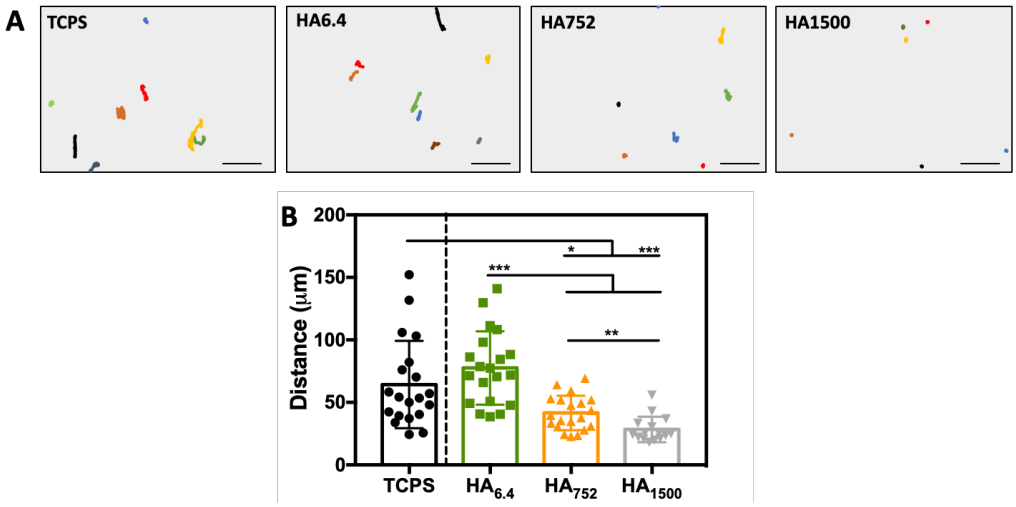

Supplementary Fig. 6-3. A. Individual cells paths (represented by different colours), obtained by time-lapse live imaging during 16h. Scale bars correspond to 100μm. B. Distance analysis of AGS cells seeded on TCPS and LbLs. Significant differences are marked with *** for $p < 0.001$, ** for $p < 0.01$ and * for $p < 0.05$.

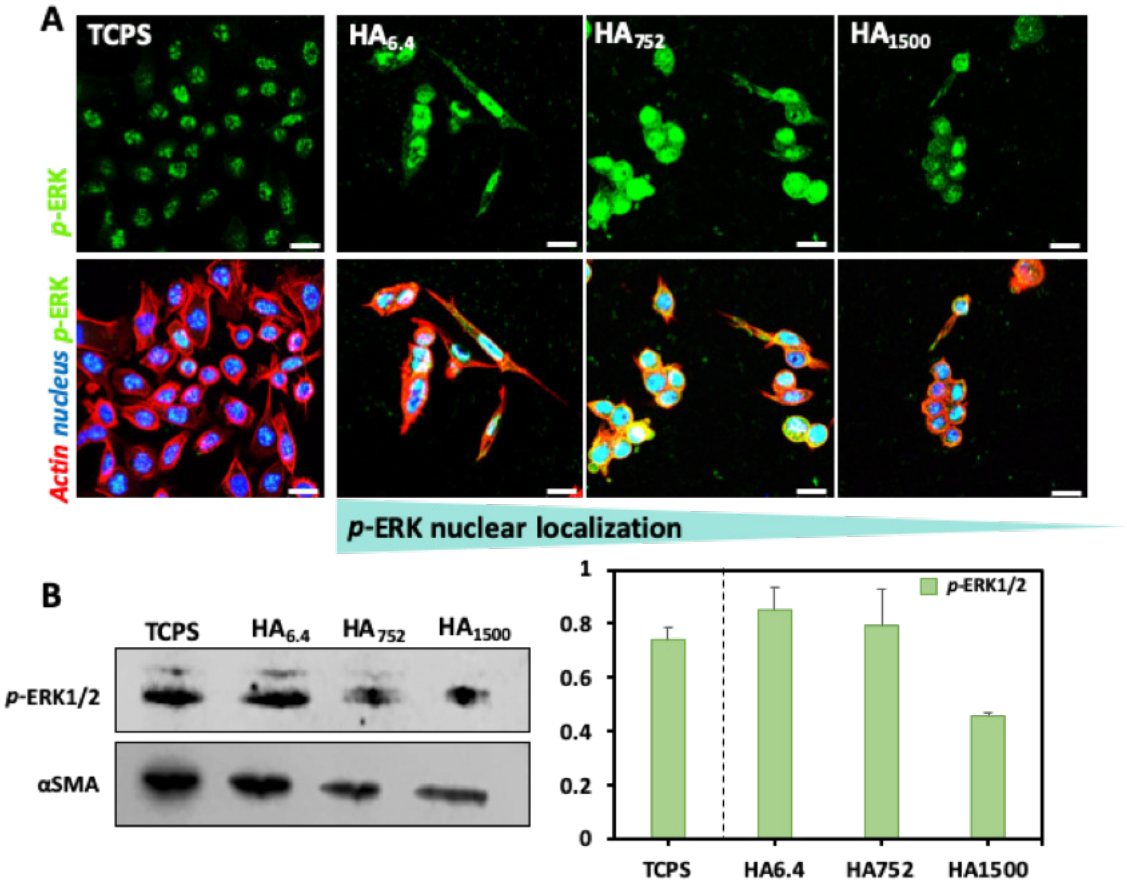

Supplementary Fig. 6-4. A. Expression of p-ERK1/2 (42/44 kDa) by AGS cells seeded on TCPS and LbLs. B. p-ERK1/2 protein expression quantified by Western Blot and densitometry.

Chapter 7

Multilayer platform to model the bioactivity of Hyaluronic acid in gastric cancer

Chapter 7

Multilayer platform to model the bioactivity of Hyaluronic acid in gastric cancer¨

ABSTRACT

Hyaluronic acid (HA) has a key role in cancer progression and invasiveness. It is overexpressed in the tumor parenchyma and stroma. Moreover, its molecular weight (Mw) is also altered in this pathological state: there is an increased concentration of shorter fragments because of the overexpressed hyaluronidases and reactive oxygen species. Aiming to mimic this microenvironment, we developed a Layer-by-Layer (LbL) platform presenting HA of different Mws, namely 6.4, 752 and 1500kDa. This platform allows to study the influence of HA Mw on the formation of focal adhesion sites (FAs), and the involvement of paxillin and CD44 in this process. High paxillin expression and formation of more FAs is observed for MKN45 cells seeded on LbLs with short HA (6.4kDa). In addition, phospho-MAPK analysis shows that low Mw HA activates the ERK1/2 pathway, responsible for cell motility, invasiveness and tumor progression. On the other hand, an activation of p38 pathway and an inhibition of the ERK1/2 pathway, usually related with cancer latency, is observed for cells seeded on LbLs with higher Mw HA (i.e. 752 and 1500kDa). Overall, it is demonstrated the suitability of the developed platform to study cancer progression and invasiveness, and the possibility to use HA of different Mw in distinct anticancer therapeutic approaches.

¨ This Chapter is based on the publication "Amorim, S., da Costa, D. S., Mereiter S., Reis, C. A., Reis, R. L., Pashkuleva, I., & Pires, R. A. (2020), *Multilayer Platform to Model the Bioactivity of Hyaluronic Acid in Gastric Cancer*. (submitted)"

7-1. INTRODUCTION

The communication between cells and their microenvironment is crucial for the regulation of cellular functions in either normal or diseased states. [1, 2] An example is the formation of cancerous tissue that is usually accompanied by an abnormal cellular metabolic activity and an altered stroma. In specific types of cancers, e.g. gastric cancer, an accumulation of hyaluronic acid (HA) in the tumor microenvironment and surrounding stroma is observed.[3, 4] HA is a negatively charged glycosaminoglycan, whose amount is tightly regulated by the interplay of HA synthetases (HAS) and hyaluronidases (HYAL). Three different transmembrane enzymes, HAS1, HAS2 and HAS3 generate HA of different molecular weight (Mw). After synthesis, HYALs are responsible for the additional modification of the size of HA.[5] [6] This process is extremely important, as most of the HA bioactivities are size-dependent, e.g. only short HA fragments are angiogenic inductors which are associated with cancer cell migration and tumor aggressiveness.[7] The expression of HYALs and HASs have been shown to be altered in tumors resulting in specific HA profiles characterized by overexpression of HA and enrichment on short oligomers.[6, 8]

These alterations affect the cellular activity via interactions of HA with cell surface receptors.[9] Previously, it was demonstrated that the HA Mws affects its interaction with CD44 (the main HA cell surface receptor) and the subsequent signalling cascades, that lead to different expression of cortactin and the formation of cell membrane protrusions.[10] The multi-domain CD44 glycoprotein presents various distinct isoforms due to alternative splicing: CD44 standard (CD44s), lacking all alternatively spliced exons and expressed by normal and cancer cells; and CD44 variant isoforms (CD44v), which can contain different exon chains (v1–v10) and are commonly overexpressed by cancer cells.[11] Additionally, CD44 function, such as HA binding, is enhanced in cancer through the altered glycosylation of CD44.[12] CD44 is involved in the activation of different signalling cascades that can alter cell proliferation rate, promote/inhibit cell migration and remodelling, among other biological outcomes.[13] It has a key role in the activation of the complex FAK-Src through interaction with Src tyrosine kinase and triggers the activation of several other protein kinase cascades that lead to the phosphorylation of proteins associated with the (re)organization of the cytoskeleton, such as paxillin.[14-16] Paxillin is a main component in the regulation of the assembly, disassembly and signalling of focal adhesions (FAs).[17]

The (dis)assembly of FAs is a dynamic process required for cell motility and migration. [18] Herein, we studied the influence of the HA Mw on these processes. HA of different Mws, namely 6.4kDa, 752kDa and 1500kDa, were incorporated in Layer-by-Layer (LbL) constructs (using poly-L-lysine, PLL, as polycation) and the interactions of these substrates with MKN45 - a gastric cancer cell line with a high expression of CD44, was evaluated. The developed LbL systems have the advantage of presenting HA in an extracellular matrix (ECM)-relevant way, i.e. with restricted mobility but still able to reorganize and bind specifically to other biomolecules, as previously demonstrated. [10]

7-2. MATERIALS AND METHODS

7-2.1. Materials

All chemicals were used as received without further purification. Poly-L-lysine hydrobromide (PLL; Mw 30-70 kDa), N-(3-dimethylaminopropyl)-N′-ethylcarbodiimide hydrochloride (EDC) ≥98.0% and N-hydroxysuccinimide (NHS) were obtained from Sigma-Aldrich (Portugal). Hyaluronic acid (HA; Mw 6.4 kDa, 752 kDa and 1500 kDa) was purchased from Lifecore (USA). Phalloidin–tetramethylrhodamine B isothiocyanate (phalloidin–TRITC), 4,6-diamidino-2-phenyindole, dilactate (DAPI) from Sigma-Aldrich (Portugal) and the Rabbit monoclonal [Y113] to Paxillin from Abcam (Cambridge, UK) were used for immunostaining. The secondary antibody, Alexa Fluor® 488 Donkey anti-Rabbit IgG, was obtained from Life Technologies (Canada). Anti-CD44 antibody [KM201] (ab25340) from Abcam (Cambridge, UK) was used for CD44 blocking.

7-2.2. Methods

7-2.2.1. Assembly of polyelectrolytes multilayers

The substrates used in this study were gold coated glasses (1x1 cm2). The LbL build-up was performed as following: the substrates were first immersed into a polycation solution (PLL, 0.5 mg.mL-1 in 0.15 M NaCl) for 15 min, then removed, washed (0.15 M NaCl, pH ≈ 6.0 – 6.5) and immersed into the polyanion solution (HA, 1 mg.mL-1 in 0.150 M NaCl) supplemented with a crosslinking agent (EDC, 0.400 M and NHS, 0.100 M) for 15 min. This procedure was repeated until a 10 layers system (PLL-

$HAn)_5$ was obtained (n represents the Mw of HA, i.e. n = 6.4, 752, 1500). The so-coated substrates were rinsed with water (to remove the excess of salt), dried at room temperature and characterized or used in further studies.

7-2.2.2. Culture, expansion and seeding of gastric cancer cell lines

Human gastric cancer cell line MKN45 were cultured in RPMI-1640 medium (Sigma-Aldrich, Portugal) supplemented with 10% heat-inactivated fetal bovine serum (FBS; Biochrom AG, Germany) and 1% antibiotic/antimycotic solution (final concentration of penicillin 100 units/mL and streptomycin 100 mg.mL-1; Gibco, UK). Cells were cultured in a 5% CO2 incubator at 37°C. Before the in vitro studies, the (PLL-HAn)5 coated substrates were sterilized by exposing them to UV light for 30 min. Confluent MKN45 were harvested and seeded on $(PLL\text{-}HAn)_5$ substrates at a density of 11000 cells/cm2. Bare gold glasses were processed as the other samples and used as controls.

7-2.2.3. Characterization of MKN45 Cell Adhesion by Real Time Quartz Crystal Microbalance with Dissipation (QCM-D)

$(PLL\text{-}HA_n)_5$ were deposited on commercially available gold coated QCM-D crystals (Biolin Scientific) using a spin-coater. Briefly, 100μL of each polyelectrolyte solution was allowed to adsorb on the quartz crystal for 15 min. Between layers adsorption, a spin coating was performed during 10 sec at 3000 rpm to remove the excess of the solution and the unbound materials, with an additional wash spinning using 0.15 M NaCl solution. The coated sensors were placed in the QCM-D flow chamber and a stable baseline was acquired by flowing the RPMI medium at flow rate of 50 µL.min-1. The MKN45 cells (0.400×106 cells/mL) were then flowed over the substrates at rate of 50 µL.min-1 for at least 1h. Then, the flow was stopped for 1h to allow cell attachment. Finally, the sensors were rinsed with RPMI to remove unbound cells, at flow rate of 100 µL.min-1. The resonance frequency shift, Δf, and the dissipative shift, ΔD, were recorded at several harmonics (n = 3, 5, 7, 9, 11, and 13). The obtained data are presented as $\Delta D/\Delta f$ (5^{nd} overtone) plots.

7-2.2.4. Cell morphology, distribution and protein expression

After the period of culture, the samples were washed twice with PBS, fixed in 10% neutral buffered formalin for 30 min at 4°C, permeabilized with 1% Triton X-100 in PBS for 30 min at 4°C, and blocked with 3% BSA in PBS for 30 min at room temperature. The Paxillin expression was evaluated by Anti-Paxillin monoclonal antibody [Y113] (AB32084, 1:250 in 1% w/v BSA/PBS), followed by anti-rabbit Alexafluor-488 (1:500 in 1% w/v BSA/PBS). A phalloidin–TRITC conjugate was used (1:200 in PBS for 30 min) to assess cytoskeleton organization. Nuclei were counter-stained with DAPI (1 mg.mL-1 in 1% BSA in PBS for 30 min). The cells were observed under confocal laser scanning microscope (TCS SP8, Leica, Germany). Scanning electron microscopy (SEM) was used to evaluate cell spreading and morphology. The (PLL-HAn)5 samples with the cultured MKN45 cells were washed with PBS, fixed with 10% formalin and dehydrated using ethanol of increasing concentrations (50%, 70%, 90% and 100%). The samples were coated with 0.6 nm Platine and examined at an accelerating voltage of 3.00 kV in a Zeiss Auriga Compact scanning electron microscope. The cells' filopodia length and number were analysed from the SEM pictures using ImageJ analysis software (Version 2.0.0-rc-68/1.52c).

7-2.2.5. Cell migration by Live imaging

MKN45 were seeded as described above on (PLL-HAn)5 samples and allowed to attach for 6h. Live monitoring of cell migration was performed at 37°C in an inverted microscope (Zeiss Axio Observer) equipped with a temperature and CO2 control device (5% CO2). Time-lapse images (40X) were captured every 5 min using Zen software. Cells were followed for 16 h. Image stacks were analysed with ImageJ analysis software (Version 2.0.0-rc-65/1.52c) using manual tracking.

7-2.2.6. Protein array. Cell lysates were subjected to Proteome Profiler™ using the Human Phospho-MAPK Array kit

MKN45 cells were cultured in the QCM-D chambers, following the procedure mentioned before. After the dynamic cell seeding, the sensors were wash with PBS and treated with the Lysis Buffer 6, provided on the array kit, to disrupt the cells and extract the protein lysate. The protein analysis and quantification were determined using the Bio-Rad Protein Assay kit, following the manufacturer instructions.

7-2.2.7. Statistical Analysis

The normality of the data was evaluated using Shapiro–Wilk test ($p<0.05$). When the data did not follow a normal distribution an initial Kruskal–Wallis test was executed followed by Mann-Whitney test. In all the cases, a significant variation was considered for $p<0.05$ (*) and $p<0.001$ (***).

7-3. RESULTS AND DISCUSSION

7-3.1. Build-up of LbL comprising hyaluronic acid of different sizes and cell adhesion monitored by real-time QCM-D

The stacking of oppositely charged polyelectrolytes (PEs) through LbL assembly is a well-established methodology to coat surfaces[19] or generate self-standing membranes.[20] The process comprises the alternate deposition of polycations and polyanions on a substrate that leads to the formation of a multilayer film maintained through electrostatic interactions between the polyions (Figure 1A-C).[21] Under physiological conditions (ionic strength of 0.15 M NaCl, neutral pH), poly-L-lysine (PLL, strong PE) and HA (weak PE) generate dynamic systems where the PEs are able to diffuse between layers. This dynamic process depends on the PE size (Mw) as well as on the addition of crosslinking agents: two factors that influence the film growth and modulate the properties of the generated assemblies. [21, 22] In our case, the different layers are crosslinked through carbodiimide chemistry to ensure the stability of the systems under physiological conditions. From a molecular mobility perspective, this system is confined but yet enough adaptive not to compromise HA ability to interact with proteins and other biologics, i.e. it mimics the HA presentation in the extracellular matrix (ECM) where its mobility is restricted by interactions with other biomolecules.

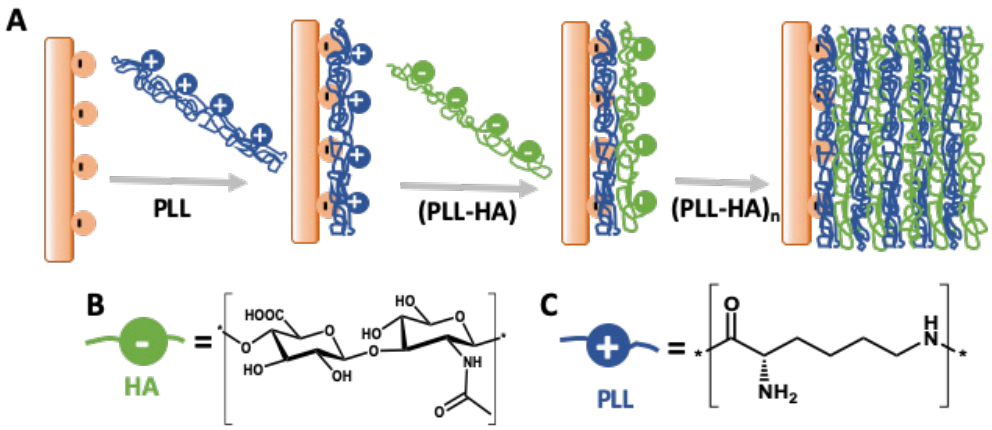

Figure 7-1. (A) Schematic presentation of $(PLL\text{-}HA_n)_5$ assembly on gold coated glasses and chemical structure of the Hyaluronic acid (B) and Poly-L-lysine (C) used for LbL.

CD44 is the main HA receptor and is overexpressed in different types of cancer.[13, 23] This receptor is selected as a pathologically relevant target to evaluate the efficiency of the generated assemblies as models to study the impact of HA Mws in the response of cancer cells. The gastric cancer cell line MKN45 overexpress CD44 and are sensitive to HA Mw. [10, 24] We, therefore, followed in situ the interactions of MKN45 cells with the LbL substrates using quartz crystal microbalance with dissipation (QCM-D). The QCM-D is an acoustic technique [25-27] that measures frequency shifts (Δf) of an oscillating piezoelectric quartz crystal in response to the hydrodynamic adsorbed mass and the energy dissipation (ΔD) of this mass, which gives an indication of its viscoelastic properties.[28-30] These characteristics make the QCM-D a valuable tool to evaluate the build-up of the LbL assemblies, their properties as function of the HA's Mw and structural changes that are induced upon cell adhesion (Figure 2). The in situ registered changes of Δf and ΔD after the injection of cells demonstrated three different stages: i) seeding of the cells; ii) cell attachment, spreading and LbL/ECM remodelling; and iii) detachment of the loosely attached cells (Supplementary Fig. 1).

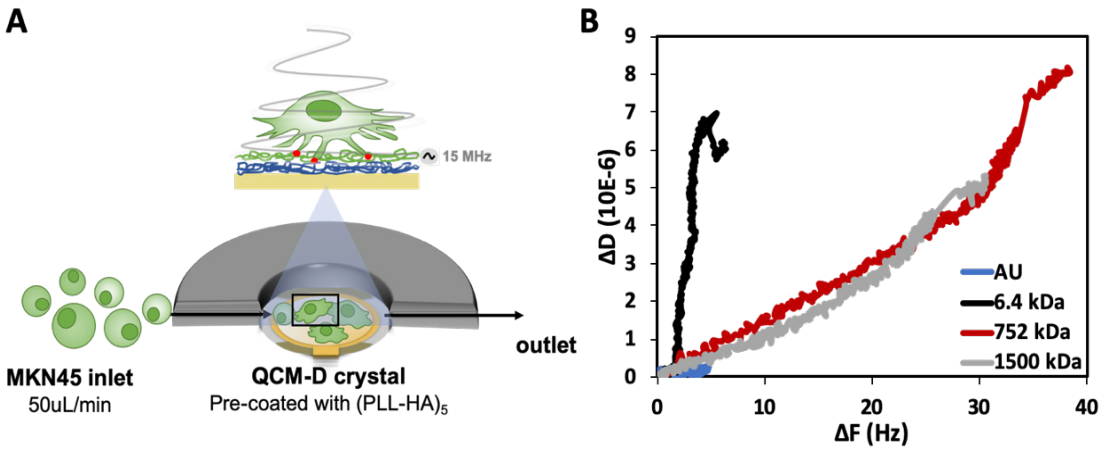

Figure 7-2. (A) Schematic presentation of QCM-D setup in the presence of cells and (B) representative ΔD/Δf plots (5th overtone) showing changes during the interaction between the MKN45 cells and the $(PLL\text{-}HA_n)_5$ samples

The correlation between Δf and the adsorbed mass is not straightforward when cells are used as sensory input because they are relatively big for the used frequency: QCM can detect changes within a layer of apx. 250 nm (at most) for the used fundamental frequency (5 MHz). [31, 32] Therefore, cells represent an acoustically "thick" layer with thickness (nearly 10 μm) much larger than the maximum penetration depth of the acoustic wave.[33] Because the cell body is above the detection limit of the QCM-D shear wave, Δf is not indicative for the number of cells deposited on the sensor. However, specific interactions taking place on the sensor surface within the detection limit (i.e. adsorption of proteins secreted by the cells, receptor-ligand interactions, etc.) can be detected but only provide qualitative information about the dynamics of cells' adhesion.[27, 31] ΔD can corroborate Δf signal as it provides data for the viscoelastic properties of the mass deposited on the quartz sensor and thus, indication about cell adhesion strength, formation of FAs and cytoskeleton assembly. [34]

The deposited LbL films have a thickness between 30-100 nm (Chapter 4) depending on the HA Mw (thicker LbLs are build-up from HA with higher Mws). Considering the limiting penetration depth of the acoustic shear waves, the QCM-D data can provide information about the following specific events occurring upon the injection of cells: 1) the rearrangements/modification of the viscoelastic properties of the LbL films induced by the MKN45 cells; 2) formation of contact points between the cells and the multilayer surface; 3) secretion of proteins by the MKN45 cells. ΔD/Δf plots show the direct relation of the deposited mass and its mechanical properties. [25] Analysis of the ΔD/Δf plots (Figure 2B) showed that MKN45 cells seeded on $(PLL\text{-}HA_{6.4})_5$ induce an abrupt increase in ΔD with no significant changes in Δf, while MKN45 cells in contact with the multilayers comprising the HAs of higher Mws, i.e. $(PLL\text{-}HA_{752})_5$

and $(PLL\text{-}HA_{1500})_5$, induce an exponential increase of the Δf and ΔD. The negligible response observed for cells seeded on bare gold is related with the lack of a viscoelastic layer underlaying the adherent MKN45 (ΔD) and secreted ECM (Δf) for the studied timeframe. The result obtained for the cells in contact with LbL with short HA (6.4 kDa) can be associated with the formation of FAs and further reorganization of the substrate layers. [25] MKN45 cells on $(PLL\text{-}HA_{752})_5$ and $(PLL\text{-}HA_{1500})_5$ behave differently: during the injection of the cell suspension and adhesion stage (I and II in Supplementary Fig. 1) the deposited mass and the energy dissipation increase linearly. These changes are an indication of the secretion of proteins by the cells (mass increase) and gradual remodelling of the underlaying LbL system.[33, 35]

7-3.2. Morphology of MKN45 cells seeded on $(PLL\text{-}HAn)_5$ under dynamic and static conditions

We evaluated the impact of the HA Mw on the morphology of MKN45 cells adhered on the $(PLL\text{-}HAn)_5$ samples. Cells were seeded either in the QCM-D chamber (dynamic cell seeding: 1h of constant flow rate, followed by 1h30 under static conditions) or under standard static conditions during 3 and 6h. These culture conditions were chosen based on our previous studies demonstrating amplification of cellular response when dynamic culture conditions are used.[25]

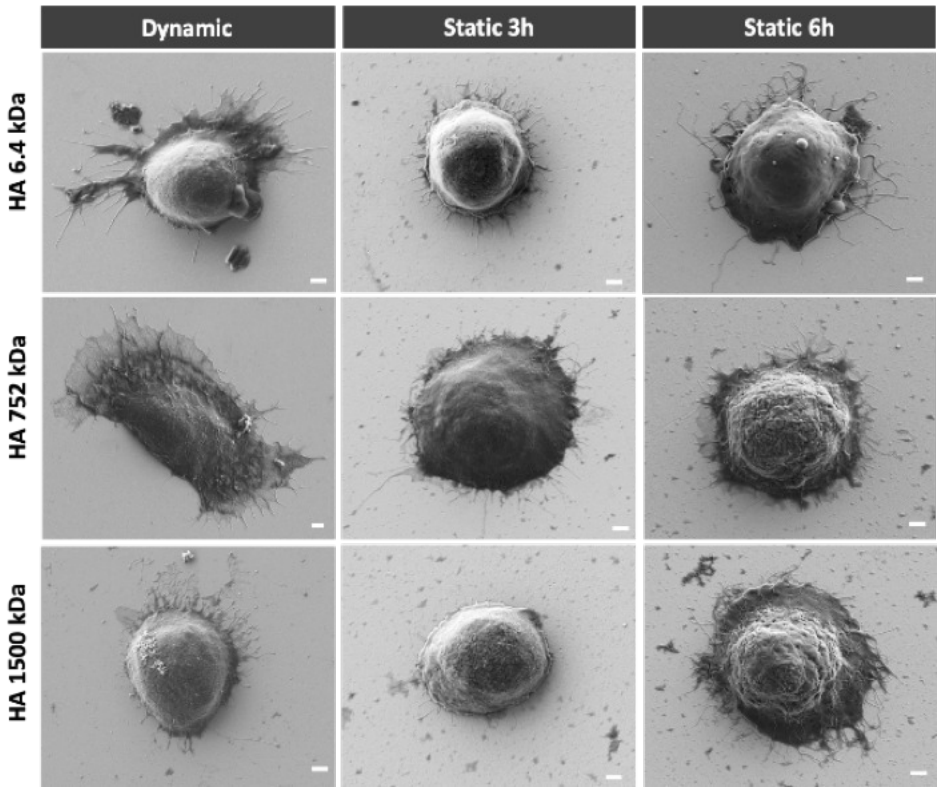

Figure 7-3. Representative SEM images of MKN45 cells cultured under dynamic (50 μL/min flow for 2h30 in QCM-D chambers) and static (3 and 6h) conditions on $(PLL\text{-}HAn)_5$ samples. Scale bar is equal to 1μm. SEM images of the cells seeded on bare gold are presented on Supplementary Fig. 2.

We observed different cellular morphology in response to the used conditions and LbLs (Figure 3): most cells have a round shape but the type of protrusive structures at the leading edge of the cells, their number and size were different.

Lamellipodia are sheet-like projections on the leading edge of the cell. They are highly dynamic and promote cell migration through formation of protrusions driven by actin polymerisation. Filopodia are thin, long and actin rich cytoplasmic protrusions, which are used by the cells to probe their microenvironment.[36, 37] We observed formation of both filopodia and lamellipodia for all cells seeded under dynamic conditions independently of the Mw of HA. Two types of filopodia are visible: ones growing from the cell body and others growing from lamellipodia. The number of the filopodia and their length are similar for cells cultured on $(PLL\text{-}HA_n)_5$ samples comprising HA of the same Mw under dynamic and 6h of static cell culture (Supplementary Fig. 3). The Mw of the HA present in the LbL significantly influenced the cellular response at any of the tested culture conditions: HA of 6.4 kDa stimulate formation of filopodia, especially the ones growing from lamellipodia (Figure 4).

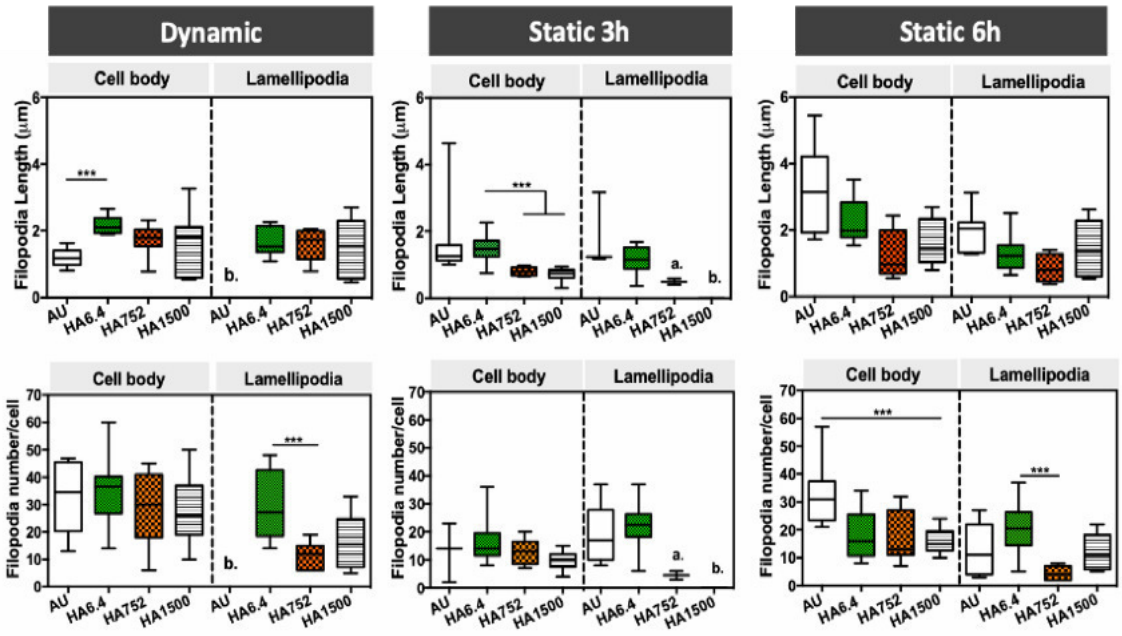

Figure 7-4. Quantitative analysis of (A) filopodia length and (B) filopodia number of MKN45 cultured at dynamic and static conditions for 3 and for 6h. Significant differences are marked for p<0.001 (***), and for n<3 (a.) and n=0 (b.).

As mentioned above, both filopodia and lamellipodia are cellular features associated with cell migration. However, in contrast to lamellipodia, filopodia cannot drive cellular migration by itself.[38] Therefore, our results (Figures 3 and 4) suggest that cells seeded on $(PLL\text{-}HA_{6.4})_5$ have higher motility as compared with the cells cultured in contact with HA of 752 and 1500kDa.

7-3.3. Cell motility depends on the HA size

Recently, we reported the influence of HA Mw on the motility of MKN45 cells cultured on one bilayer $(PLL\text{-}HA_n)_1$ system: we observed shorter cellular tracks for samples with HA of 6.4kDa. Cellular motility increased on samples comprising HA of higher Mw due to the binding and clustering of CD44 receptors leading to formation of invadopodia.[10] Herein, it is used thicker LbL systems, composed by 5 bilayers of $(PLL\text{-}HA_n)_5$. Surprisingly, the opposite trend was observed for the motility of MKN45 cells seeded on these thicker systems, i.e. MKN45 cells in contact with $(PLL\text{-}HA_{6.4})_5$ have longer displacement tracks, while cells cultured on $(PLL\text{-}HA_{752})_5$ and $(PLL\text{-}HA_{1500})_5$ have shorter displacements (Figure 5). Moreover, pronounced morphological changes are visible for the motile cells on $(PLL\text{-}HA_{6.4})_5$ samples (Figure 5 – yellow/green arrows).

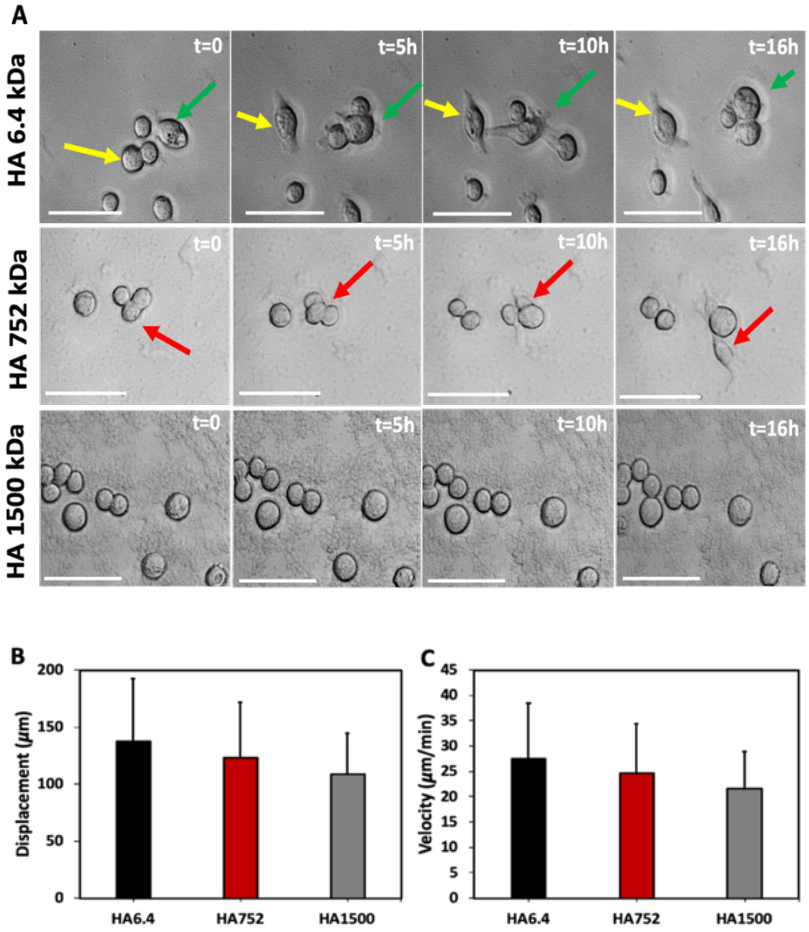

Figure 7-5. (A) Time-lapse images of MKN45 cells seeded on the different $(PLL\text{-}HAn)_5$ samples up to 16h (arrows with the same colour point to the same cell). Scale bars correspond to 50 m. (B) Displacement and (C) velocity of the cells (n = 10 of 2 replicas) calculated from the time-lapse imaging.

Cellular adhesion and migration on $(PLL\text{-}HAn)_5$ samples can be regulated by biochemical signals, as well as by mechanotransduction - a phenomenon associated with the mechanosensing ability of the CD44 receptors.[39, 40] The increasing of layers' number results in formation of softer constructs especially in the case of LbLs comprising long HA chains, i.e. $(PLL\text{-}HA_{752})_5$ and $(PLL\text{-}HA_{1500})_5$.[41] These results indicate that the observed response of MKN45 cells seeded on $(PLL\text{-}HA_{6.4})_5$ samples (higher cellular adhesion, Supplementary Fig. 4, migration and cytoskeleton rearrangement) is driven by both mechano- and biochemical cues, mediated by CD44 cell surface receptors.[7, 42]

7-3.4. Influence of HA Mw on the activation of focal adhesion sites

To better understand the impact of the HA's Mw on cell adhesion and migration it was analysed the expression of paxillin at the FAs and in the stress fibres. Paxillin is a molecular adaptor – it contains binding sites for different proteins and thus, is crucial in the activation of various pathways (by facilitating the binding of different proteins), their signalling specificity and their crosstalk with other pathways. Upon cellular adhesion, paxillin is recruited to the FAs where is involved in the activation of intracellular signalling cascades that lead to the reorganization of FAs and actin fibres. The tyrosine phosphorylation of paxillin is important in regulating FAs dynamics, through their assembly and disassembly, leading to cell adhesion and migration.[17, 43, 44] Herein, it is evaluated the expression of paxillin by MKN45 cells in contact with $(PLL\text{-}HA_n)_5$ samples (Figure 6). Our results demonstrated a correlation between the paxillin expression and the Mw of HA: cells attached to the LbL presenting HA of 6.4kDa express more paxillin at all studied conditions and this expression is reduced with the increment of the HA Mws' (Figure 6). Of note, paxillin was mainly located in the cytoplasm for cells cultured under static conditions and on the cellular membrane when dynamic cell culture was used instead. Formation of FAs is observed for MKN45 cells cultured on $(PLL\text{-}HA_{6.4})_5$ either under dynamic, on the membrane, or static (6h) conditions, on peripheral filopodia (Figure 6, white arrows).

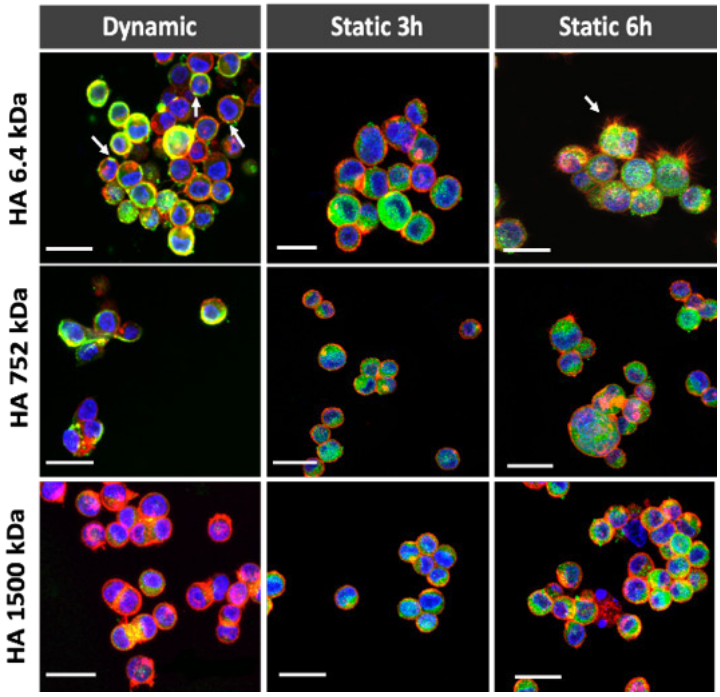

Figure 7-6. Paxillin expression (green) of MKN45 cells cultured on $(PLL\text{-}HAn)_5$ samples (n = 6.4, 752 and 1500kDa) under dynamic (QCM-D) and static conditions (3 and 6h). Scale bars correspond to 25µm. Actin is stained in red and nuclei in blue. These results are in good agreement with the cell motility data (Figure 5): cells seeded on $(PLL\text{-}HA_{6.4})_5$ samples are more motile and express more paxillin. Paxillin staining of cells seeded on bare gold are presented on Supplementary Fig. 5.

7-3.5. HA mediated activation of mitogen-activated protein kinases (MAPKs)

The observed correlation between the size of HA and cellular motility, FAs formation and paxillin expression suggests that cellular mechanisms responsible for cancer invasiveness and aggressiveness can be also altered as a function of HA size. Therefore, it is analysed the phosphorylation of three major families of mitogen-activated protein kinases (MAPKs): the ERK1/2 and JNK1-3 kinases, the p38 isoforms $\alpha/\beta/\delta/\gamma$, and additional key signalling molecules, such as Akt, GSK-3, p70 S6 kinase, TOR, p53 and CREB. The MAPK signalling pathways can be activated by different cellular receptors, proteins, growth factors or/and hormones. The activated pathways are fundamental in regulating processes such proliferation, differentiation, migration, stress response and apoptosis.

We analysed the protein lysate from the MKN45 cells seeded under dynamic conditions because this culture is closer to the in vivo environment where both biochemical signalling and mechanotransduction determine cellular response. The Phospho-MAPK array kit was used to analyse

the lysates from cells cultured on $(PLL\text{-}HA_{6.4})_5$ and $(PLL\text{-}HA_{1500})_5$ because of the distinct behaviour that it is observed for cells cultured on these samples (Figures 7 and Supplementary Fig. 6).

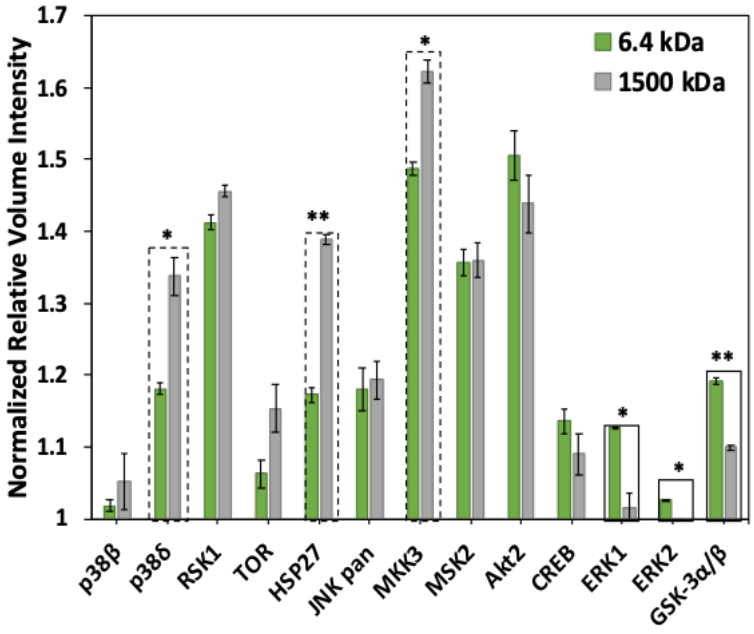

Figure 7-7. Activated pathways in MKN45 cells seeded on LbL samples presenting HA of 6.4 and 1500kDa under dynamic conditions. Phosphorylated proteins activated in response to HA of 6.4kDa are marked with solid black line and to HA of 1500kDa are marked with dashed black line. Significant differences are marked for $p<0.05$ (*) and $p<0.01$ (**).

The activation of two distinct mutually inhibitory signalling cascades in response to different sizes of HA, is observed. MKN45 cells attached to $(PLL\text{-}HA_{6.4})_5$ have high levels of ERK1/2 and GSK-3α/β phosphorylation, while cells seeded on $(PLL\text{-}HA_{1500})_5$ have upregulated p38α, HSP27 and MKK3 phosphorylation. The relationship between the phosphorylated proteins of p38-MAPK family are known: MKK3 is responsible for the phosphorylation of p38α and p38δ, but not p38β while p38α is responsible for the activation of HSP27.[45, 46] These results confirmed the hypothesis that HA of different Mw induce the activation of different pathways: short HA activates the ERK1/2 downstream cascade that regulates cell differentiation and spreading, whereas HA of high Mw is related to p38 phosphorylation considered to be stress activator, regulating cellular apoptosis (Figure 8A).[47] These results are consistent with the ones showing cell adhesion, migration and paxillin expression. The role of low HA Mw on triggering ERK1/2 pathway, through the activation of FAK-Src signalling is enabled by the phosphorylation of paxillin.[43, 48] The crosstalk between these two pathways on tumor cell behaviour is described: high p38 MAPK activity in combination with low ERK1/2 pathway action is

associated to tumor cell latency,[49] which can be correlated to the results obtained for cells seeded on the samples presenting HA of 1500kDa.

However, this data does not clearly identify the mechanism by which HA induces paxillin phosphorylation. As mentioned before, CD44 is one of the main receptors for HA, and it is known to induce phosphorylation of the complex Src/FAK leading to the formation FA complexes. To evaluate if the HA/CD44 interaction participates on the recruitment of paxillin to the FA sites, the CD44 receptors were blocked and paxillin expression evaluated under dynamic conditions (Figure 8B).

Blocking CD44 affected tremendously the expression of paxillin by the cells cultured on $(PLL\text{-}HA_{6.4})_5$ samples (Figure 8B): these MKN45 cells express less paxillin that is mostly localised in the cytoplasm (Figure 8B vs Figure 6). Paxillin expression does not change significantly with the blocking of CD44 for cells in contact with samples presenting HA of 752kDa and 1500kDa, (Figure 6 vs Figure 8). Of note, the blocking of the CD44 receptors of cells cultured on bare gold does not alter significantly the paxillin expression (Supplementary Fig. 8). In this case, i.e. when HA is not present on the surface, cell adhesion and spreading is not mediated by CD44 but via different mechanisms, e.g. integrin-mediated ones, where proteins such as Src, focal adhesion kinases (FAK) and paxillin are recruited to form the FA complexes.[50]

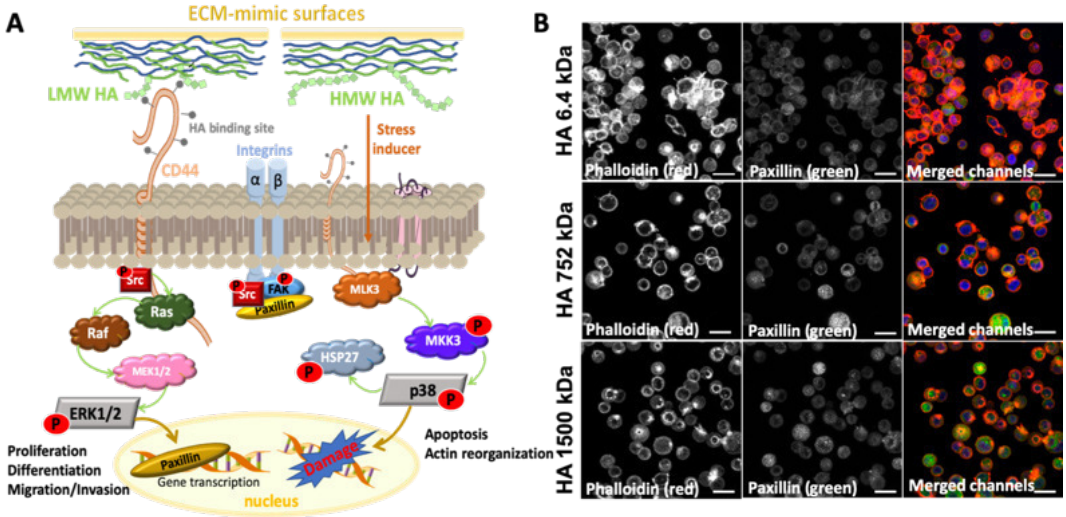

Figure 7-8. (A) Schematic presentation of MAPK signalling cascades activated by HA of different sizes: low Mw and high Mw HA. (B) Effect of CD44 blocking on paxillin expression (actin in red, paxillin in green and nuclei in blue) of MKN45 cells seeded on $(PLL\text{-}HAn)_5$ samples under dynamic conditions. Scale bars correspond to 25µm.

7-4. CONCLUSION

We developed a feasible and versatile platform that can incorporate HA of different Mws without compromising its recognition by specific cellular receptors, i.e. its bioactivity. We demonstrated that the Mw of HA influences dramatically the response of gastric cancer cells: short HA oligomers (6.4kDa) induce the formation of FAs and cell migration via the activation of the MAPK-ERK signalling cascade, which is responsible for the invasiveness and aggressiveness of gastric cancers. In contrast, surfaces presenting higher Mw HA (i.e. 752kDa and 1500kDa) inhibits cell migration, thus triggering tumor cell latency through activation of the p38 signalling cascade and inhibition of the ERK1/2 pathway. The obtained results contribute to the understanding of HA involvement in tumor progression and allow the development of therapeutic approaches based on HA that target specific pathways.

7-5. REFERENCES

1. Baranyi, M., M. Lippai, and Z. Szatmari, *[Role of the stroma in the initiation and progression of tumors].* Orv Hetil, 2015. **156**(45): p. 1816-23.

2. Quail, D. and J. Joyce, *Microenvironmental regulation of tumor progression and metastasis.* Nat Med, 2013. **19**(11): p. 1423-37.

3. Kultti, A., et al., *Accumulation of extracellular hyaluronan by hyaluronan synthase 3 promotes tumor growth and modulates the pancreatic cancer microenvironment.* Biomed Res Int, 2014. **2014**: p. 817613.

4. Chen, J.E., et al., *Influence of Hyaluronic Acid Transitions in Tumor Microenvironment on Glioblastoma Malignancy and Invasive Behavior.* Front Mater, 2018. **5**.

5. Toole, B.P., *Hyaluronan: from extracellular glue to pericellular cue.* Nat Rev Cancer, 2004. **4**(7): p. 528-39.

6. Chanmee, T., P. Ontong, and N. Itano, *Hyaluronan: A modulator of the tumor microenvironment.* Cancer Lett, 2016. **375**(1): p. 20-30.

7. Slevin, *Oligosaccharides of hyaluronan induce angiogenesis through distinct CD44 and RHAMM-mediated signalling pathways involving Cdc2 and γ-adducin.* International Journal of Oncology, 2009. **35**(4): p. 761-773.

8. Misra, S., et al., *Interactions between Hyaluronan and Its Receptors (CD44, RHAMM) Regulate the Activities of Inflammation and Cancer.* Frontiers in Immunology, 2015. **6**.

9. Chanmee, T., et al., *Key Roles of Hyaluronan and Its CD44 Receptor in the Stemness and Survival of Cancer Stem Cells.* Front Oncol, 2015. **5**: p. 180.

10. Amorim, S., et al., *Molecular weight of surface immobilized hyaluronic acid influences CD44-mediated binding of gastric cancer cells.* Sci Rep, 2018. **8**(1): p. 16058.

11. Dicker, K.T., et al., *Hyaluronan: a simple polysaccharide with diverse biological functions.* Acta Biomater, 2014. **10**(4): p. 1558-70.

12. Mereiter, S., et al., *O-glycan truncation enhances cancer-related functions of CD44 in gastric cancer.* FEBS Lett, 2019. **593**(13): p. 1675-1689.

13. Senbanjo, L.T. and M.A. Chellaiah, *CD44: A Multifunctional Cell Surface Adhesion Receptor Is a Regulator of Progression and Metastasis of Cancer Cells.* Front Cell Dev Biol, 2017. **5**.

14. McFarlane, S., et al., *CD44-mediated activation of alpha5beta1-integrin, cortactin and paxillin signaling underpins adhesion of basal-like breast cancer cells to endothelium and fibronectin-enriched matrices.* Oncotarget, 2015. **6**(34): p. 36762-73.

15. Turley, E.A., P.W. Noble, and L.Y.W. Bourguignon, *Signaling properties of hyaluronan receptors.* The Journal of biological chemistry, 2002. **277**(7): p. 4589-92.

16. Dzwonek, J. and G.M. Wilczynski, *CD44: molecular interactions, signaling and functions in the nervous system.* Front Cell Neurosci, 2015. **9**: p. 175.

17. López-Colomé, A.M., et al., *Paxillin: a crossroad in pathological cell migration.* J Hematol Oncol, 2017. **10**.

18. Parsons, J.T., *Focal adhesion kinase: the first ten years.* J Cell Sci, 2003. **116**(Pt 8): p. 1409-16.

19. Wu, C., et al., *Porous Nanofilm Biomaterials Via Templated Layer-by-Layer Assembly.* Advanced Functional Materials, 2013. **23**(1): p. 66-74.

20. Boudou, T., et al., *Internal composition versus the mechanical properties of polyelectrolyte multilayer films: the influence of chemical cross-linking.* Langmuir, 2009. **25**(24): p. 13809-19.

21. Picart, C., et al., *Buildup Mechanism for Poly(l -lysine)/Hyaluronic Acid Films onto a Solid Surface.* Langmuir, 2001. **17**(23): p. 7414-7424.

22. Lavalle, P., et al., *Modeling the buildup of polyelectrolyte multilayer films having exponential growth.* Journal of Physical Chemistry B, 2004. **108**(2): p. 635-648.

23. Chen, C., et al., *The biology and role of CD44 in cancer progression: therapeutic implications.* J Hematol Oncol, 2018. **11**(1): p. 64.

24. da Cunha, C.B., et al., *CD44 alternative splicing in gastric cancer cells is regulated by culture dimensionality and matrix stiffness.* Biomaterials, 2016. **98**: p. 152-162.

25. Araujo, A.R., et al., *Surfaces Mimicking Glycosaminoglycans Trigger Different Response of Stem Cells via Distinct Fibronectin Adsorption and Reorganization.* ACS Appl Mater Interfaces, 2016. **8**(42): p. 28428-28436.

26. Amorim, S., et al., *Interactions between Exogenous FGF-2 and Sulfonic Groups: in Situ Characterization and Impact on the Morphology of Human Adipose-Derived Stem Cells.* Langmuir, 2013. **29**(25): p. 7983-7992.

27. Chen, J.Y., L.S. Penn, and J. Xi, *Quartz crystal microbalance: Sensing cell-substrate adhesion and beyond.* Biosens Bioelectron, 2018. **99**: p. 593-602.

28. Reviakine, I., D. Johannsmann, and R.P. Richter, *Hearing what you cannot see and visualizing what you hear: interpreting quartz crystal microbalance data from solvated interfaces.* Anal Chem, 2011. **83**(23): p. 8838-48.

29. Teixeira, R., R.L. Reis, and I. Pashkuleva, *Influence of the sulfation degree of glycosaminoglycans on their multilayer assembly with poly-l-lysine.* Colloids Surf B Biointerfaces, 2016. **145**: p. 567-575.

30. Borges, J., et al., *Nanoengineering Hybrid Supramolecular Multilayered Biomaterials Using Polysaccharides and Self-Assembling Peptide Amphiphiles.* Advanced Functional Materials, 2017. **27**(17): p. 1605122.

31. Saitakis, M. and E. Gizeli, *Acoustic sensors as a biophysical tool for probing cell attachment and cell/surface interactions.* Cell Mol Life Sci, 2012. **69**(3): p. 357-71.

32. Nimeri, G., et al., *Neutrophil interaction with protein-coated surfaces studied by an extended quartz crystal microbalance technique.* Colloids and Surfaces B-Biointerfaces, 1998. **11**(5): p. 255-264.

33. Tymchenko, N., et al., *Reversible changes in cell morphology due to cytoskeletal rearrangements measured in real-time by QCM-D.* Biointerphases, 2012. **7**(1-4): p. 43.

34. Monemian Esfahani, A., et al., *On the Measurement of Energy Dissipation of Adhered Cells with the Quartz Microbalance with Dissipation Monitoring.* Anal Chem, 2018.

35. Kushiro, K., C.H. Lee, and M. Takai, *Simultaneous characterization of protein-material and cell-protein interactions using dynamic QCM-D analysis on SAM surfaces.* Biomaterials Science, 2016. **4**(6): p. 989-997.

36. Mattila, P.K. and P. Lappalainen, *Filopodia: molecular architecture and cellular functions.* Nat Rev Mol Cell Biol, 2008. **9**(6): p. 446-54.

37. Carretero, A., et al., *Extracellular matrix-inspired assembly of glycosaminoglycan–collagen fibers.* Journal of Materials Chemistry B, 2017. **5**(17): p. 3103-3106.

38. Hoffmann, B. and C. Schaefer, *Filopodial focal complexes direct adhesion and force generation towards filopodia outgrowth.* Cell Adhesion & Migration, 2010. **4**(2): p. 190-193.

39. Kim, Y. and S. Kumar, *CD44-mediated adhesion to hyaluronic acid contributes to mechanosensing and invasive motility.* Mol Cancer Res, 2014. **12**(10): p. 1416-29.

40. Razinia, Z., et al., *Stiffness-dependent motility and proliferation uncoupled by deletion of CD44.* Sci Rep, 2017. **7**(1): p. 16499.

41. Shen, L., et al., *pH-Amplified multilayer films based on hyaluronan: influence of HA molecular weight and concentration on film growth and stability.* Biomacromolecules, 2011. **12**(4): p. 1322-31.

42. Berdiaki, A., et al., *bFGF induces changes in hyaluronan synthase and hyaluronidase isoform expression and modulates the migration capacity of fibrosarcoma cells.* Biochim Biophys Acta, 2009. **1790**(10): p. 1258-65.

43. Badowski, C., et al., *Paxillin phosphorylation controls invadopodia/podosomes spatiotemporal organization.* Mol Biol Cell, 2008. **19**(2): p. 633-45.

44. Hu, Y.L., et al., *FAK and paxillin dynamics at focal adhesions in the protrusions of migrating cells.* Sci Rep, 2014. **4**: p. 6024.

45. Cuadrado, A. and A.R. Nebreda, *Mechanisms and functions of p38 MAPK signalling.* Biochem J, 2010. **429**(3): p. 403-17.

46. Koul, H.K., M. Pal, and S. Koul, *Role of p38 MAP Kinase Signal Transduction in Solid Tumors.* Genes Cancer, 2013. **4**(9-10): p. 342-59.

47. Wang, Q., et al., *Glycogen synthase kinase-3 is a negative regulator of extracellular signal-regulated kinase.* Oncogene, 2006. **25**(1): p. 43-50.

48. Webb, D.J., et al., *FAK-Src signalling through paxillin, ERK and MLCK regulates adhesion disassembly.* Nature Cell Biology, 2004. **6**(2): p. 154-+.

49. Sosa, M.S., et al., *ERK1/2 and p38alpha/beta signaling in tumor cell quiescence: opportunities to control dormant residual disease.* Clin Cancer Res, 2011. **17**(18): p. 5850-7.

50. Mitra, S.K. and D.D. Schlaepfer, *Integrin-regulated FAK-Src signaling in normal and cancer cells.* Curr Opin Cell Biol, 2006. **18**(5): p. 516-23.

SUPPLEMENTARY INFORMATION

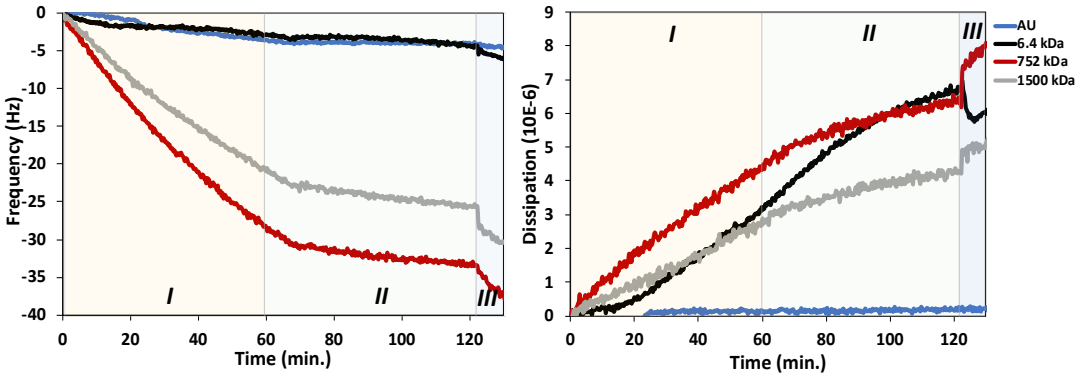

Supplementary Fig. 7-1. Real-time frequency and dissipation shifts during the injection of MKN45 cells (I), cellular adhesion without flow and (II) during the washing step (III).

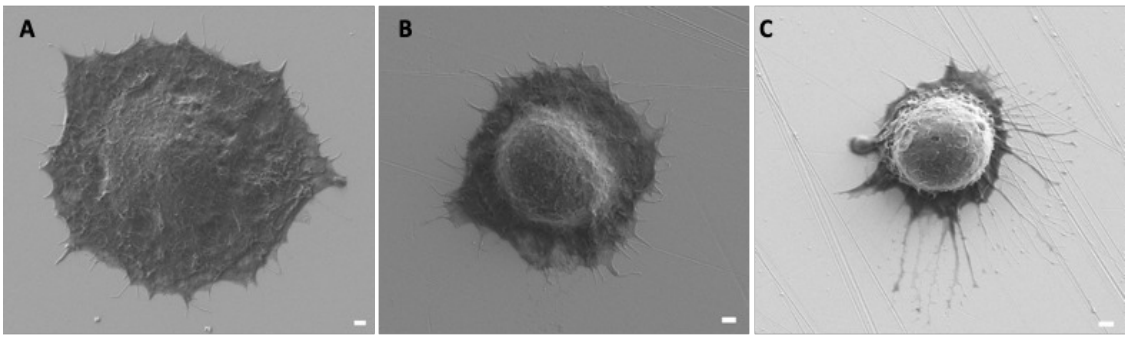

Supplementary Fig. 7-2. SEM micrographs of MKN45 cells cultured on bare gold QCM-D sensors, i.e. dynamic conditions (A), and gold coated glasses, i.e. static conditions for 3h (B) and 6h (C). Scale bars correspond to 1µm.

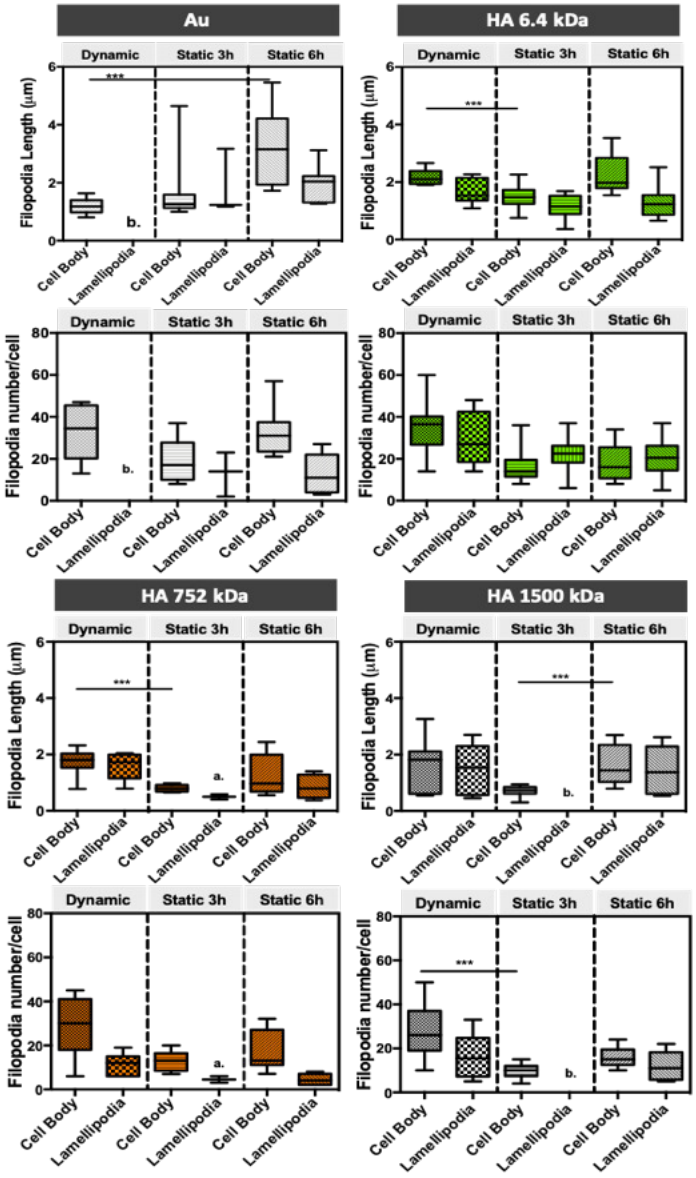

Supplementary Fig. 7-3. Quantitative analysis of filopodia length and number of MKN45 during QCM-D analysis (dynamic conditions) and standard cell culture (static conditions). MKN45 cells were cultured on bare gold surfaces and on (PLL-HA)5 surfaces of HA 6.4kDa, HA 752kDa and HA 1500kDa. Significant differences are marked with $p<0.001$ (***) and insufficient data for statistical analysis is marked for $n < 4$ (a.) and $n=0$ (b.).

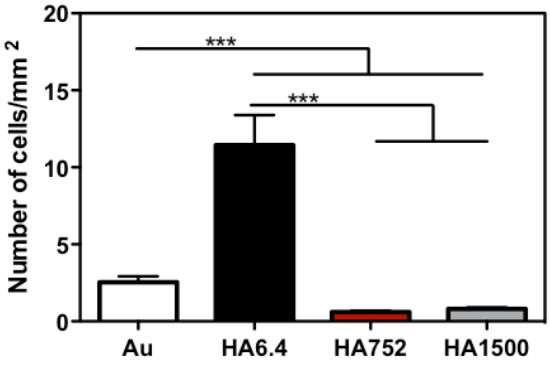

Supplementary Fig. 7-4. Number of MKN45 cells adhered after 24h of cell culture. Significant differences are marked for $p<0.001$ (***).

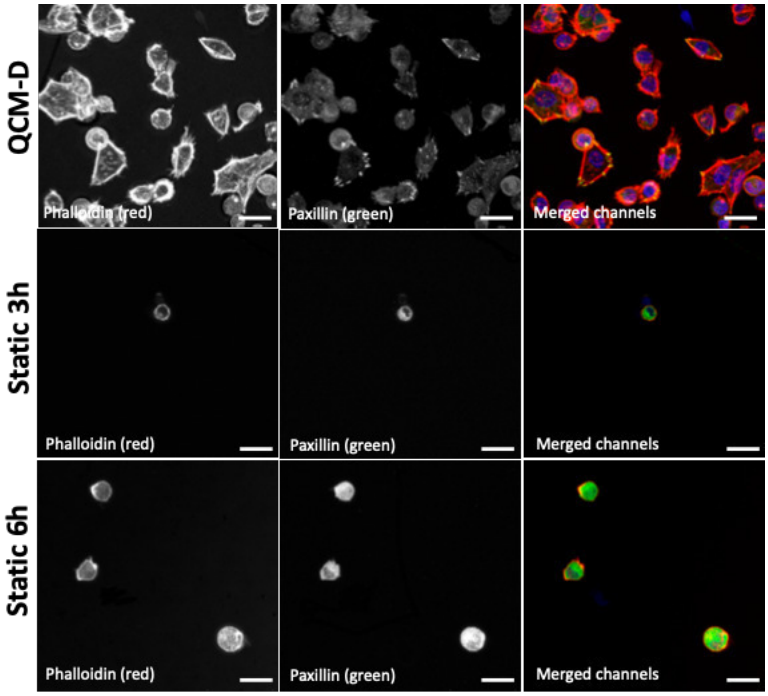

Supplementary Fig. 7-5. Paxillin expression analysis by immunofluorescence (paxillin in green, actin in red, and nuclei in blue) of MKN45 cells cultured on bare gold surfaces, under dynamic cell culture conditions, i.e. QCM-D experiment and under standard culture conditions for 3 and 6h. Scale bar correspond to 25µm.

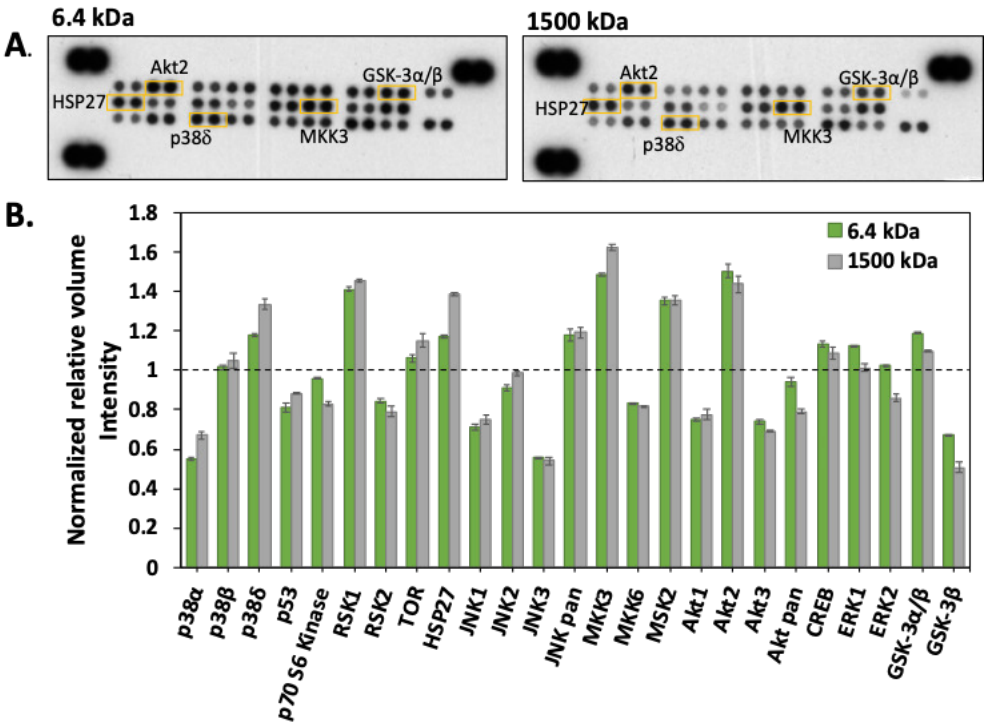

Supplementary Fig. 7-6. Analysis of the Phospho-MAPK protein array for the surfaces presenting HA of 6.4 and 1500kDa. The strong signals of p38δ, MKK3, Akt2 or Hsp27 in response to the LbL surfaces are highlighted (A). Normalized results obtained for the MKN45 cells seeded on the surfaces presenting HA of 6.4 and 1500kDa, under dynamic conditions (QCM-D) (B).

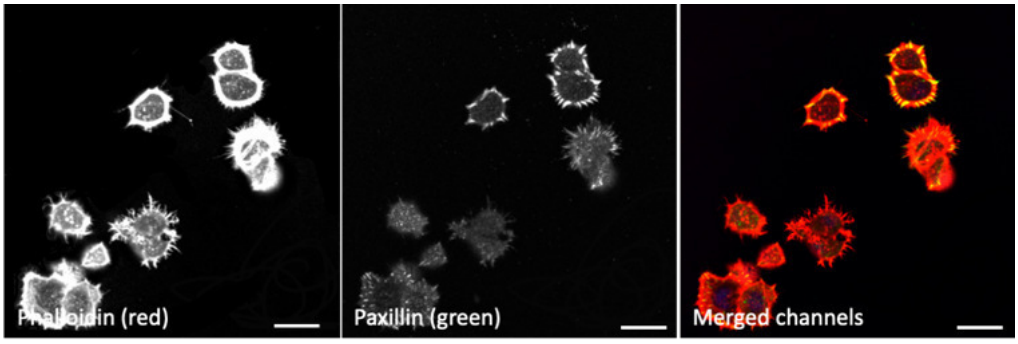

Supplementary Fig. 7-7. Expression of paxillin (paxillin in green, actin in red, and nuclei in blue) by MKN45 cells cultured under dynamic conditions, on bare gold surfaces after blocking the CD44 cell surface receptor. Scale bar correspond to 25μm.

Chapter 8

3D mimics of the tumor microenvironment: interplay between hyaluronic acid, stem and cancer cells

Chapter 8

3D mimics of the tumor microenvironment: interplay between hyaluronic acid, stem and cancer cells[††]

ABSTRACT

The present work reports on a 3D model of the tumor microenvironment that contains hyaluronic acid (HA) and alginate, and demonstrate the utility of this model to study the effect of HA size on the crosstalk between cancer cells and mesenchymal stem cells (MSCs). The system incorporates a core that contains HA of specific size (*i.e.* 6.4, 741 or 1500 kDa) with encapsulated epithelial MKN45 cancer cells and a shell with MSCs that mimic the presence of stem cells next to the tumor site. It is found that short HA (*i.e.* 6.4 kDa) promotes the migration of cancer cells from the core to the shell, whereas longer HA (*i.e.* 741 and 1500 kDa) induces the migration of MSCs into the core, *i.e.* the tumor site, where a reduction of the formation of cancer cells aggregates was observed. In a summary, the developed 3D model recapitulates some key tumor features, related with the effect of HA size on both the cancer cell invasiveness, as well as on the MSC behavior at the tumor site.

[††] This Chapter is based on the publication "Amorim, S., da Costa, D. S., Reis, C. A., Reis, R. L., Pashkuleva, I., & Pires, R. A. (2020), *3D mimics of tumor microenvironment: interplay between hyaluronan*, stem and cancer cells. (submitted)"

8-1. INTRODUCTION

The interactions of cancer cells (CCs) with the components of the surrounding microenvironment, such as proteins, glycoproteins, proteoglycans, signaling molecules and different cell types, determine a complex tumor microenvironment (TME). [1-3] Changes in TME impacts cancer progression: unbalanced synthesis and degradation of its components lead to altered stiffness, elasticity, permeability [4], and biochemical composition. [5, 6] One of the TME components that plays a critical role in cancer invasiveness is hyaluronic acid (HA). [7, 8] The abnormal synthesis of HA by the synthases and the deregulated digestion by hyaluronidases, lead to the accumulation of HA with different molecular weights (Mws) in the basement membrane of cancer cells. [7] The accumulated HA can trigger various signaling pathways (*e.g. via* interaction with HA specific transmembrane receptor CD44) that affect cell proliferation, migration or even latency and apoptosis. [6] The cell response is dependent on the Mw of HA [9, 10]: low Mw HA (<100 kDa) is pro-inflammatory and promote CC migration and invasiveness; while high Mw (>1000 kDa) HA induces CC latency.[7, 11] TME is also governed by the crosstalk between CCs and healthy cells from the surrounding microenvironment (*e.g.* mesenchymal stem cells - MSCs, macrophages, fibroblasts, among others). [12-14] MSCs are linked to tumor progression but their role is controversial. Some authors show that MSCs induce tumor growth by disrupting cell-to-cell contacts and promoting CC migration. [15] Other works suggest that MSCs inhibit the invasiveness of CCs by reducing their drug resistance. [16] In fact, the MSCs' activity depend on their density. It has been reported that a 1:1 MSCs:CCs ratio induces upregulation of metastatic genes; whereas a lower ratio (*e.g.* 1:2) results in the tumor remission. [17-19] The presence of MSCs can also influence the CCs aggregation: MSCs added to pre-formed aggregates disorganized the structures, while MSCs present since the beginning of the formation of CC spheroids enhanced spatial organization and homogeneity. [20]

The complexity of the TME, as well as the mismatch between different animal models and the human cellular environment impose the development of 3D models that mimic the biochemical and mechanical features of the TME as a valuable tool to study cancer progression and/or the efficiency of different treatments. [21, 22] Herein, we developed a 3D co-culture system that recapitulates some important features of the TME: the core is the cancer site with encapsulated CCs exposed to HA of specific Mws that are known to elicit different CC responses, *e.g.* migration or latency; and the surrounding shell contains healthy MSCs that can crosstalk to the CCs present at the cancer site (*i.e.*

core of the hydrogel). We demonstrate that this system can replicate key features of cancer progression and invasiveness.

8-2. MATERIALS AND METHODS

8-2.1. Materials

Sodium Hyaluronate (HA) with Mws of 6.4kDa, 741kDa and 1500kDa was acquired from Lifecore (USA) and sodium Alginate (Alg, UP VLVG, <75kDa) from Pronova (Norway). CD44 monoclonal antibody (Ascites, AM06286SU-N) was purchased from ACRIS. FITC labelled CDD90 (Thy-1) monoclonal Antibody (eBio5E10 (5E10)) was obtained from eBioscience™. The other antibodies: rabbit monoclonal to Vimentin [EPR3776], rabbit monoclonal to E-cadherin [EP700Y] and rabbit monoclonal to alpha smooth muscle actin [E184] were obtained from Abcam. The secondary antibodies IRDye® 800CW Goat-anti-Rabbit and IRDye® 800CW Goat-anti-Mouse were obtained from LI-COR Biosciences.

8-2.2. Methods

8-2.2.1. Hyaluronic acid modification with FITC

Fluoresceinamine (FITC) was coupled to the carboxylic groups of HA of different Mws (*i.e.* 6.4kDa, 741kDa and 1500kDa) using N-(3-dimethylaminopropyl)-N′-ethylcarbodiimide hydrochloride (EDC) chemistry as previously described. [23]

8-2.2.2. Preparation of hydrogels

Alg and HA were dissolved in Milli-Q water and NaCl 0.15M, respectively. Both solutions were mixed to a final concentration of 20mg.mL^{-1} of Alg and 1mg.mL^{-1} of HA. Spheres (core of the 3D systems) were extruded (27G syringe) into a $CaCl_2$ solution (100mM) under constant magnetic stirring. After gelation, the spheres were washed with Tris-buffered saline (TBS) supplemented with 15mM of $CaCl_2$. The Alg or Alg-HA_{Mw} spheres were embedded on a pre-gelated Alg disc and the core-shell hydrogels were allowed to crosslink on a QGel® mold immersed in 50 mM of $CaCl_2$ during 15min. The final construct was washed with TBS-$CaCl_2$.

8-2.2.3. Culture, expansion and seeding of gastric cancer cell line and bone marrow mesenchymal stem cells

Human gastric cancer cell line MKN45 (passages 6 or 7) were cultured in RPMI-1640 medium (Sigma-Aldrich, Portugal) supplemented with 10% fetal bovine serum (FBS; Gibco) and 1% antibiotic/antimycotic solution (final concentration of penicillin 100units/mL, streptomycin 100mg.mL^{-1} and 25μg.mL^{-1} amphotericin B; Gibco, UK). Human bone marrow aspirates were collected from patients subjected to total hip replacement surgery, under the scope of an agreement with Hospital da Prelada (Porto, Portugal). Bone marrow mesenchymal stem cells (bmMSCs) were isolated from the tissue according to a previously published procedure. [24] Afterwards, bmMSCs were expanded in Minimum Essential Medium (MEM) alpha Medium (αMEM; Sigma-Aldrich, Germany) supplemented with 1% Antibiotic/Antimycotic (Gibco), 10% FBS and used at passage 3. Both cell types, MKN45 and bmMSCs, were cultured in a 5% CO_2 incubator maintained at 37°C. For cells encapsulation in the hydrogel, MKN45 and bmMSCs were washed with PBS and harvested with TrypLE™ Express. MKN45 cells (at a cell density of 5x10^6 cells/mL) were dispersed in Alg or Alg-HA_{Mw} solution and extruded as described above (*i.e.* 47μL sphere volume). The spheres with the cells were further embedded in an Alg disc (70μL shell disc) containing bmMSCs (2x10^6 cells/mL) that were previously encapsulated during processing and expanded in αMEM for 3 days. The core-shell system was incubated for 10 days in the presence of αMEM or with bmMSCs conditioned media (CM) from 3 days of stem cells expansion (1:1 ratio of CM: fresh αMEM).

8-2.2.4. Cellular viability, morphology and distribution

To evaluate the cellular viability after 10 days of culture, cells were stained with calcein-AM (1μg/mL - green staining, live cells) and propidium iodide (1μL/mL - red staining, dead cells). To assess the cellular distribution and the expression of specific cellular markers for MKN45 and for bmMSCs (*i.e.* CD44 and CD90, respectively), the hydrogels were washed with TBS-$CaCl_2$, fixed with 16% formaldehyde (Pierce™, P1304MP) for at least 1h at room temperature under shaking. After washing with TBS-$CaCl_2$, the cells were permeabilized with 0.1% Triton X-100 in TBS-$CaCl_2$ for 15min under stirring, and blocked with 3% BSA in TBS-$CaCl_2$ for 1h at room temperature. The CD44 and CD90 expression was evaluated using the CD44 monoclonal antibody (1:350 in 1% w/v BSA/TBS-$CaCl_2$),

followed by rabbit anti-mouse Alexa Fluor-594 (1:500 in 1% w/v BSA/TBS-$CaCl_2$) and CD90-FITC (1:250 in 1% w/v BSA/TBS-$CaCl_2$), respectively. Nuclei were counter-stained with DAPI (1 mg/mL in 1% BSA in TBS-$CaCl_2$). After 1h of incubation with the antibodies, the gels were washed with TBS-$CaCl_2$ and observed under a confocal laser scanning microscope (TCS SP8, Leica, Germany).

8-2.2.5. Immunoblotting

Cell lysates were obtained from the MKN45 cells extracted from the spheres of the core-shell hydrogels. The total protein was extracted with radioimmunoprecipitation assay, RIPA buffer (150mM Sodium chloride; 1% Triton-X100; 0.5% Sodium Deoxycholate; 0.1% Sodium Dodecyl Sulphate; 50mM Tris-Base – pH = 8) supplemented with 1x Protease (cOmplete™ ROCHE, Sigma-Aldrich, Portugal) and 1x Phosphatase (PhosSTOP™ ROCHE, Sigma-Aldrich, Portugal) inhibitor cocktails. Briefly, the spheres were carefully removed from the core-shell hydrogels and washed with cold TBS-$CaCl_2$. The protein lysates were extracted in RIPA buffer for 30min with 5min intervals of vortexing. The extracts were centrifuged (18,000 *g*, 16min, 4°C), and the supernatant was further analyzed by Western-Blotting (WB). Each protein, under Laemmli buffer, was denatured at 37°C for 1h 30min and 95°C for 5min prior to use. The lysates, containing 20μg of protein, were dissolved using 4-12% Bis-Tris Protein Gels (Invitrogen NuPAGE, ThermoFisher Scientific, USA) and transferred to nitrocellulose membranes (Thermo Fischer Scientific, USA). The membranes were incubated in 4% (m/v) bovine serum albumin in Tris-buffered saline-Tween (TBS-T, Cell Signaling Technology) and probed with α-smooth muscle actin (1:5000), Vimentin (1:1000) and E-cadherin (1:5000) antibodies. After 3 cycles of 5min washing with TBS-T, the membranes were incubated with IRDye®800CW anti-Rabbit or anti-Mouse (1:10000) for 1h and imaged on the Odyssey Infrared Imaging System (LI-COR Biosciences, USA).

8-2.2.6. Mechanical properties

The cores of the hydrogels were analyzed by Atomic Force Microscopy (AFM) using a JPK NanoWizard 3 (JPK, Germany). The stiffness of Alg and Alg-HA_{Mw} spheres were measured in TBS buffer, under QI Advanced Mode using qp-BioAC-CB1 probes (resonance frequency between 65-115kHz; spring constant between 0.15-0.55N/m; NanoSensors, Germany). Prior to any experiments, the probes were calibrated using the JPK non-contact method. Young's modulus was calculated from fitting of the approach curves with the Hertz/Sneddon model, using a cone tip shape.

8-2.2.7. Image analysis

The Volume (V) of the clusters was calculated from confocal laser scanning microscopy images, by measuring the radius (r) of the cellular agglomerates according to the equations:

Equation 8-1

$$r = \frac{1}{2}\sqrt{d1 * d2}$$

Equation 8-2

$$V = \frac{4}{3}\pi * r^3$$

where $d1$ and $d2$ is the length and width of the cells' clusters, respectively.

The quantification of fluorescence from the confocal images and the densitometric analysis of WB membranes were performed using ImageJ software (Version 2.0.0-rc-34/1.50a).

8-2.2.8. Statistical analysis

The normality of the data was analyzed using the Shapiro–Wilk test ($p < 0.05$). The data that did not followed a normal distribution, Kruskal–Wallis test followed by Mann-Whitney test was used. In all the cases, significant variations were considered for * $p < 0.03$, ** $p < 0.002$, *** $p < 0.0002$ and **** $p < 0.0001$.

8-3. RESULTS AND DISCUSSION

8-3.1. Development of core-shell 3D hydrogel

Mimicking the complexity of the TME is challenging due to its complexity. [25] Cells' spheroids and 3D scaffolds are the current *in vitro* TME models used on cancer studies. Whereas spheroids are based on clustering of one (*e.g.* CCs) or more cell types (*e.g.* cancer associated fibroblasts (CAFs) and MSCs), but lacks on the dynamic crosstalk between CCs and the surrounding environment [26]; the 3D hydrogel models mimic the features of the extracellular matrix (ECM) composition by using specific components of the ECM, with controlled porosity and mechanical properties. [27]

Here, we developed a core-shell 3D cancer model that resembles the complexity of the TME, combining: 1) the presence of HA of different Mws in the ECM of the cancer tissue; 2) its influence in the behavior of gastric CCs (*i.e.* MKN45) at the cancer site and of healthy bone marrow (bm)MSCs in the neighboring regions; as well as 3) the interplay between HA, CCs and healthy bmMSCs (Figure 1A).

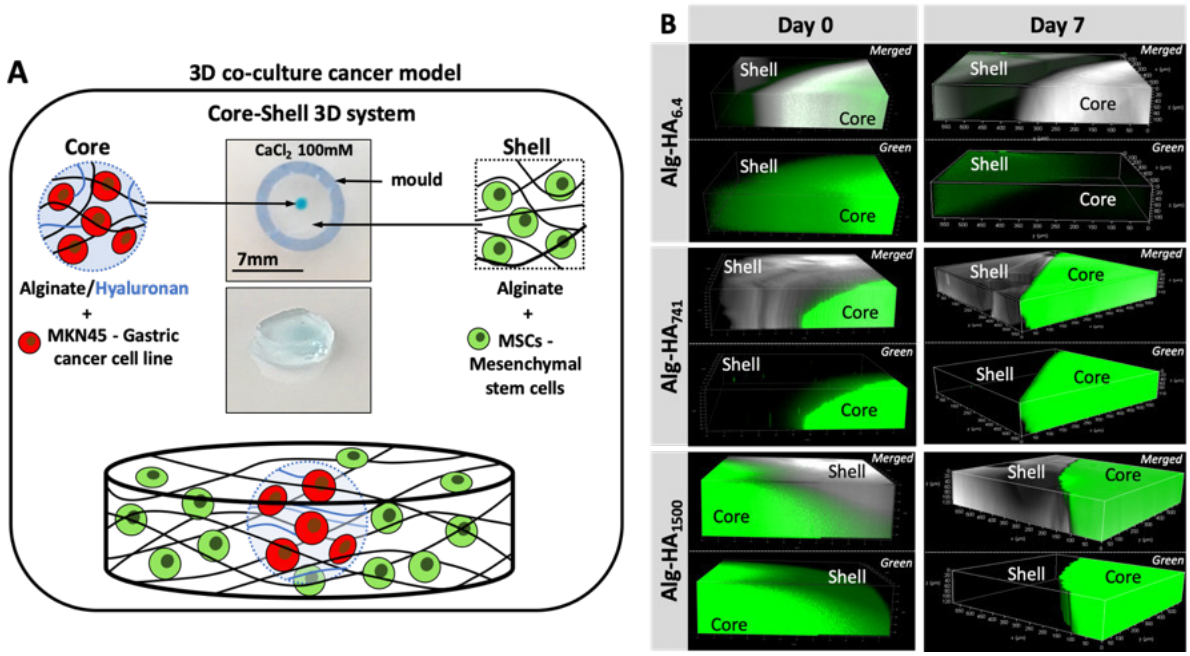

Figure 8-1. (A) Graphical illustration of the developed 3D core-shell system used for the co-culture of cancer MKN45 cells and bone marrow mesenchymal stem cells (bmMSCs). (B) Characterization of the constructs' core incorporating HA with different Mws (i.e. 6.4, 752 and 1500kDa): confocal microscopy images showing the diffusion of the HA (green) from the core to the shell (bottom images, where green corresponds to HA-FITC incorporated in the Alg core; top images merged channels from the transmitted and fluorescence images of the Alg/HA-FITC).

The proposed system is composed by a core hydrogel's microparticle that present HA of different Mws, blended with the biocompatible Alg to generate the 3D polymer network cross-linked under mild conditions, *i.e.* with Ca^{2+}. [28] We performed an initial assessment of the suitability of this system to present the HA in the core of the 3D hydrogel. This was executed using labelled HA (*i.e.* HA-FITC) making it possible to confirm its incorporation in the core of the construct (Figure 1B) by fluorescence microscopy. As expected, short HA (*i.e.* 6.4kDa) are more diffusive: fluorescence can be seen beyond the core of the system even at very short immersion times. This diffusion can explain the similarity between the mechanical properties and stability of Alg and Alg-$HA_{6.4}$ cores (Figure 2A). However, in general we observe a reduction of stiffness when HA is combined with Alg, with higher impact as the HA Mw increases. We believe that HA is contributing differently to the stability of the hydrogels, with a clear distinction between shorter HA chains (*i.e.* $HA_{6.4}$) and the longer HA chains (*i.e.* HA_{741} and HA_{1500}). Our results are consistent with the ability of the longer chains of HA to partially block the ionic crosslinking of Alg, leading to the formation of hydrogels of lower stiffness (Figure 2B2). In contrast, the shorter chains of $HA_{6.4}$ are not able to significantly block the activity of the Ca^{2+} ions presenting a more limited impact in the Alg cross-linking (Figure 2B1). [29, 30] Another important point to consider is the fact that the very high viscosity of HA_{1500} produces a mechanical support to the Alg matrix, partially reverting the loss of stiffness observed for the core composed by Alg-HA_{741}.

After 7 days of immersion (5% CO_2 incubator at 37°C in cell culture medium, but in the absence of cells), the Alg and Alg-$HA_{6.4}$ spheres lose their integrity due to the release of Ca^{2+} (*i.e.* the Alg crosslinking agent) from the hydrogel network, resulting in a disruption of the Alg matrix. [31]

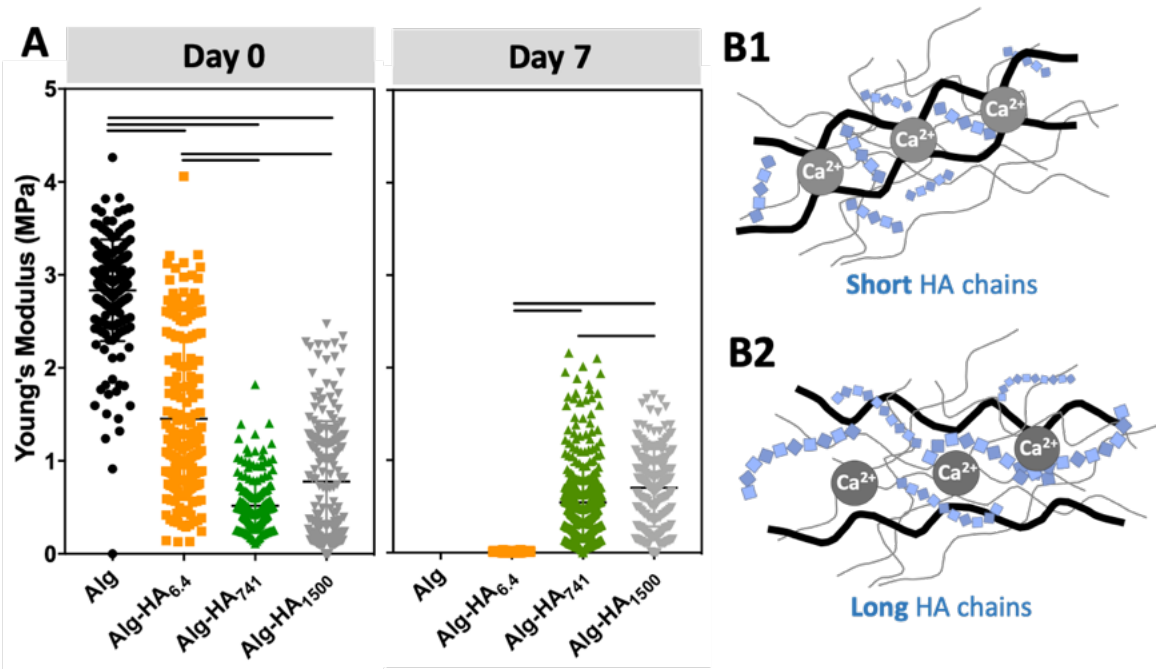

Figure 8-2. (A) Mechanical characterization of the constructs' cores incorporating HA with different Mws (i.e. 6.4, 752 and 1500kDa). (B) schematic presentation of the molecular structure of the cores made from Alg (black) and (B1) short or (B2) long HA chains (blue) that results in the formation of an interpenetrating network. Statistical differences are marked for $p < 0.001$.

Longer HA chains (*i.e.* 741 and 1500kDa) remained within the core even after 7 days of immersion (Figure 1B) due to the interpenetrating network formed by Alg and the lower mobility and diffusion of the HA of high Mw compared with the low Mw variant. Overall, the generated Alg-HA_{741} and Alg-HA_{1500} networks had lower stiffness values as compared to Alg (Figure 2A), however they were more stable after 7 days of immersion. In fact, their mechanical properties did not change significantly over time, while the Alg and Alg-$HA_{6.4}$ disassembled at the same time period.

8-3.2. The incorporation of MKN45 cells influence the mechanical properties and stability of the hydrogels' core

The stiffness of 3D matrices affects cellular adhesion and proliferation. [32-35] In turn, cells also modulate the stiffness of the surrounding environment through the secretion of different proteins. [36]

In fact, the higher deposition of ECM components in the TME usually leads to a stiffening of the cancer site. [36]

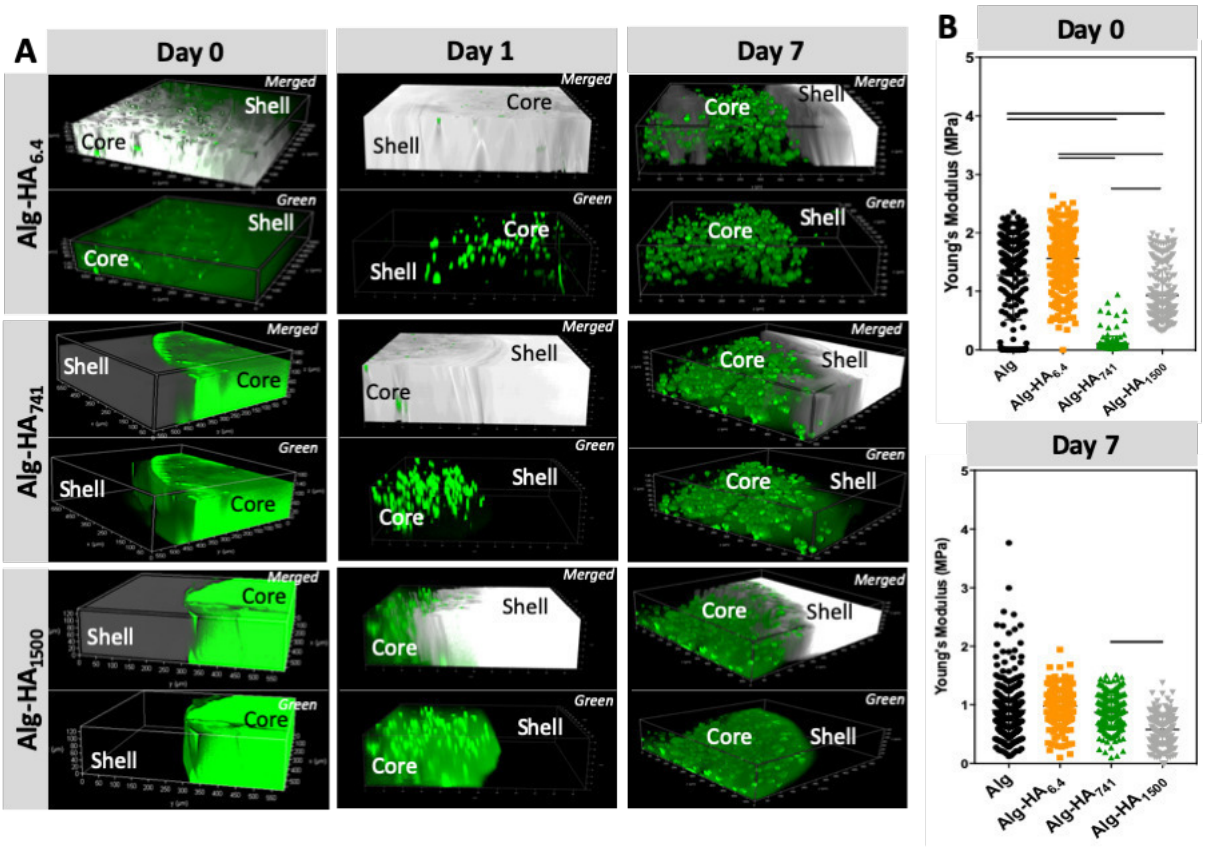

Figure 8-3. A) Confocal microscopy images showing the reorganization of HA (green) by the encapsulated MKN45 cells for different culture times (bottom images, green corresponds to HA-FITC incorporated in the Alg core; top images correspond to the merged channels from the transmitted and fluorescence images of the Alg/HA-FITC). (B) Young's modulus of Alg and Alg-HAMw hydrogels (core) in the presence of encapsulated MKN45 cells. Statistical differences are marked for $p < 0.001$.

Indeed, we observed that the MKN45 cells encapsulated in the construct's core affected its mechanical properties (Figure 3). MKN45 cell formed aggregates with increased cell viability in the presence of HA. This result can be explained with the recognition of HA by the MKN45 cells. [37] Indeed, confocal microscopy showed a scattered fluorescence signal indicating HA reorganization in the presence of cells (Figure 3A). At day 0, this change is visible only for the short and diffusive $HA_{6.4}$, *i.e.* immediately after the cell encapsulation. However, after 1 day of culture, similar redistribution is also visible for the longer HA_{741} and HA_{1500}. However, in these cases (especially for HA_{1500}) a blur fluorescence

co-exists with the scattered signal suggesting engagement of HA in two processes: interpenetrating network formation (blur fluorescence) and cells-HA interactions.

Cellular encapsulation reduced the stiffness of the hydrogels (Figure 2B *vs* Figure 3B, at day 0) but the dependence of the HA size was similar to the one obtained for the hydrogels without cells. The main difference was observed after 7 days of culture: MKN45 cells significantly improved the stability of the Alg or Alg-$HA_{6.4}$ hydrogels. These results are consistent with the ability of the encapsulated cells to proliferate and produce ECM under these experimental conditions leading to improved stability of the 3D hydrogel structure over time. [38]

The use of Alg to generate the 3D polymer network (through crosslinking with Ca^{2+}) is compatible with cell culture conditions. [39] While being biocompatible, Alg also lacks adhesive epitopes and, thus, can serve as a bioinert background that allows to evaluate the bioactivity of the added HA. Such approach is advantageous because HA can be immobilized in the 3D construct without any modification. The core containing HA was loaded with CCs (mimicking the cancer site), which was embedded in a hydrogel disc, to which healthy bmMSCs were encapsulated (mimicking the surrounding environment). Moreover, the proposed core-shell model where CCs are confined on the hydrogel's core, mimic the hypoxic tumor physiological conditions and reduced flow of nutrients. [40] This system was used to evaluate the impact of HA's Mw in cancer invasiveness and the influence of the surrounding healthy cells.

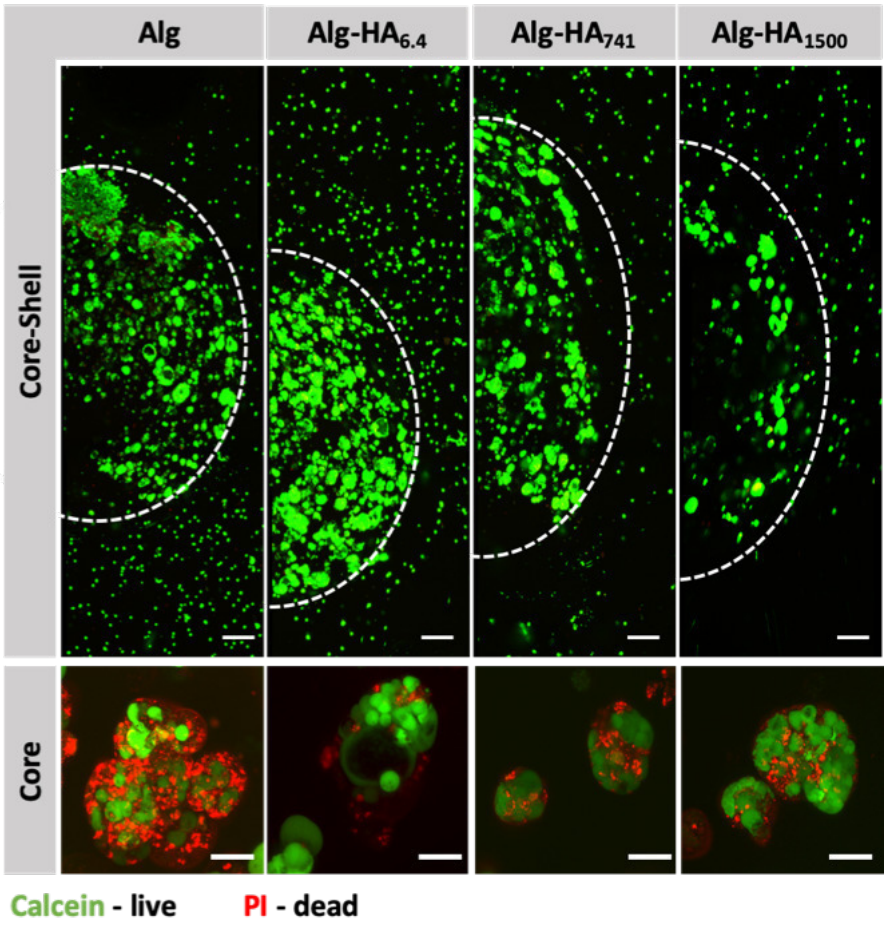

Figure 8-4. Live/Dead staining of co-cultures of MKN45 cells (in the core, i.e. inside the circle maked by a dashed line) and bmMSCs (in the shell, i.e. outside the circle) after 10 days of culture. Scale bars correspond to 200µm. Lower images correspond to the viability of the MKN45 cell's clusters present inside the core (higher magnification). Scale bars correspond to 50µm.

The viability of the cancer (*i.e.* MKN45) and healthy (*i.e.* bmMSCs) cells, cultured on the developed 3D system, was evaluated after 10 days of cell culture. Our Live/Dead staining results show a high viability of both cell types in the core and shell of the 3D system (Figure 4). The formation of MKN45 cell clusters are visible in the core of the hydrogel, with increased cell death in the Alg-only sphere. The addition of HA into the core improves cellular viability, which could be related with the internalization of HA by the MKN45 cells, as suggested by the fluorescence images obtained using HA-FITC (Figure 3A, day 1 and 7). [37]

8-3.3. Cancer cell migration and protein expression in the presence of mesenchymal stem cells

The influence of MSCs on CCs behavior is mediated through the release of pro-inflammatory cytokines and/or growth factors (*e.g.* TGF-beta1 and VEGF). [41] However, direct MSCs-CCs contacts can also occur and lead to the disruption of CCs agglomerates mainly through the cleavage of the cell-cell junctions, which are maintained by E-Cadherin. [15, 42] The presence of MSCs in the TME also increases the sensitivity of CCs to anti-cancer drugs. [43] The MSCs:CCs ratio is also critical for any outcome, including changes in CCs invasiveness and tumor progression. [18, 26]

To mimic the complexity of the TME, we encapsulated MSCs in the shell of the construct, which was designed to be in direct contact with the core (representing the cancer site) containing the encapsulated CCs. To track the migration of each cell type, we tagged cells for the mesenchymal stem cells marker, CD90 [44], and the transmembrane HA receptor, CD44, in all the studied cells. [45] Both cell types express CD90 and CD44 (Supplementary Fig. 2 and 3) but the relative expression intensity is very different and can be used to distinguish MKN45 from bmMSCs cells. Our results show that MKN45 cells (encapsulated in the Alg-$HA_{6.4}$ core) migrated to the Alg shell. When the core contained longer HA chains (*i.e.* 741 and 1500kDa) no MKN45 migration was observed but bmMSCs migrated from the shell into the core of the construct (Figure 5A and Supplementary Fig. 4).

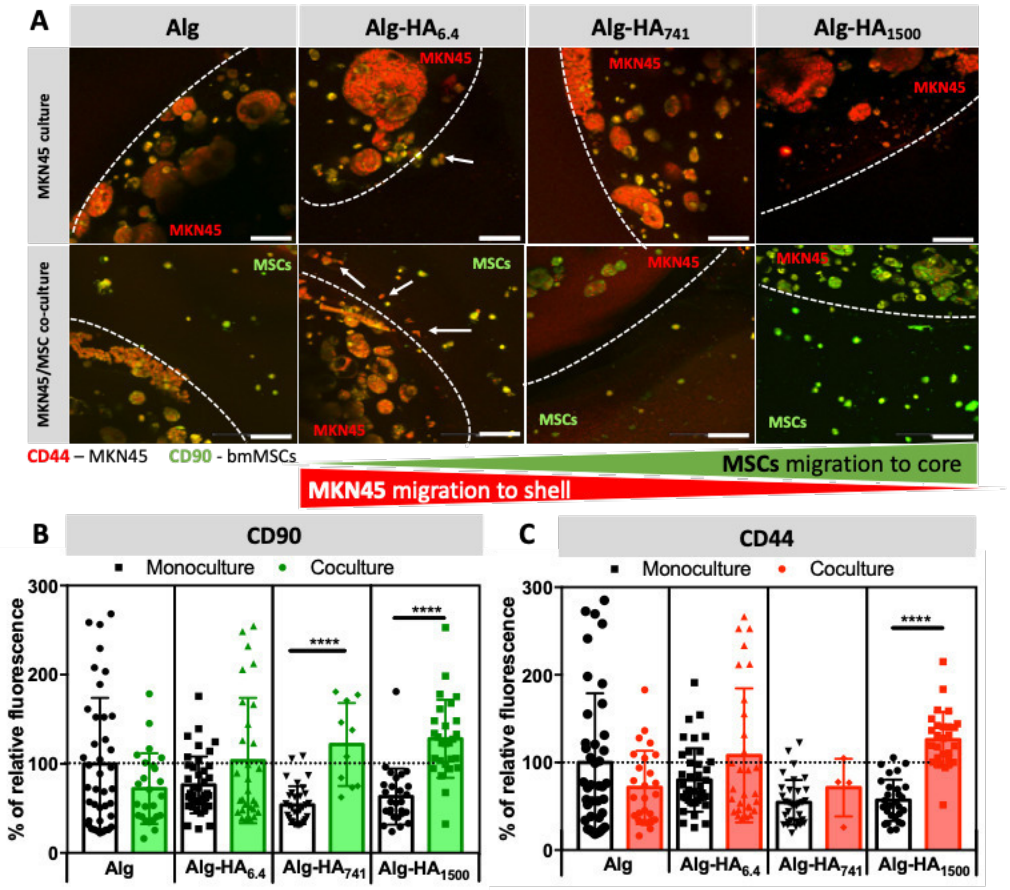

Figure 8-5. A) Migration of MKN45 cells (mono- and co-culture) and bmMSCs (co-culture) cells within the constructs. (B, C) Relative fluorescence intensity (normalised to Alg construct under monoculture conditions) measured for the cells' agglomerates in the core that were immunolabelled for (B) CD90 and (C) CD44. Scale bars correspond to 200µm. Statistical differences ** are marked for $p < 0.0001$.**

The migration of MKN45 cells from the Alg-$HA_{6.4}$ core was also observed in the absence of bmMSCs (Figure 5A; monoculture, white arrows) and can be associated with: 1) fast solubilization of the core structure, through the release of Ca^{2+} cations (as previously shown in Figure 1 and 2) leads to the reorganization of the core matrix increasing the migration of MKN45 cells; 2) the HA gradient generated upon the diffusion of HA into the shell (Figure 1B) acting as directional cues for CCs migration; and 3) the internalization of $HA_{6.4}$ by CCs, as suggested by the fluorescence images of HA-FITC on the CCs sites (core, Figure 3A) that could act as a signaling mechanism to induce CCs' migration. [38, 46] bmMSCs cultured alone did not migrate from the shell to the HA rich core (Supplementary Fig. 3), however, in the presence of MKN45 cells, it seems that the stem cells colonized the Alg-HA_{1500} (Figure 5A). The observed result (high relative intensity of green in the core, Figure 5) can be also due to an increased CD90 expression by the MKN45 in the presence of bmMSCs

in the vicinity of the CCs. The same variation of CD90 expression was observed for MKN45 cell cultures supplemented with medium from bmMSCs expansion (Supplementary Fig. 5). This result showed that MSCs-secretome alone is able to modulate the MKN45 behavior but the direct MSCs-MKN45 contacts amplifie this response.

8-3.4. Disruption of MKN45 cell-cell contacts in the presence of MSCs

The ability of bmMSCs to modulate the cell-to-cell contacts in tumors was assessed by the capacity of MKN45 cells to form aggregates when cultured alone or together with bmMSCs (Figure 6). We observed significantly smaller MKN45 aggregates in Alg and Alg-HA_{1500} in the presence of bmMSCs (Figure 6B). We believe that the co-culture on Alg-only system induces a faster degradation of the hydrogel, compromising cellular adhesion and proliferation. On the other hand, bmMSCs cultured in the shell of the Alg-HA_{1500} rich-core system promotes the formation of smaller CCs' aggregates and therefore inhibit tumor growth. In fact, it has been previously reported the same tumor inhibition when low, but relevant, number of MSCs (a CC:MSCs ratio of 2:1) were injected in the tumor site. [47]

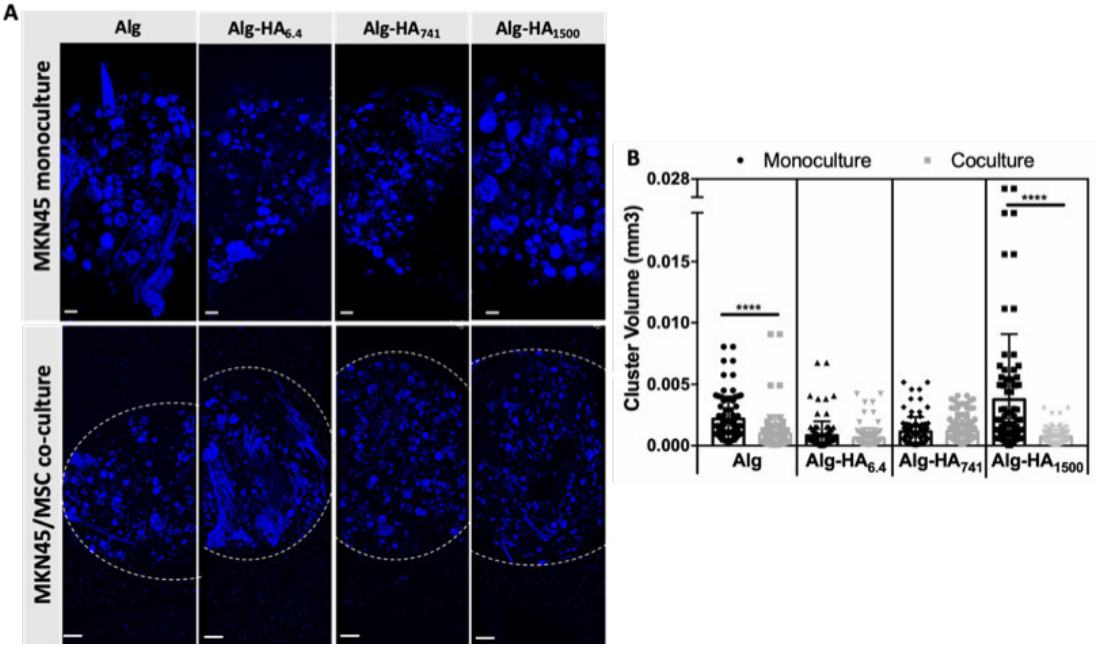

Figure 8-6. Influence of the bmMSCs cells (cultured in the shell of the hydrogels) on the aggregation of MKN45 cells in the core of the construct: (A) Confocal microscopy images of MKN45 cells cultured alone (monoculture) and together with bmMSCs (co-culture) and immunostained with DAPI (cell nuclei). (B) Volume analysis of the CCs' aggregates generated under different cell culture conditions. Scale bars correspond to 200µm. Statistical differences ** are marked for $p < 0.0001$.**

The mesenchymal/epithelial markers expressed by the MKN45 cells encapsulated in the core of the constuct was evaluated by Western Blot (WB, Figure 7). Under co-culture conditions, the cells present in the core increment the expression of vimentin, a mesenchymal marker [44] for the Alg, Alg-HA_{741} and Alg-HA_{1500} hydrogels' core. Of note, vimentin was not expressed by MKN45 cells cultured alone or supplemented with bmMSCs conditioned media (Supplementary Fig. 6). This observation is consistent with, either vimentin is derived from the epithelial to mesenchymal transition of the MKN45 cells, or the bmMSCs attracted to the core are the source of this vimentin expression. Overall, our results are consistent with the latter possibility as bmMSCs are observed in the core of the hydrogel formulated with HA of higher Mw (Figure 5A). Moreover, the presence of HA of high Mw has been reported to induce CCs to produce chemotaxic factors, such as cytokines and growth factors, that act as chemoattractant for MSCs, further supporting our results that show the migration of bmMSCs to the core of the 3D system. [48-50]

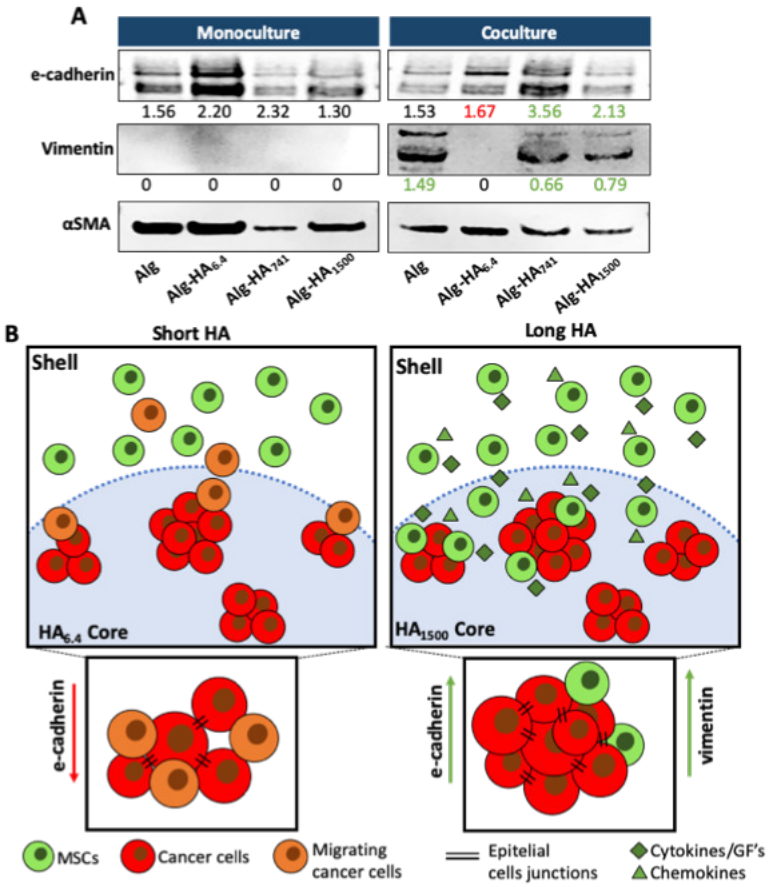

Figure 8-7. (A) Western blot analysis of E-cadherin (120kDa), vimentin (55kDa) and smooth muscle actin (40kDa), from the protein lysates of the cells present in the core of the hydrogel. (B) Graphical representation of the effect of the HA size on MKN45 (red) and bmMSCs (green) cellular response.

For the same samples (*i.e.* Alg, Alg-HA_{741} and Alg-HA_{1500}) we also observed overexpression of E-Cadherin by the cells present in the core of the 3D system showing an increment on the cell-cell contacts. This result indicates promotion of epithelial transition of MKN45 cells when they are in contact with bmMSCs. The absence of vimentin expression and a downregulation of E-Cadherin (responsible for the epithelial cell-cell junctions) in the MKN45 cells encapsulated in the Alg-$HA_{6.4}$ core suggests that the CCs are not in direct contact with MSCs in the core of the hydrogel, but instead induces the CCs migration to the shell (loss of E-Cadherin expression), as previously reported. [51]

8-4. Conclusion

We developed a 3D core-shell model that is able to recapitulate a series of mechanical, biochemical and biological features of a gastric TME. Using co-culturing conditions (MKN45 cells at the tumor site and bmMSCs in its periphery) we were able to mimic the influence of healthy bmMSCs in the CCs' behavior. We further demonstrate that the HA's Mw at the cancer site is able to modulate CCs' behavior. Low Mws, *e.g.* $HA_{6.4}$, induces a migratory phenotype in MKN45 cells, which also internalize HA immediately after cell seeding. In contrast, HA of high Mw, *e.g.* HA_{1500}, does not promote an invasive behavior on MKN45 CCs, however, instead, it attracts bmMSCs to the cancer site reducing the growth of CCs' clusters. Overall, with the developed core-shell 3D model, we were able to mimic the TME and to assess the influence of the biochemical features of specific components of the cancer ECM, *e.g.* HA and its Mw, as well as the presence of bmMSCs, in CC's behavior.

8-5. References

1. Hui, L.L. and Y. Chen, *Tumor microenvironment: Sanctuary of the devil.* Cancer Letters, 2015. **368**(1): p. 7-13.

2. Wang, M., et al., *Role of tumor microenvironment in tumorigenesis.* J Cancer, 2017. **8**(5): p. 761-773.

3. Pinho, S.S. and C.A. Reis, *Glycosylation in cancer: mechanisms and clinical implications.* Nat Rev Cancer, 2015. **15**(9): p. 540-55.

4. Taubenberger, A.V., et al., *3D extracellular matrix interactions modulate tumour cell growth, invasion and angiogenesis in engineered tumour microenvironments.* Acta Biomater, 2016. **36**: p. 73-85.

5. Venning, F.A., L. Wullkopf, and J.T. Erler, *Targeting ECM Disrupts Cancer Progression.* Front Oncol, 2015. **5**: p. 224.

6. Mereiter, S., et al., *O-glycan truncation enhances cancer-related functions of CD44 in gastric cancer.* FEBS Lett, 2019. **593**(13): p. 1675-1689.

7. Chanmee, T., P. Ontong, and N. Itano, *Hyaluronan: A modulator of the tumor microenvironment.* Cancer Lett, 2016. **375**(1): p. 20-30.

8. Setälä, L.P., et al., *Hyaluronan expression in gastric cancer cells is associated with local and nodal spread and reduced survival rate.* British Journal of Cancer, 1999. **79**(7): p. 1133-1138.

9. Walker, C., E. Mojares, and A. Del Rio Hernandez, *Role of Extracellular Matrix in Development and Cancer Progression.* Int J Mol Sci, 2018. **19**(10).

10. Price, Z.K., N.A. Lokman, and C. Ricciardelli, *Differing Roles of Hyaluronan Molecular Weight on Cancer Cell Behavior and Chemotherapy Resistance.* Cancers (Basel), 2018. **10**(12).

11. Yang, C., et al., *The high and low molecular weight forms of hyaluronan have distinct effects on CD44 clustering.* J Biol Chem, 2012. **287**(51): p. 43094-107.

12. Chen, F., et al., *New horizons in tumor microenvironment biology: challenges and opportunities.* BMC Med, 2015. **13**: p. 45.

13. Sawayama, H., T. Ishimoto, and H. Baba, *Microenvironment in the pathogenesis of gastric cancer metastasis.* Journal of Cancer Metastasis and Treatment, 2018. **4**(2).

14. Mereiter, S., et al., *Glycosylation in the Era of Cancer-Targeted Therapy: Where Are We Heading?* Cancer Cell, 2019. **36**(1): p. 6-16.

15. Dittmer, A., et al., *Human mesenchymal stem cells induce E-cadherin degradation in breast carcinoma spheroids by activating ADAM10.* Cellular and Molecular Life Sciences, 2009. **66**(18): p. 3053-3065.

16. Khakoo, A.Y., et al., *Human mesenchymal stem cells exert potent antitumorigenic effects in a model of Kaposi's sarcoma.* J Exp Med, 2006. **203**(5): p. 1235-47.

17. Zhu, W., et al., *Engineering a biomimetic three-dimensional nanostructured bone model for breast cancer bone metastasis study.* Acta Biomater, 2015. **14**: p. 164-74.

18. Yen, B.L. and M.-L. Yen, *Mesenchymal Stem Cells and Cancer — for Better or for Worse?* 2008. **4**(1): p. 5-9.

19. Djouad, F., et al., *Earlier onset of syngeneic tumors in the presence of mesenchymal stem cells.* Transplantation, 2006. **82**(8): p. 1060-6.

20. Klopp, A.H., et al., *Mesenchymal stem cells promote mammosphere formation and decrease E-cadherin in normal and malignant breast cells.* PLoS One, 2010. **5**(8): p. e12180.

21. Mak, I.W., N. Evaniew, and M. Ghert, *Lost in translation: animal models and clinical trials in cancer treatment.* Am J Transl Res, 2014. **6**(2): p. 114-8.

22. Melissaridou, S., et al., *The effect of 2D and 3D cell cultures on treatment response, EMT profile and stem cell features in head and neck cancer.* Cancer Cell Int, 2019. **19**: p. 16.

23. Ferreira, D.S., et al., *Hyaluronan and self-assembling peptides as building blocks to reconstruct the extracellular environment in skin tissue.* Biomaterials Science, 2013. **1**(9): p. 952-964.

24. da Costa, D.S., et al., *Sulfonic groups induce formation of filopodia in mesenchymal stem cells.* Journal of Materials Chemistry, 2012. **22**(15): p. 7172-7178.

25. Infanger, D.W., M.E. Lynch, and C. Fischbach, *Engineered culture models for studies of tumor-microenvironment interactions.* Annu Rev Biomed Eng, 2013. **15**(1): p. 29-53.

26. Ferreira, L.P., V.M. Gaspar, and J.F. Mano, *Bioinstructive microparticles for self-assembly of mesenchymal stem Cell-3D tumor spheroids.* Biomaterials, 2018. **185**: p. 155-173.

27. Rijal, G. and W. Li, *A versatile 3D tissue matrix scaffold system for tumor modeling and drug screening.* Sci Adv, 2017. **3**(9): p. e1700764.

28. Hached, F., et al., *Polysaccharide Hydrogels Support the Long-Term Viability of Encapsulated Human Mesenchymal Stem Cells and Their Ability to Secrete Immunomodulatory Factors.* Stem Cells Int, 2017. **2017**: p. 9303598.

29. Costa, M.J., et al., *Physicochemical properties of alginate-based films: Effect of ionic crosslinking and mannuronic and guluronic acid ratio.* Food Hydrocolloids, 2018. **81**: p. 442-448.

30. Braccini, I. and S. Perez, *Molecular basis of Ca2+-induced gelation in alginates and pectins: The egg-box model revisited.* Biomacromolecules, 2001. **2**(4): p. 1089-1096.

31. Chan, G. and D.J. Mooney, *Ca2+ released from calcium alginate gels can promote inflammatory responses in vitro and in vivo.* Acta Biomaterialia, 2013. **9**(12): p. 9281-9291.

32. Kim, H.N. and N. Choi, *Consideration of the Mechanical Properties of Hydrogels for Brain Tissue Engineering and Brain-on-a-chip.* Biochip Journal, 2019. **13**(1): p. 8-19.

33. Cavo, M., et al., *Microenvironment complexity and matrix stiffness regulate breast cancer cell activity in a 3D in vitro model.* Scientific Reports, 2016. **6**.

34. Kim, J.E., et al., *Characterization of the mechanical properties of cancer cells in 3D matrices in response to collagen concentration and cytoskeletal inhibitors.* Integr Biol (Camb), 2018. **10**(4): p. 232-241.

35. Liu, C., et al., *Potential effect of matrix stiffness on the enrichment of tumor initiating cells under three-dimensional culture conditions.* Exp Cell Res, 2015. **330**(1): p. 123-34.

36. Yu, H., J.K. Mouw, and V.M. Weaver, *Forcing form and function: biomechanical regulation of tumor evolution.* Trends Cell Biol, 2011. **21**(1): p. 47-56.

37. Canibano-Hernandez, A., et al., *Alginate Microcapsules Incorporating Hyaluronic Acid Recreate Closer in Vivo Environment for Mesenchymal Stem Cells.* Mol Pharm, 2017. **14**(7): p. 2390-2399.

38. Kratochvil, M.J., et al., *Engineered materials for organoid systems.* Nature Reviews Materials, 2019. **4**(9): p. 606-622.

39. Bohari, S.P., D.W. Hukins, and L.M. Grover, *Effect of calcium alginate concentration on viability and proliferation of encapsulated fibroblasts.* Biomed Mater Eng, 2011. **21**(3): p. 159-70.

40. Rijal, G. and W. Li, *Native-mimicking in vitro microenvironment: an elusive and seductive future for tumor modeling and tissue engineering.* J Biol Eng, 2018. **12**: p. 20.

41. Ridge, S.M., F.J. Sullivan, and S.A. Glynn, *Mesenchymal stem cells: key players in cancer progression.* Mol Cancer, 2017. **16**(1): p. 31.

42. Ferreira, L.P., et al., *Mesenchymal Stem Cells Relevance in Multicellular Bioengineered 3D In Vitro Tumor Models.* Biotechnol J, 2017. **12**(12).

43. Dittmer, A., et al., *Mesenchymal stem cells and carcinoma-associated fibroblasts sensitize breast cancer cells in 3D cultures to kinase inhibitors.* Int J Oncol, 2011. **39**(3): p. 689-96.

44. Secunda, R., et al., *Isolation, expansion and characterisation of mesenchymal stem cells from human bone marrow, adipose tissue, umbilical cord blood and matrix: a comparative study.* Cytotechnology, 2015. **67**(5): p. 793-807.

45. Amorim, S., et al., *Molecular weight of surface immobilized hyaluronic acid influences CD44-mediated binding of gastric cancer cells.* Sci Rep, 2018. **8**(1): p. 16058.

46. Stern, R., A.A. Asari, and K.N. Sugahara, *Hyaluronan fragments: an information-rich system.* Eur J Cell Biol, 2006. **85**(8): p. 699-715.

47. Djouad, F., et al., *Earlier Onset of Syngeneic Tumors in the Presence of Mesenchymal Stem Cells.* Transplantation, 2006. **82**(8): p. 1060-1066.

48. Lee, H.Y. and I.S. Hong, *Double-edged sword of mesenchymal stem cells: Cancer-promoting versus therapeutic potential.* Cancer Sci, 2017. **108**(10): p. 1939-1946.

49. Spaeth, E., et al., *Inflammation and tumor microenvironments: defining the migratory itinerary of mesenchymal stem cells.* Gene Ther, 2008. **15**(10): p. 730-8.

50. Rattigan, Y., et al., *Interleukin 6 mediated recruitment of mesenchymal stem cells to the hypoxic tumor milieu.* Experimental Cell Research, 2010. **316**(20): p. 3417-3424.

51. Zhao, Y.F., et al., *Modulating Three-Dimensional Microenvironment with Hyaluronan of Different Molecular Weights Alters Breast Cancer Cell Invasion Behavior.* ACS Appl Mater Interfaces, 2017. **9**(11): p. 9327-9338.

SUPPLEMENTARY INFORMATION

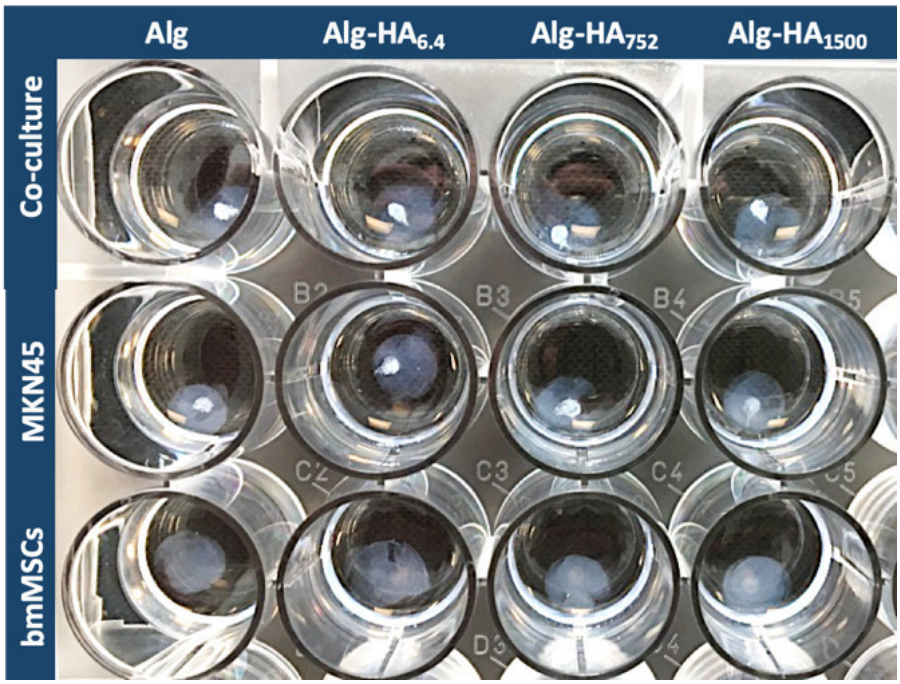

Supplementary Fig. 8-1. 3D hydrogels constructs made from an alginate (Alg) shell with encapsulated bone marrow mesenchymal stem cells (bmMSCs) and a core containing MKN45 cancer cells encapsulated in a mixture of Alg and hyaluronic acid (HA) of different molecular weights (Mws, *i.e.* 6.4, 752 and 1500kDa).

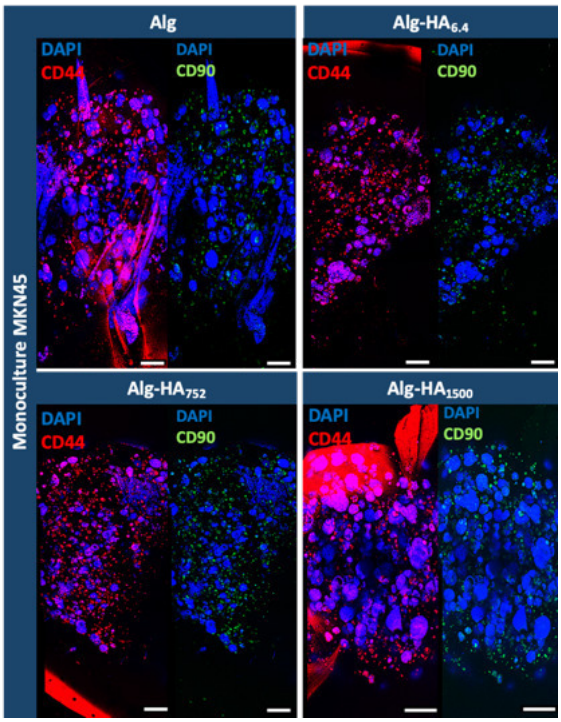

Supplementary Fig. 8-2. Constructs generated with the encapsulation of MKN45 cells in the core (cell-free shell). Cells were immunostained for CD44 (red), CD90 (green) and nuclei (blue). Scale bar corresponds to 200µm.

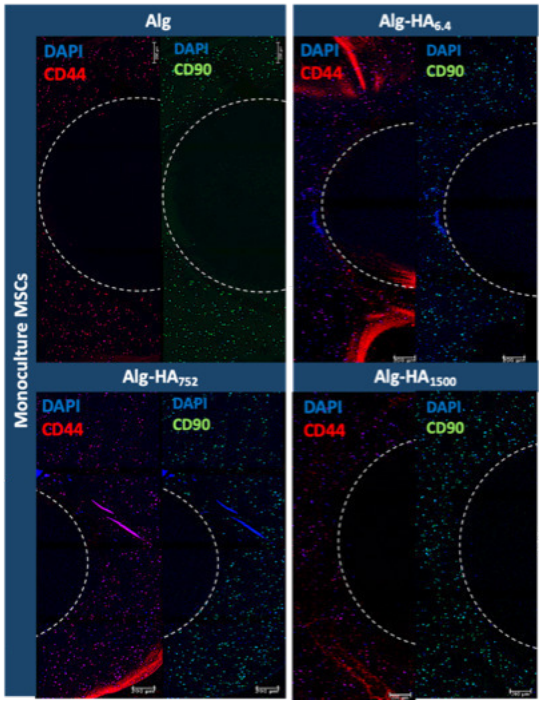

Supplementary Fig. 8-3. Constructs with bone marrow mesenchymal stem cells (bmMSCs) encapsulated in the shell (cell-free core) and immunostained for CD44 (red), CD90 (green) and nuclei (blue). Scale bar corresponds to 200µm.

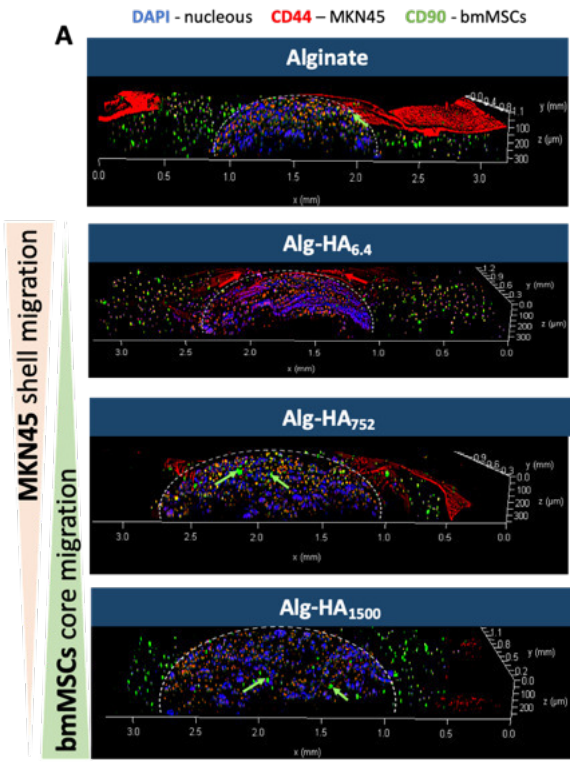

Supplementary Fig. 8-4. Constructs co-cultured with bmMSCs (encapsulated in the shell) and MKN45 cells (encapsulated in the core). Both cell types were immunostained for CD44 (red), CD90 (green) and nuclei (blue). Scale bar corresponds to 200μm. The arrows show the MKN45 cells migration to the shell (red arrows) and bmMSCs migration to the core (green arrows).

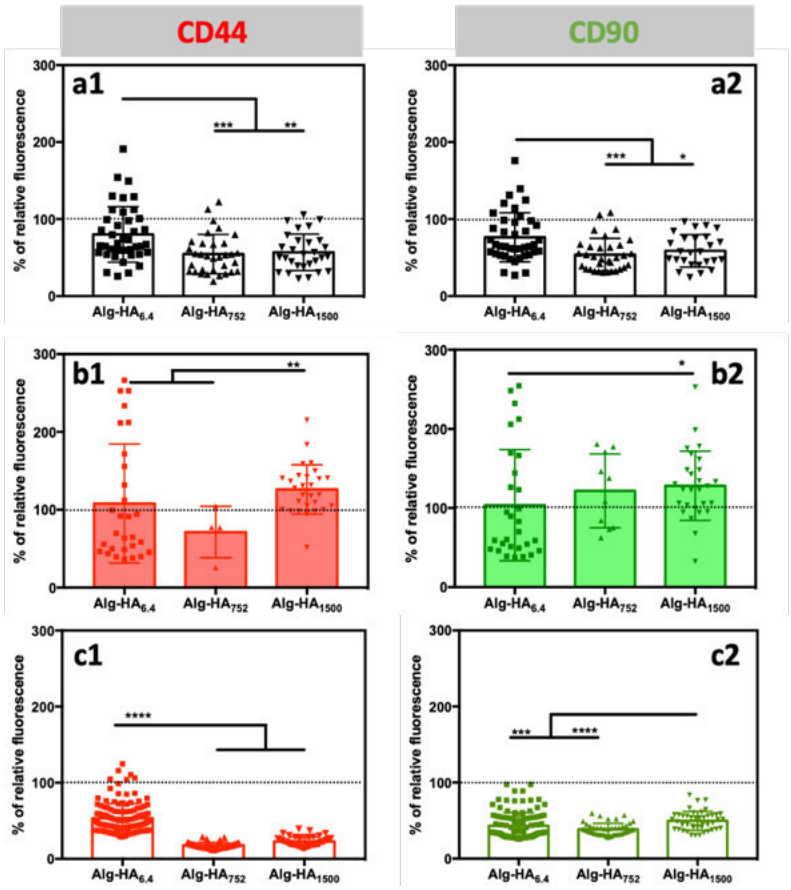

Supplementary Fig. 8-5. Relative fluorescence intensity of the construct's core stained for CD44 and CD90 in the presence of (a1, a2) monoculture of MKN45, (b1, b2) co-culture of MKN45/bmMSC and (c1, c2) MKN45 under conditioned medium as control. Statistical differences **** are marked for $p < 0.0001$ and *** for $p < 0.0002$, ** for $p < 0.002$ and * for $p < 0.03$. All results are referenced to the fluorescence obtained for the HA-free Alg core.

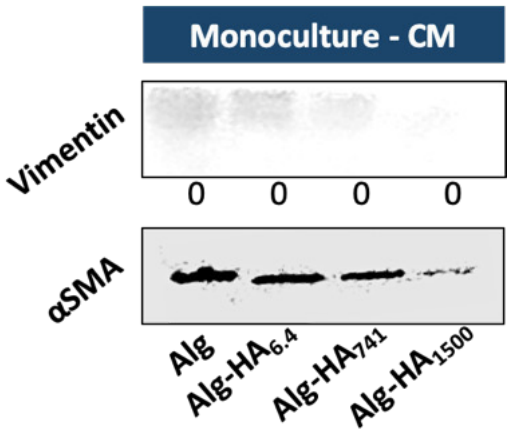

Supplementary Fig. 8-6. Western blot analysis of protein lysates from cells present in the core, seeded in the presence of conditioned medium obtained from the bmMSCs expansion.

Section IV

Final Conclusions and Perspectives

Chapter 9

General conclusions and Final Remarks

Chapter 9

General Conclusions and Final remarks

9-1. General Conclusions

Gastric cancer (GC) is responsible for, approximately, 750 000 deaths per year. The current therapies are restricted to the use of chemotherapeutic drugs, the use of radiotherapy and surgery to remove the affected area. However, the current therapies are still non-specific, which leads to side-effects where a large number of healthy cells and tissues are also affected. Even under these circumstances, the complete cure of a cancer patient is still not a common outcome of the therapies, being common relapses where cancer appears again after some years.

Under this framework, significant effort is being made to understand the intrinsic properties of the tumor microenvironment (in particular of the extracellular matrix, ECM) and the interplay between changes in the biochemical/physical composition/properties of the ECM and cancer onset, growth and metastasis. In fact, it is currently established that the ECM is a key contributor to the transformation of healthy cells to the malignant phenotype, and is a key modulator of cancer cell behavior, as in the case of the triggering of the cancer invasive character. Different elements of the ECM have been studied and reported to be take part of these transformations. One of such elements is the glycosaminoglycan hyaluronic acid (HA). HA is of particular interest due to the fact that HA of different molecular weights accumulate on ECM of the tumor microenvironment. HA is known to interfere on cellular adhesion and proliferation, as well as the triggering of the invasive character of cancer cells. In fact, the length of the HA's chains is known to be important modulators of the HA's bioactivity, playing a crucial role on cancer progression/recession. Cancer cell behavior is not only influenced by the HA's biochemical properties mediated by its molecular weight, it is also important to consider the mechanical stimulus that the remodeled HA-rich cancer ECM play in the apply on the embedded cancer cells.

In this thesis, we used different strategies to mimic the accumulation of HA on the cancer ECM and to evaluate its influence on cancer cell behaviour. The controlled side-on immobilization of HA with

different Mws (6.4, 752 and 1500kDa) on 2D surfaces were performed using the Layer-by-Layer (LbL) approach using PLL as the support polycation layer. The easy handling and mild conditions used during the LbL assembly allowed us to immobilize HA on 2D surfaces without compromising its bioactivity. In addition, we also developed a 3D model through the combination of alginate (Alg) and HA, where cancer cells were encapsulated in a spherical Alg-HA core (simulating the cancer site), that was further embedded into the center of and Alg disc containing healthy mesenchymal stem cells (mimicking the surrounding environment).

During Chapter 3, we describe the assembly of LbL films composed by 10 layers, *i.e.* $(PLL\text{-}HA)_5$, using HA of different Mws, *i.e.* 6.4, 751 and 1500kDa. We characterized these films in terms of their viscoelastic/mechanical properties, hydration and binding affinity with CD44, one of the major receptors for HA. We performed this evaluation using different characterization techniques, namely, QCM-D, SPR and AFM. The stability of the films was evaluated under two types of cross-linking, using the typical electrostatic forces used during LbL assembly and the promotion of covalent cross-linking by carbodiimide chemistry. The covalently stabilized $(PLL\text{-}HA)_5$ films showed reduced thickness and hydration, variations that were more pronounced for the films assembled using HA of low Mw (*i.e.* 6.4kDa). The mechanical properties of the films showed the same tendency, where HA of 6.4kDa presented the highest Young's modulus, compatible with a densification of the film. In addition, the enhanced stability of the cross-linked $(PLL\text{-}HA)_5$ coatings allowed them to interact with the CD44 without the disruption of the films, showing an enhanced affinity to all the LbL assemblies, independently of the HA's Mw used to assemble the film.

Under Chapter 4, we seeded two different GC cell lines, *i.e.* MKN45 and AGS, on the surface of the LbL films. Our first approach was based on the use of LbL film of 2 layers, *i.e.* (PLL-HA), to study the GC cells adhesion, CD44 expression, motility and invasiveness. We observed different CD44 expression depending on the cell line. In the case of the MKN45 cells, they presented a high CD44 expression on the cellular membrane, which was at the basis of the observation of a relationship between cellular behavior and the Mw of the immobilized HA. In this case, a higher number of cells was observed as the Mw of the immobilized HA increased. In the case of AGS cells, their adhesion was not influenced by the blocking of CD44, which we correlated with the expression of CD44 in the cytoplasm and not in the cell membrane. Of note, this observation was consistent with a CD44-independent adhesion process. We also found that the Mw of HA modulates E-cadherin and cortactin expression. The immobilization of HA of high Mw (*i.e.* 1500kDa) induced a high expression of cortactin. The upregulated expression of CD44, a cancer stem cell marker, together with high cell motility and upregulated expression of cortactin, a key

component of invadopodia, demonstrated the invasive character of MKN45 cells when seeded on LbL films containing HA_{1500}.

In Chapter 5, we used the crosslinked LbL films (characterized under Chapter 3) to evaluate the impact of the HA's Mw on the behavior of AGS cancer cells. The invasive character of AGS cancer cells are usually associated with the infection with *Helicobacter pylori*, which is at the basis of GC malignancy and therapeutic resistance. We observed that cells seeded on the $(PLL\text{-}HA)_5$ films presenting HA of 6.4kDa, exhibited an elongated morphology with increased polarity, similar to the typical invasive "hummingbird" phenotype. Moreover, the cells in contact with $HA_{6.4}$ presented increased motility associated to the overexpression of *p*-ERK1/2 and *p*-AKT signaling cascades, typically observed in invasive cancer cells. We demonstrated that the increment in the number of layers of the LbL film, altered its mechanical and chemical properties, with relevant impact on cellular behavior. In contrast with the induction of cancer invasiveness by HA of 6.4kDa, in the case of the films that presented of HA of high Mw, *i.e.* HA_{1500}, we observed a reduction of the migration of AGS cells, being compatible with the promotion of cancer latency.

Chapter 6 focused in the evaluation of the behavior of MKN45 cells using the 10-layered films, *i.e.* $(PLL\text{-}HA)_5$. While in Chapter 4 it was observed that MKN45 presented a high expression of CD44 on the cell membrane, and as a consequence, the cells were responsive for the immobilized HA; in this case, we followed in real-time the adhesion of MKN45 cells and the remodeling of the LbL layers using the QCM-D technique. We observed that the dynamic cell seeding, under a constant flow rate, accelerated the cellular adhesion with the formation of filopodia and lamellipodia, with enhanced expression of focal adhesion sites. When we compared the dynamic and static cell culture conditions, the latter ones induced a lower filopodia number and length, in particular for higher HA's of higher Mws (*i.e.* 752 and 1500kDa). Moreover, the surfaces presenting HA of 6.4kDa showed the activation of the MAPK-ERK signalling cascade, which is responsible for the invasive character of GC. In contrast, HA of high Mw (*i.e.* 1500kDa) showed the activation of signalling cascades associated to cells apoptosis and cancer latency.

Finally, under Chapter 7, we developed a 3D core-shell model combining Alg and HA of different Mws. This system was used to culture MKN45 cancer cells in an Alg-HA sphere that was embedded in a disc of Alg hydrogel, to which bone marrow mesenchymal stem cells, bmMSCs, were encapsulated. This strategy was used to mimic the influence of healthy bmMSCs in the behavior of cancer cells. While the hydrogel core (comprising the MKN45 cells) resembled the confined tumor site, the bmMSCs on

the shell mimicked the stem cells present on the periphery of the tumor site. Similar to the 2D surfaces, the Mws of HA at the modeled cancer site (*i.e.* Alg-HA sphere) influenced the 3D mechanical properties of the hydrogel, being softer as the HA's Mw increased. However, we observed by using fluorescently marked HAs, that the proposed system was able to retain the HA chains at the hydrogel sphere, which were recognized by the encapsulated cancer cells, *i.e.* MKN45. We also showed that the HA's Mw modulated the cancer cells behavior, where: the $HA_{6.4}$ induced the migration of cancer cells; the HA_{1500} retained the MKN45 cell in the hydrogels' core. In addition, the high Mw of HA were able to attract bmMSCs from the shell to the core, reducing the size of the cancer cells clusters. This co-culture model was a faithful mimic of the TME, where cancer and healthy cells were able to interact under a 3D environment that mimicked the *in vivo* scenario.

The scientific works presented in this thesis describes several models, techniques and methodologies that can be exploited to study the influence of HA in the behavior of cancer cells. From a biophysical perspective, we were able to contribute to a better understanding of the HA-mediated interaction with CD44 using QCM-D and SPR. At a biochemical characterization level, we used different techniques, such as western blot and protein arrays, which were important contributors to unravel the influence of Mw of HA in the behavior of GC cells.

9-2. FINAL REMARKS

This thesis reports different strategies to study the interaction of HA with GC cells. The evaluation of the pathological involvement of the Mw of HA (that naturally occurs on the ECM of tumors) on the adhesion, migration and invasiveness of cancer cells was achieve using the traditional 2D cell culture onto LbL films. In this case, it was possible to mimic the entanglement of HA usually observed on the ECM while maintaining the bioactivity of HA. Typical limitations associated with the 2D surfaces that usually does not completely resemble the spatial organization of the ECM in the *in vivo* scenario, led us to propose the development of 3D co-culture systems with the presentation of HA in the center of the 3D hydrogels. The presence of HA influenced not only influenced directly cancer cell behavior, but also promoted changes in the mechanical and viscoelastic properties of the models which, *per se*, also impacted on the cellular response. In this thesis we show the remarkable influence of the ECM mechanical properties, and its biochemical features, on the adhesion, remodeling and migration of cancer cells. However, further studies should be pursued, to separate the contributions of the chemical or physical properties of the models to the observed biological outcomes. Moreover, the proposed 2D

and 3D models can be further tested to study the efficacy of cancer therapeutic drugs, a line of research that is gaining increasing importance due to 2 main reasons: 1) limitations related with the relevance of the present *in vivo* models, where results cannot be translated to the human scenario; and 2) increasing limitations on the use of animal models. Finally, based on the findings presented in this thesis, clearly showing the involvement of HA and its Mw on GC cellular behaviour, an important future line of research is the development of therapeutic approaches based on the manipulation of the composition of the HA-rich ECM of GC tissue.